PACIFIC EARTHQUAKE ENGINEERING
RESEARCH CENTER

Reference-Rock Site Conditions for Central and Eastern North America:

Part I – Velocity Definition

Developed by

NGA-East Geotechnical Working Group

Youssef M.A. Hashash, Albert R. Kottke, Jonathan P. Stewart, Kenneth W. Campbell, Byungmin Kim, Ellen M. Rathje, and Walter J. Silva

In Collaboration with:

Sissy Nikolaou and Cheryl Moss

PEER 2014/11
AUGUST 2014

Reference-Rock Site Conditions for Central and Eastern North America:

Part I – Velocity Definition

Developed by

NGA-East Geotechnical Working Group

Youssef M.A. Hashash, Albert R. Kottke, Jonathan P. Stewart, Kenneth W. Campbell, Byungmin Kim, Ellen M. Rathje, and Walter J. Silva

In Collaboration with:

Sissy Nikolaou and Cheryl Moss

Report PEER 2014-11
Pacific Earthquake Engineering Research Center
Headquarters, University of California at Berkeley

August 2014

ABSTRACT

As part of the Next Generation Attenuation Relationships for Central and Eastern North America (NGA-East) Project, we have gathered data to define an appropriate reference-rock site condition for CENA. The reference-rock site condition is defined by the *S*- and *P*-wave velocities, as well as the local crustal damping (κ_0). This report deals solely with the definition of the reference *P*- and *S*-wave velocities. The significance of the reference-rock definition is that it represents the site condition for which ground motions will be predicted using semi-empirical ground motion prediction equations (GMPEs). Moreover, it represents the site condition to which site amplification factors are referenced (i.e., site amplification is unity for reference rock). There are significant differences in the reference-rock site conditions between active tectonic regions, such as Western North America (WNA), and mid-plate regions, such as Central and Eastern North America (CENA).

Using velocity measurements reported in the license applications at nuclear power plants as well as published data, we developed criteria to assess the presence of the reference-rock site condition that is based on the seismic velocities and their gradient with respect to depth. We apply the criteria to the available profiles, which are included with this report, from which we recommend that seismic velocities for reference rock in CENA be defined as follows:

- $V_{s,ref}$ = 3000 m/sec or 9800ft/sec (2700 to 3300 m/sec or 8900 to 10,800 ft/sec)
- $V_{p,ref}$ =5500 m/sec or 18,000 ft/sec. (5000 to 6100 m/sec or 16,400 to 20,000 ft/sec)

The range given for seismic velocities is based on a ±5% change in amplification using quarter wavelength theory.

We do not find evidence for regional dependence of the reference velocities, which are derived principally from three general geographic regions: (1) the Atlantic Coast; (2) continental interior; and (3) Appalachian Mountains. Our data do not provide reference velocities for the Gulf Coast region. In this region the depth to the CENA reference-rock condition is expected to be much greater than other CENA regions due to several kilometers of overlying sediments. We do not provide a reference-rock condition for the Gulf Coast. Our recommendation is to adopt a consistent reference-rock condition for the entire CENA region, as given above, and then estimate transfer functions to a softer reference condition (such as 760 m/sec) for application of the NGA-East GMPEs.

ACKNOWLEDGMENTS

This project would not have been possible without support from the following individuals and companies: Farhang Ostadan and Tarek Elkhoraibi of Bechtel; Jeff Bachuber and Michael Gray of Fugro Consultants for providing digital velocity profiles for a number of nuclear power plant applications; Richard Rivera-Lugo of the United States Nuclear Regulatory Commission for assisting with navigation of regulatory documents and license applications; Sissy Nikolau and Cheryl Moss for providing data in the New York City areas as well as laboratory measurements on rock; Michael Musgrove and Khatereh Khodaverdi for selecting reference-rock velocity profiles; and, finally, Ataya Eltibi and Paul Khauli who digitized velocity profiles for this project.

CONTENTS

LIST OF TABLES

LIST OF FIGURES

1 Introduction

Site amplification represents the differences in ground motions for a particular site condition relative to a reference condition, hereby referred to as the reference-rock site condition. The reference-rock site condition is defined by the *S*- and *P*-wave velocities, as well as the local crustal damping (κ_0). There are significant differences in the reference-rock site condition between active tectonic regions, e.g., Western North America (WNA), and mid-plate regions, e.g., Central and Eastern North America (CENA) [Boore and Joyner 1997].

As part of the Next Generation Attenuation Relationships for Central and Eastern North America (NGA-East) Project, we have gathered data to define an appropriate reference-rock site condition for CENA. Using velocity measurements reported in the license applications at 16 nuclear power plants as well as published data, we have developed criteria to assess the presence of the reference-rock site condition. The criteria were then used to select reference-rock velocities ($V_{s,ref}$ and $V_{p,ref}$) from the profiles that are representative of the reference-rock site condition.

These reference-rock site parameters will be used for the derivation of the NGA-East ground motion prediction equations (GMPEs). In separate work, site amplification factors will also be derived in which the amplification is relative to the reference-rock condition (i.e., site amplification for the reference condition is unity).

2 Prior Recommendation on Reference Rock

The Electric Power Research Institute (EPRI) [1993] report established the state-of-practice for defining ground motions in the CENA region for nuclear facilities. The report identified 16 crustal structure regions within CENA developed using P-wave inversions, and *S*-wave velocities were estimated using an assumed Poisson's ratio of 0.25. The *S*-wave velocities in the EPRI [1993] report are not based on direct measurements. The characteristics of the surface layer in the crustal structure regions are presented in Table 1. As shown in Figure 1, the estimated V_s of the surface layer ranges from 2.31 to 2.83 km/sec with a value of 2.83 km/sec for 12 of 16 profiles. The results of ground motion simulations showed small differences among 15 of the 16 crustal models (with the exception of the Gulf Coast Plain). Accordingly, the 15 models producing similar motions were combined using a representative surface layer $V_{\mathrm{S},ref} = 2.83$ km/sec ([EPRI) 1993]. This combined region was referred to as the Midcontinental region. Toro et al. [1997] developed GMPEs for these two regions (Midcontinental and Gulf Coast).

Table 1 Surface layer characteristics from the sixteen crustal structure regions proposed by EPRI [1993].

Region	V_p (km/sec)	V_s (km/sec)	Thickness (km)
Offshore New England	4.9	2.83	1.0
Northern Appalachians	4.9	2.83	1.0
Atlantic Coastal Plain	4.9	2.83	1.0
Southern Appalachians	4.9	2.83	1.0
Lake Superior Basin	4.9	2.83	5.0
Midcontinent	4.9	2.83	1.0
Northern Great Plains	4.9	2.83	1.0
Southern Great Plains	4.9	2.83	2.0
Wilison Basin	4.9	2.83	1.0
Western Tennessee	4.9	2.83	1.5
Central Tennessee	4.9	2.83	1.0
Ozarks	4.9	2.83	1.0
New Madrid Rift	4.7	2.72	4.0
Central Plains	4.5	2.60	3.0
Northern Grenville-Superior	5.0	2.34	1.0
Gulf Coast Plain	4.0	2.31	7.0

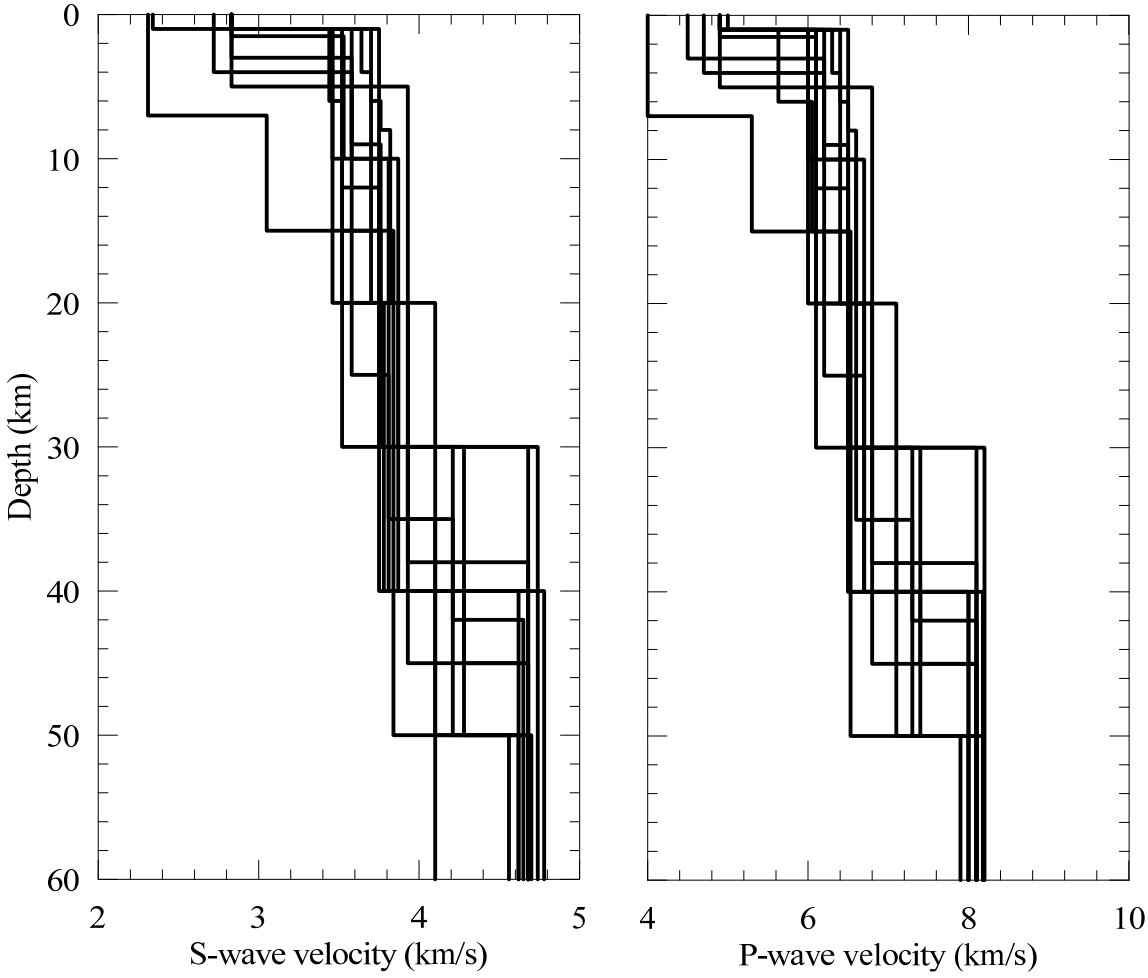

Figure 1 Summary of velocity models for the 16 regions in the EPRI [1993] study.

The U.S. Nuclear Regulatory Commission (NRC) provides the following guidance on the selection of $V_{s,ref}$ in NUREG-1.208 [NRC 2007]:

> *The hazard curves from the PSHA are defined for general surficial rock conditions that are consistent with the definition of rock for the attenuation relationships used in the PSHA. For example, existing attenuation relationships for the CEUS typically define generic rock conditions as materials with a shear wave velocity (V_s) of 2.8 km/sec (9,200 ft/sec).*

The recommendation of 2.8 km/sec (9200 ft/sec) in NUREG-1.208 was adopted by the NRC to maintain compatibility with contemporaneous GMPEs used in the nuclear industry (e.g., Toro et al. [1997]), which are based on the estimated $V_{\mathrm{S},ref}$ values from EPRI [1993]. Table 2 shows reference site condition ranging from 2.00 to 2.83 km/sec for a number of GMPEs applicable to the CENA region (see Toro et al. [1997]; Campbell [2003]; Atkinson and Boore [2006]; and Pezeshk et al. [2011]). Those models are based on simulations; hence the reference velocities

reflect conditions at the top of assumed crustal profiles used during the simulation process. It is important to recognize the divergence in reference site conditions in GMPEs does not reflect varying interpretations of available profiles derived from data. In fact, since the seminal EPRI [1993] work, no systematic data compilation has been undertaken to support a defensible definition of reference rock. The work described in this report is meant to fill this need, using prescribed protocols applied to high quality data in a transparent, reviewable manner.

Table 2 Reference *S*-wave velocities used by CENA GMPEs.

Reference	$V_{S,ref}$ (km/sec)
Atkinson and Boore [2006]	≥ 2.00
Campbell [2003]	2.80
Toro, Abrahamson, and Schneider [1997][1]	2.83
Pezeshk, Zandieh, and Tavakoli [2011]	≥ 2.00

[1]Midcontinental region.

3 Evaluation of Reference *S*- and *P*-Wave Velocities

3.1 DATA COLLECTION

We have collected *S*- and *P*-wave velocity profiles that penetrate intact hard rock from published reports and Nuclear Power Plant (NPP) license applications for sites in the CENA. The following sites/references were considered:

- Bell Bend NPP [UniStar Nuclear Services LLC 2010)
- Bellefonte NPP [Tennessee Valley Authority 2009]
- Beresnev and Atkinson [Beresnev and Atkinson 1997]
- Callaway NPP [Union Electric Company 2009)
- Calvert Cliffs NPP [Calvert Cliffs 3 Nuclear Project LLC. UniStar Nuclear Operating Services LLC 2011]
- Clinton NPP [Exelon Generation Company 2006]
- Comanche Peak [Luminant Generation Company LLC 2009]
- Dames and Moore [1974]*
- Daniels et al. [1983]
- Dorman and Smalley [1994]
- Fermi NPP [Detroit Edison Company 2010]
- Grand Gulf NPP [Entergy Operations Florida Inc. 2011]
- Kafka and Skehan [1990)
- Levy County NPP [Progress Energy Florida Inc. 2011]
- Luetgert et al. [1994]
- Moos and Zoback [1983]
- Motazedian et al. [2011]*

- Nine Mile NPP [Nine Mile Point Nuclear Project LLC and UniStar Nuclear Operating Services LLC 2011]
- North Anna NPP [Dominion Virginia Power 2009]
- PSEG NPP [PSEG Power 2011]
- River Bend Station NPP [Entergy Operations Inc 2008]
- Shearon Harris NPP [Progress Energy Carolinas 2011]
- South Texas NPP [STP Nuclear Operating Company 2011]
- Turkey Point NPP [Florida Power and Light Company 2010]
- V. C. Summer NPP [South Carolina Electric & Gas 2011]
- Victoria County NPP [Exelon Nuclear Texas Holdings LLC 2008]
- Vogtle NPP [Southern Nuclear Operating Company 2008]
- William States Lee III NPP [Duke Energy 2010]

This data was screened for quality and then analyzed, as described in the next section, to develop criteria to identify the reference-rock site condition in the CENA. Data from both Midcontinental and Gulf Coast regions are included in this compilation. Two datasets marked by an asterisk are excluded:

1. The Dames and Moore [1974] dataset provides geology, V_s, and V_p profiles at 61 nuclear power plants across the CENA region. The major concern with inclusion of this dataset was the poor quality of the measurements and the inability to clearly identify the assumptions that were made in the development of the profiles.
2. The Motazedian et al. [2011] dataset is from a micro-zonation study for a portion of Ottawa, Canada. The data consists of refraction profiles at 531 sites with 508 measurements of the bedrock V_s ranging from 940 to 6124 m/sec. Motazedian et al. [2011] screened the data by removing outliers using the Grubbs' [1969] and Chavenet's [Worthing and Geffner 1943] rejection criteria. The resulting data ranged from 940 to 4895 m/sec with mean of 2700 m/sec and a standard deviation of 680 m/sec and COV = 0.25. Crow [*personal communication*, 2011] has suggested that high velocity values resulted from uneven stratigraphic surfaces at the sites. With or without outlier removal, we consider the range of the reported velocities to be unrealistic. Moreover, there is significant uncertainty regarding whether the penetration depth of the refraction surveys is sufficiently large that the underlying intact rock is sampled. Accordingly, we did not utilize this dataset.

3.2 EVALUATION OF PROFILES

3.2.1 Reference Rock Definition

We have found that velocity profiles from the CENA region comprising a sufficiently large sampling depth to penetrate intact bedrock show some common characteristics. For example, as illustrated in Figures 2 to 5 from Bell Bend NPP, *S*- and *P*-wave velocities increase with depth as the materials transition from soils into weathered rock and eventually intact rock. A striking feature of profiles from a significant majority of the available sites is the lack of increase with depth of shear wave velocity within firm materials encountered near the bases of profiles. We have found that defining the reference-rock site condition on the basis of written descriptions of relatively intact rock from boring logs is not sufficient, because highly variable conditions in the rock V_s profile can be present even for materials logged as intact rock. This is thought to result in part from the wide range of rock types sampled in our dataset. Instead, visual inspection of the profiles revealed key features that are commonly encountered were used to define reference rock as follows:

1. We require V_s > 2000 m/sec and V_p > 3500 m/sec for a layer potentially defined as reference rock.
2. Reference-rock layers must be sampled over a sufficiently large depth range so that velocity gradients and potential weathered zones can be identified. For the case of velocity profiles based on depth-controlled geophysical measurements (i.e., test types where the geophysical receivers are located at depth; for example, suspension logging, cross hole, and down hole), logs must penetrate at least 10 m into a layer being considered as a reference-rock material. For velocity profiles derived using geophysical methods without depth-control (e.g., reflection or refraction surveys, surface wave methods), no such penetration criteria are used. Profiles developed from surface wave methods are only considered if the layers judged to have the reference velocity are not the first layer in the profile below shallower materials having relatively slow velocities and relatively steep velocity gradients.
3. The velocity gradient with respect to depth (dV/dz) is negligible to small within the reference rock. Typically, this condition is achieved over depth intervals at least 5–10 m in thickness and associated gradients are generally less than 25 (m/sec)/m. More information on this topic is provided in Section 0.
4. Reference-rock units should be from materials of Paleozoic and older (>251 Myr) age, although this criteria is not enforced in cases where age is unknown.

For each site satisfying the above criteria, a mean profile velocity, $\left(\bar{V}_{s,ref}\right)_{pr}$ was evaluated within the reference-rock layer, see Figures 2–5.

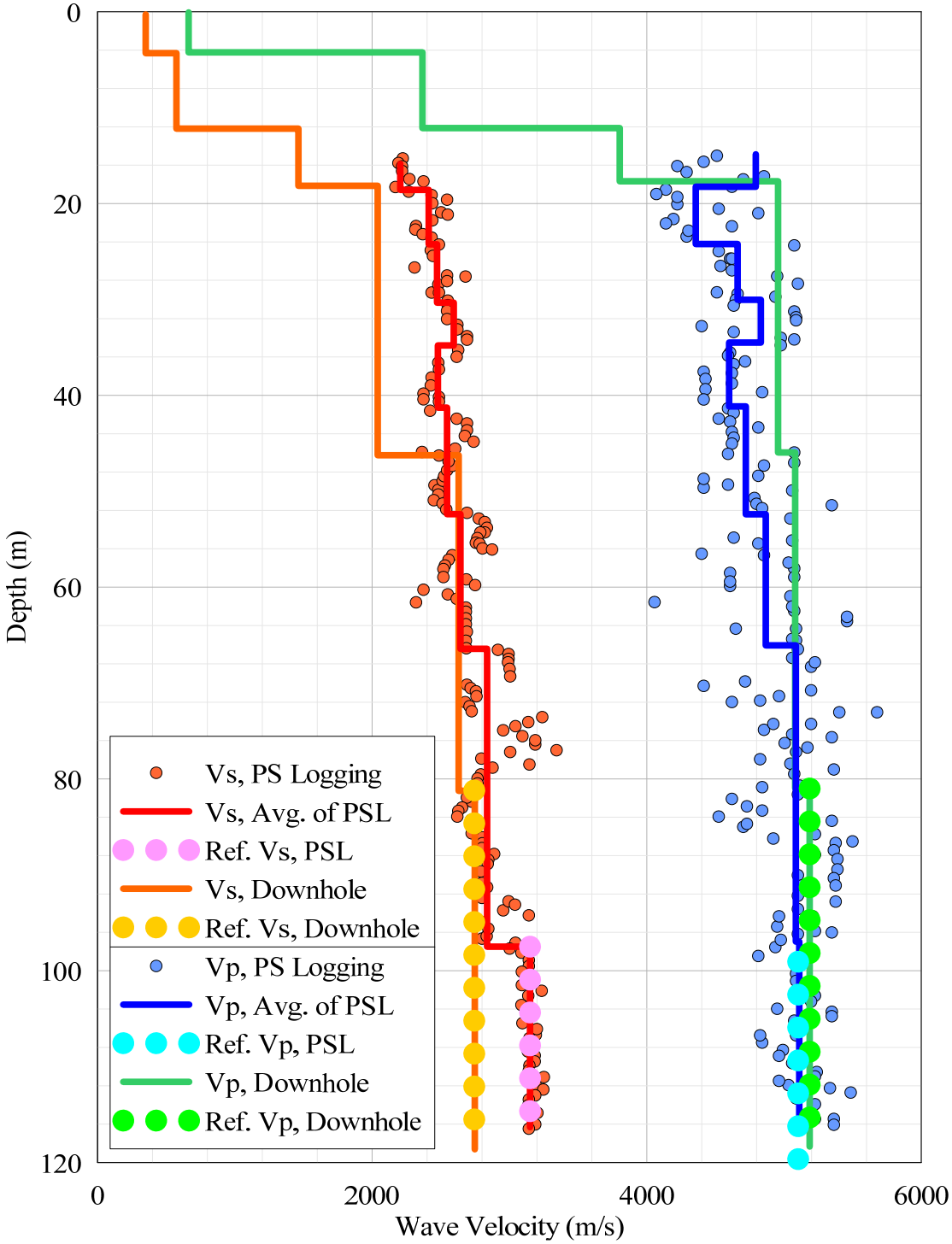

Figure 2 **Wave velocities at Bell Bend NPP (FSAR Figure 2.5-151).**

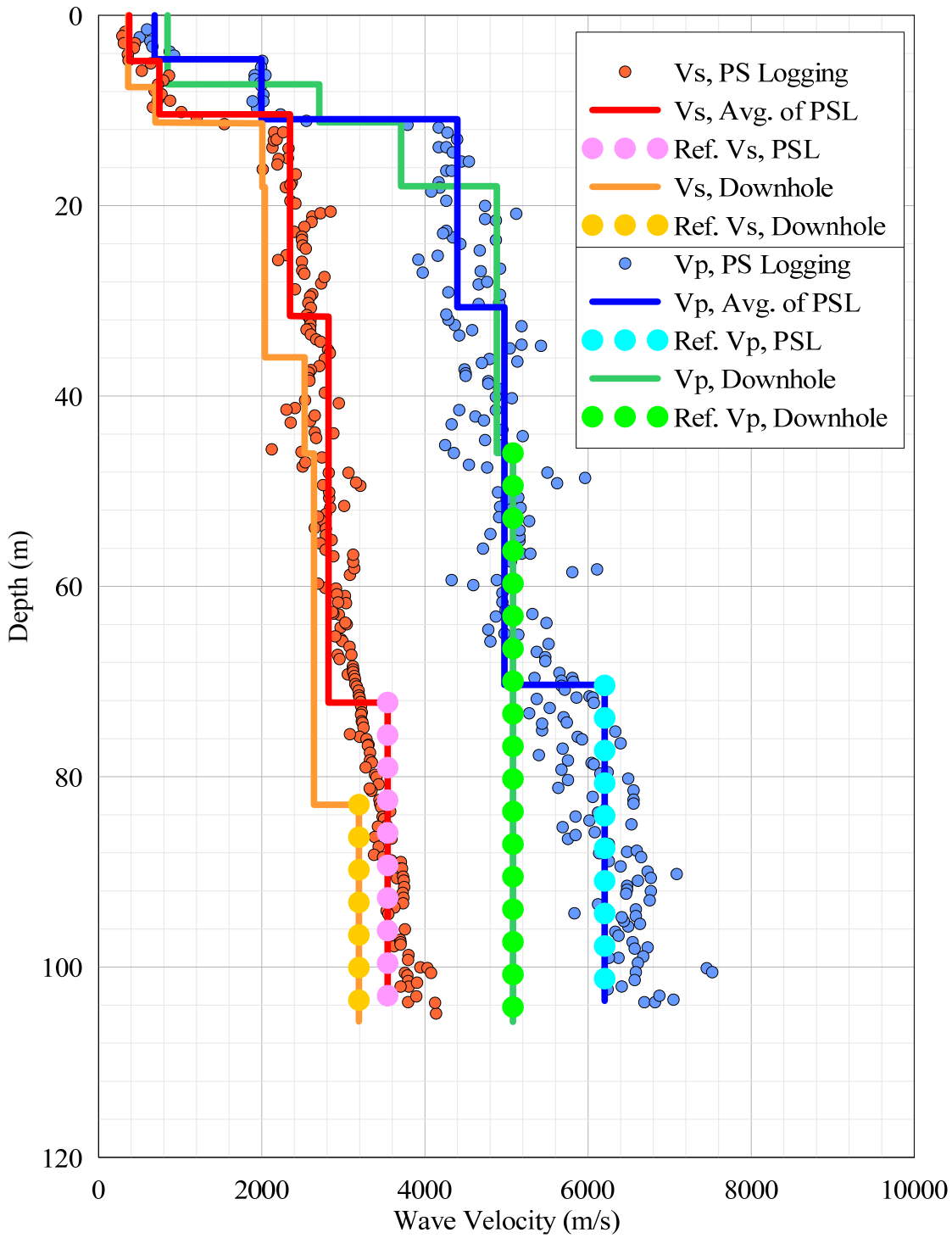

Figure 3 **Wave velocities at Bell Bend NPP (FSAR Figure 2.5-152).**

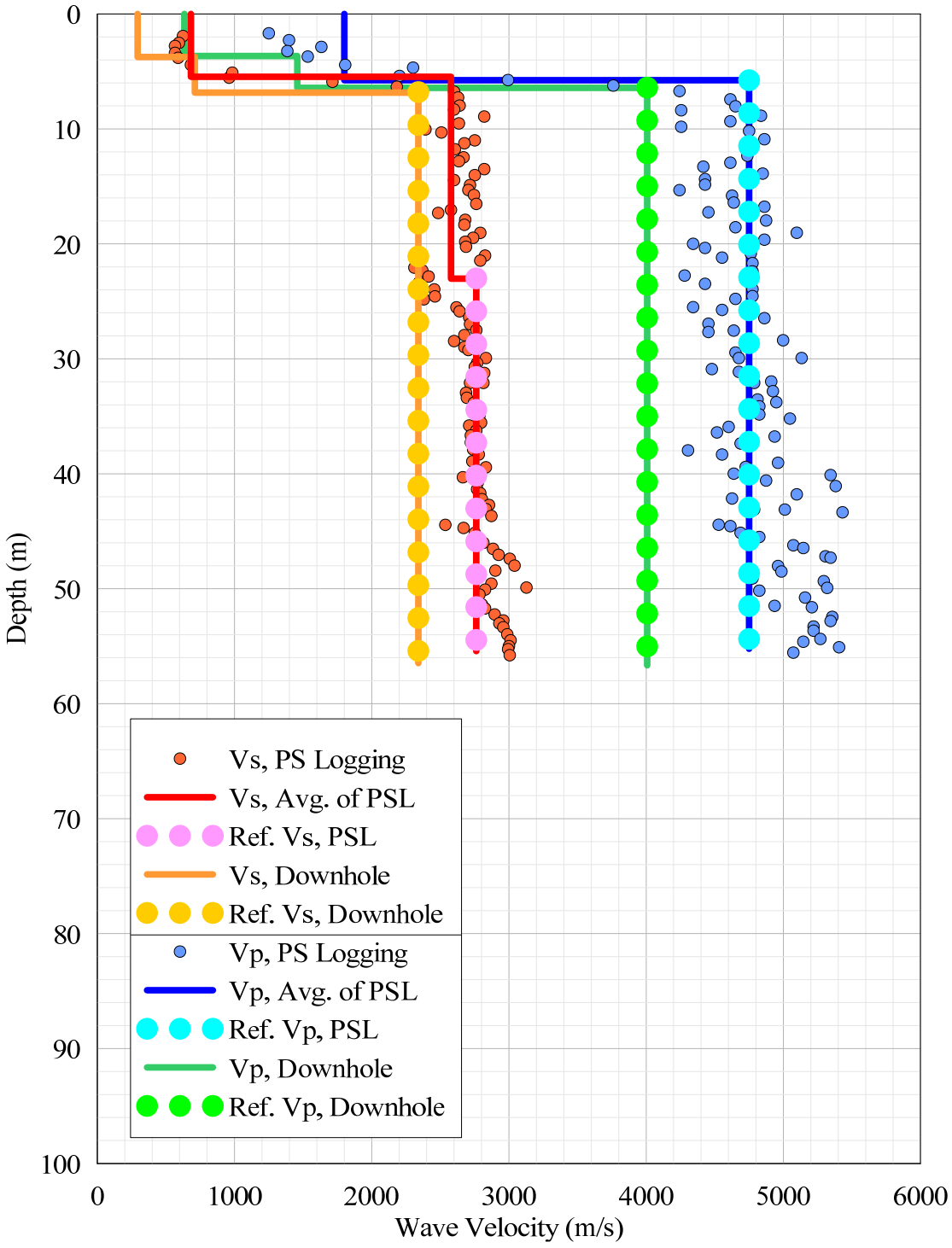

Figure 4 **Wave velocities at Bell Bend NPP (FSAR Figure 2.5-153).**

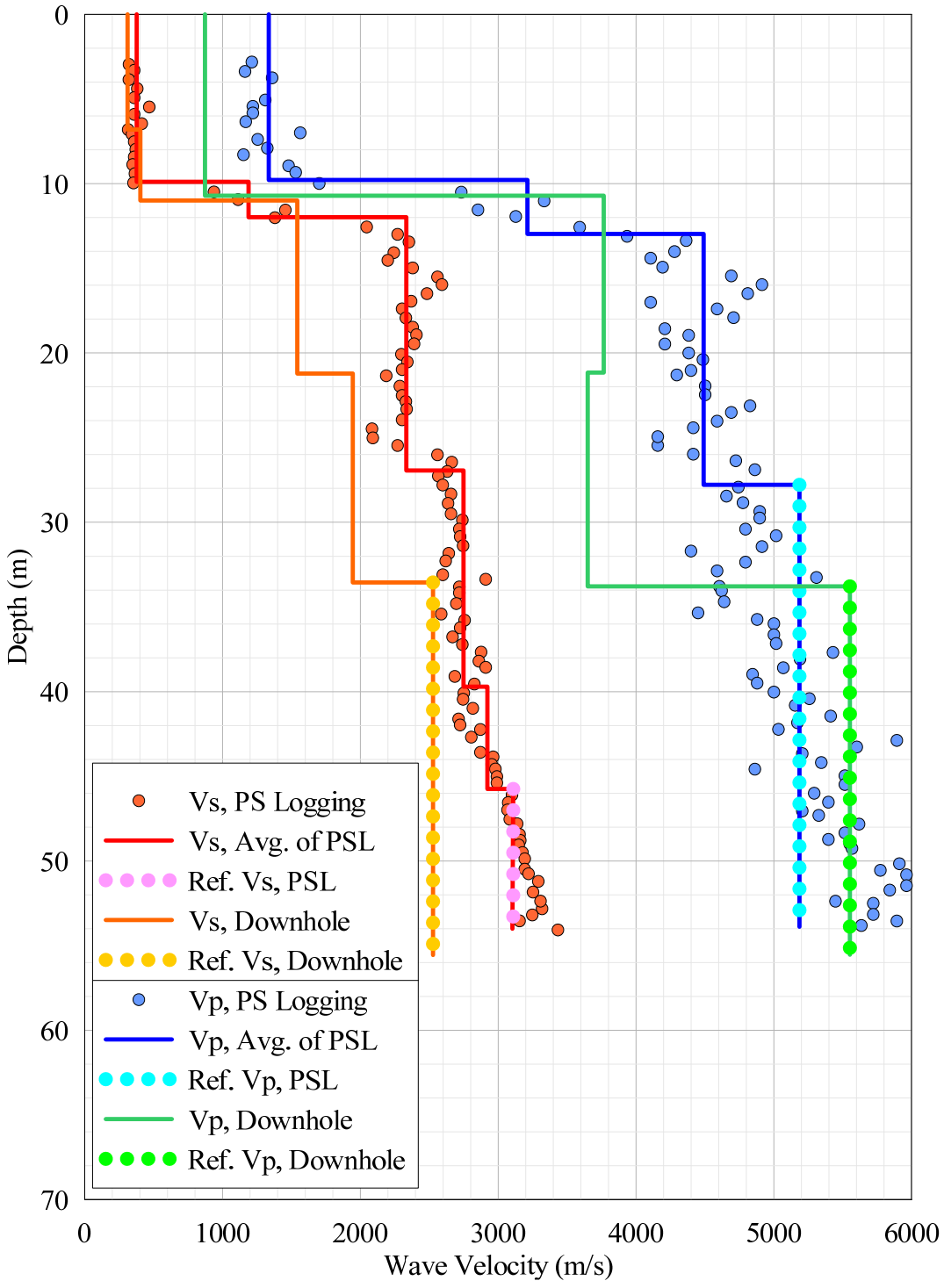

Figure 5 **Wave velocities at Bell Bend NPP (FSAR Figure 2.5-154).**

3.2.2 Selected $V_{s,ref}$ and $V_{p,ref}$ Values

The total number of profiles examined in this work was 283, of which 128 satisfied the reference-rock velocity conditions described in Section 3.2.1. Those 128 profiles were digitized and the mean reference-rock velocity was computed over the interpreted depth range. This process yielded 68 *S*-wave velocities at 27 different locations and 60 *P*-wave velocities at 22 different locations; see Table 3.

Figure 6 shows the locations of the sites with reference velocities. Chulick and Mooney [2002], later updated by Mooney [personal communication, 2012], define crustal properties within four general regions of the CENA: (1) the continental interior; (2) Gulf Coast; (3) Appalachian Mountains; and (4) Atlantic Coast. These regional designations are indicated for each site in Table 3. All but one of the sites with reference-rock velocities are located within the continental interior (13 sites), Atlantic Coast region (17 sites), or Appalachian Mountains (2 sites). We have relatively limited coverage along the Gulf Coast region. The velocity profiles from three Gulf-Coast nuclear plants (Levy County, South Texas, and Victoria County) were not sufficiently deep to sample the reference-rock condition despite measurements at depths of 1400 to 4000 m.

Of the 68 *S*-wave measurements, 58 are from direct measurements of the *in situ S*-wave velocity. The remaining 10 values estimated V_s using measured V_p and an assumed Poisson's ratio, as listed in Table 3. Figures 7 and 8 present box plots of the reference velocity at the various sites showing the range of data. The selected *S*- and *P*-wave reference velocities show essentially no trend with depth, as shown in Figure 9, which is consistent with the criteria described in Section 3.2.1.

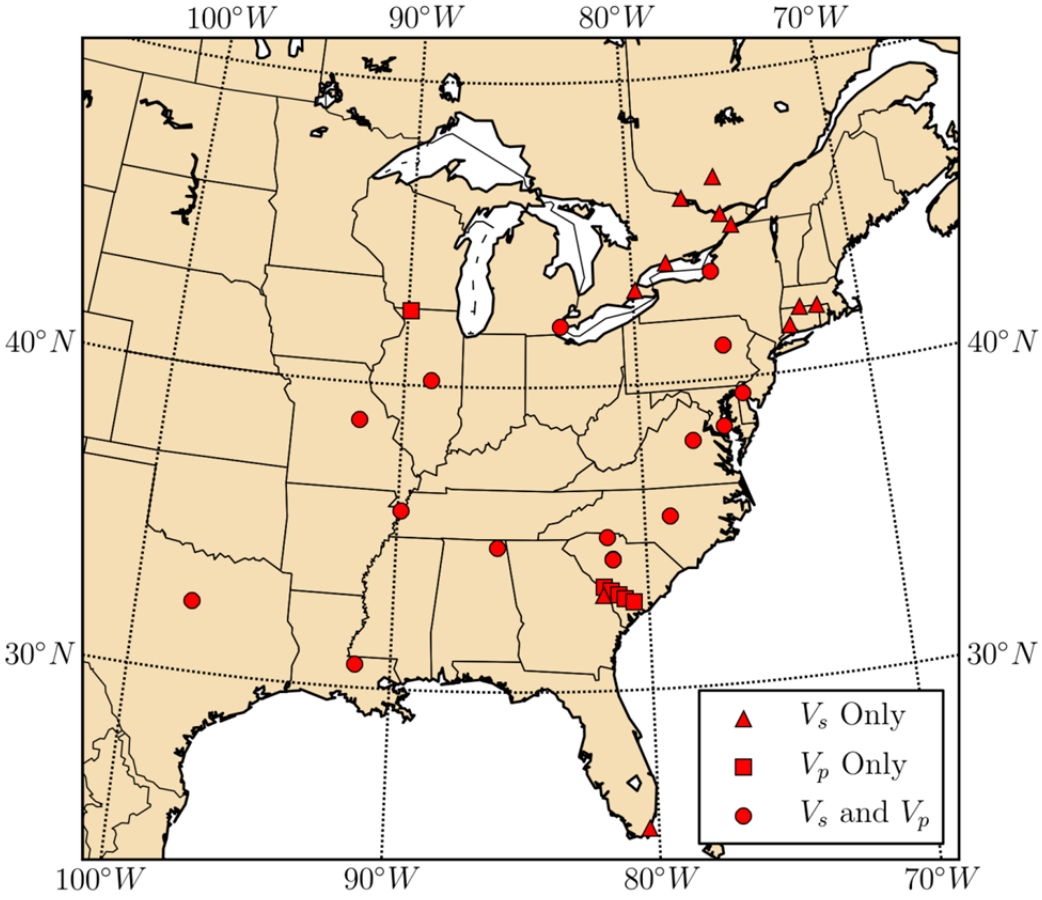

Figure 6 **Locations of the reference *S*- and *P*-wave velocity measurements.**

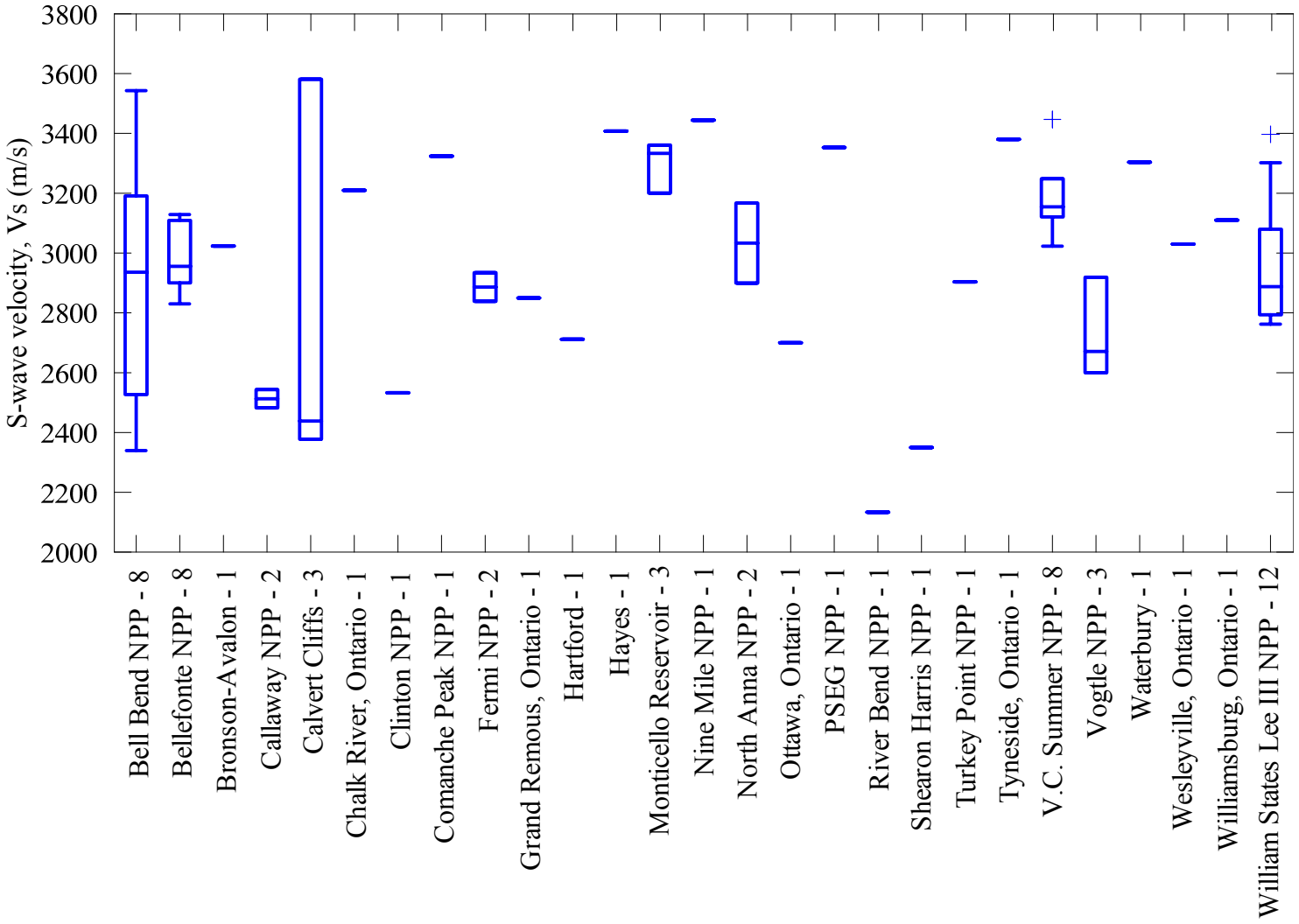

Figure 7 **Boxplots of the reference *S*-wave velocity and number of values, which shows the minimum and maximum (outside bars), 25th and 75th percentile (blue box), and the median (bar inside of blue box).**

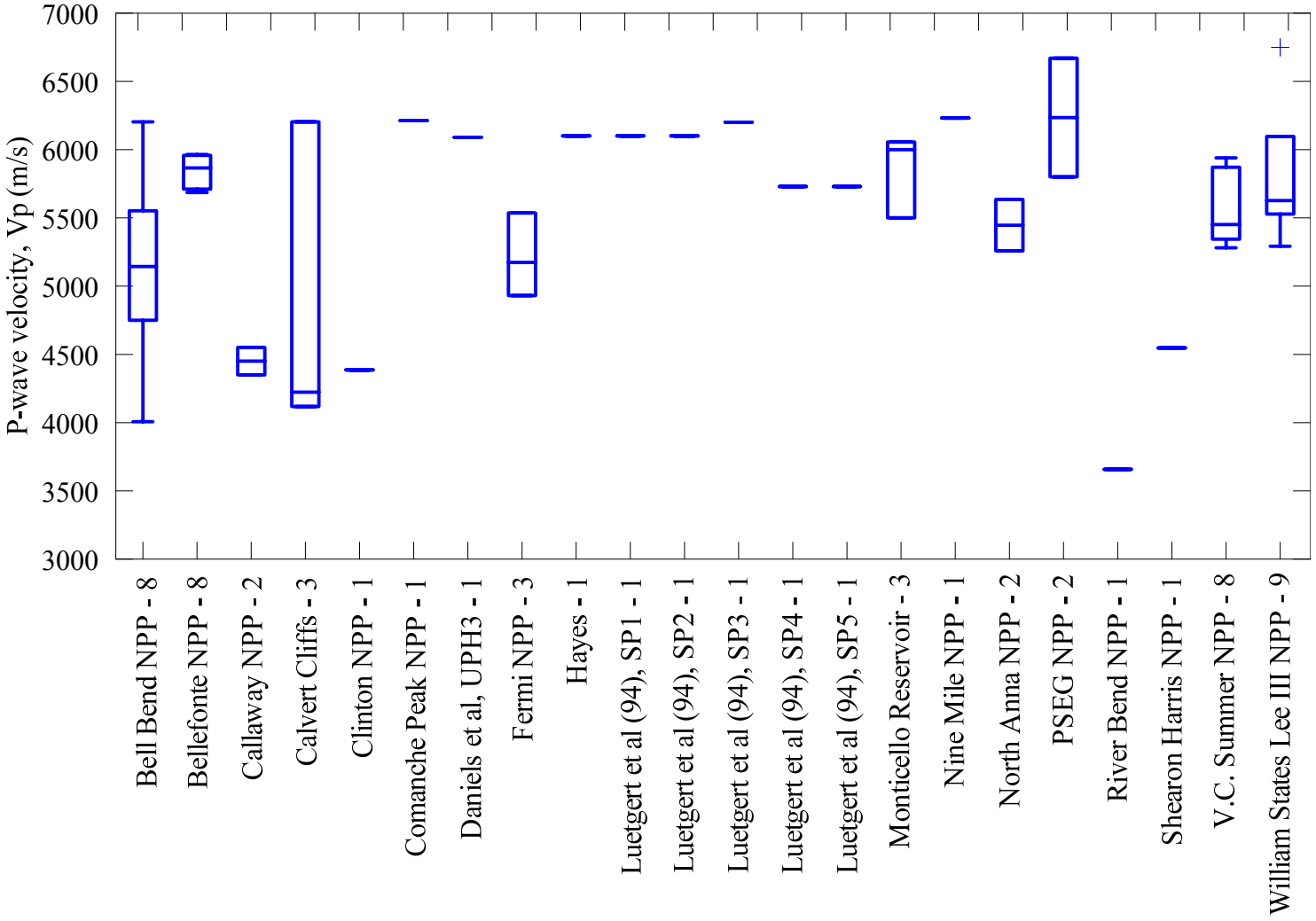

Figure 8 **Boxplots of the reference *P*-wave velocity and number of values. See Figure 7 for boxplot description.**

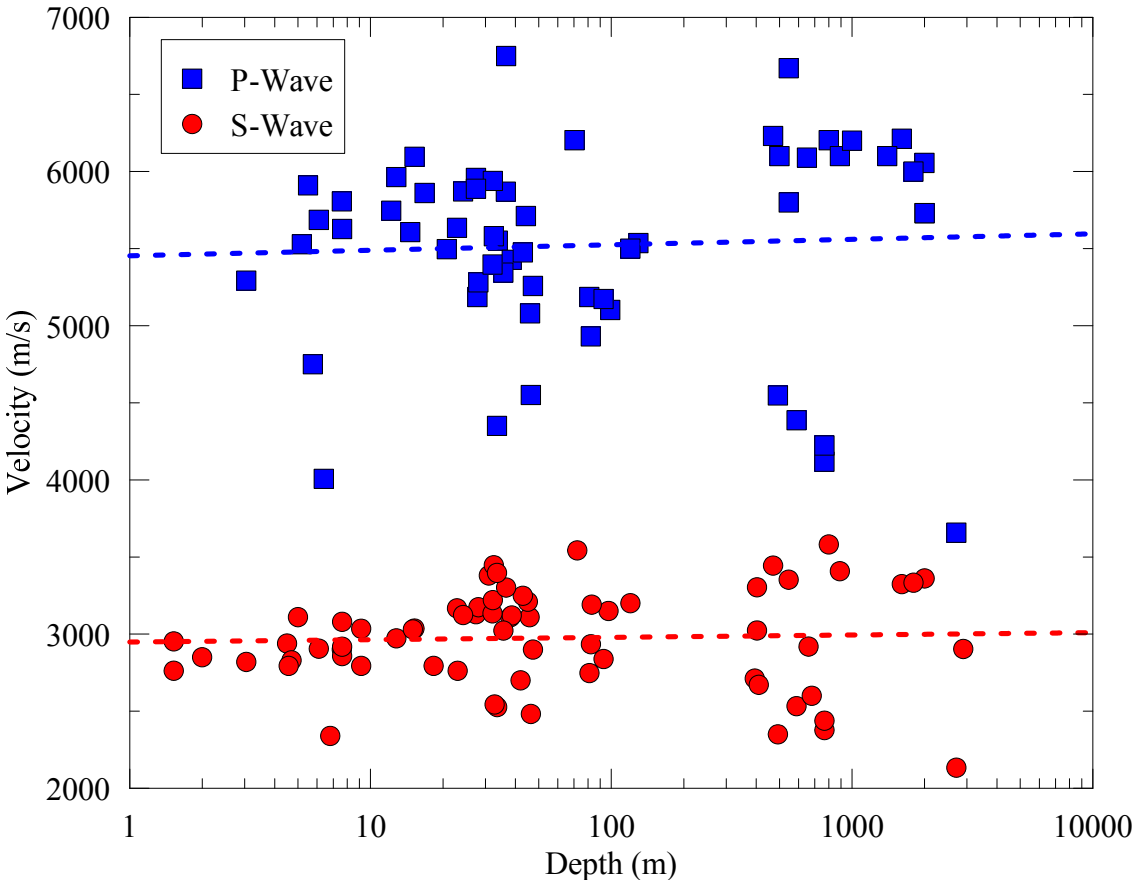

Figure 9 **Influence of depth on the reference *P*- and *S*-wave velocities with semi-log-linear models fit through the *S*- and *P*-wave data.**

Table 3 Reference *S*- and *P*- wave velocities for all profiles.

Site	Lat. (N)	Lon. (E)	Region	$V_{p,ref}$ (m/sec)	$\sigma^{pr}_{V_{p,ref}}$ (m/sec)	$V_{s,ref}$ (m/sec)	$\sigma^{pr}_{V_{s,ref}}$ (m/sec)	Assumed Poisson's Ratio	Method	Reference
Bell Bend NPP	41.086	-76.165	App.	5186		2747			downhole	FSAR Figure 2.5-151
Bell Bend NPP	41.086	-76.165		5102	151	3150	52		ps logging	FSAR Figure 2.5-151
Bell Bend NPP	41.086	-76.165		5080		3191			downhole	FSAR Figure 2.5-152
Bell Bend NPP	41.086	-76.165		6203	456	3543	228		ps logging	FSAR Figure 2.5-152
Bell Bend NPP	41.086	-76.165		4007		2340			downhole	FSAR Figure 2.5-153
Bell Bend NPP	41.086	-76.165		4750	318	2762	142		ps logging	FSAR Figure 2.5-153
Bell Bend NPP	41.086	-76.165		5552		2527			downhole	FSAR Figure 2.5-154
Bell Bend NPP	41.086	-76.165		5186	415	3110	76		ps logging	FSAR Figure 2.5-154
Bellefonte NPP	34.713	-85.925	App.	5910	356	2939	185		ps logging	FSAR Figure 2.5-331
Bellefonte NPP	34.713	-85.925		5686		2905			downhole	FSAR Figure 2.5-333
Bellefonte NPP	34.713	-85.925		5806	337	2900	194		ps logging	FSAR Figure 2.5-333
Bellefonte NPP	34.713	-85.925		5964	385	2973	209		ps logging	FSAR Figure 2.5-334
Bellefonte NPP	34.713	-85.925		5861	282	3036	223		ps logging	FSAR Figure 2.5-335
Bellefonte NPP	34.713	-85.925		5870		2830			downhole	FSAR Figure 2.5-336
Bellefonte NPP	34.713	-85.925		5711	213	3109	86		ps logging	FSAR Figure 2.5-336
Bellefonte NPP	34.713	-85.925		5958	252	3129	129		ps logging	FSAR Figure 2.5-337
Chalkn River, Ontario	45.990	-77.450	Int.			3210			refraction	Beresnev and Atkinson (1997)
Grand Remous, Ontario	46.610	-75.860	Int.			2850			refraction	Beresnev and Atkinson (1997)
Ottawa, Ontario	45.390	-75.720	Int.			2700			refraction	Beresnev and Atkinson (1997)
Tyneside, Ontario	43.090	-79.870	Int.			3380			refraction	Beresnev and Atkinson (1997)
Williamsburg, Ontario	45.000	-75.250	Int.			3110			refraction	Beresnev and Atkinson (1997)
Wesleyville, Ontario	43.920	-78.400	Int.			3030			refraction	Beresnev and Atkinson (1997)
Callaway NPP	38.763	-91.782	Int.	4350		2544			downhole	FSAR Figure 2.5.4-19
Callaway NPP	38.763	-91.782		4551	372	2482	181		ps logging	FSAR Figure 2.5.4-19
Calvert Cliffs	38.432	-76.442	Atl	4118		2377	422	0.25	p logging	FSAR Figure 2.5-142
Calvert Cliffs	38.432	-76.442		6203		3581	612	0.25	p logging	FSAR Figure 2.5-143
Calvert Cliffs	38.432	-76.442		4223		2438		0.25	p logging	FSAR Figure 2.5-144

Site	Lat. (N)	Lon. (E)	Region	$V_{p,ref}$ (m/sec)	$\sigma^{pr}_{V_{p,ref}}$ (m/sec)	$V_{s,ref}$ (m/sec)	$\sigma^{pr}_{V_{s,ref}}$ (m/sec)	Assumed Poisson's Ratio	Method	Reference
Clinton NPP	40.172	-88.835	Int	4387		2533		0.25	p logging	ESP, Figure 4.2-8
Comanche Peak NPP	32.302	-97.793	Int	6212		3324		0.3	p logging	FSAR Table 2.5.2-227
Daniels et al, UPH3	42.438	-89.871	Int	6090	389				p logging	Daniels el al. (1983)
Hayes	35.865	-89.849	Int	6100		3408		0.28	p logging	Dorman and Smalley (1994)
Fermi NPP	41.962	-83.260	Int	5174	467	2838	195		ps logging	FSAR Figure 2.5.4-220
Fermi NPP	41.962	-83.260		4930					downhole	FSAR Figure 2.5.4-221
Fermi NPP	41.962	-83.260		5536	429	2934	199		ps logging	FSAR Figure 2.5.4-221
Bronson-Avalon	42.026	-71.868	Atl			3024			group velocity	Kafka and Skehan (1990)
Hartford	42.055	-72.648	Atl			2712			group velocity	Kafka and Skehan (1990)
Waterbury	41.485	-73.158	Atl			3304			group velocity	Kafka and Skehan (1990)
Luetgert et al (94), SP1	33.411	-81.707	Atl	6100					reflection	Luetgert, Benz, and Madabhushi (1994)
Luetgert et al (94), SP2	33.267	-81.441	Atl	6100					reflection	Luetgert, Benz, and Madabhushi (1994)
Luetgert et al (94), SP3	33.128	-81.162	Atl	6200					reflection	Luetgert, Benz, and Madabhushi (1994)
Luetgert et al (94), SP4	33.007	-80.919	Atl	5730					reflection	Luetgert, Benz, and Madabhushi (1994)
Luetgert et al (94), SP5	32.883	-80.581	Atl	5730					reflection	Luetgert, Benz, and Madabhushi (1994)
Monticello Reservoir	34.320	-81.334	Atl	6056	295	3361	180		ps logging	Moos and Zoback (1983), Figure 4
Monticello Reservoir	34.320	-81.334		6000	397	3333	276		ps logging	Moos and Zoback (1983), Figure 5
Monticello Reservoir	34.320	-81.334		5500	190	3200	135		ps logging	Moos and Zoback (1983), Figure 7
Nine Mile NPP	43.521	-76.407	Int	6231		3444			ps logging	FSAR Table 2.5-58
North Anna NPP	38.059	-77.795	Atl	5258	398	2900	365		ps logging	ESP Geophysics Figure 5
North Anna NPP	38.059	-77.795		5635	316	3167	256		ps logging	ESP Geophysics Figure 8
PSEG NPP	39.463	-75.536	Atl			3353		0.3	p logging	ESP, Figure 2.5.4.7-15
PSEG NPP	39.463	-75.536		5800					refraction	ESP, Figure 2.5.4.7-14
PSEG NPP	39.463	-75.536		6670					refraction	ESP, Figure 2.5.4.7-14
River Bend NPP	30.756	-91.334	GC	3658		2134	299	0.25	p logging	FSAR Figure 2.5.4-245

Site	Lat. (N)	Lon. (E)	Region	$V_{p,ref}$ (m/sec)	$\sigma^{pr}_{V_{p,ref}}$ (m/sec)	$V_{s,ref}$ (m/sec)	$\sigma^{pr}_{V_{s,ref}}$ (m/sec)	Assumed Poisson's Ratio	Method	Reference
Shearon Harris NPP	35.633	-78.955	Atl	4548	309	2350	150	0.3	p logging	Figure 2.5.2-262
V.C. Summer NPP	34.285	-81.321	Atl	5428	89	3121	79		ps logging	FSAR Figure 2.5.4-224/225, BP-201
V.C. Summer NPP	34.285	-81.321		5345	225	3023	191		ps logging	FSAR Figure 2.5.4-224/225, BP-206
V.C. Summer NPP	34.285	-81.321		5281	180	3174	161		ps logging	FSAR Figure 2.5.4-224/225, BP-207
V.C. Summer NPP	34.285	-81.321		5871	267	3124	200		ps logging	FSAR Figure 2.5.4-224/225, BP-211
V.C. Summer NPP	34.285	-81.321		5475	290	3249	185		ps logging	FSAR Figure 2.5.4-224/225, BP-301
V.C. Summer NPP	34.285	-81.321		5397	182	3134	133		ps logging	FSAR Figure 2.5.4-224/225, BP-306
V.C. Summer NPP	34.285	-81.321		5581	136	3447	76		ps logging	FSAR Figure 2.5.4-224/225, BP-307
V.C. Summer NPP	34.285	-81.321		5939	227	3220	168		ps logging	FSAR Figure 2.5.4-224/225, BP-311
Turkey Point NPP	25.424	-80.333	Atl			2903	100	0.3	p logging	FSAR Figure 2.5.4-211
Vogtle NPP	33.141	-81.763	Atl			2671	344		ps logging	FSAR Figure 2.5.4-8
Vogtle NPP	33.141	-81.763				2919	240		ps logging	FSAR Figure 2.5.4-8
Vogtle NPP	33.141	-81.763				2600	223		ps logging	FSAR Figure 2.5.4-8
William States Lee III NPP	35.037	-81.512	Atl			3397	287		downhole	FSAR Figure 2.5.4-219
William States Lee III NPP	35.037	-81.512		6749	280	3302			ps logging	FSAR Figure 2.5.4-219
William States Lee III NPP	35.037	-81.512		5746	504	3035	331		ps logging	FSAR Figure 2.5.4-220
William States Lee III NPP	35.037	-81.512		5888	531	2858	283		ps logging	FSAR Figure 2.5.4-221
William States Lee III NPP	35.037	-81.512				2762			downhole	FSAR Figure 2.5.4-222
William States Lee III NPP	35.037	-81.512		5292	333	2953	230		ps logging	FSAR Figure 2.5.4-222
William States Lee III NPP	35.037	-81.512		5627	413	2918	337		ps logging	FSAR Figure 2.5.4-223
William States Lee III NPP	35.037	-81.512		5607	342	2794	229		ps logging	FSAR Figure 2.5.4-224
William States Lee III NPP	35.037	-81.512		5528	445	2819	338		ps logging	FSAR Figure 2.5.4-225
William States Lee III NPP	35.037	-81.512				2794			downhole	FSAR Figure 2.5.4-226
William States Lee III NPP	35.037	-81.512		6096	401	3080	290		ps logging	FSAR Figure 2.5.4-226
William States Lee III NPP	35.037	-81.512		5497	335	2794	287		ps logging	FSAR Figure 2.5.4-232

3.2.3 Statistical Evaluation of the Data

The data collected in this study provides information on the aleatory uncertainty at three different scales: profile, site, and region. At each of these scales, the data are used to quantify the expected value and uncertainty, as well as to test statistical distributions.

At the profile level, the reference-rock depth range is identified and used to select individual within-profile measurements of reference-rock velocities $\left(V_{s,ref} \text{ and } V_{p,ref}\right)$. Measurements by different methods (e.g., donwhole and ps logging methods) were treated as separate profiles. For profiles with more than five measurements of $V_{s,ref}$ and $V_{p,ref}$ histograms of the reference-rock velocities are included in Appendix B. The Shapiro-Wilk test [Shapiro and Wilk 1965] was used to test if the distribution of within-profile measurements follows a normal or log-normal distribution. If the p-value from the test is lower than a chosen confidence level, typically 0.05 to 0.10, then the null hypothesis that the data is from the assumed distribution can be rejected. Using a confidence level of 0.10, the test was found to reject the normal and log-normal distributions for the majority of the $V_{s,ref}$ and $V_{p,ref}$ profiles shown in Figure 10. To better understand the distribution of within-profile measurements, the $V_{s,ref}$ data are combined together after removing the within-profile mean value. This transformation is applied to original dataset under the assumption of a normal distribution with constant uncertainty, as well as to the natural log of the data under the assumption of a log-normal distribution. Figure 11 shows the test of the normal distribution, and indicates that the data is more strongly clustered at the center than expected from the theoretical distribution with the sample standard deviation. There are also differences at tails of the histogram (quantiles <-3 and >+3). The data has more than the expected observations at the tails with several observations that differ by more than $\pm$ 1000 m/sec from the mean. Similar trends are observed for the log-normal distribution; see Figure 12. The Shapiro-Wilk test was used to test for normality rejected both the normal and log-normal distributions due to wider than expected tails. As shown in Figures 13 and 14, a similar evaluation of the $V_{p,ref}$ data found that both of the assumed distributions provided better fits to the data.

Subsequent analysis of velocity statistics requires the selection of a distribution so that the proper form of the standard deviation is used (e.g., COV for normal, $\sigma_{\ln V}$ for log-normal). Neither distribution is clearly preferred based on the Shapiro-Wilk tests, as described above. Previous researchers have generally applied log-normal distributions to characterize soil velocity data (e.g., Roblee et al. [1996]; Andrus et al. [2006]). Nonetheless, we elected to proceed with the normal distribution principally because it is more representative of the within-site and within-region distributions considered subsequently.

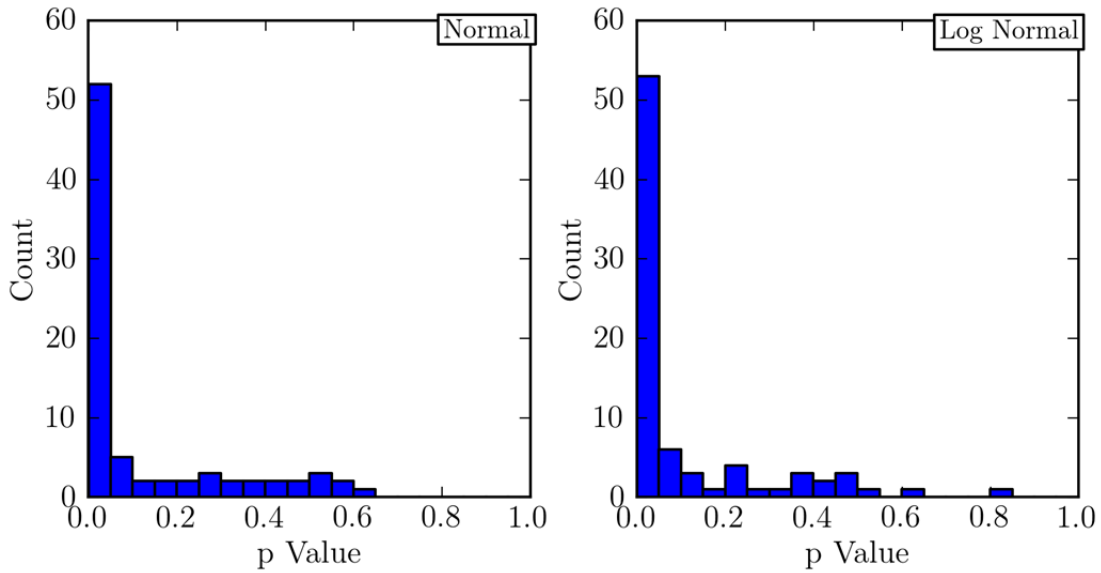

Figure 10 **Histograms of the p-value from Shapiro-Wilk tests on distributions of within-profile measurements of the reference velocity. Typical thresholds for rejection of the assumed distribution are < 0.05 or < 0.10.**

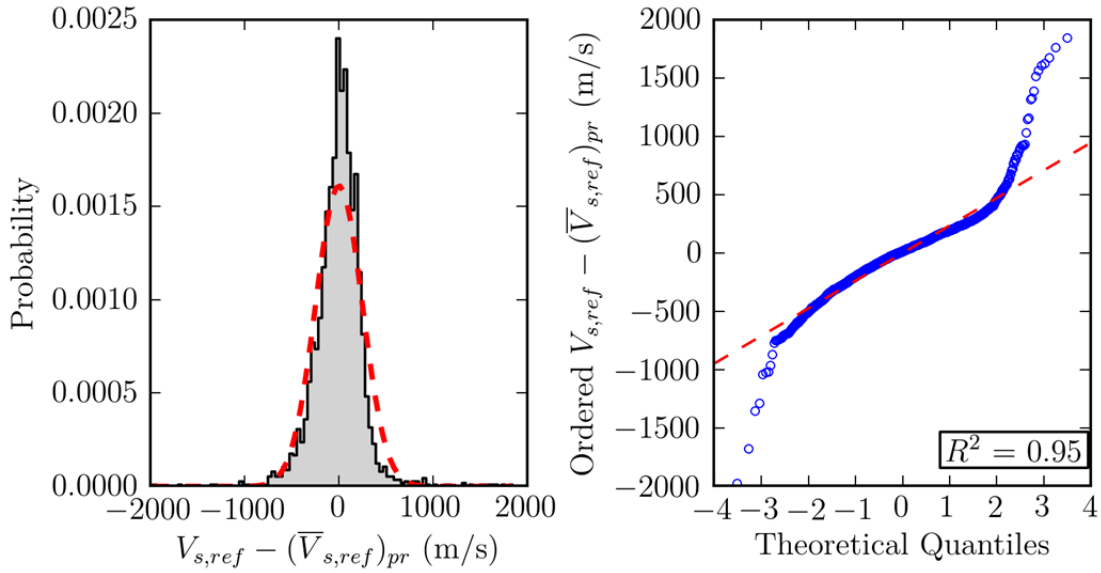

Figure 11 **Comparison of the within-profile $V_{s,ref}$ data to a normal distribution.**

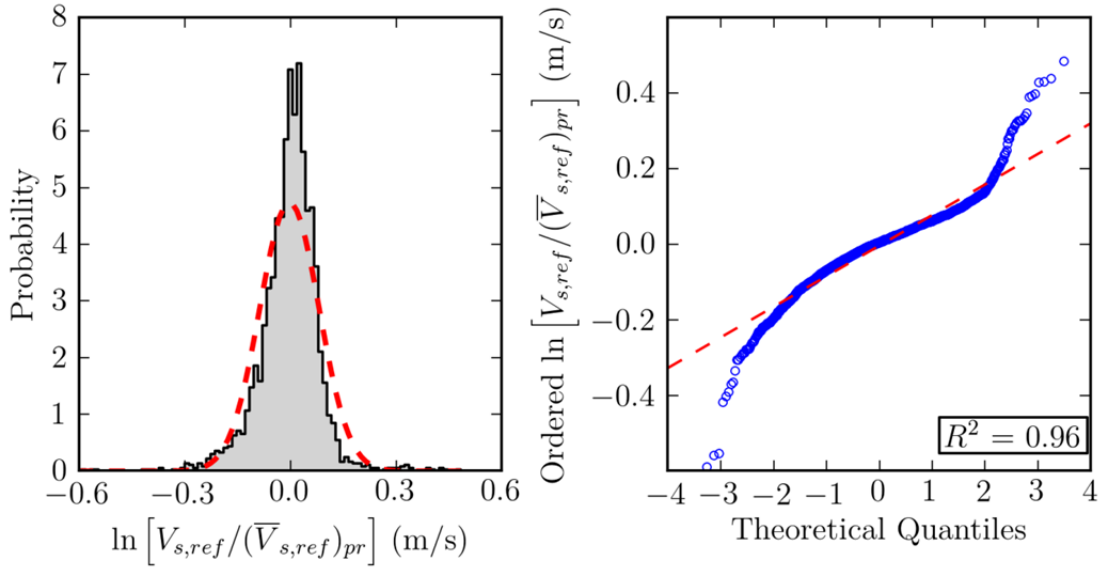

Figure 12 **Comparison of the within-profile $V_{s,ref}$ data to a log-normal distribution.**

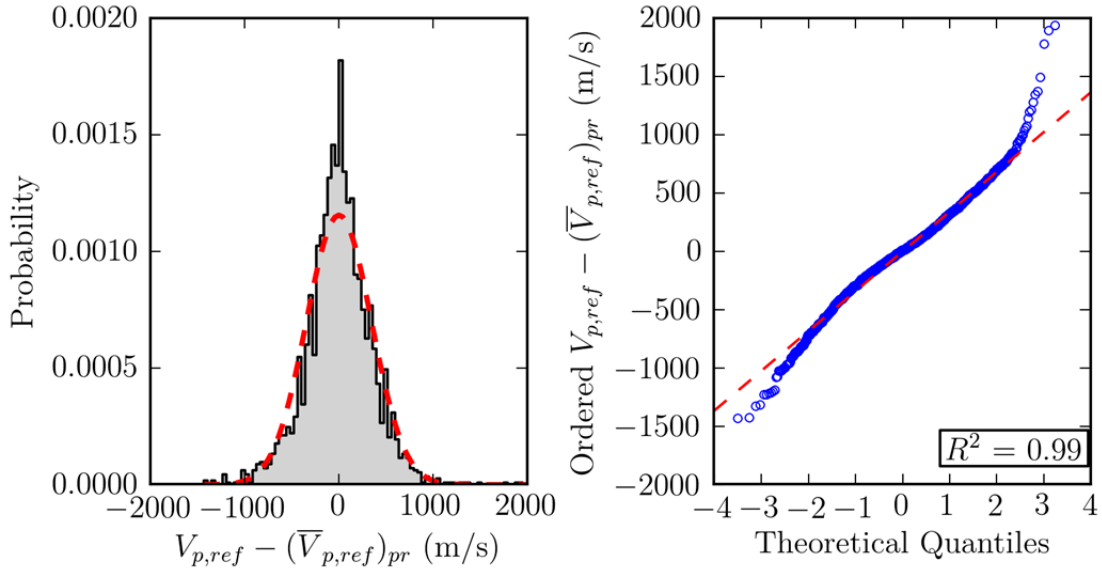

Figure 13 **Comparison of the within-profile $V_{p,ref}$ data to a normal distribution.**

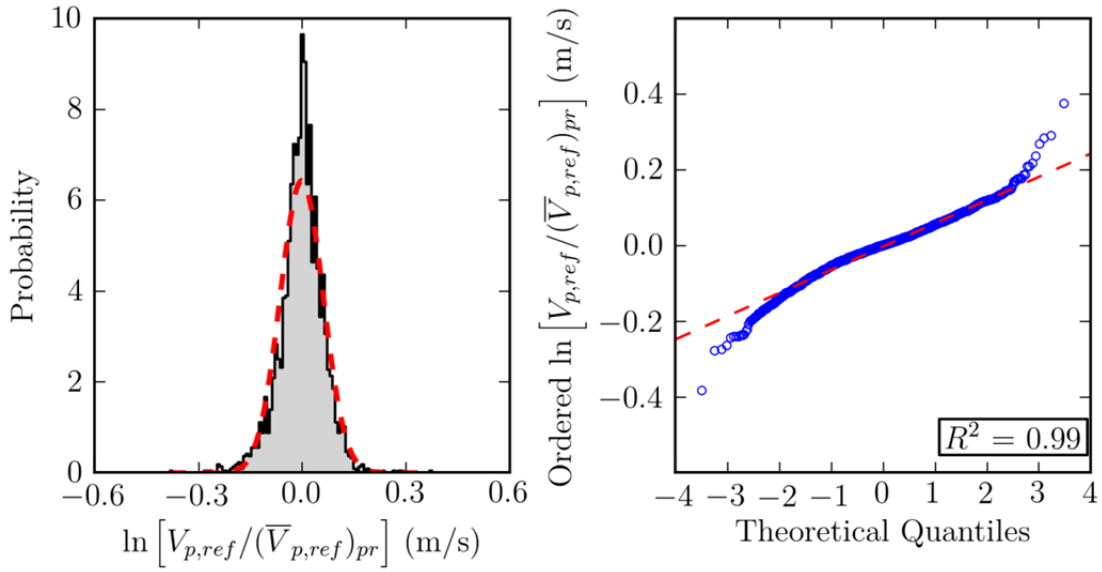

Figure 14 Comparison of the within-profile $V_{p,ref}$ data to a log-normal distribution.

Each of the profiles has a median reference velocity, $\left(\overline{V}_{s,ref}\right)_{pr}$ and $\left(\overline{V}_{p,ref}\right)_{pr}$, and an within-profile standard deviation, $\sigma^{pr}_{V_{s,ref}}$ and $\sigma^{pr}_{V_{p,ref}}$. These standard deviation terms, provided in Table 3, range from 52 to 612 m/sec. As shown in Figure 15, there is a slight trend in within-profile standard deviation with mean profile velocity; , thus, dispersion is represented with a coefficient of variation (COV) instead of standard deviation. The within-profile coefficients of variation range from 0.02 to 0.18 for $\text{COV}^{pr}_{V_{s,ref}}$ and 0.02 and 0.09 for $\text{COV}^{pr}_{V_{p,ref}}$; see Figure 16. The average COV of *S*- and *P*-wave values (0.067) is used as the estimate of within-profile coefficient of variation ($\text{COV}_{\text{profile}}$).

The mean *S*-wave velocities at each of the profiles, provided in Table 3 and shown in Figure 7, range from 2134 m/sec at River Bend NPP located in Louisiana to 3581 m/sec at Calvert Cliffs NPP located in Maryland. For sites with multiple profiles (multiple measurements in one or more boreholes in close proximity), the mean can be taken across the datasets for the site as a whole, $\left(\overline{V}_{s,ref}\right)_{site}$ and $\left(\overline{V}_{p,ref}\right)_{site}$, and a between-profile standard deviation of reference velocity can be computed, $\sigma^{site}_{V_{s,ref}}$ and $\sigma^{site}_{V_{p,ref}}$. Distributions of the reference *S*- and *P*-wave velocity measurements at sites with more than seven profiles are shown in Figures 17 and 18, respectively. This between-profile variability is evaluated from four sites with 8 to 12 profiles (i.e., Bell Bend NPP, Bellefonte NPP, V.C. Summer NPP, and William States Lee NPP); see Table 4. Using the Shapiro-Wilk test and a confidence level of 0.10, 7 of the 8 profiles were not rejected against normal and log-normal distributions, with the William States Lee III NPP *S*-wave data being rejected for both distributions. The normal distributed is used based on better performance and judgment. The between-profile coefficients of variation range from 0.033 to

0.127 for $\mathrm{COV}_{V_{s,ref}}^{site}$ and 0.017 to 0.114 for $\mathrm{COV}_{V_{p,ref}}^{site}$. Given the similar range in coefficients of variations and the relationship between *S*- and *P*-wave velocities, a single coefficient variation of 0.063 is recommended for both $\mathrm{COV}_{V_{s,ref}}^{site}$ and $\mathrm{COV}_{V_{p,ref}}^{site}$, which is quite similar to $\mathrm{COV}_{\mathrm{profile}}$ of 0.067.

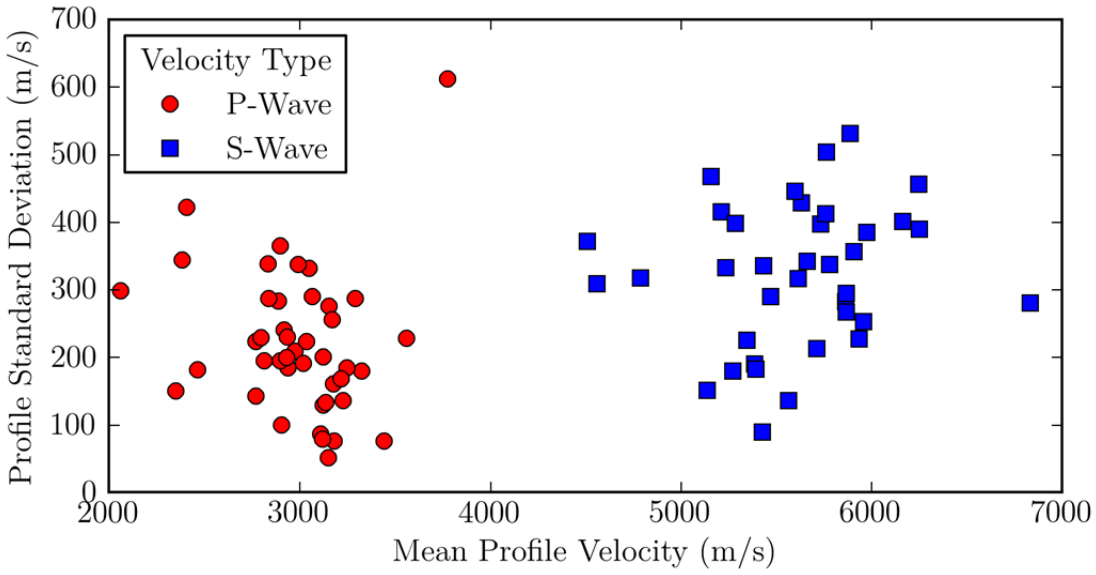

Figure 15 **Influence of mean profile velocity on profile standard deviation.**

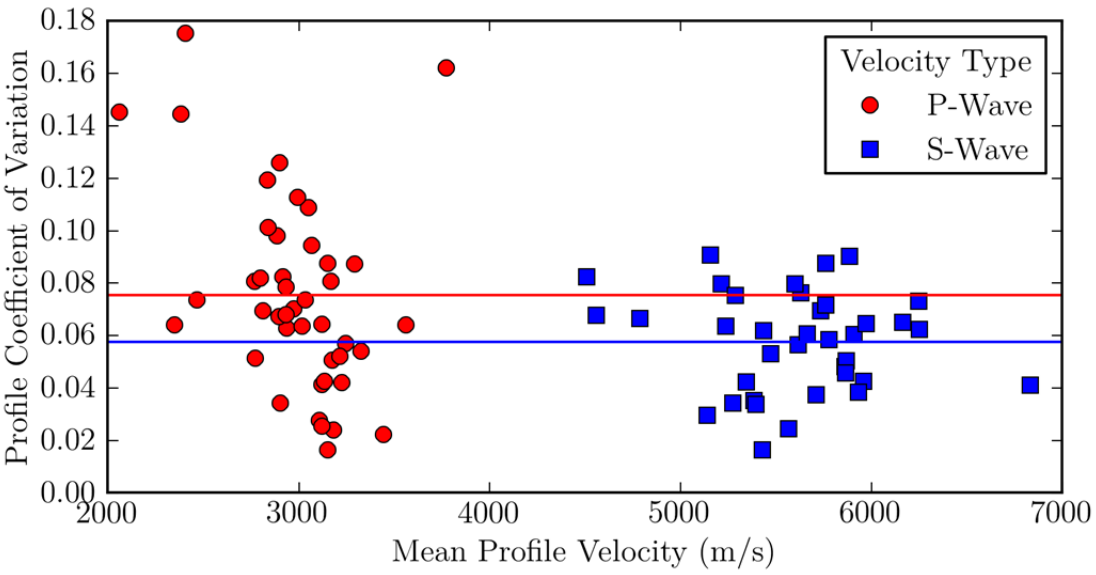

Figure 16 **Influence of mean profile velocity on profile coefficient of variation.**

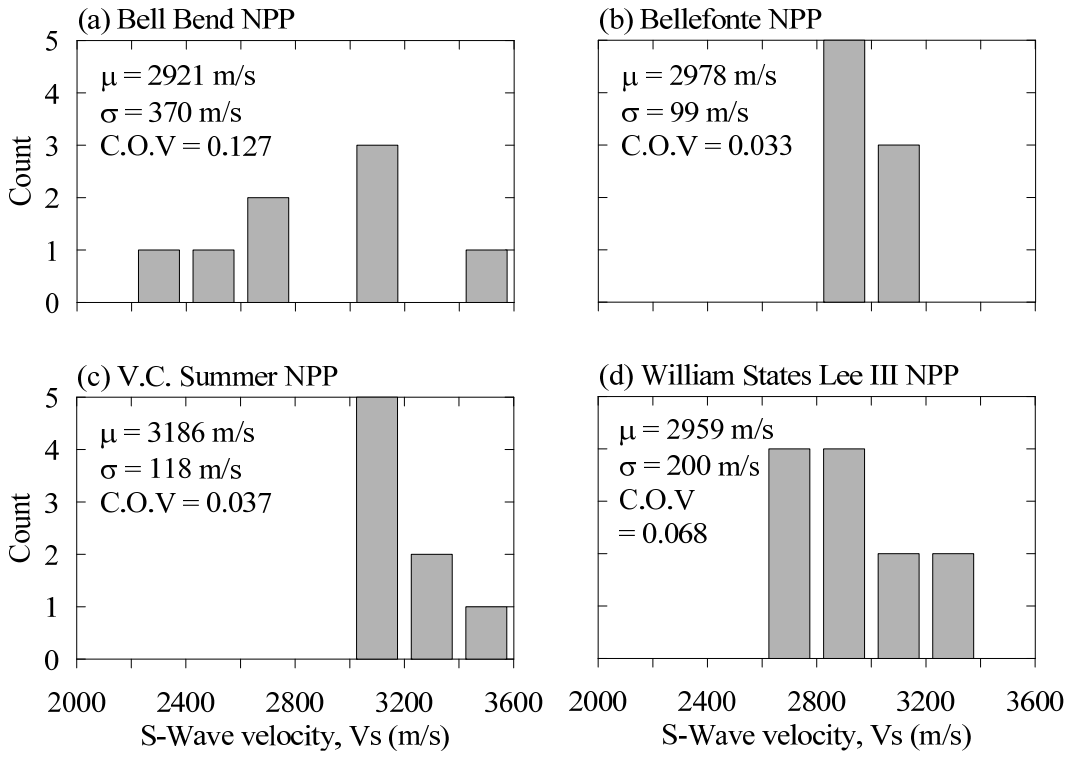

Figure 17 **Distribution of the reference *S*-wave velocity measurements at sites with more than seven profiles.**

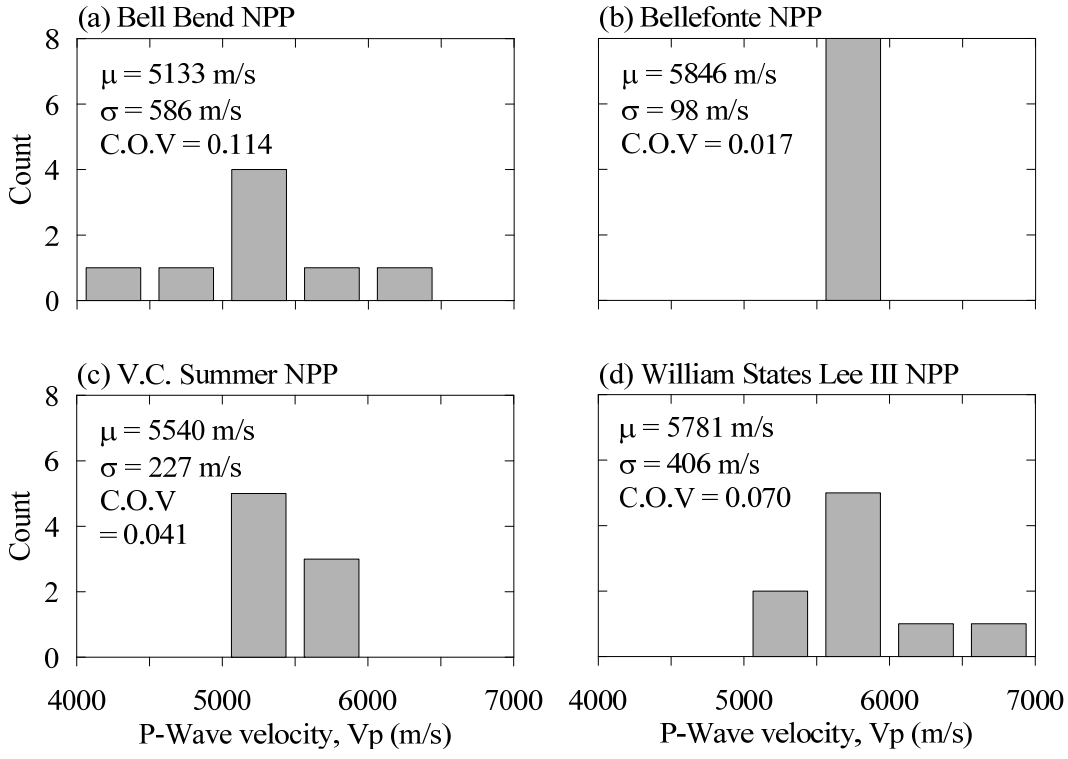

Figure 18 **Distribution of the reference *P*-wave velocity measurements at sites with more than seven profiles.**

Table 4 **Standard deviation and coefficient of variation (COV) of reference-rock values from sites with more than 7 values.**

Site	Count	Standard deviation.	COV
***P*-wave velocity**			
Bell Bend NPP	8	586	0.114
Bellefonte NPP	8	98	0.017
V.C. Summer NPP	8	227	0.041
William States Lee III NPP	9	406	0.070
Mean		329	0.061
***S*-wave velocity**			
Bell Bend NPP	8	370	0.127
Bellefonte NPP	8	99	0.033
V.C. Summer NPP	8	118	0.037
William States Lee III NPP	12	200	0.068
Mean		197	0.066

Histograms of $\left(\bar{V}_{s,ref}\right)_{site}$ and $\left(\bar{V}_{p,ref}\right)_{site}$ are shown in Figures 19 and 20, respectively. The histograms of the *S*- and *P*-wave velocities skew towards higher velocities. Using the reference *S*-wave velocity data, the Shapiro-Wilk test was used to test for normality. Using an alpha factor of 0.10, the computed p-value of 0.30 does not reject assumed normal distribution for $\left(\bar{V}_{s,ref}\right)_{site}$, but the p-value of 0.006 does reject the assumed normal distribution for $\left(\bar{V}_{p,ref}\right)_{site}$. Considering site-to-site variability of median reference velocities, a regional weighted mean is computed with weights taken as proportional to the reciprocal of the standard error, defined by the $\mathrm{COV}_{V_{s,ref}}^{pr}$ and $\mathrm{COV}_{V_{\mathrm{p},ref}}^{pr}$ values divided by the square root of the number of profiles, which provide a maximum likelihood estimate of the mean [denoted $\left(\bar{V}_{s,ref}\right)_{reg}$ and $\left(\bar{V}_{p,ref}\right)_{reg}$]. For the four well-sampled sites, the standard deviations in Table 4 are used for weighting. For more sparsely sampled sites (having one to three profile medians), the standard deviation is computed from mean COV of 0.063. Weighted standard deviations are similarly computed [denoted as $\mathrm{COV}_{V_{s,ref}}^{reg}$ and $\mathrm{COV}_{V_{\mathrm{p},ref}}^{reg}$, which represent regional site-to-site variability of the median velocity. Results for both weighted mean and standard deviation are given in Table 5. Combining site-to-site and between-profile standard deviations yields a total standard deviation of $\mathrm{COV}_{V_{s,ref}}^{reg}$ and $\mathrm{COV}_{V_{\mathrm{p},ref}}^{reg}$ = 0.144 and 0.128, respectively. The mean values and their 95%

confidence intervals are $\left(\bar{V}_{s,ref}\right)_{reg}$ = = 2951 $\pm$ 831 m/sec (i.e., 2120 to 3782 m/sec) and $\left(\bar{V}_{p,ref}\right)_{reg}$ = 5517 $\pm$ 1380 m/s (i.e., 4137 to 6897 m/sec).

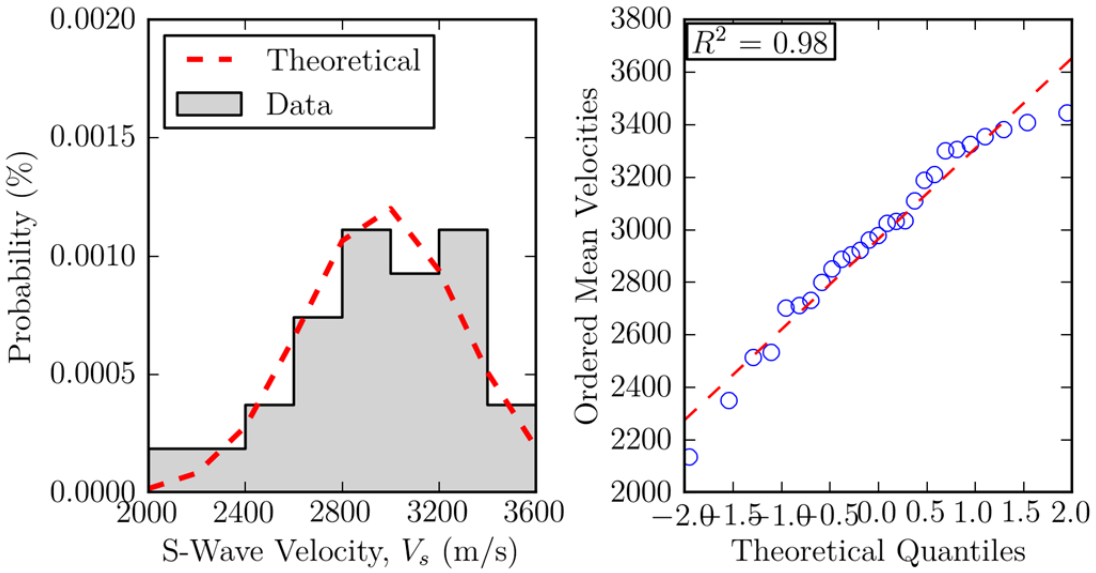

Figure 19 **Distribution of the mean reference *S*-wave velocity measurements at all sites. The ordered mean values versus theoretical quantiles (or Q-Q plot) comparisons the shape of the distribution with the assumed normal distribution. Deviations from the 1-to-1 line indicate deviations from the assumed distribution.**

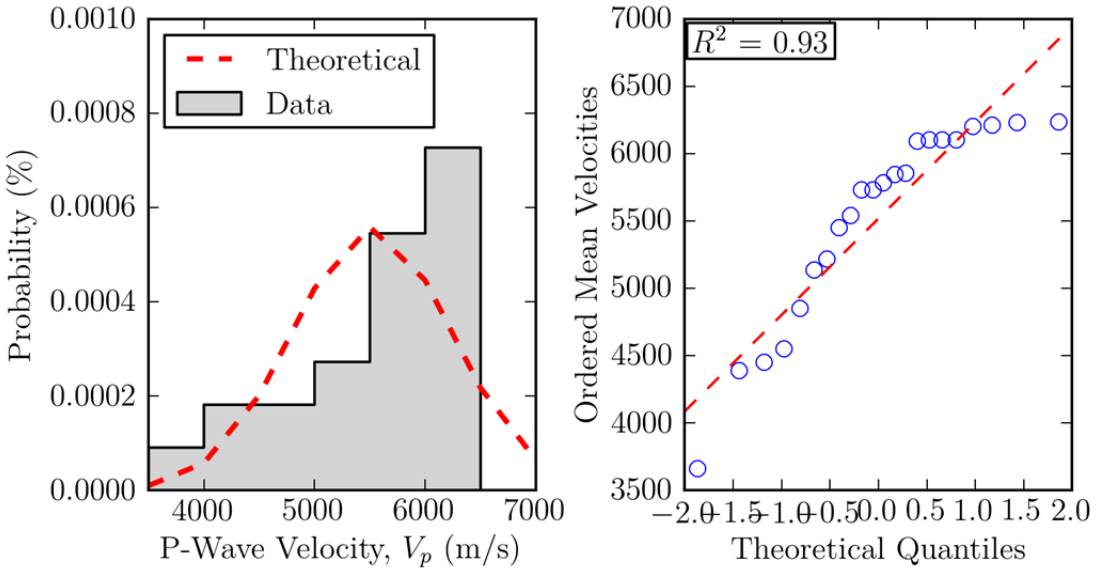

Figure 20 **Distribution of the mean reference *P*-wave velocity measurements at all sites. See Figure 19 for a description of the figure.**

If mean values and confidence intervals are computed on the basis of the regions proposed by Chulick and Mooney [2002] and Mooney [*personal communication*, 2012], we find negligible changes, as indicated by the following satistics in which each site within the respective regions is weighted equally and confidence intervals reflect site-to-site variability:

- Interior: $\left(\overline{V}_{s,ref}\right)_{reg}$ = 3030 ± 770 m/sec; $\left(\overline{V}_{p,ref}\right)_{reg}$ = 5530 ± 210 m/sec
- Atlantic: $\left(\overline{V}_{s,ref}\right)_{reg}$ = 2970 ± 330 m/sec; $\left(\overline{V}_{p,ref}\right)_{reg}$ = 5680 ± 190 m/sec
- Appalachian: $\left(\overline{V}_{s,ref}\right)_{reg}$ = 2950 m/sec; $\left(\overline{V}_{p,ref}\right)_{reg}$ = 5490 m/sec

This indicates that the reference velocities have no statistically significant regional dependence among the continental interior, Appalachian Mountain, and Atlantic Coast regions.

Slowness, which is defined as the reciprocal of velocity, was considered as an alternate method for calculating the mean reference velocity. The regional weighted mean reference *S*-wave slowness was found to be 0.3450 ms/m with a standard deviation of 4.278e-5 ms/m. The mean *S*-wave slowness corresponds to a $\left(\overline{V}_{s,ref}\right)_{pr}$ of approximately 2900 m/sec. The statistics computed using velocities, not slowness, are recommended because of the insignificant difference between these two numbers and the simplicity of directly computing the statistics from velocity.

Table 5 **Statistics computed for the reference-rock velocities weighted by the reciprocal of the standard deviation. The within-site standard deviation is estimated using a coefficient of variation of 0.063.**

Velocity type	Mean	Standard Deviation (COV)		
		Within Site	Between Site	Total
P-wave	5517	348 (0.063)	612 (0.111)	704 (0.128)
S-wave	2951	186 (0.063)	381 (0.129)	424 (0.144)

3.3 DISCUSSION OF PROFILE CHARACTERISTICS

3.3.1 Poisson's Ratios

For each profile in reference rock, we use $\left(\overline{V}_{s,ref}\right)_{pr}$ and $\left(\overline{V}_{p,ref}\right)_{pr}$ to compute the mean profile Poisson's ratio, $\left(\overline{v}_{s,ref}\right)_{pr}$, as follows [Mavko et al. 2003]:

$$\left(\bar{v}_{ref}\right)_{pr} = \frac{\left(\bar{V}_{p,ref}\right)_{pr}^{2} - 2\left(\bar{V}_{\mathrm{s},ref}\right)_{pr}^{2}}{2\left(\bar{V}_{p,ref}\right)_{pr}^{2} - 2\left(\bar{V}_{\mathrm{s},ref}\right)_{pr}^{2}} \tag{3.1}$$

The computed Poisson's ratios range from 0.24 to 0.33 with a mean of 0.28, see Figure 21. The computed values fall within the range expected for intact rock presented by Gercek [2007]. The mean value of 0.28 is similar to the assumed value of 0.25 used by EPRI [1993].

3.3.2 Weathering Zone

At the Bellefonte, North Anna, V.C. Summer, and William States Lee III sites, information regarding the transition from weathered rock to intact rock could be inferred from the characteristics of velocity profiles (i.e., steep transition from low velocities to the reference-rock velocity) and borehole geology. At the other sites, no weathering zone could be identified. The range in depths and *S*-wave velocities associated with the identified weathered zones is shown in Figure 22. The top of the weathered zone occurs at depths ranging from 4.5 to 35 m, with thicknesses varying from 3 to 83 m. The velocity at the top of the weathered zone varies from 1500 to 2450 m/sec and at the base of the weathered zone varies from 2590 to 3540 m/sec. The ratio of the *S*-wave velocity of the intact rock to the weathered rock, referred to as *S*-wave velocity ratio, ranges from 1.3 to 2, see Figure 23. The geometric mean of the thickness is 15 m, and the *S*-wave velocity ratio is 1.53.

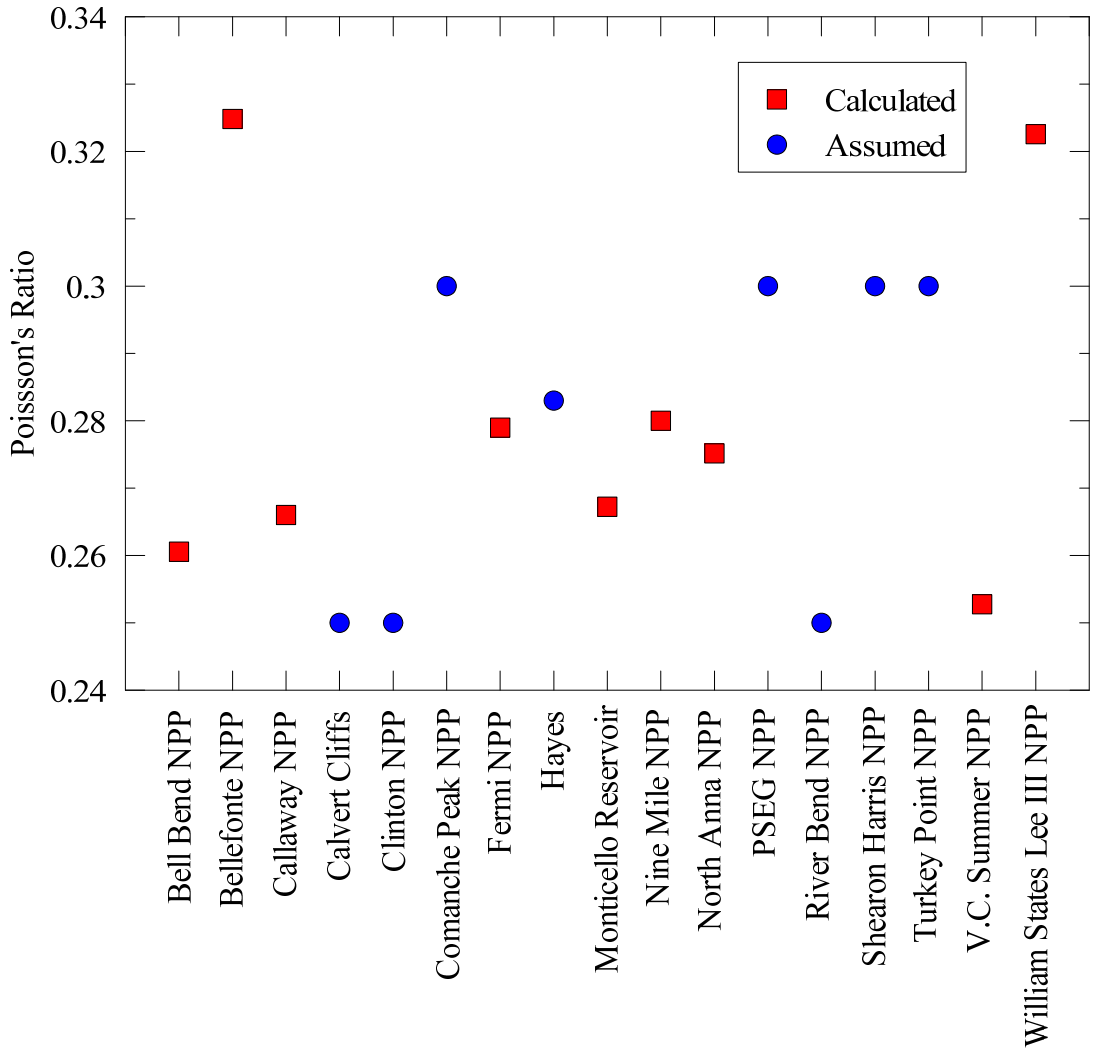

Figure 21 **Poisson's ratio computed from mean reference velocity measurements, as well as reported assumed values. The mean (μ) and standard deviation (σ) was computed to be 0.28 and 0.025, respectively.**

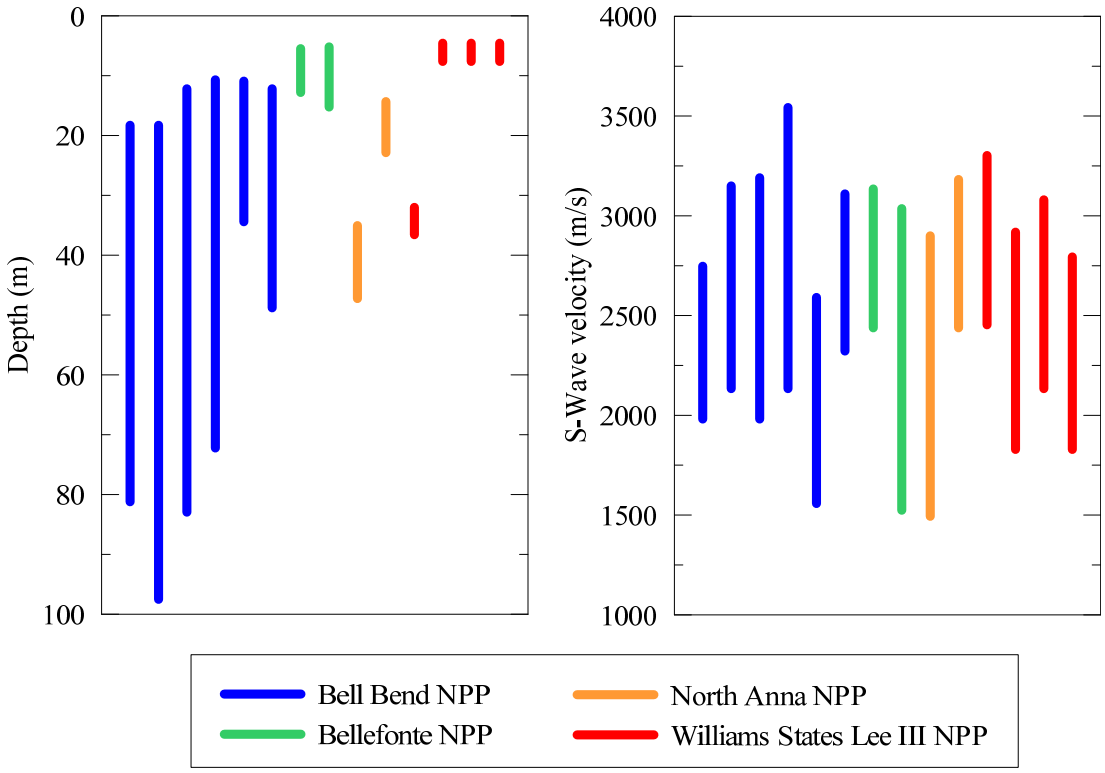

Figure 22 **The range in depths and velocities observed in the identified weathered zones.**

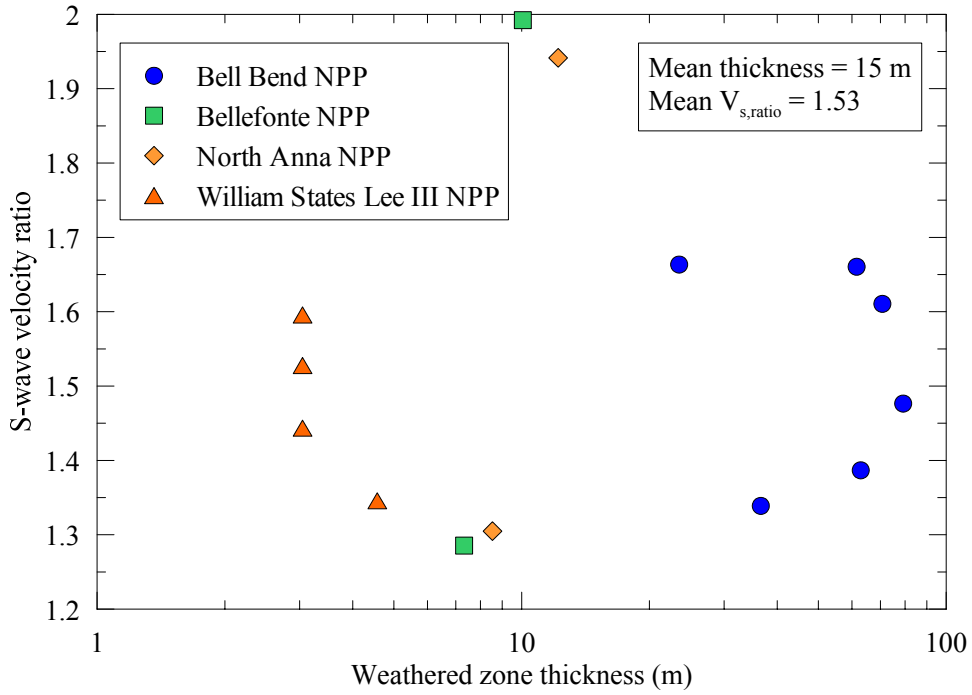

Figure 23 **The relationship between on the weathered zone thickness and ratio of *S*-wave velocity at the top and base of the weathered zone. The geometric mean of the thickness is 15 m, and the median *S*-wave velocity ratio is 1.53.**

3.3.3 Velocity Gradient within the Reference Rock

The velocity gradient is defined as the change in velocity with respect to depth *(dV/dz*). It can be computed over a depth range and used as a parameter to assist in identifying reference-rock conditions within a profile. Within the reference rock, the velocity gradient is computed for all profiles with at least 4 measurements spanning at least 5 m by fitting a linear model through the data. There are 82 profiles with a sufficient amount of data to compute the velocity gradient. The reference velocity gradient ranges from *dV/dz* = -64 to 46 (m/sec)/m with a mean of 2 (m/sec)/m and standard deviation of 13 (m/sec)/m. The associated 95% confidence interval is -24 to 28 (m/sec)/m. The velocity gradient within the weathered zone can be computed as well. In this calculation, the gradient is computed by the change in velocity before and after the identified zone without fitting a linear trend to the data. The computed velocity gradient within the weathered zone ranges from 12 to 360 (m/sec)/m with a mean of 125 (m/sec)/s. A comparison of the reference and weathered zone velocity gradients is shown in Figure 24. The magnitude of the velocity gradient within the weathered and reference zones do overlap for some sites. For a specific profile, the difference between the velocity gradient in the weathered rock and reference rock is always greater than zero, as shown in Figure 25, indicating a decrease in the velocity gradient as the profile transitions from the weathered zone into the reference velocity zone.

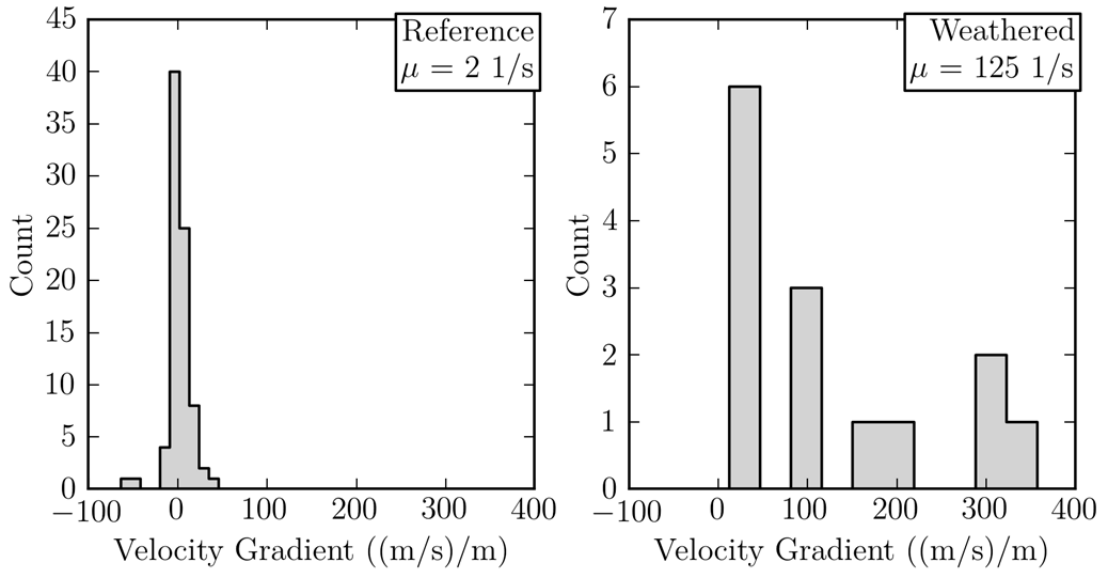

Figure 24 Velocity gradients of the within the reference rock and weathered zones.

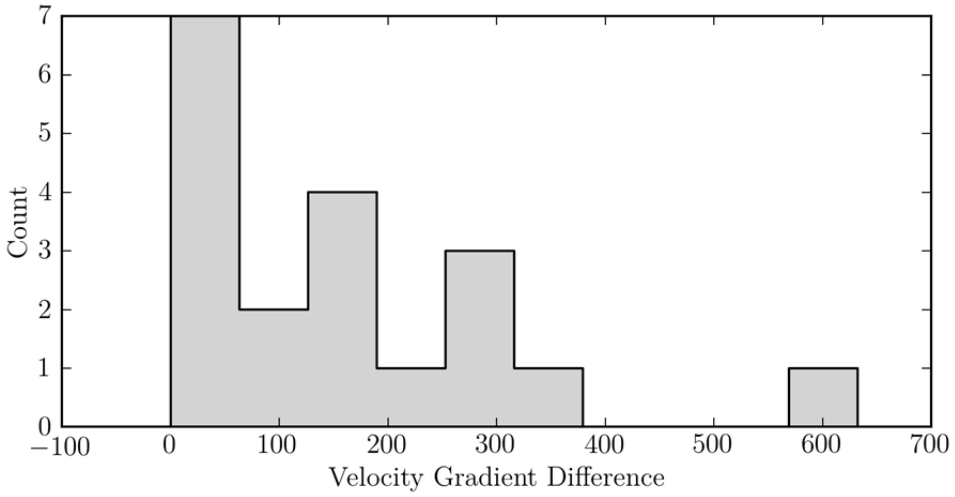

Figure 25 Difference between the weathered and reference velocity zone velocity gradients.

3.4 ESTIMATION OF EPISTEMIC UNCERTAINTY

Epistemic uncertainty in the reference-rock velocities arises from two principal sources: (1) insufficient data–namely, if we had a larger database, the statistics on regional median and standard deviations would surely change; and (2) the judgment involved with the selection of reference-rock intervals within profiles when the protocols from Section 3.2.1 are applied. We do not attempt to quantify the first source, which is always present in any data-driven study. In this section, we attempt to quantify the second source associated with user judgment.

Our process for estimating the judgment-driven epistemic uncertainty was to provide 46 *P*- and/or *S*-wave velocity profiles that penetrate reference rock to three experts. They were asked to select profile mean reference-rock velocities based on their visual assessment of the profile and by reading the velocities manually off the plot (i.e., they did not perform statistical calculations using digitized versions of the profiles). We recognize that this process overestimates epistemic uncertainty due to the potential for plot reading errors, but this is actually somewhere desirable given the omission of the first source of epistemic uncertainty from our process.

For each of the profiles, the differences between the experts selected profile mean reference velocities and $\left(\overline{V}_{s,ref}\right)_{pr}$ and $\left(\overline{V}_{p,ref}\right)_{pr}$ were computed, as given in Table 6 and Figure 26. These differences represent epistemic uncertainty in the evaluation of the reference-rock velocity associated with variable expert judgment regarding the depth interval associated with the reference-rock condition and errors associated with visual reading of mean velocities from printed figures. The mean and standard deviation of these differences is presented in Table 6. The mean of the mean profile velocities provided by the three experts were essentially unbiased relative to the values from Table 3. The standard deviation of the mean estimates was 100 m/sec, which is significantly less than the between-profile aleatory variability represented by $\sigma^{site}_{\ln Vsref}$ and $\sigma^{site}_{\ln Vpref}$ = 186 and 348 m/sec, respectively.

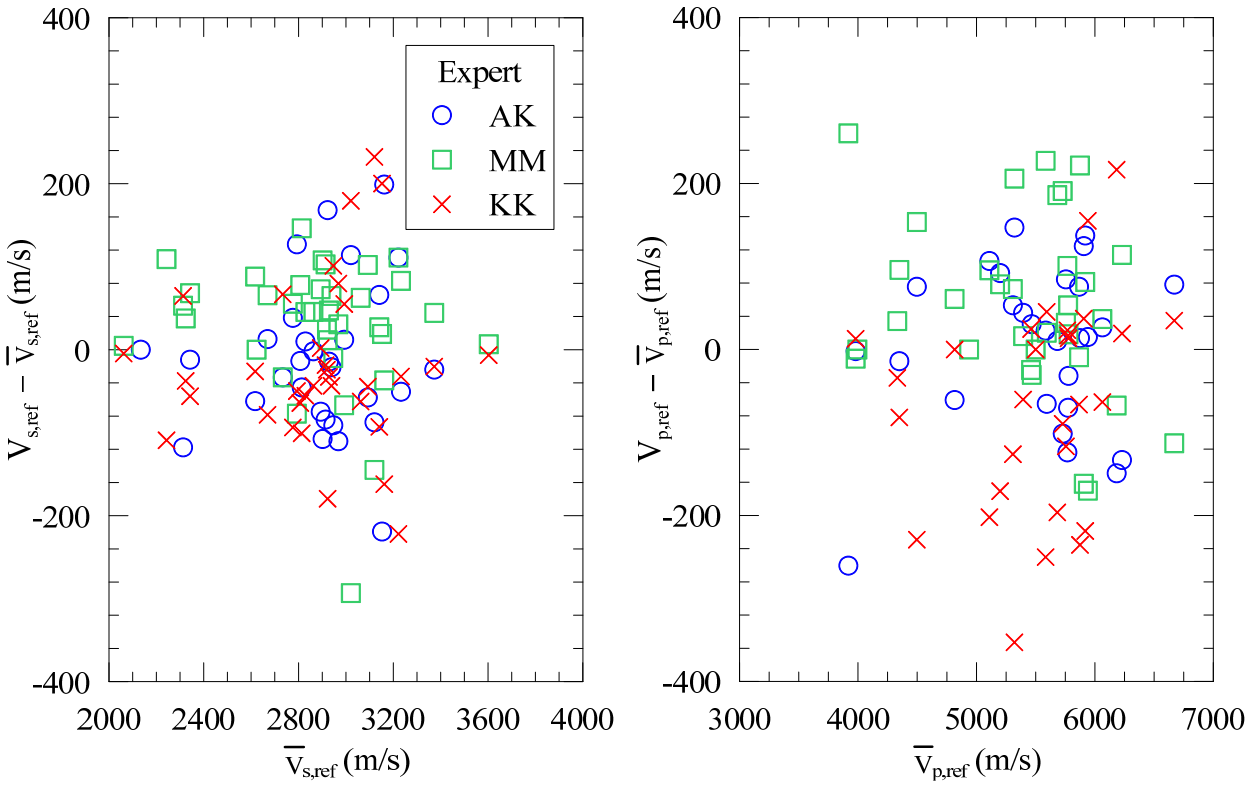

Figure 26 **Difference between reference velocity selected by an expert and the mean reference velocity. (AK: Albert Kottke, MM: Michael Musgrove, and KK: Khatereh Khodaverdi).**

Table 6 **Mean and standard deviation of the difference between the velocity selected by three experts and the mean of the selected velocities.**

Expert	$V_{s,ref}$		$V_{p,ref}$	
	Mean	**Standard Deviation**	**Mean**	**Standard Deviation**
Albert Kottke (AK)	-12.3	90.9	4.5	97.18
Michael Musgrove (MM)	-20.0	98.8	-65.3	128.6
Khatereh Khodaverdi (KK)	29.2	80.9	53.6	105.4
Average	-1.1	90.2	-2.4	110.4

3.5 COMPARISON WITH LABORATORY MEASUREMENTS

Brant et al. [2012] conducted *in situ* and laboratory measurements on metamorphic and igneous rock cores from the New York area. These tests are of interest because the cores are composed of competent, relatively unweathered bedrock that is generally compatible with the descriptions of reference rock on boring logs. The laboratory measurements were conducted using the resonant

frequency method with impulse excitation [ASTM International 2009]. No confinement was applied to the samples. The 118 *S*-wave velocities from the laboratory measurements of rock cores ranged from 1520 to 4570 m/sec with a mean of 3050 m/sec; see Figure 27. For each laboratory test, an associated *in situ* velocity measurement is available from geophysical crosshole, downhole, or suspension logging methods. As shown in Figure 28, Brant et al. [2012] compared the lab and *in situ* velocity measurements and found the laboratory measurements provide an upper bound on the *S*-wave velocity of the *in situ* rock mass. This is due to the presence of joints and shears in the rock mass that are not present in the cores due both to their small size and to the need to test intact (as opposed to fractured) specimens. While we do not advocate the direct use laboratory measurements for the evaluation of reference-rock velocities, we are nonetheless encouraged that the mean regional *S*-wave velocity of $\left(\overline{V}_{s,ref}\right)_{reg}$ = 2950 m/sec is very close to the rock core mean of 3050 m/sec.

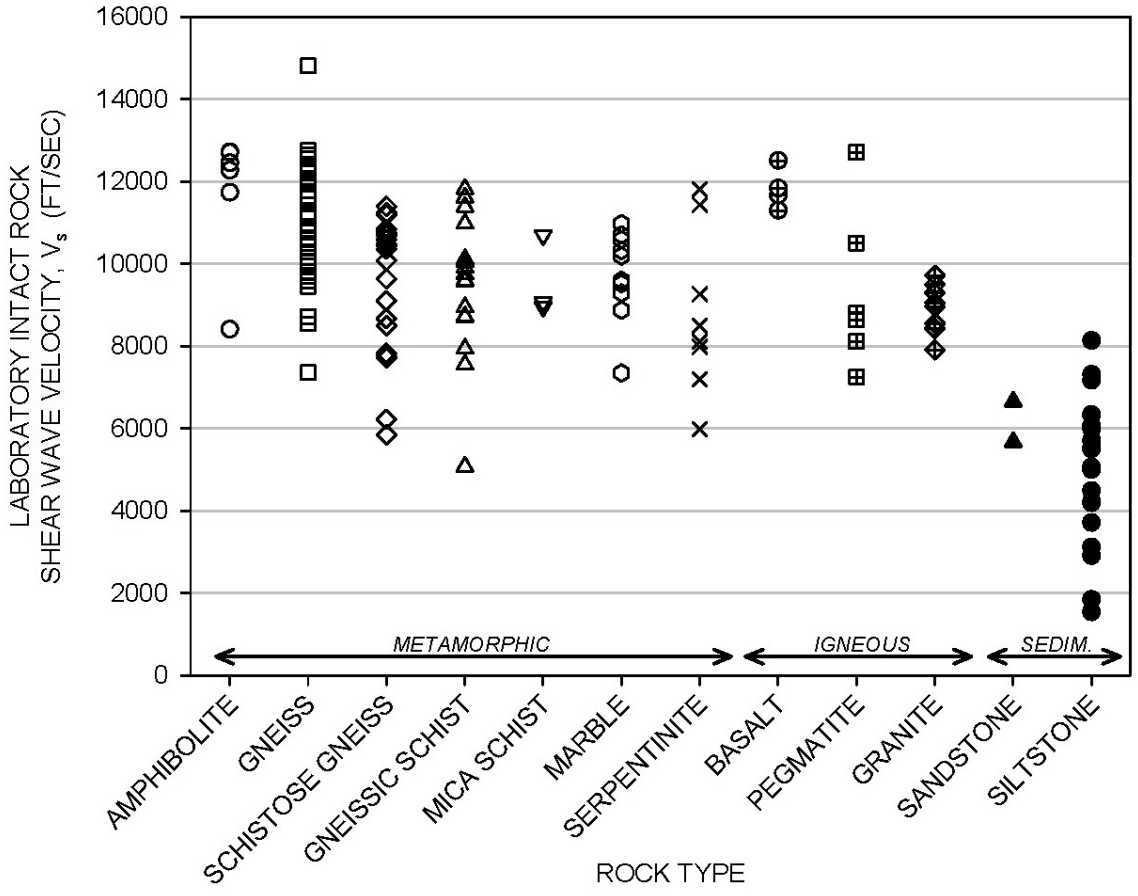

Figure 27 Laboratory measured intact shear-wave velocity by rock type [Brant et al. 2012].

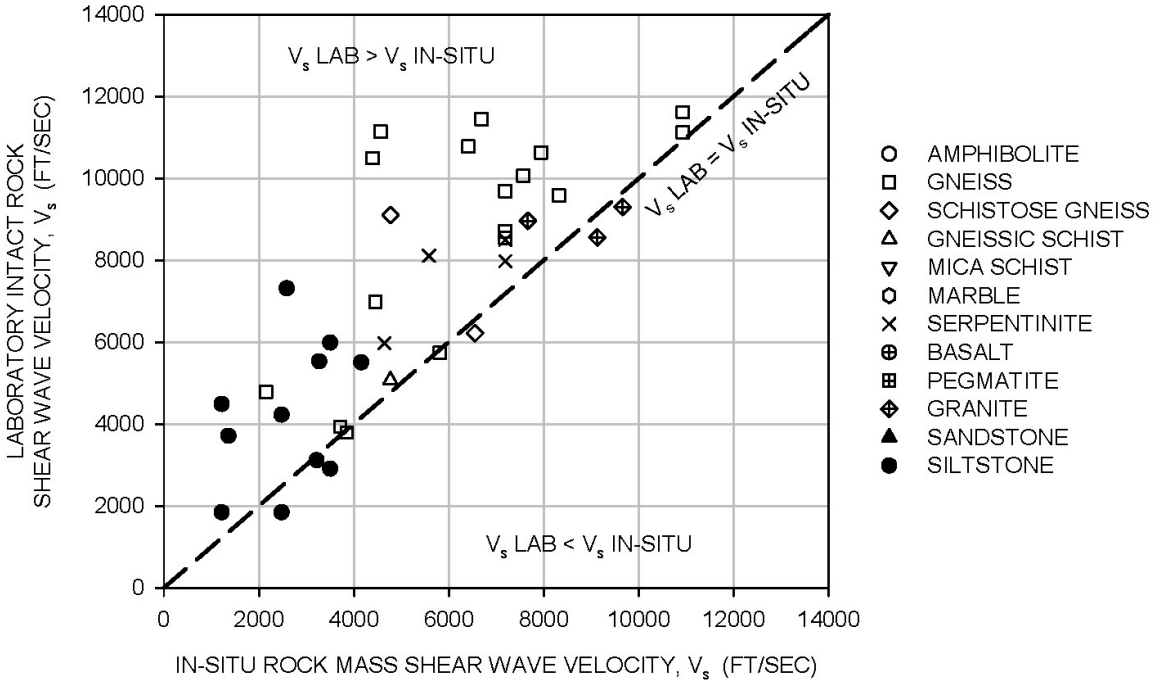

Figure 28 **Relationship between laboratory measured intact and *in situ* shear-wave velocity by rock type [Brant et al. 2012].**

4 Recommendations

As described in Section 3.2.3, the mean regional reference velocities for CENA, with their 95% confidence intervals, were found from the data assembled in this study to be $\left(\overline{V}_{s,ref}\right)_{reg}$ = 2951 $\pm$ 831 m/sec (i.e., 2120 to 3782 m/sec) and $\left(\overline{V}_{p,ref}\right)_{reg}$ = 5517 $\pm$ 1380 m/sec (i.e., 4137 to 6897 m/sec). We prefer to provide these mean values to no more than two significant digits; for application, therefore, we recommend:

$V_{s,ref}$ = 3000 m/sec or 9800ft/sec, and $V_{p,ref}$ = 5500 m/sec or 18,000 ft/sec

Note that formal statistical nomenclature for these recommendations is dropped, because they are interpreted (and slightly modified) from the formal statistics.

The data gathered in this study reveal substantial site-to-site variability of mean reference velocities. This is of substantial practical importance for site-specific ground motion studies, where geotechnical and geophysical logging to depths corresponding to the reference conditions may be required by regulatory agencies. Given the aforementioned site-to-site variability, we do not advocate strict adherence to reaching the $V_{s,ref}$ and $V_{p,ref}$ values given above. Our principal recommendation is that the depth of exploration be sufficiently large that the reference condition, as described in Section 3.2.1, is demonstrated by the data.

With that said, we recognize that many applications require articulation of a specific reference velocity (or range). We propose that the definition of such a velocity range is more rationally defined from its impact on site amplification than by the width of confidence intervals. For this reason, the velocity range is based on its impact on site amplification. The amplification in a vertically-propagating horizontally-polarized *S*-wave between two layers is related to the mass density (ρ) and velocity (V) in the layers by [Joyner et al. 1981]:

$$A = \sqrt{\frac{\rho_1 V_1}{\rho_2 V_2}} \tag{4.1}$$

If the layers have the same mass densities, then the amplification across those two layers is equal to the square root of the velocity ratio (i.e., $\sqrt{V_1/V_2}$). We select an admittedly subjective limit on amplification change of 5%, which implies that for a given soil layer velocity the range in

reference-rock velocity is 0.907 to 1.108 of the central value. This corresponds to a computed range of 2700 to 3300 m/sec for $V_{s,ref}$ and 5000 to 6100 m/sec for $V_{p,ref}$. The range is somewhat smaller than the 95% confidence interval given above. The EPRI [1993] recommendation for $V_{s,ref}$ falls within this range, which means that prior seismic hazard analyses for nuclear power plants utilizing this value are not incompatible with our recommendations. However, the *P*-wave reference velocity from EPRI [1993] of $V_{p,ref}$ = 4900 m/sec falls outside the recommended range in this report.

Based on the above reasoning, the recommended range of $V_{s,ref}$ is 2700 to 3300 m/sec (8900 to 10,800 ft/sec) and of $V_{p,ref}$ is 5000 to 6100 m/sec (16,400 to 20,000 ft/sec).

We do not find evidence for regional dependence of the reference velocities, which are derived principally from three general geographic regions: (1) the Atlantic Coast; (2) continental interior; and (3) Appalachian Mountains. Our data is does not provide reference velocities for the Gulf Coast region. In this region the depth to the CENA reference-rock condition is expected to be much greater than other CENA regions due to several kilometers of overlying sediments. We do not provide a reference-rock condition for the Gulf Coast. Our recommendation is to adopt a consistent reference-rock condition for the entire CENA region, as given above, and then estimate transfer functions to a softer reference condition (such as 760 m/sec) for application of the NGA-East GMPEs.

5 Limitations of the Study

This study represents the most complete survey of hard-rock velocity in the CENA region; however, it is not without limitations. The collected dataset does not uniformly sample the spatial distribution of the study region (Figure 6) due to limitations in the available data. However, the data does include a range of different geologic conditions; therefore, the lack of spatial coverage may not be significant. Future efforts can be focused on acquiring additional data to ensure greater spatial coverage. As noted previously, the data is especially sparse in the Gulf Coast region.

REFERENCES

Andrus R.D., Fairbanks C.D., Zhang J., Camp W.M., Casey T.J., Wright W.B. (2006). Shear-wave velocity and seismic response of near-surface sediments in Charleston, South Carolina, *Bull. Seismol. Soc. Am*., 96(5): 1897–1914.

ASTM International (2009). *ASTM E1876-09 Standard test method for dynamic Young's Modulus, Shear Modulus, and Poisson's ratio by impulse excitation of vibration*, West Conshohocken, PA.

Atkinson G.M., Boore D.M. (2006). Earthquake ground-motion prediction equations for eastern North America, *Bull. Seismol. Soc. Am*., 96(6): 2181–2205.

Beresnev I.A., Atkinson, G.M. (1997). Shear-wave velocity survey of seismographic sites in eastern Canada: Calibration of empirical regression method of estimating site response, *Seismol. Res. Lett*., 68(6): 981–987.

Boore D.M., Joyner W.B. (1997). Site amplifications for generic rock sites, *Bull. Seismol. Soc. Am*., 87(2): 327–341.

Brant L.C., Nikolaou S., Moss C. (2012). Resonant frequency testing of New York City rock types, *Proceedings, Symposium on Dynamic Testing of Soil and Rock: Field and Laboratory*, San Diego, CA.

Calvert Cliffs 3 Nuclear Project LLC. UniStar Nuclear Operating Services LLC (2011). Calvert Cliffs, Unit 3: Combined Licensing Agreement: Final Safety Analysis Report, Revision 8, *http://www.nrc.gov/reactors/new-reactors/col/calvert-cliffs/documents.html*.

Campbell K.W. (2003). Prediction of strong ground motion using the hybrid empirical method and its use in the development of ground-motion (attenuation) relations in eastern North America, *Bull. Seismol. Soc. Am*., 93(3): 1012–1033.

Chulick G.S., Mooney W.D. (2002). Seismic structure of the crust and uppermost mantle of North America and adjacent oceanic basins: A synthesis, *Bull. Seismol. Soc. Am.*, 92(6): 2478–2492.

Dames and Moore (1974). Site parameter sutdy: Gassar seismic design for General Atomic Company, *Report No. 2395–001–02*, San Franciso, CA.

Daniels J.J., Olhoeft G.R., Scott J.H. (1983). Interpretation of core and well log physical property data from drill hole UPH-3, Stephenson County, Illinois (Illinois Deep Hole Project, USA), *J. Geophys. Res.*, 88(B9): 7346–7354.

Detroit Edison Company (2010). Fermi Unit 3, Combined License Application, Part 2: Final Safety Analysis Report, Revision 2, *http://www.nrc.gov/reactors/new-reactors/col/fermi/documents.html*.

Dominion Virginia Power (2009). North Anna Unit 3, Combined License Application, Part 2: Final Safety Analysis Report, Revision 3, *http://www.nrc.gov/reactors/new-reactors/col/north-anna/documents.html*.

Dorman J., Smalley R. (1994). Low-frequency seismic surface waves in the upper Mississippi embayment, *Seismol. Res. Lett.*, 65(2): 137–148.

Duke Energy (2010). William States Lee III Nuclear Station Units 1 and 2, Combined License Application, Part 2: Final Safety Analysis Report, Revision 3, *http://www.nrc.gov/reactors/new-reactors/col/lee/documents.html*.

Electric Power Research Institute (EPRI) (1993). Guidelines for determining design basis ground motions, *Report No. TR–102293*, Palo Alto, CA.

Entergy Operations Florida Inc. (2011). Grand Gulf, Unit 3: Combined Licensing Agreement: Final Safety Analysis Report, Revision 0, *http://www.nrc.gov/reactors/new-reactors/col/grand-gulf/documents.html*.

Entergy Operations Inc (2008). River Bend Station 3, Combined License Application, Part 2: Final Safety Analysis Report, Revision 0, *http://www.nrc.gov/reactors/new-reactors/col/river-bend/documents.html*.

Exelon Generation Company (2006). Clinton Nuclear Plant, Early Site Permit, Revision 4, *http://www.nrc.gov/reactors/new-reactors/esp/clinton.html*.

Exelon Nuclear Texas Holdings LLC (2008). Victoria County Station Units 1 and 2, Combined License Application, Part 2: Final Safety Analysis Report, Revision 0, *http://www.nrc.gov/reactors/new-reactors/col/victoria/documents.html*.

Florida Power and Light Company (2010). Turkey Point Units 6 and 7, Combined License Application, Part 2: Final Safety Analysis Report, Revision 3, *http://www.nrc.gov/reactors/new-reactors/col/turkey-point/documents.html*.

Gercek H. (2007). Poisson's ratio values for rocks, *Int. J. Rock Mech. Mining Sci*., 44(1): 1–13.

Grubbs F.E. (1969). Procedures for detecting outlying observations in samples, Technometrics, 11(1): 1.

Joyner W.B., Warrick R.E., Fumal T.E. (1981). The effect of Quaternary alluvium on strong ground motion in the Coyote Lake, California, earthquake of 1979, *Bull. Seismol. Soc. Am*., 71(4): 1333–1349.

Kafka A.L., Skehan J.W. (1990). Major geological features and lateral variation of crustal structure in southern New England, *Tectonophys*., 178(2–4): 183–192.

Luetgert J.H., Benz H.M., Madabhushi S. (1994). Crustal structure beneath the Atlantic coastal plain of South Carolina, *Seismol. Res. Lett*., 65(2): 180–191.

Luminant Generation Company LLC (2009). Comanche Peak Nuclear Plants 3 and 4, Combined License Application, Part 2: Final Safety Analysis Report, Revision 1, *http://www.nrc.gov/reactors/new-reactors/col/comanche-peak/documents.html*.

Mavko G., Mukerji T., Dvorkin J. (2003). *The Rock Physics Handbook: Tools for Seismic Analysis of Porous Media*, Cambridge University Press.

Moos D., Zoback M.D. (1983). In situ studies of velocity in fractured crystalline rocks, *J. Geophys. Res.*, 88(B3): 2345–2358.

Nine Mile Point Nuclear Project LLC and UniStar Nuclear Operating Services LLC (2011). Nine Mile Point, Unit 3: Combined Licensing Agreement: Final Safety Analysis Report, Revision 1, *http://www.nrc.gov/reactors/new-reactors/col/nine-mile-point/documents.html*.

NRC (2007). A performance-based approach to define the site-specific earthquake ground motion. United States Nuclear Regulatory Commission, *Regulatory Guide 1.208*, Washington, DC.

Pezeshk S., Zandieh A., Tavakoli, B. (2011). Hybrid empirical ground-motion prediction equations for Eastern North America using NGA models and updated seismological parameters, *Bull. Seismol. Soc. Am*., 101(4): 1859–1870.

Progress Energy Carolinas, I. (2011). Progress Energy Harris Nuclear Units 2 & 3, Combined License Application, Part 2: Final Safety Analysis Report, Revision 3, *http://www.nrc.gov/reactors/new-reactors/col/harris/documents.html*.

Progress Energy Florida Inc. (2011). Levy County, Units 1 and 2: Combined Licensing Agreement: Final Safety Analysis Report, Revision 2, *http://www.nrc.gov/reactors/new-reactors/col/levy/documents.html*.

PSEG Power, L., and PSEG Nuclear, LLC (2011). PSEG Site, Early Site Planning Application: Part 2, Site Safety Analysis Report, Revision 0, *http://www.nrc.gov/reactors/new-reactors/esp/pseg.html*.

Roblee C.J., Suva W.J., Toro G.R., Abrahamson N.A. (1996). Variability in site-specific seismic ground-motion design predictions, *Geotechnical Special Publication* (58 II): X24–1133.

Shapiro S.S., Wilk M. B. (1965). An analysis of variance test for normality (complete samples), *Biometrika*, 52(3-4): 591–611.

South Carolina Electric & Gas (2011). V. C. Summer Nuclear Station Units 2 & 3, Combined License Application, Part 2: Final Safety Analysis Report, Revision 5, *http://www.nrc.gov/reactors/new-reactors/col/summer/documents.html*.

Southern Nuclear Operating Company (2008). Vogtle Units 3 and 4, Combined License Application, Part 2: Final Safety Analysis Report, Revision 3, *http://www.nrc.gov/reactors/new-reactors/col/vogtle.html*.

STP Nuclear Operating Company (2011). South Texas Project Units 3 & 4, Combined License Application, Part 2: Final Safety Analysis Report, Revision 5, *http://www.nrc.gov/reactors/new-reactors/col/south-texas-project/documents.html*.

Tennessee Valley Authority (2009). Bellefonte Nuclear Plants 3 & 4, Combined License Application, Part 2: Final Safety Analysis Report, Revision 1, *http://www.nrc.gov/reactors/new-reactors/col/bellefonte/documents.html*.

Toro G.R., Abrahamson N.A., Schneider J. F. (1997). Model of strong ground motions from earthquakes in central and eastern North America: Best estimates and uncertainties, *Seismol. Res. Lett*., 68(1): 41–57.

Union Electric Company (2009). Callaway Plant Unit 2, Combined License Application, Part 2: Final Safety Analysis Report, Revision 2, *http://www.nrc.gov/reactors/new-reactors/col/callaway/documents.html*.

UniStar Nuclear Services LLC (2010). Bell Bend Nuclear Power Plant, Combined License Application, Part 2: Final Safety Analysis Report, Revision 2, *http://www.nrc.gov/reactors/new-reactors/col/bell-bend/documents.html*.

Worthing A.G., Geffner J. (1943). *Treatment of Experimental Data*, John Wiley and Sons, Inc. New York.

Appendix A: Velocity Profiles

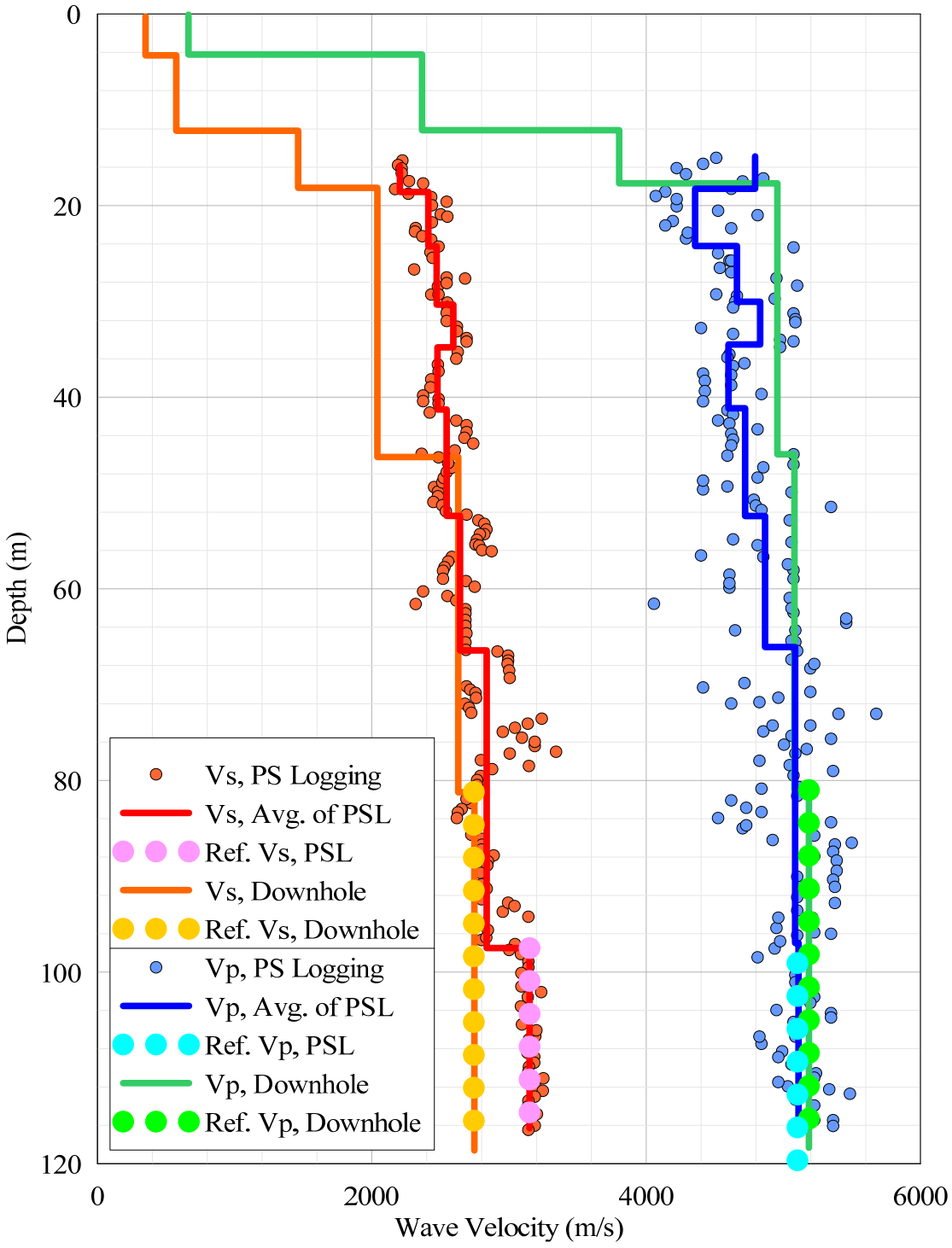

Figure A-1 Wave velocities at Bell Bend NPP (FSAR Figure 2.5-151).

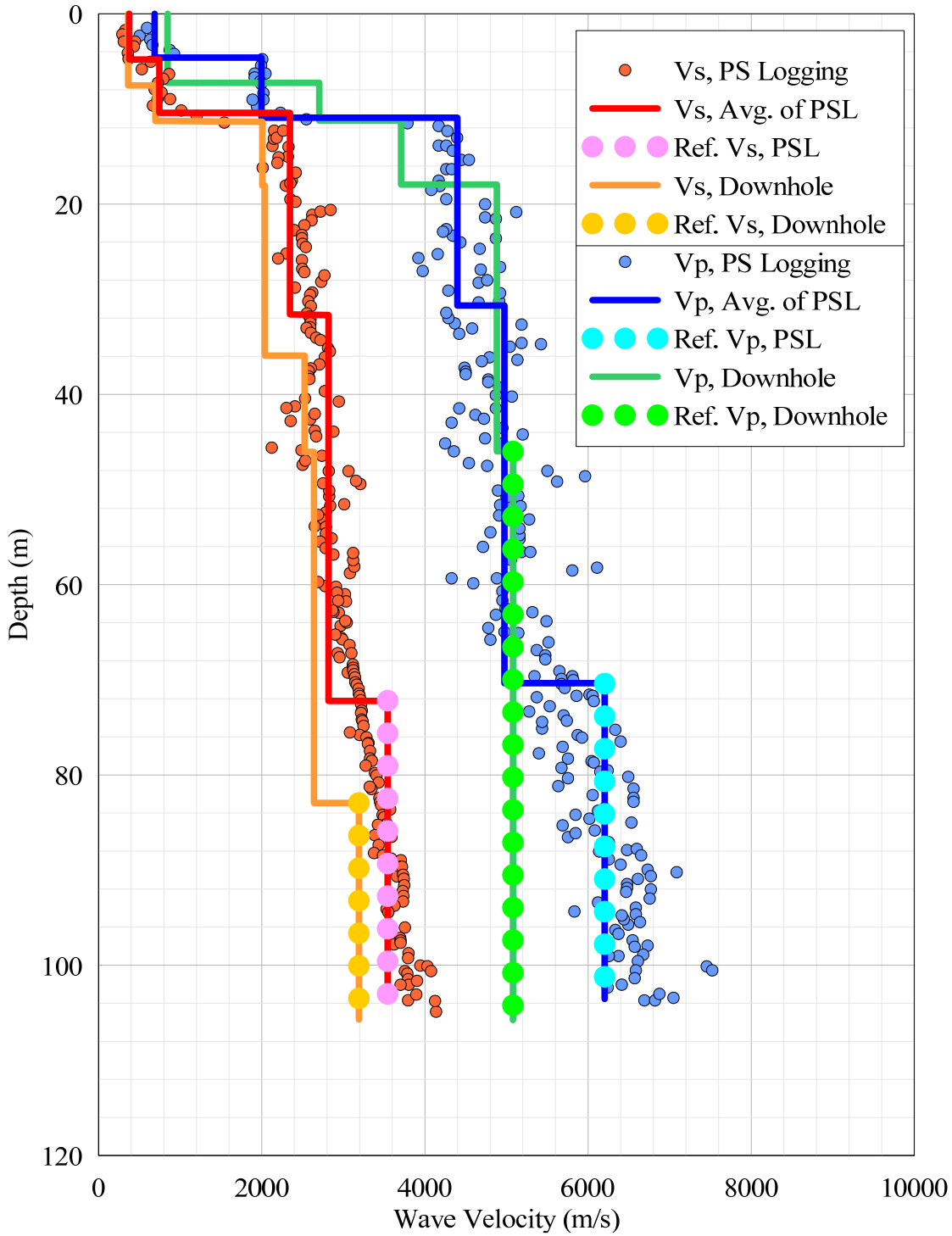

Figure A-2 Wave velocities at Bell Bend NPP (FSAR Figure 2.5-152).

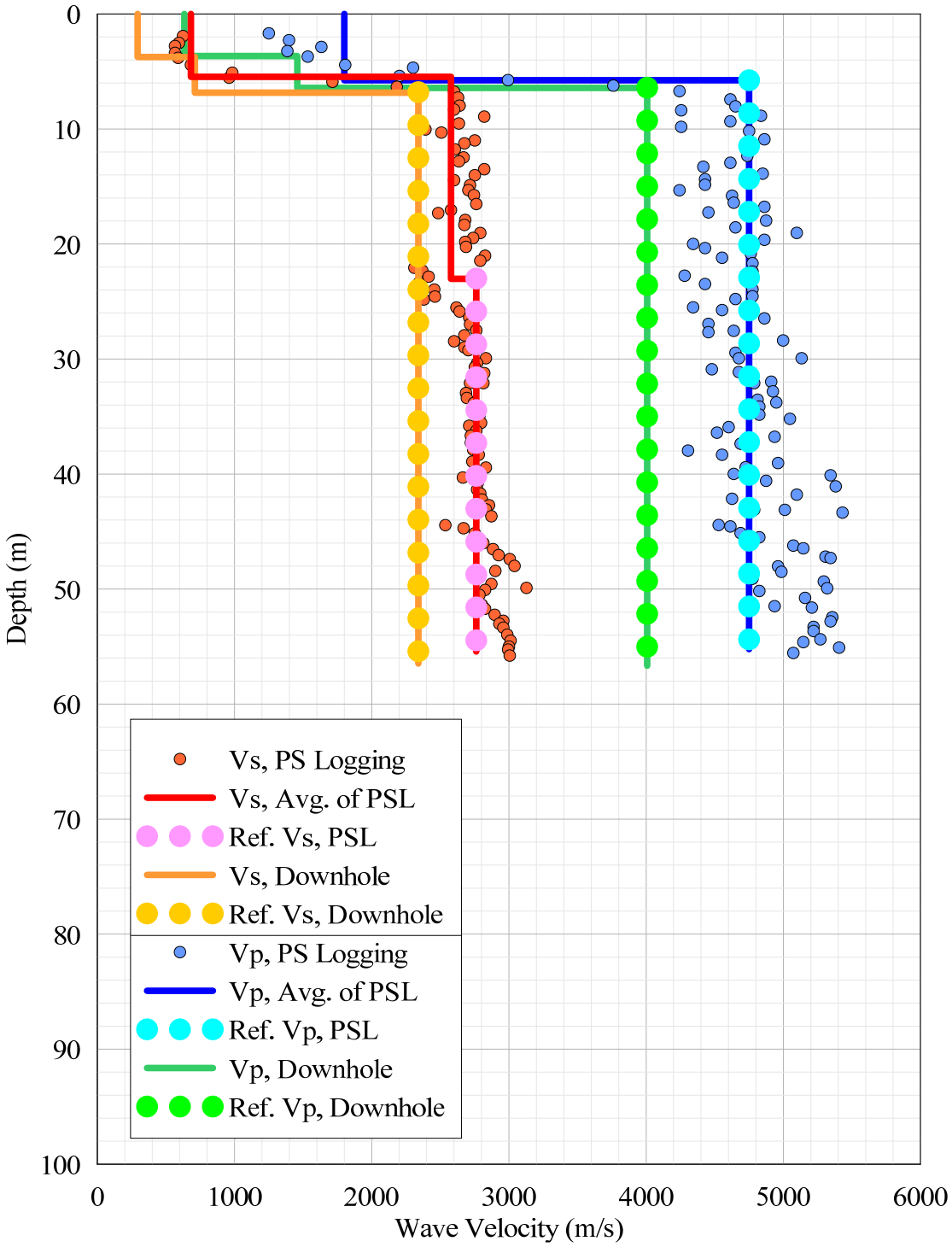

Figure A-3 Wave velocities at Bell Bend NPP (FSAR Figure 2.5-153).

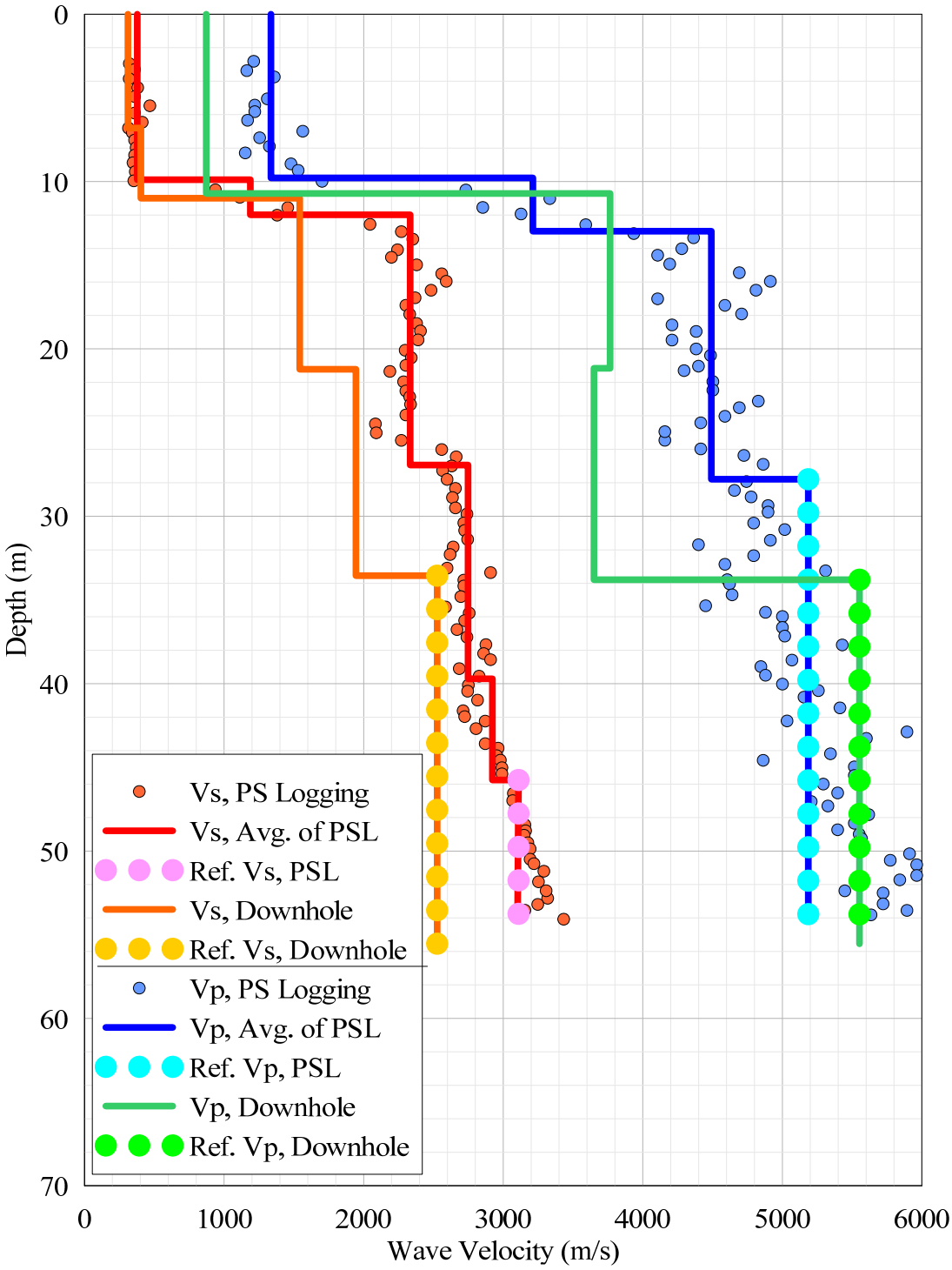

Figure A-4 Wave velocities at Bell Bend NPP (FSAR Figure 2.5-154).

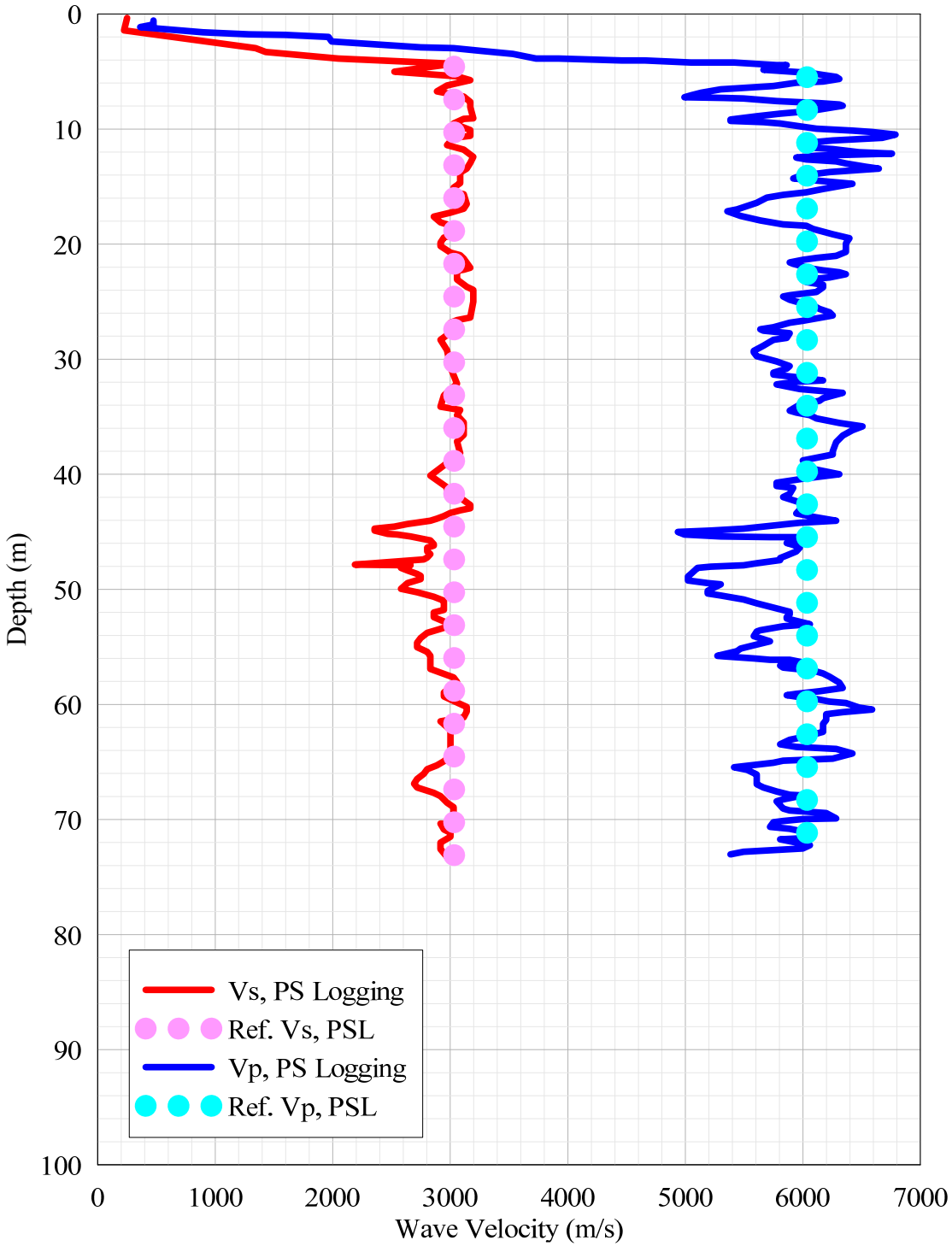

Figure A-5 Wave velocities at Bellefonte NPP (FSAR Figure 2.5-331).

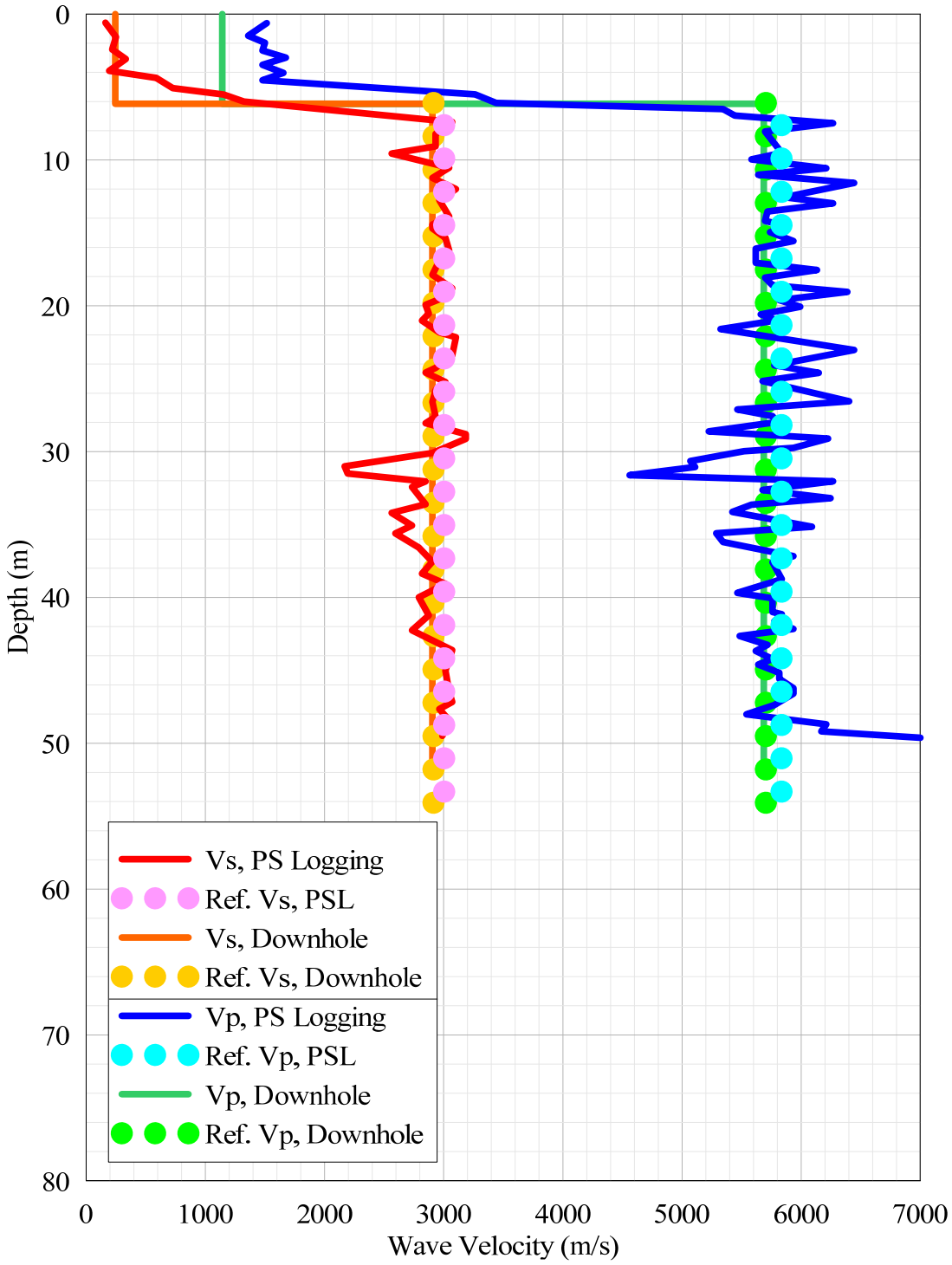

Figure A-6 Wave velocities at Bellefonte NPP (FSAR Figure 2.5-333).

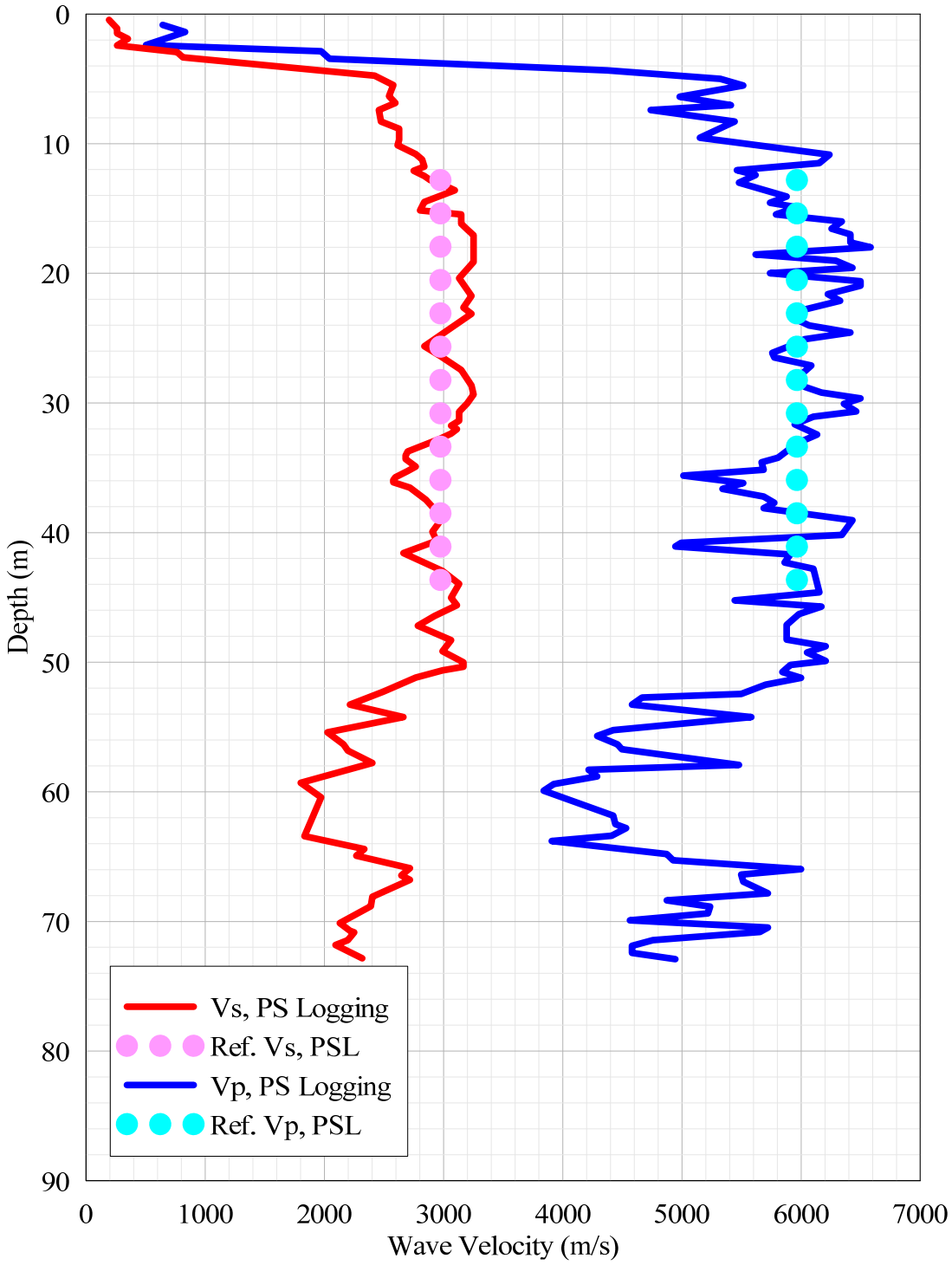

Figure A-7 Wave velocities at Bellefonte NPP (FSAR Figure 2.5-334).

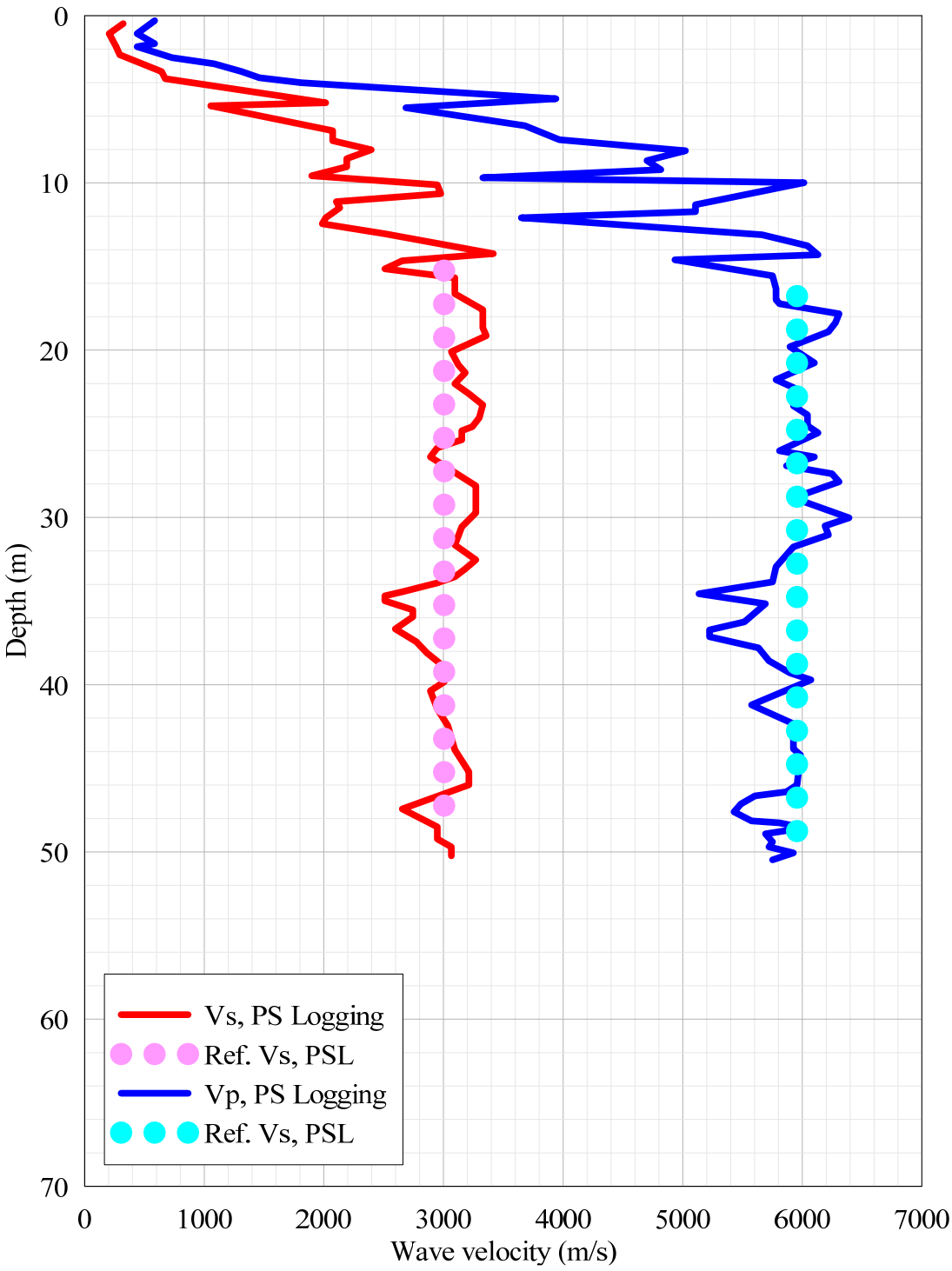

Figure A-8 Wave velocities at Bellefonte NPP (FSAR Figure 2.5-335).

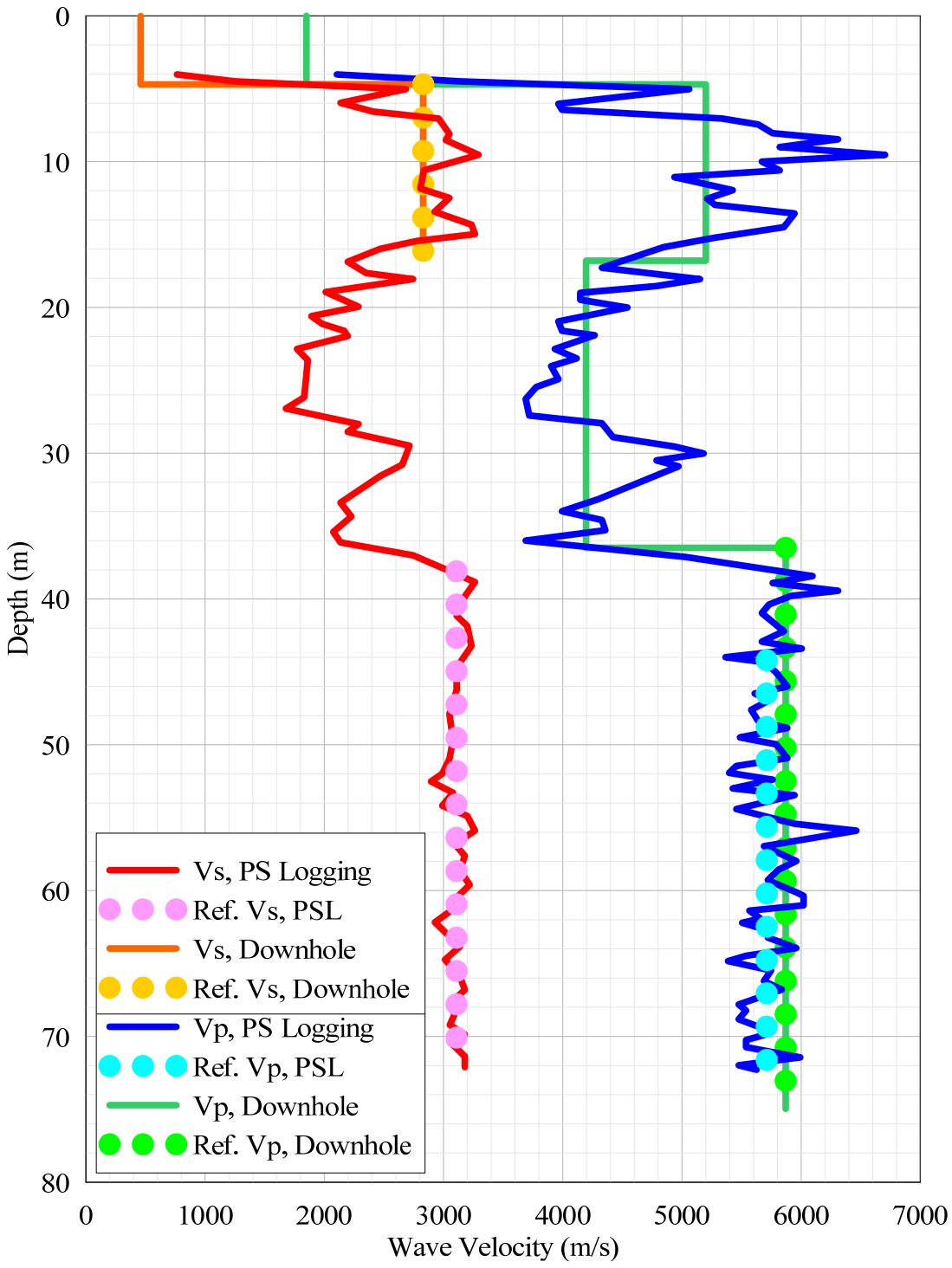

Figure A-9 Wave velocities at Bellefonte NPP (FSAR Figure 2.5-336).

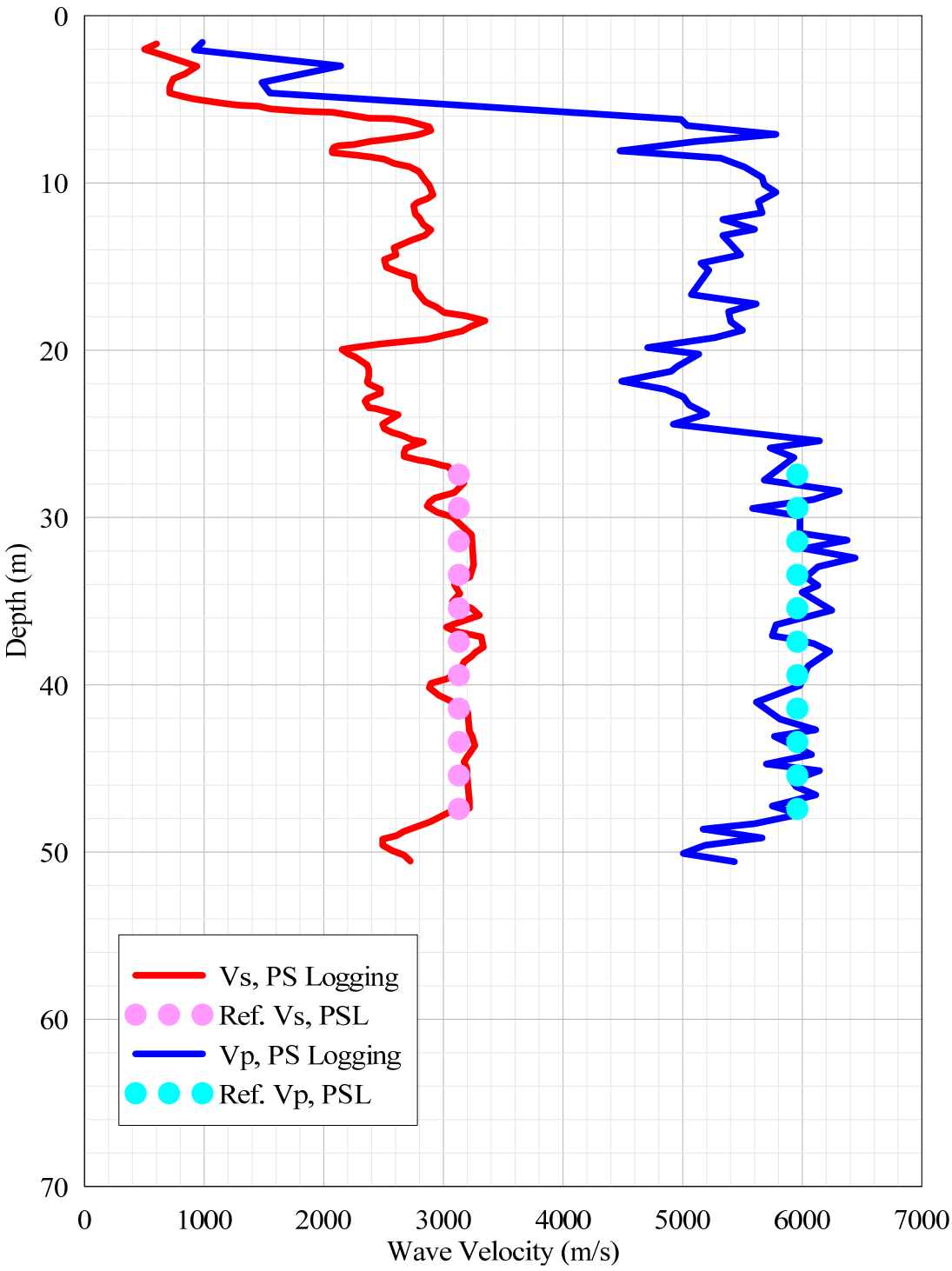

Figure A-10 Wave velocities at Bellefonte NPP (FSAR Figure 2.5-337).

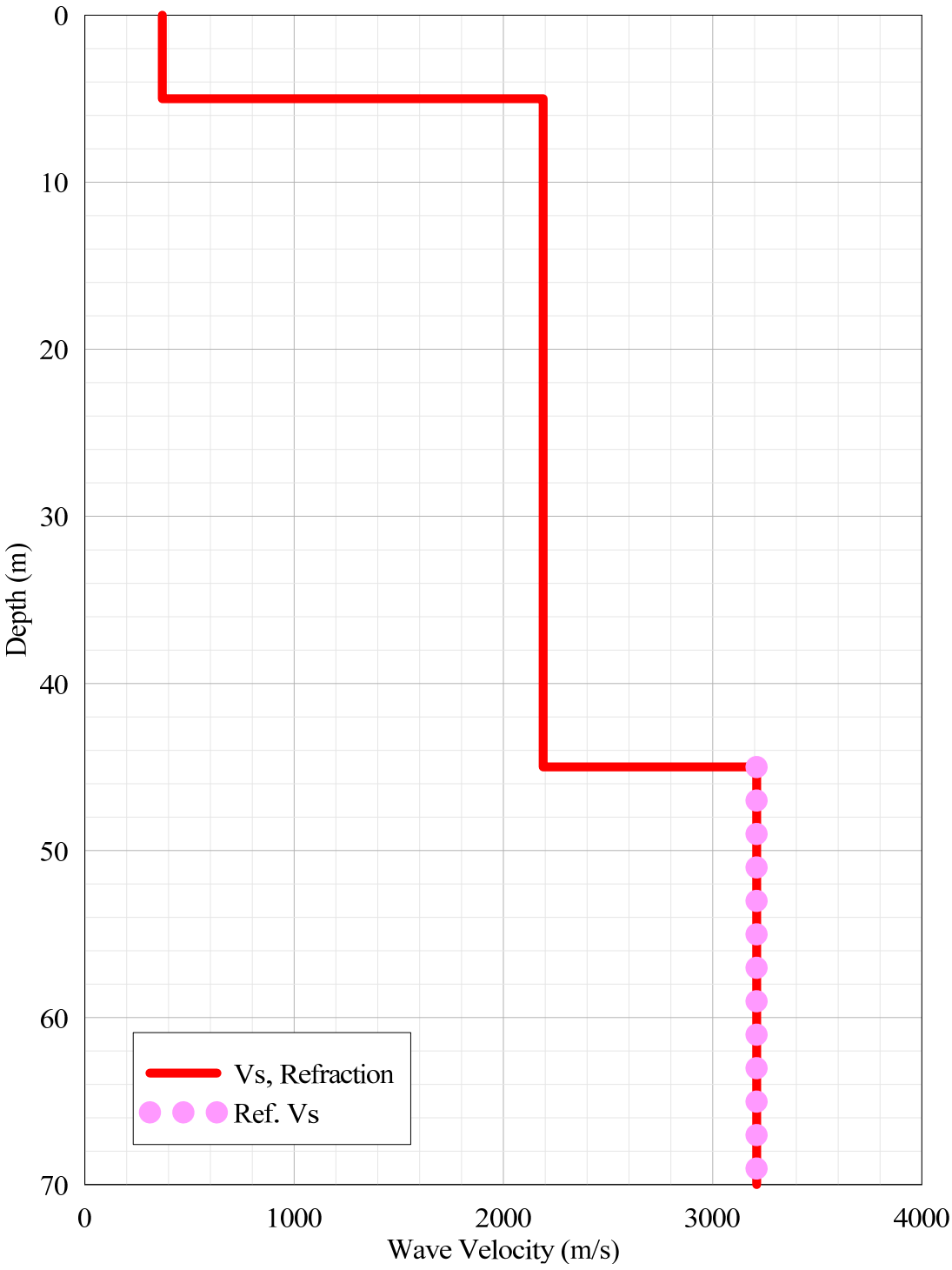

Figure A-11 Wave velocity at Chalk River, Ontario [Beresnev and Atkinson 1997].

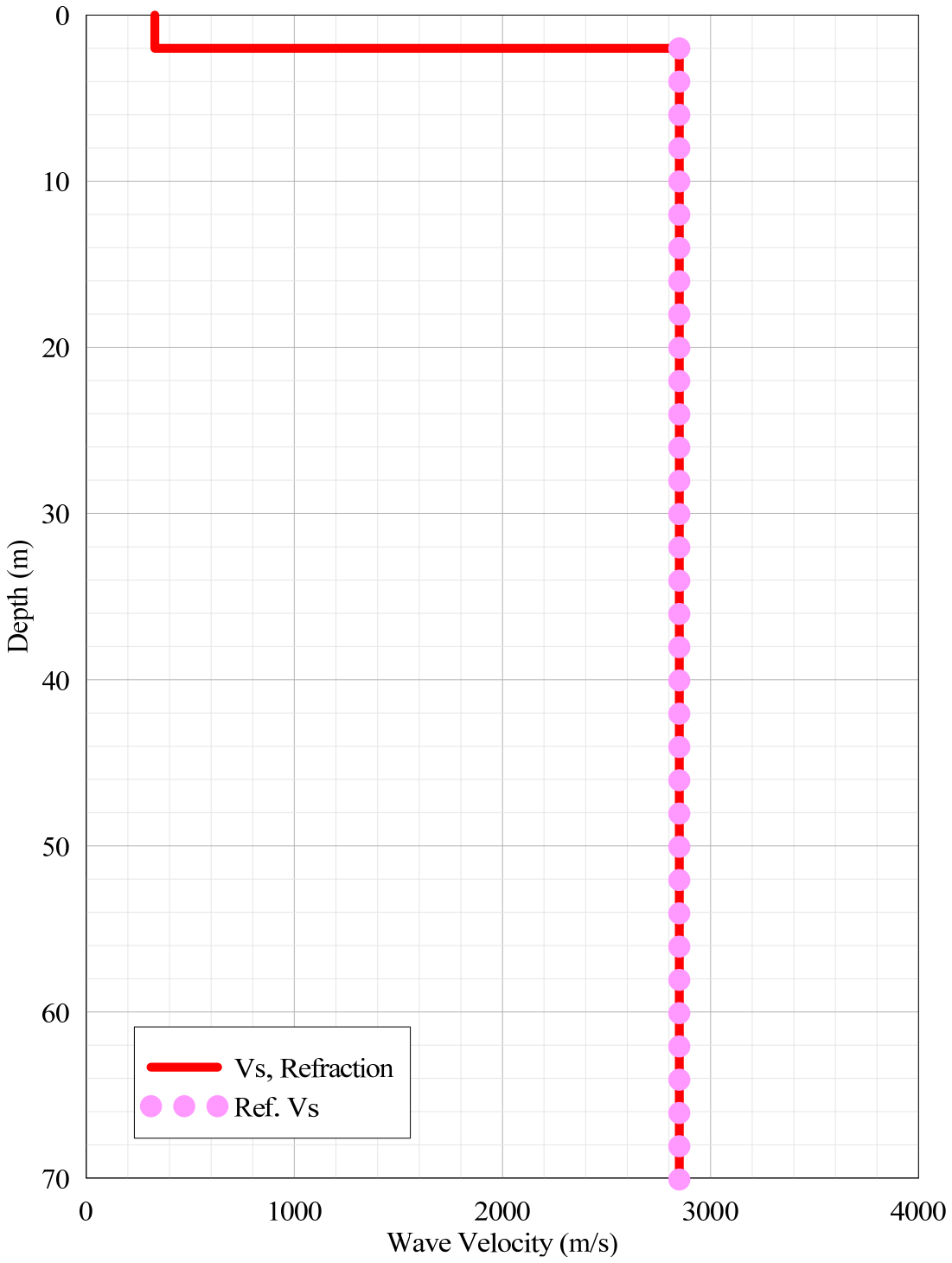

Figure A-12 Wave velocity at Grand Remous, Ontario [Beresnev and Atkinson 1997].

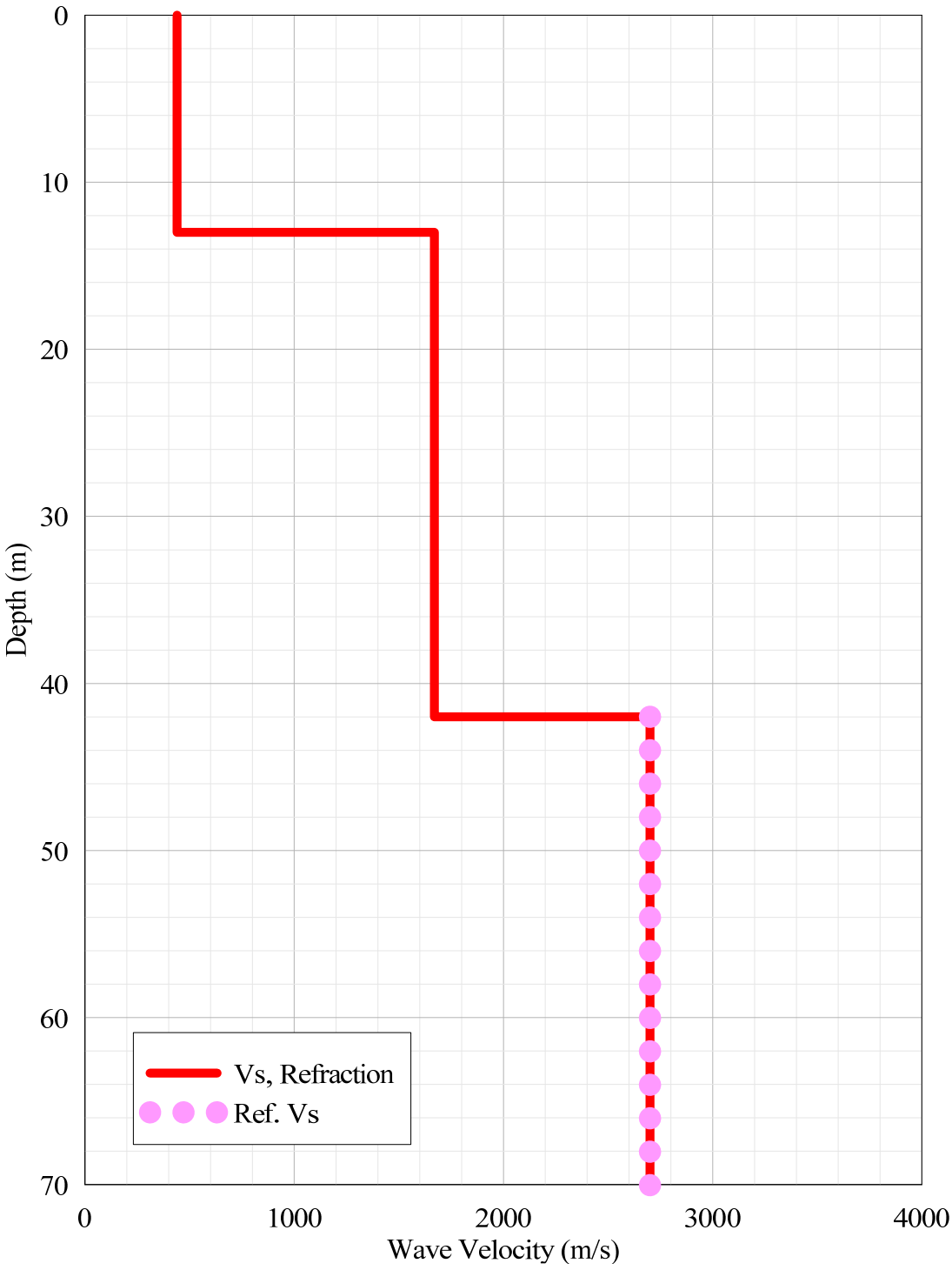

Figure A-13 Wave velocity at Ottawa, Ontario [Beresnev and Atkinson 1997].

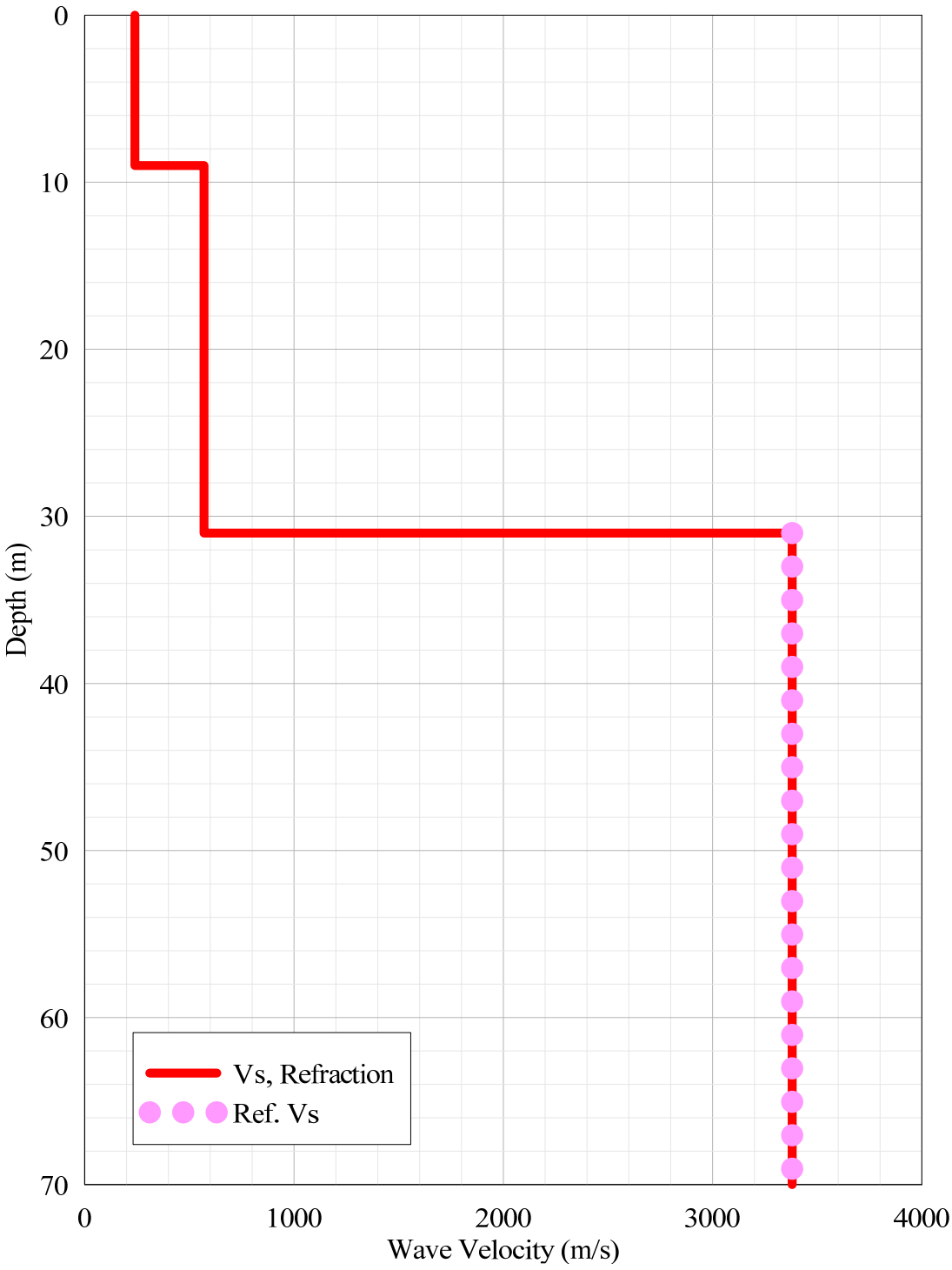

Figure A-14 Wave velocity at Tyneside, Ontario [Beresnev and Atkinson 1997].

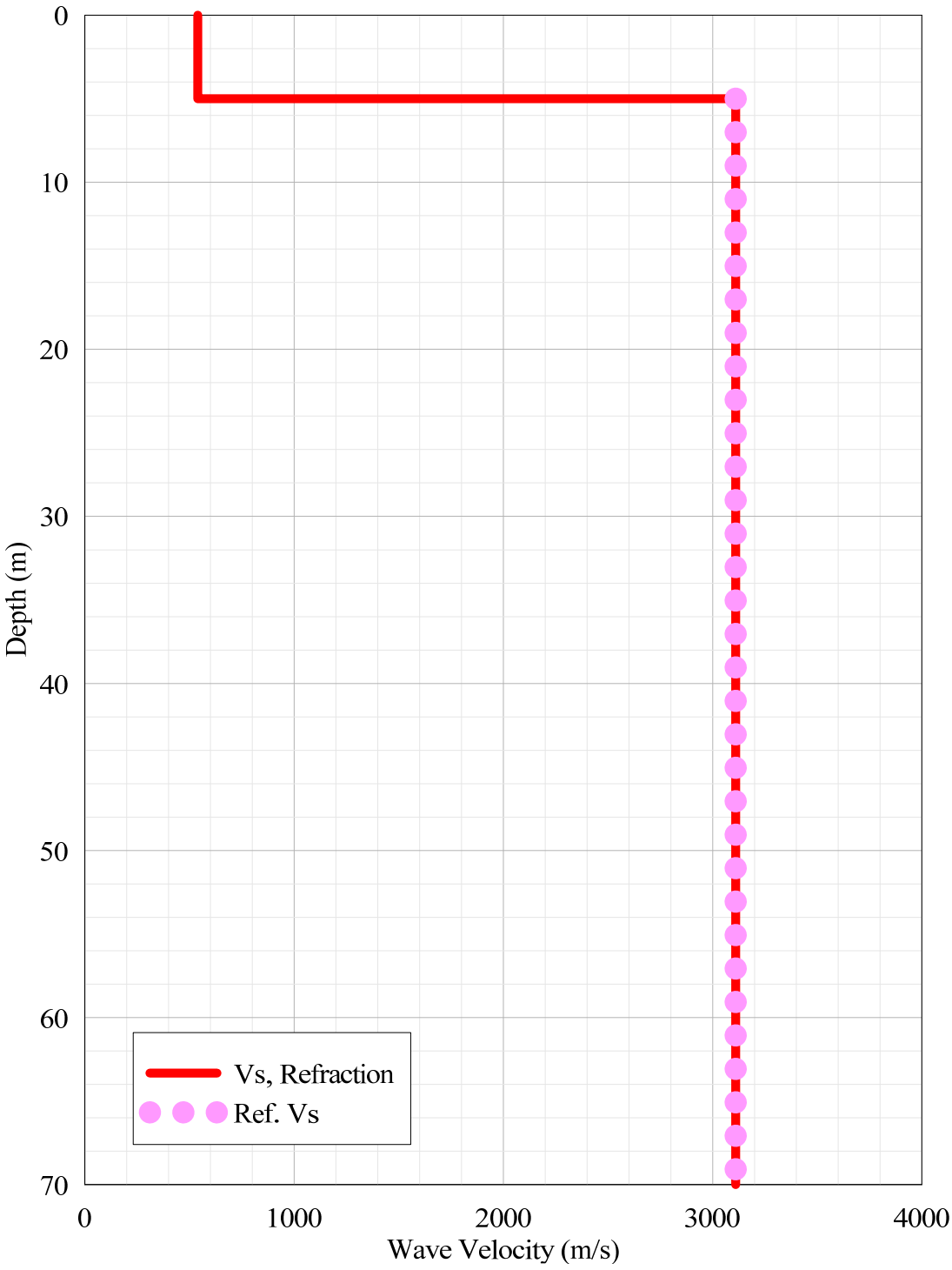

Figure A-15 Wave velocity at Williamsburg, Ontario [Beresnev and Atkinson 1997].

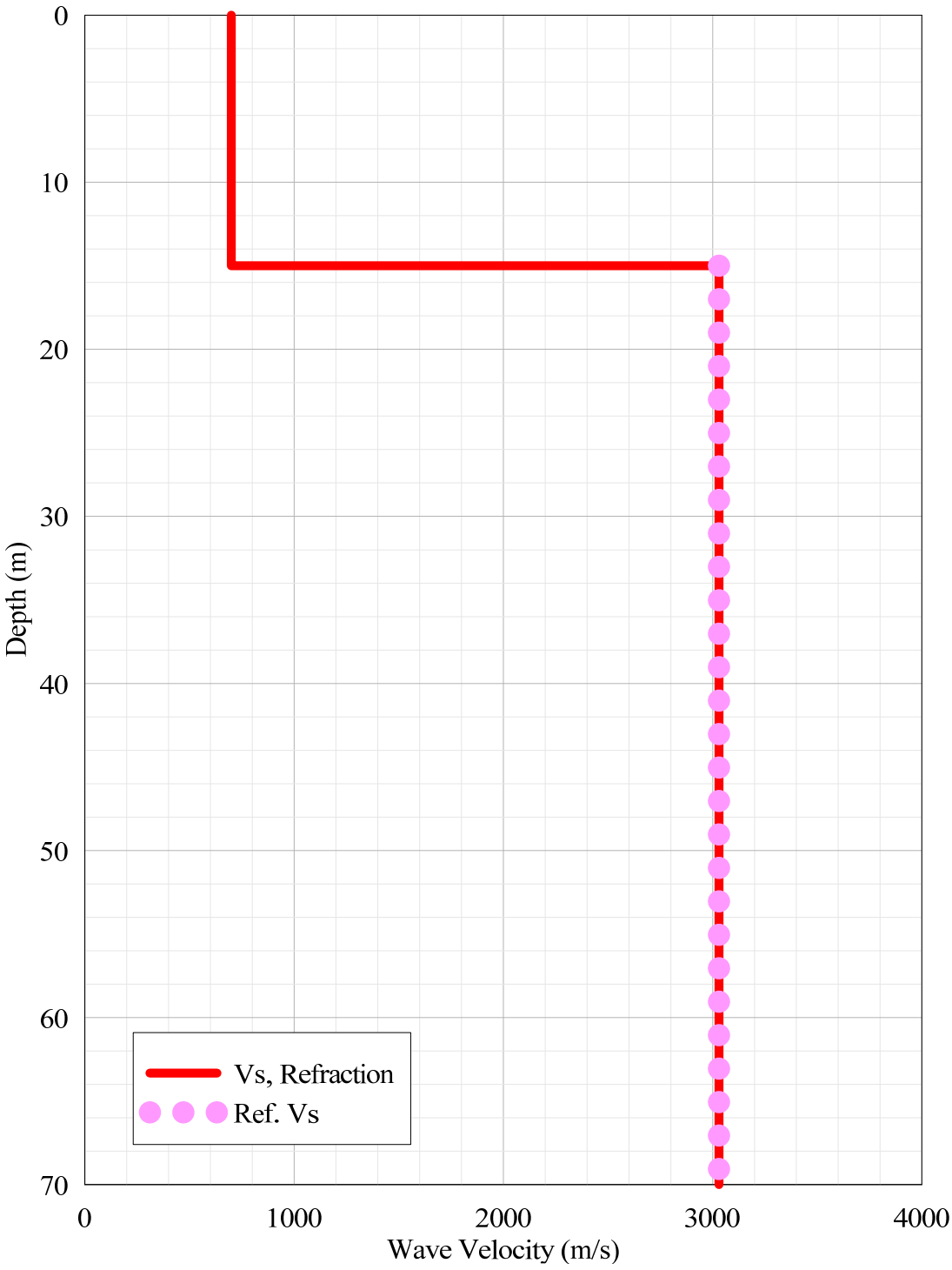

Figure A-16 Wave velocity at Wesleyville, Ontario [Beresnev and Atkinson 1997].

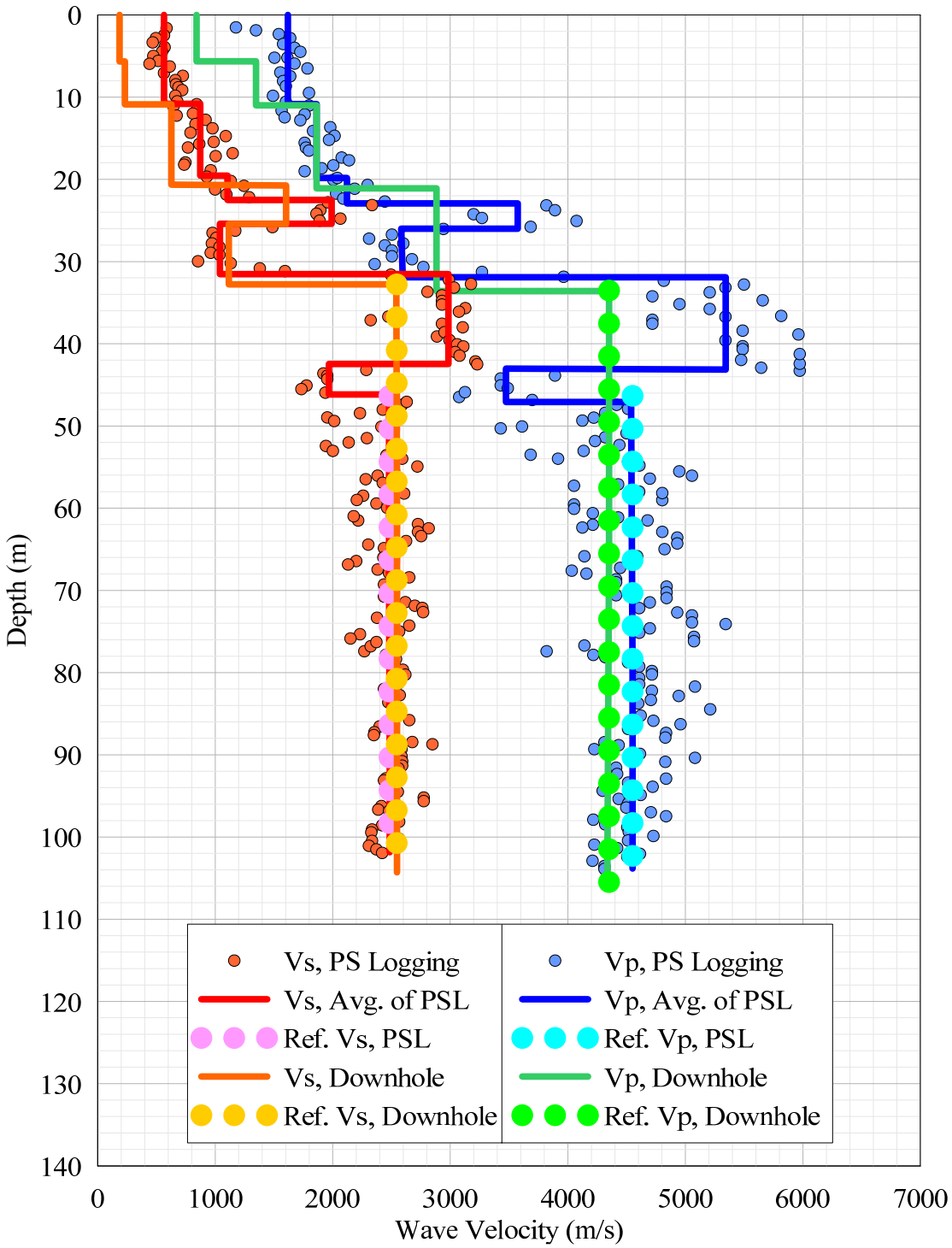

Figure A-17 Wave velocities at Callaway NPP (FSAR Figure 2.5.4-19).

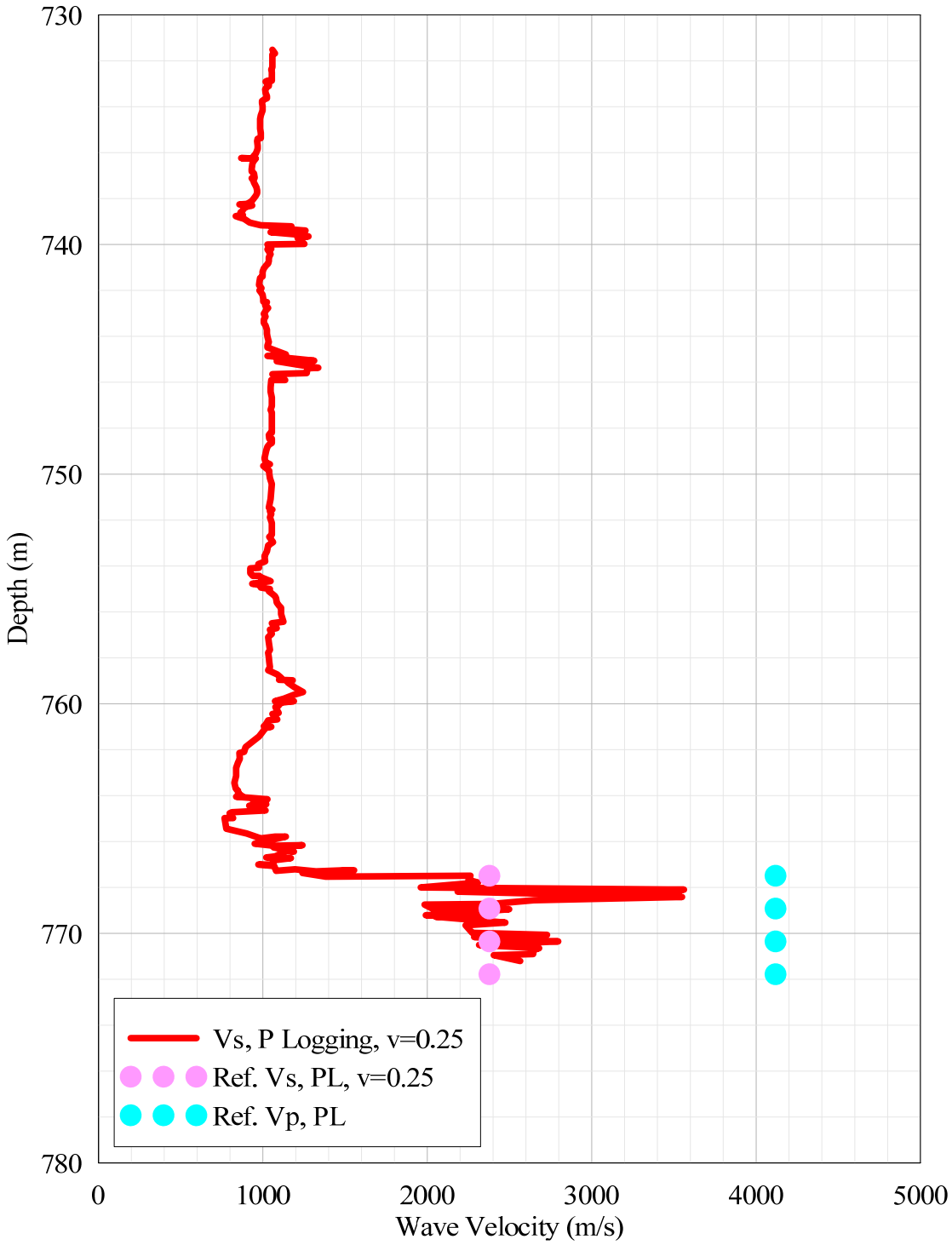

Figure A-18 Wave velocities at Calvert NPP (FSAR Figure 2.5-142).

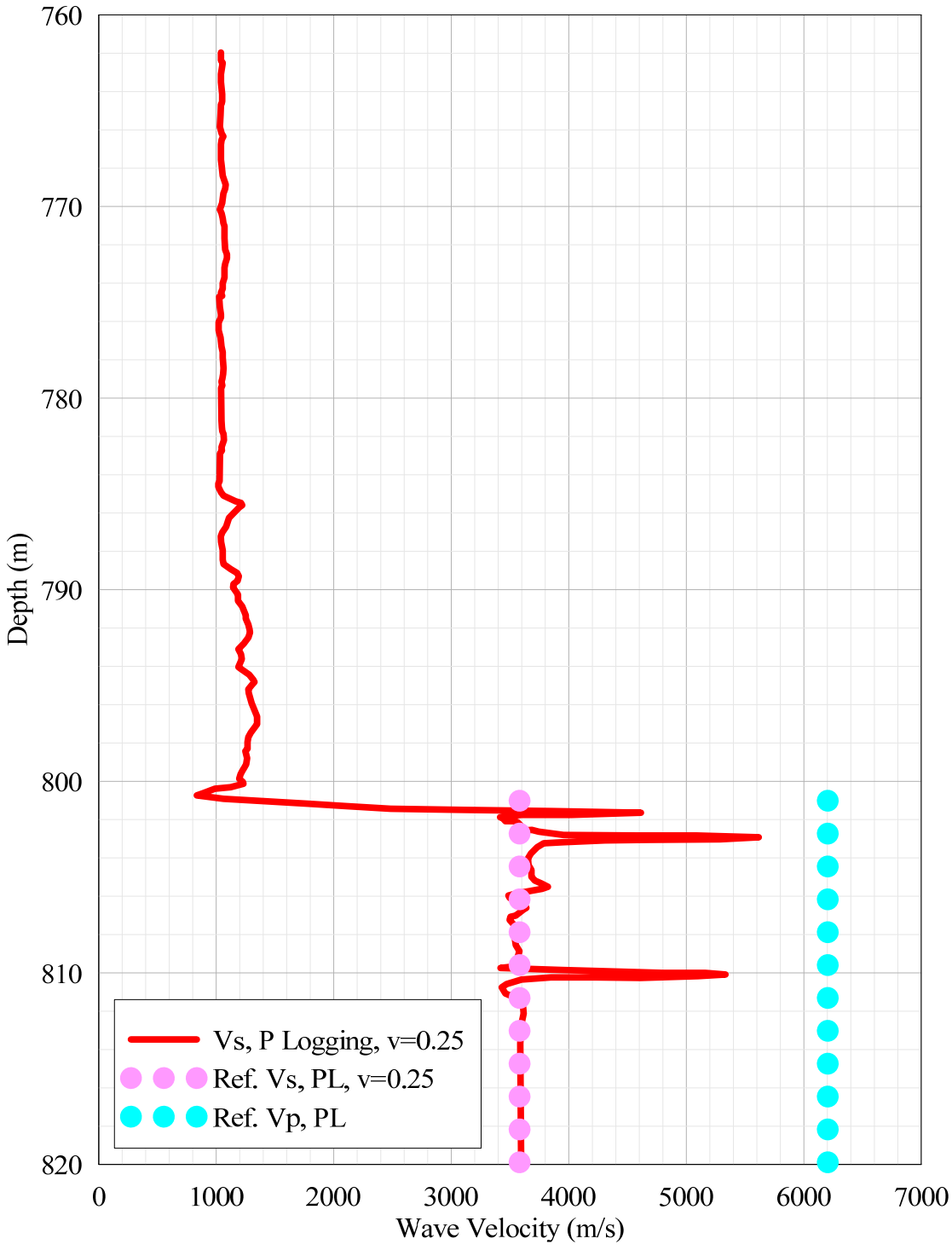

Figure A-19 Wave velocities at Calvert NPP (FSAR Figure 2.5-143).

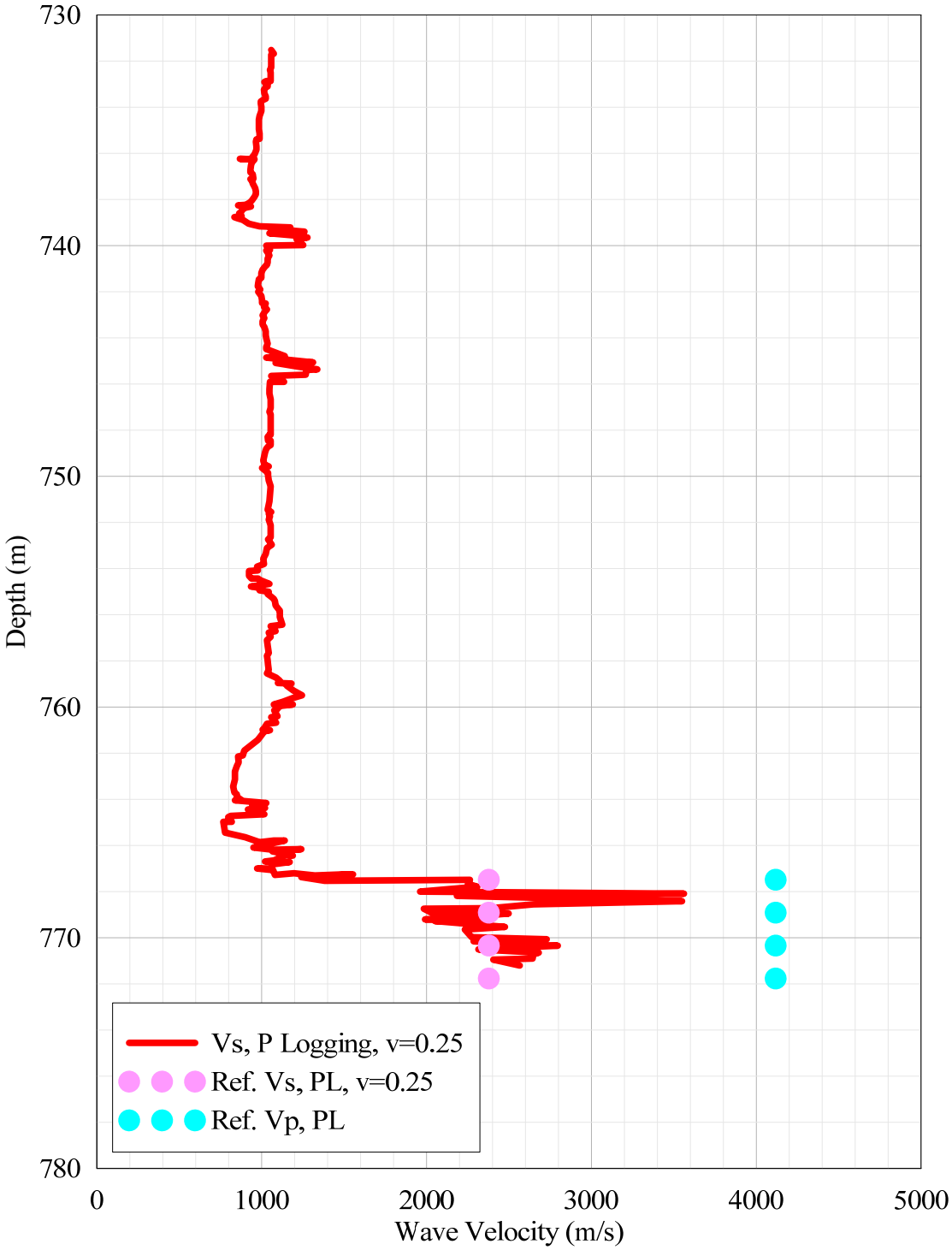

Figure A-20 Wave velocities at Calvert NPP (FSAR Figure 2.5-144).

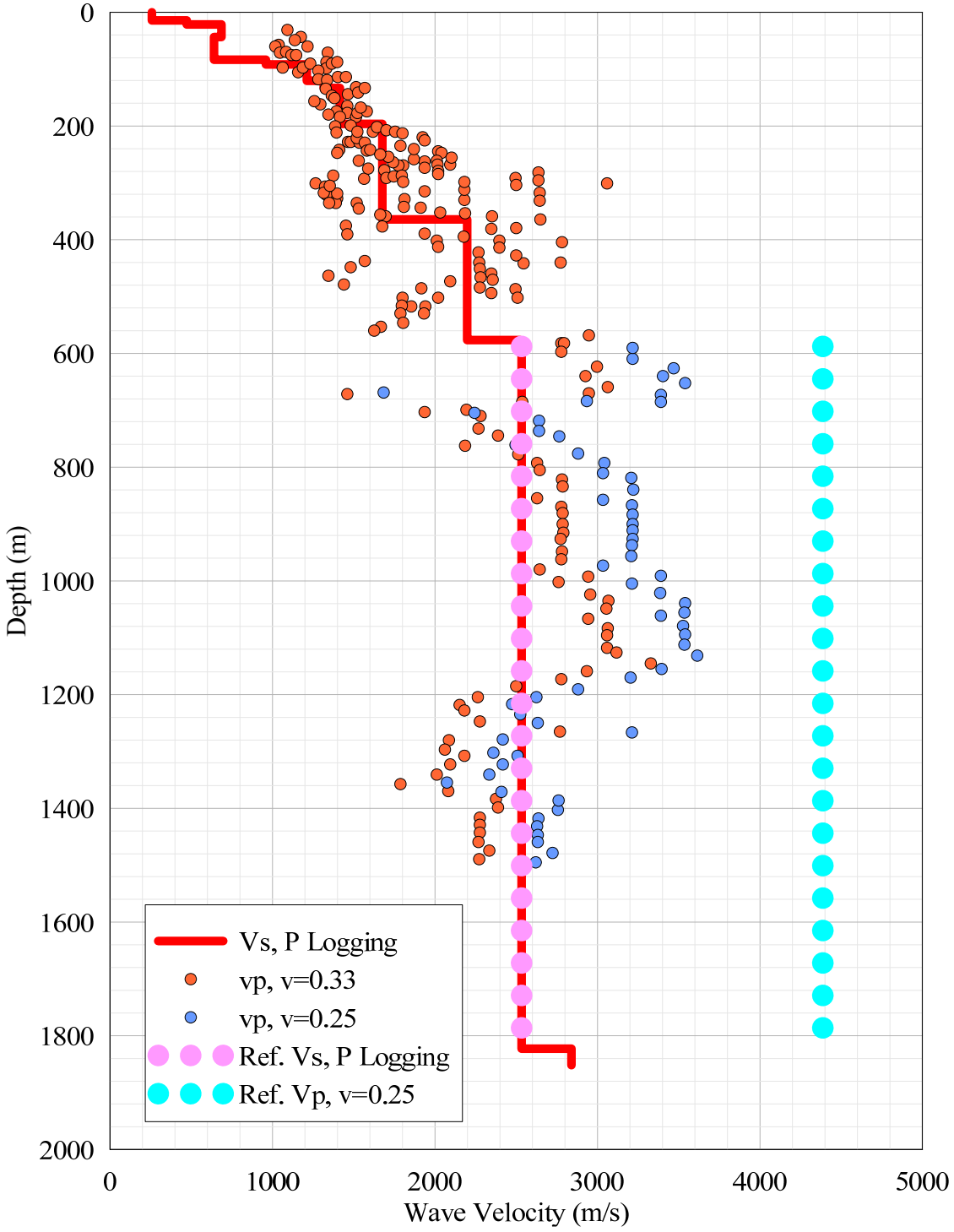

Figure A-21 Wave velocities at Clinton NPP (ESP Figure 4.2-8).

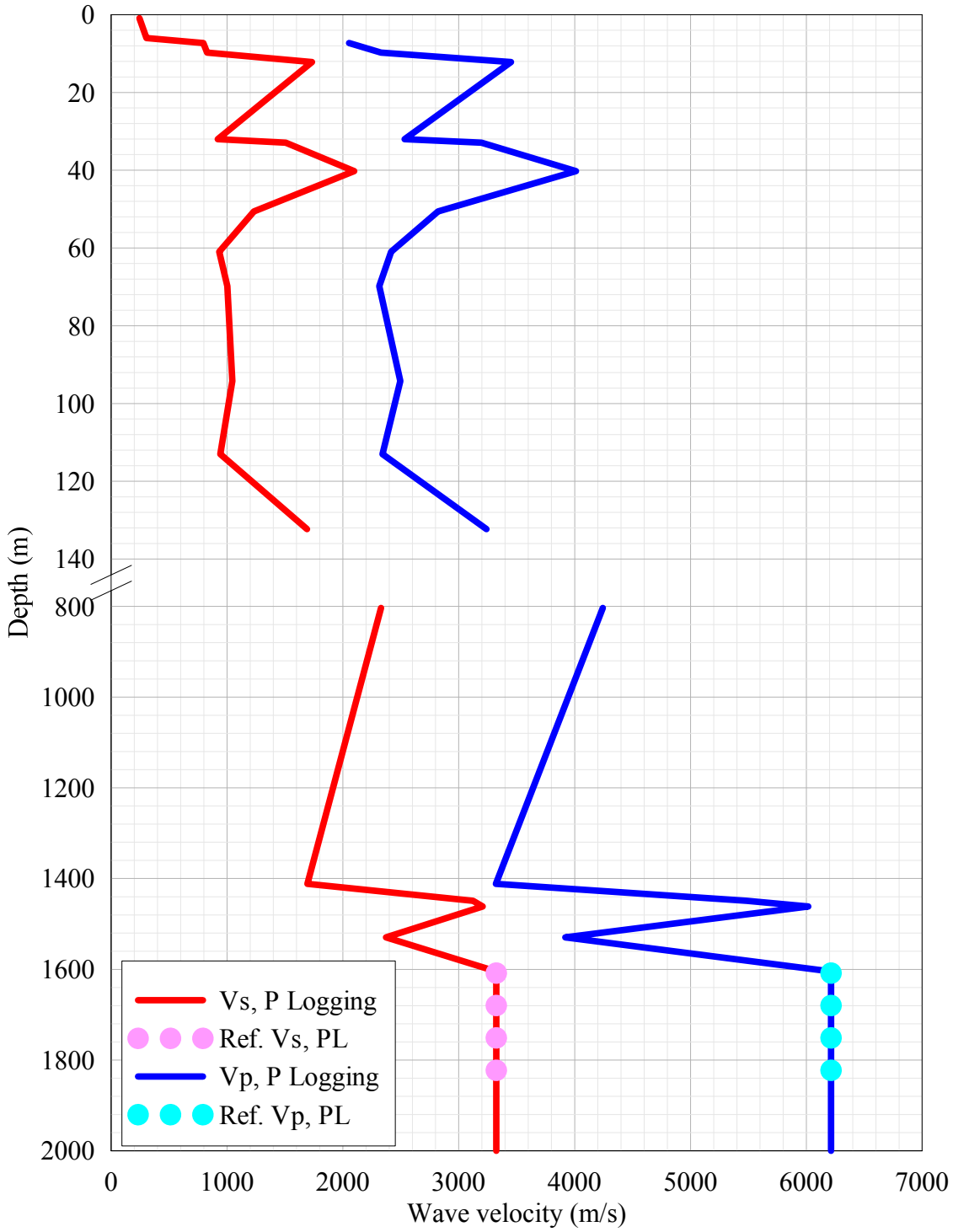

Figure A-22 Wave velocities at Comanche Peak NPP (FSAR Table 2.5.2-227).

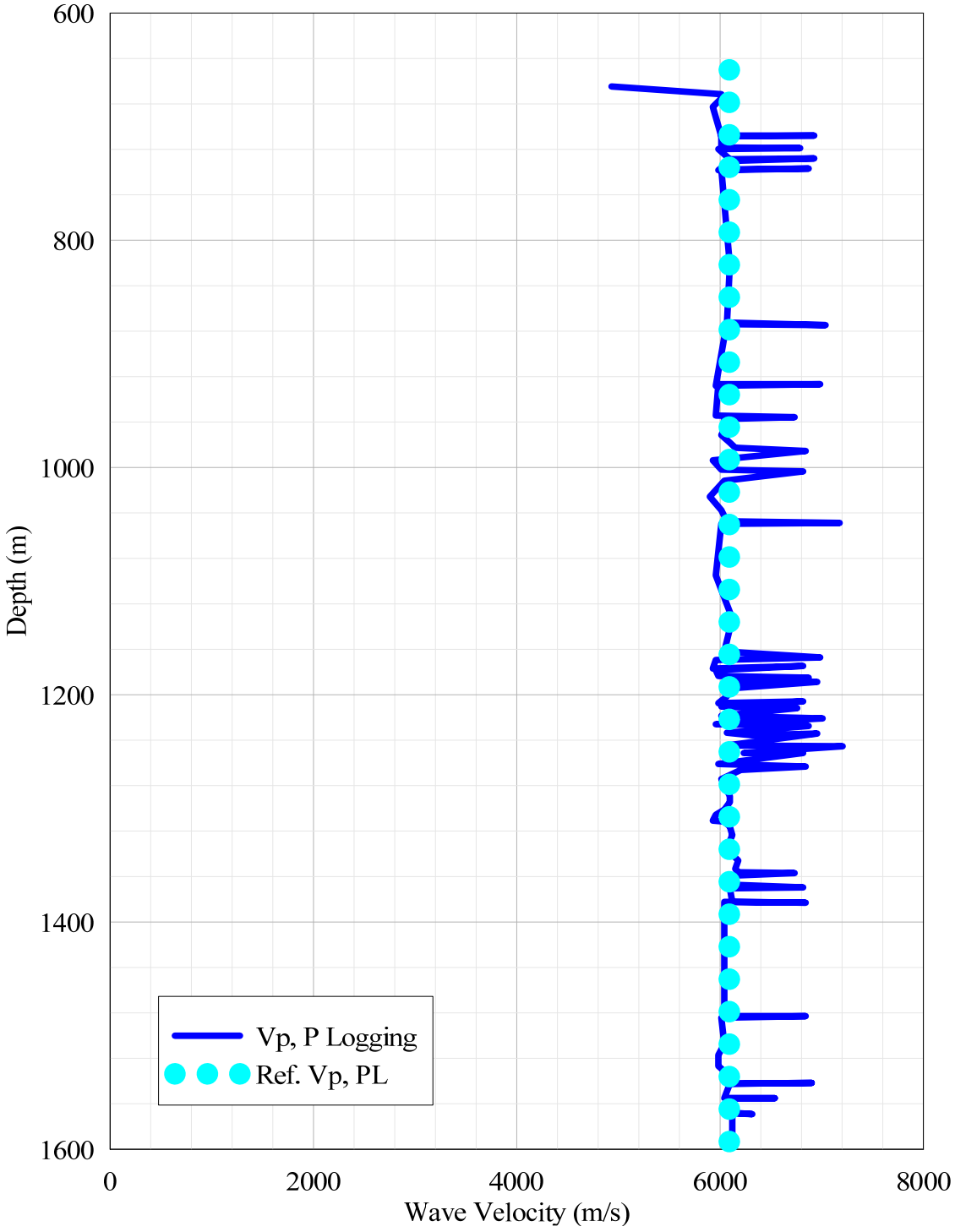

Figure A-23 Wave velocity at UPH3 [Daniels el al. 1983].

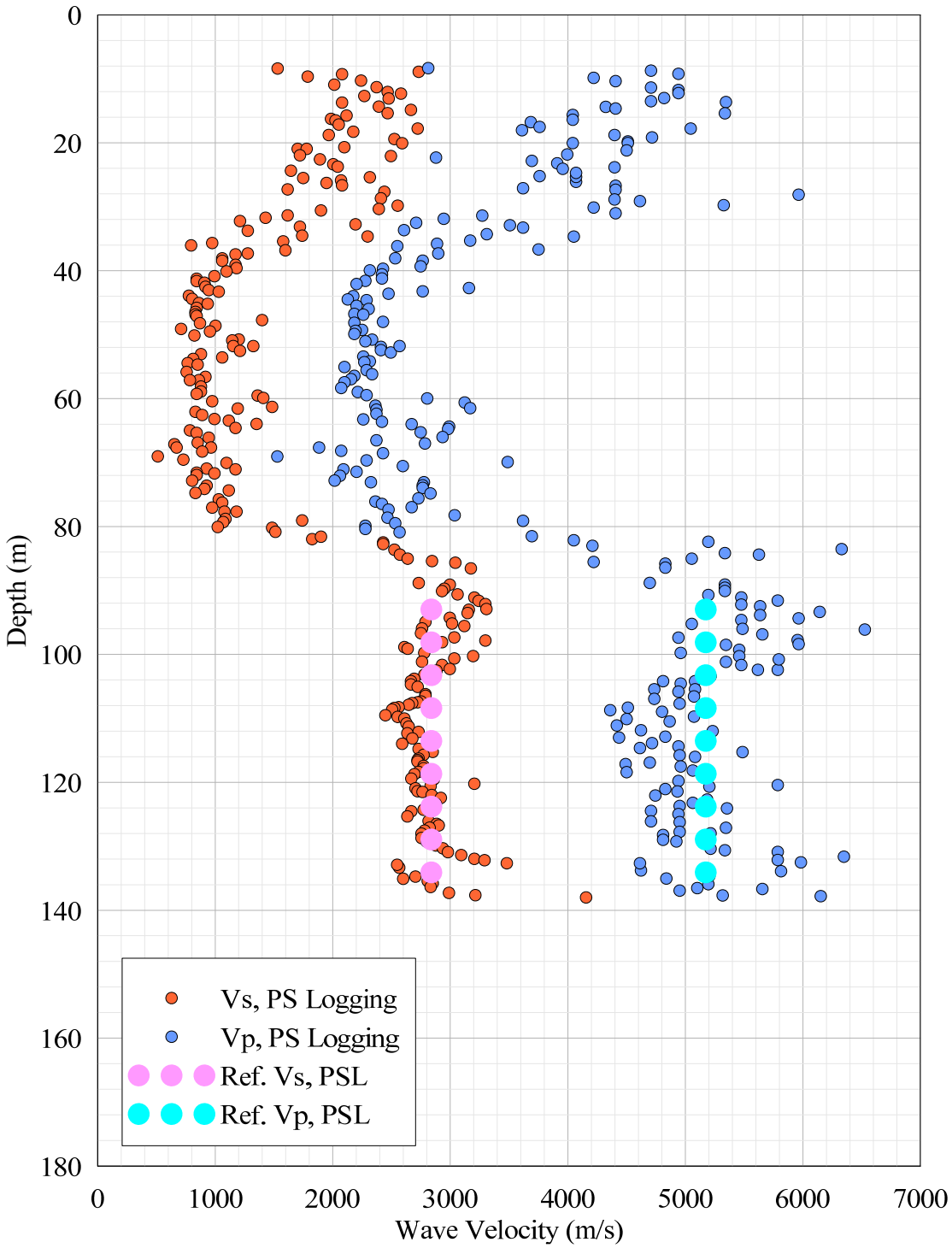

Figure A-24 Wave velocities at Fermi NPP (FSA Figure 2.5.4-220).

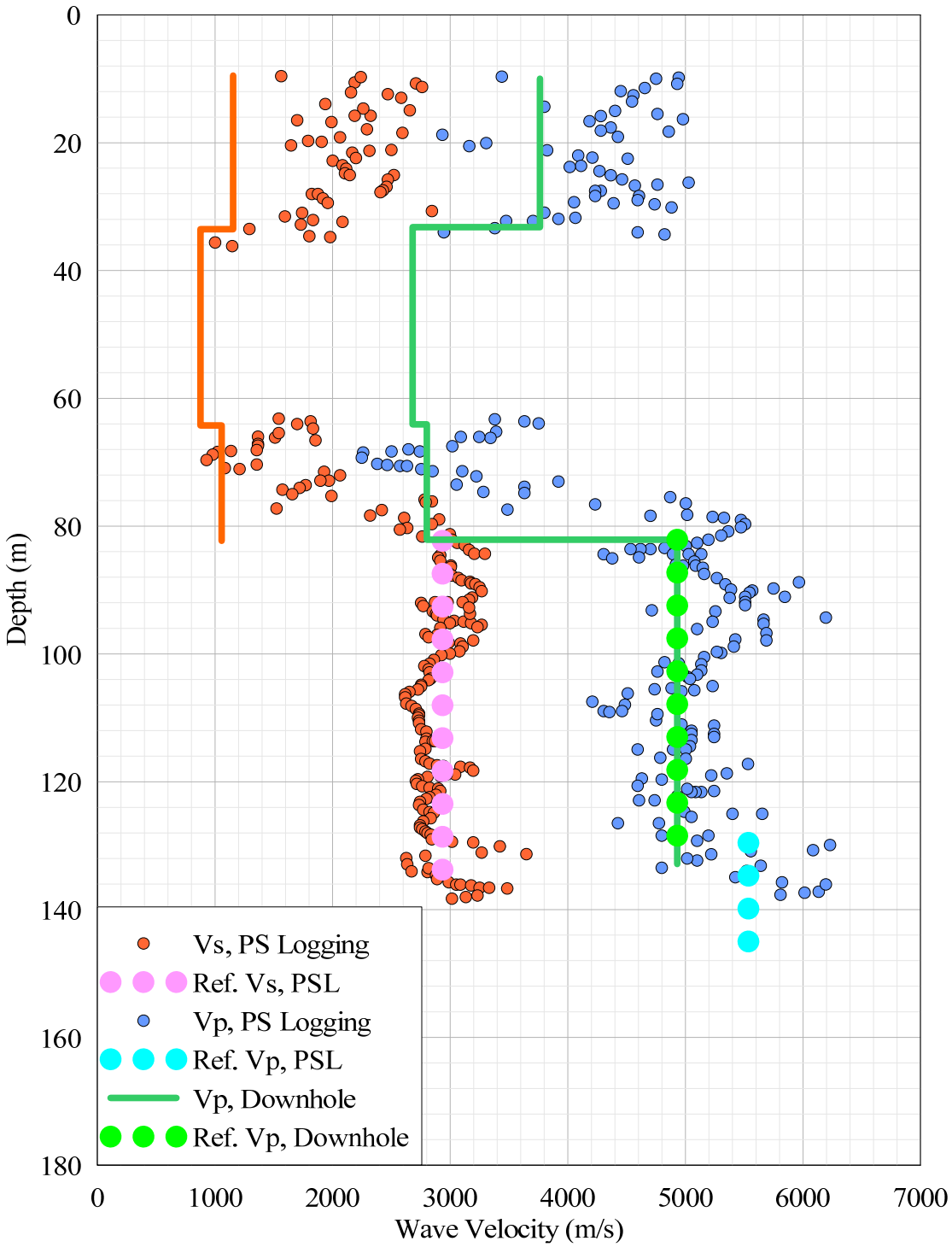

Figure A-25 Wave velocities at Fermi NPP (FSA Figure 2.5.4-221).

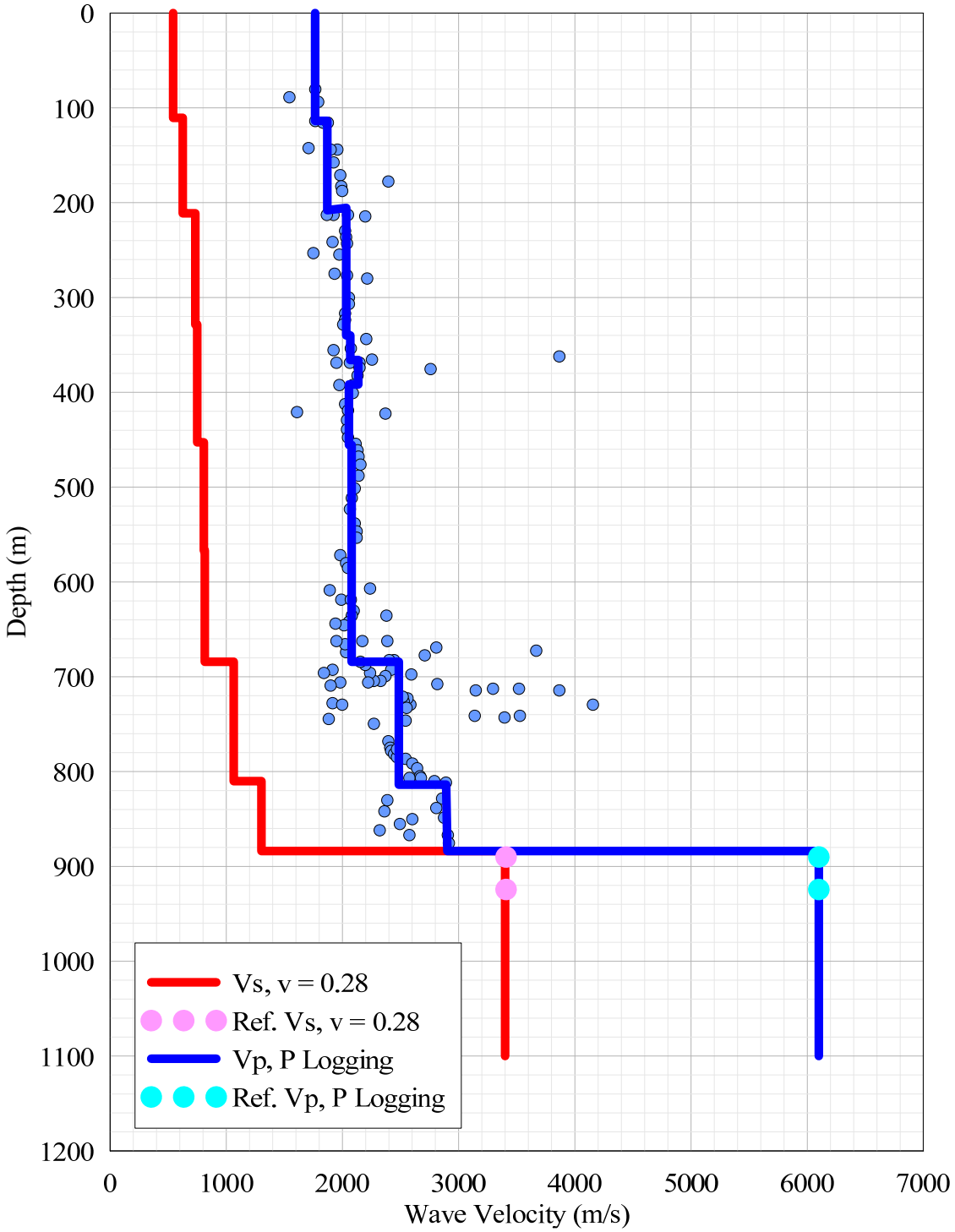

Figure A-26 Wave velocities at Hayes [Dorman and Smalley 1994].

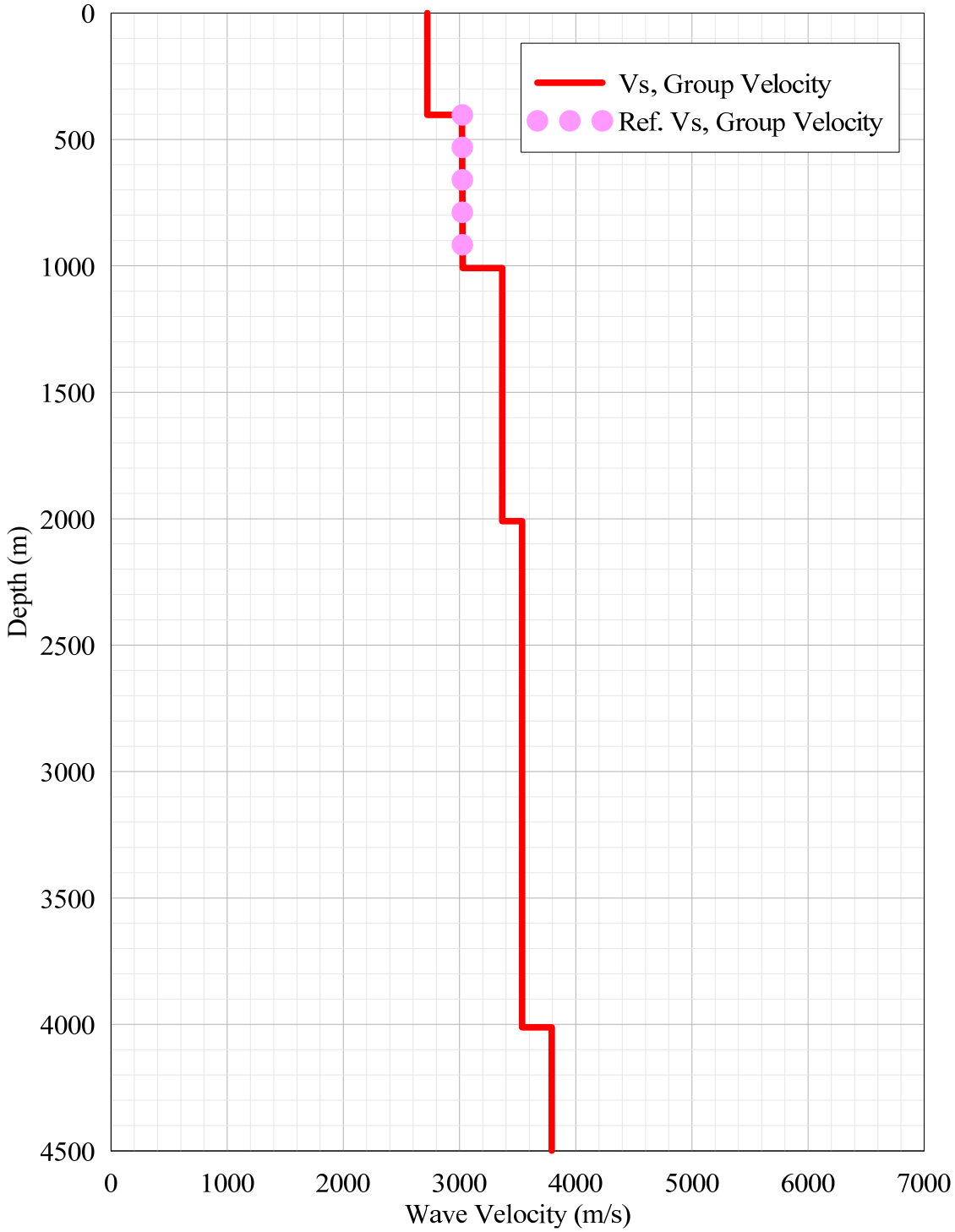

Figure A-27 Wave velocity at Bronson-Avalon [Kafka and Skehan 1990].

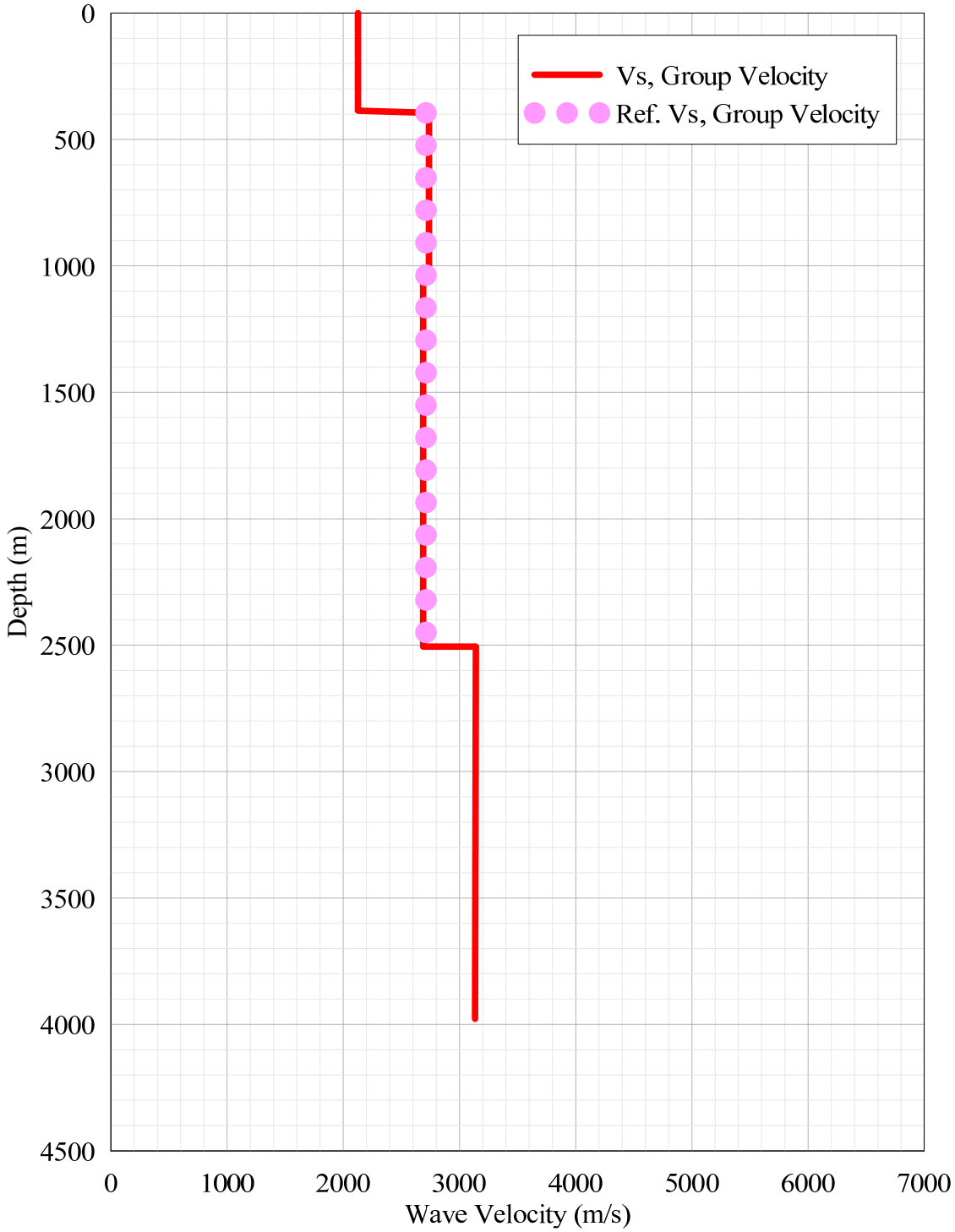

Figure A-28 Wave velocity at Hartford [Kafka and Skehan 1990].

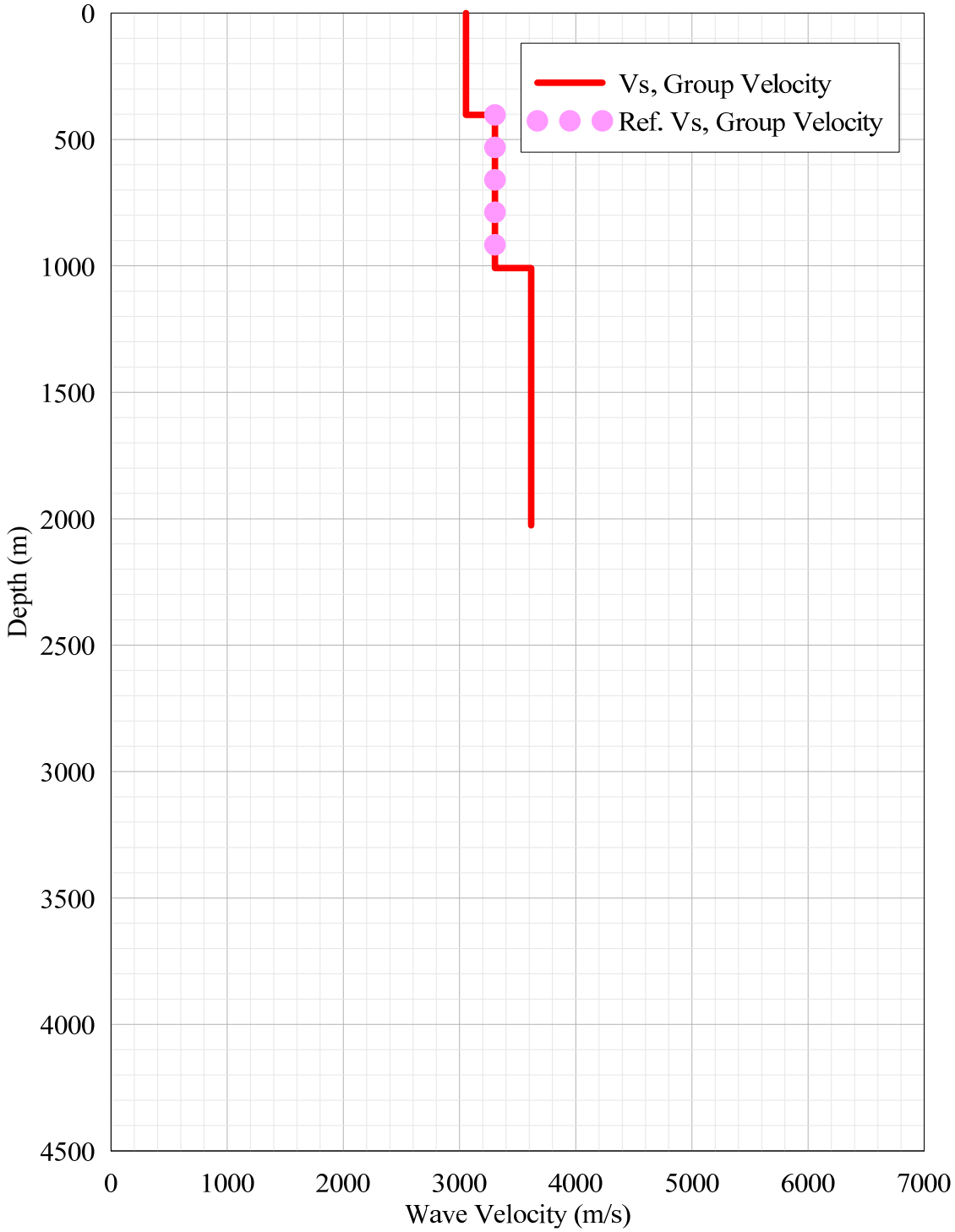

Figure A-29 Wave velocity at Waterbury [Kafka and Skehan 1990].

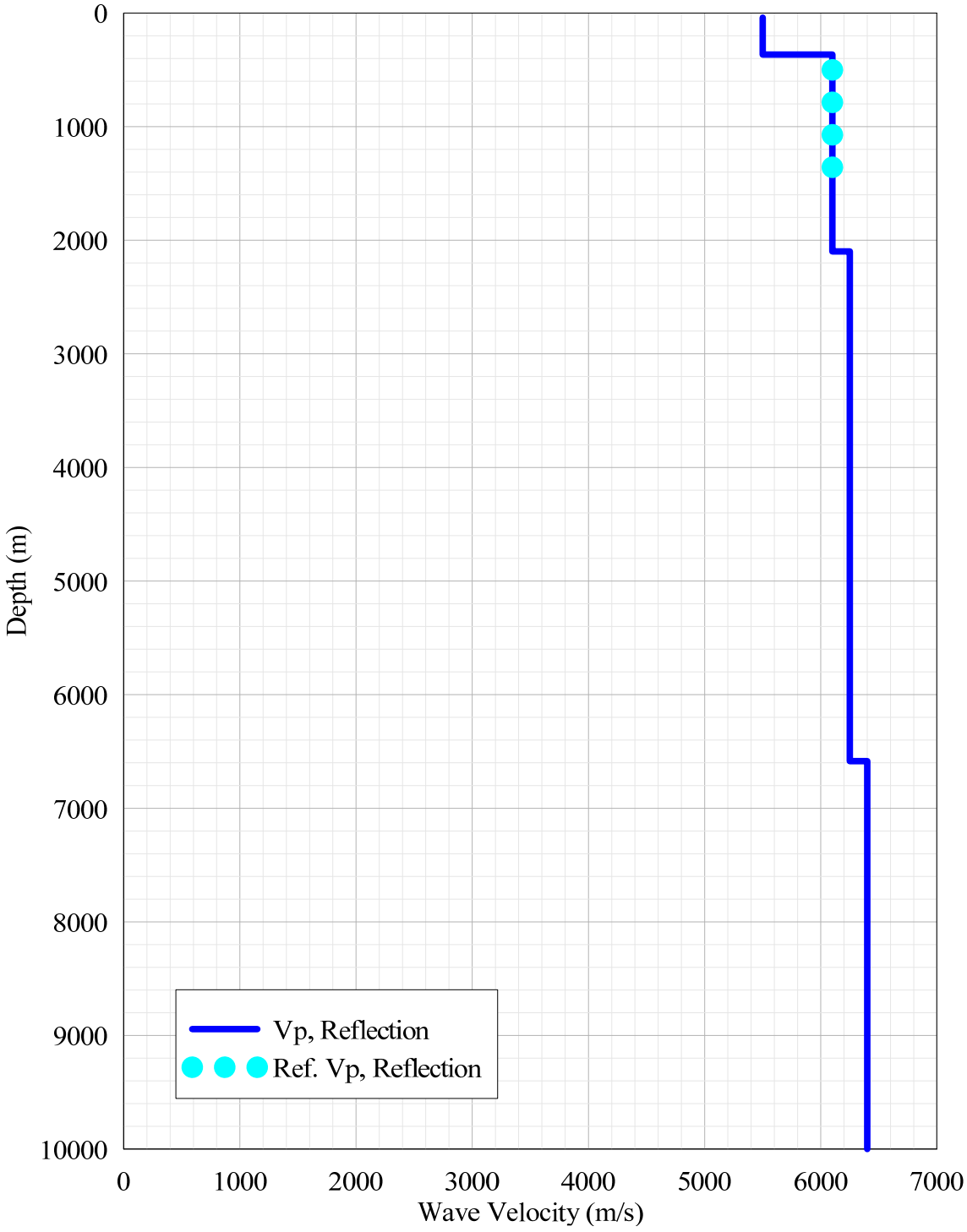

Figure A-30 Wave velocity at SP1 [Luetgert et al. 1994].

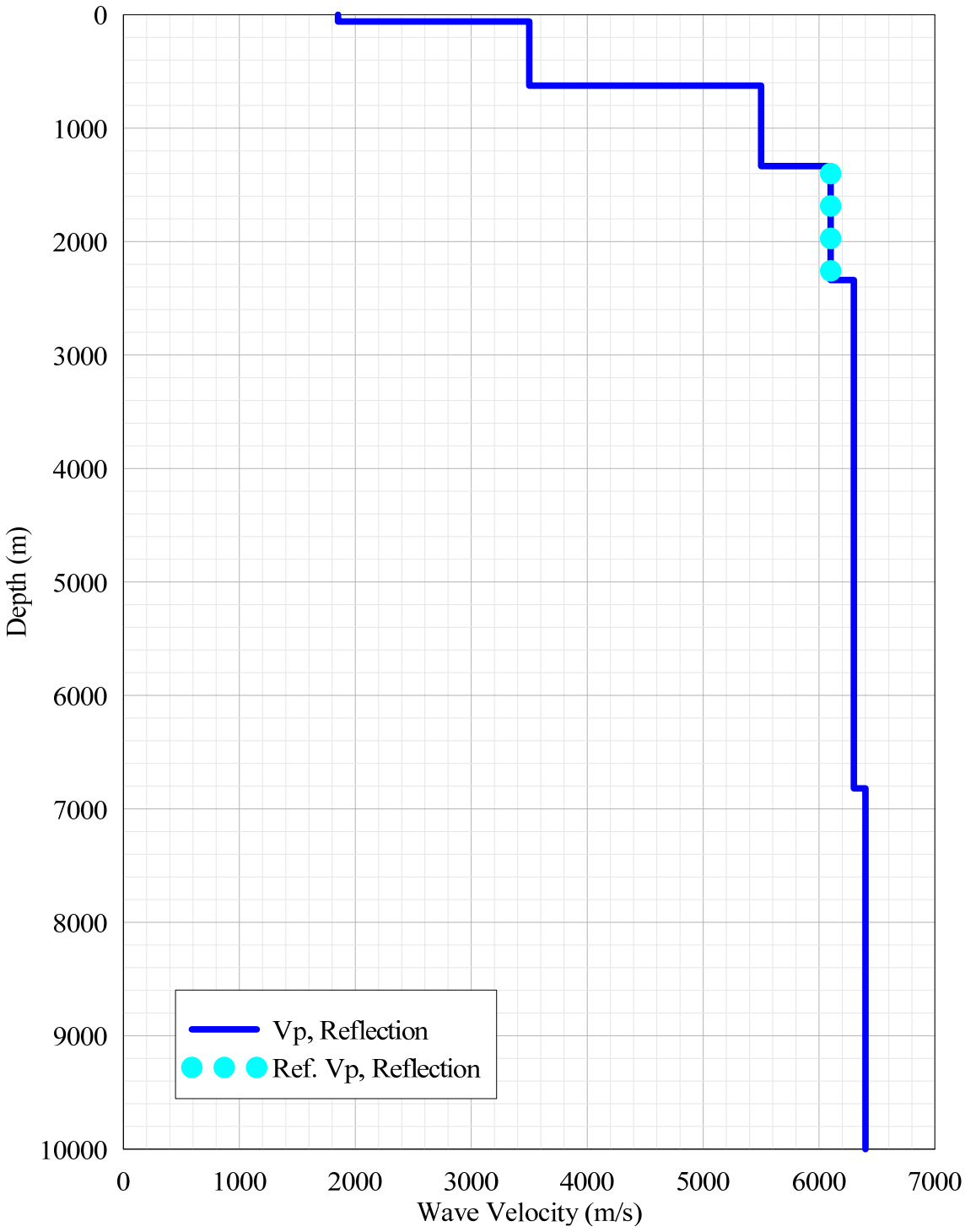

Figure A-31 Wave velocity at SP2 [Luetgert et al. 1994].

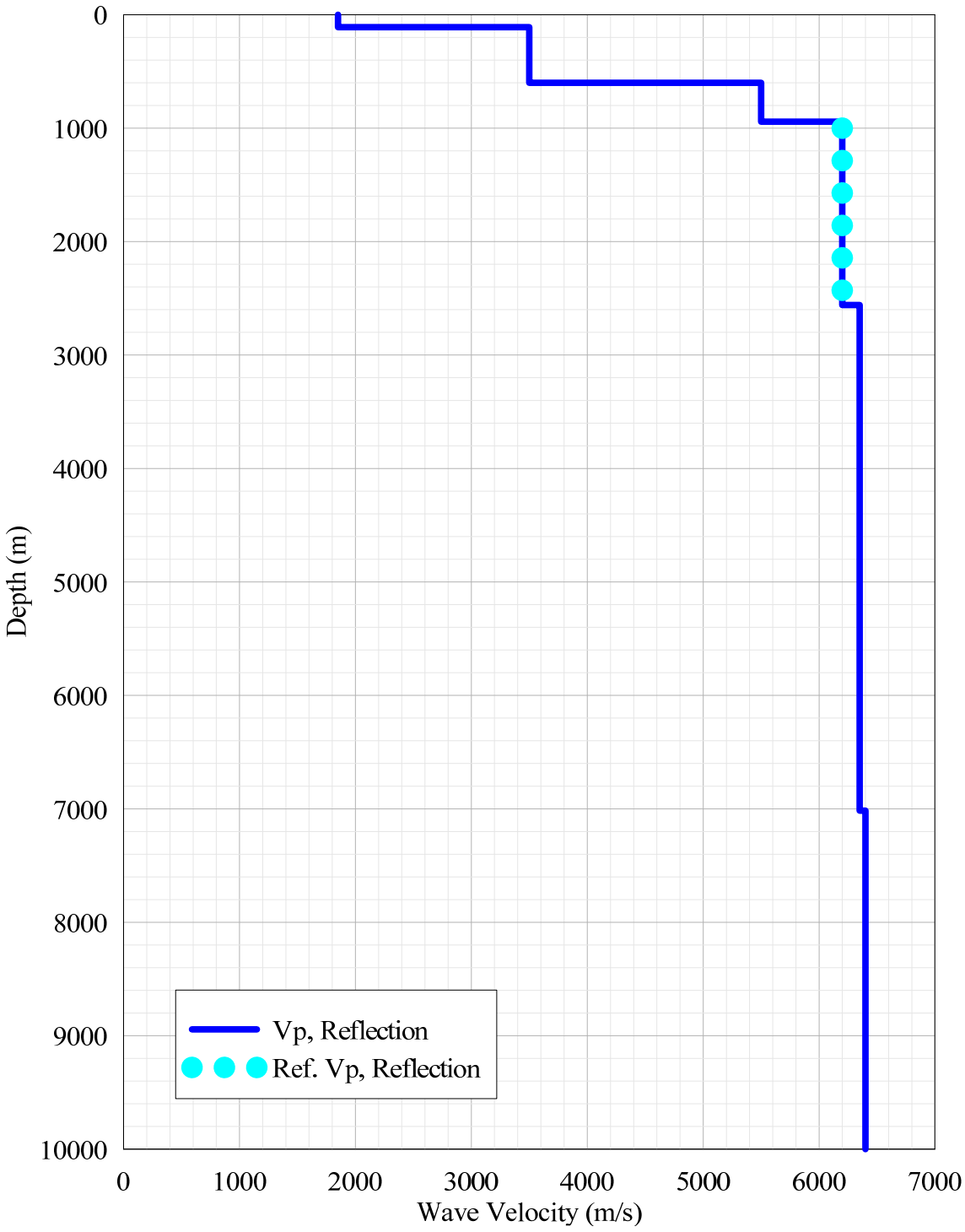

Figure A-32 Wave velocity at SP3 [Luetgert et al. 1994].

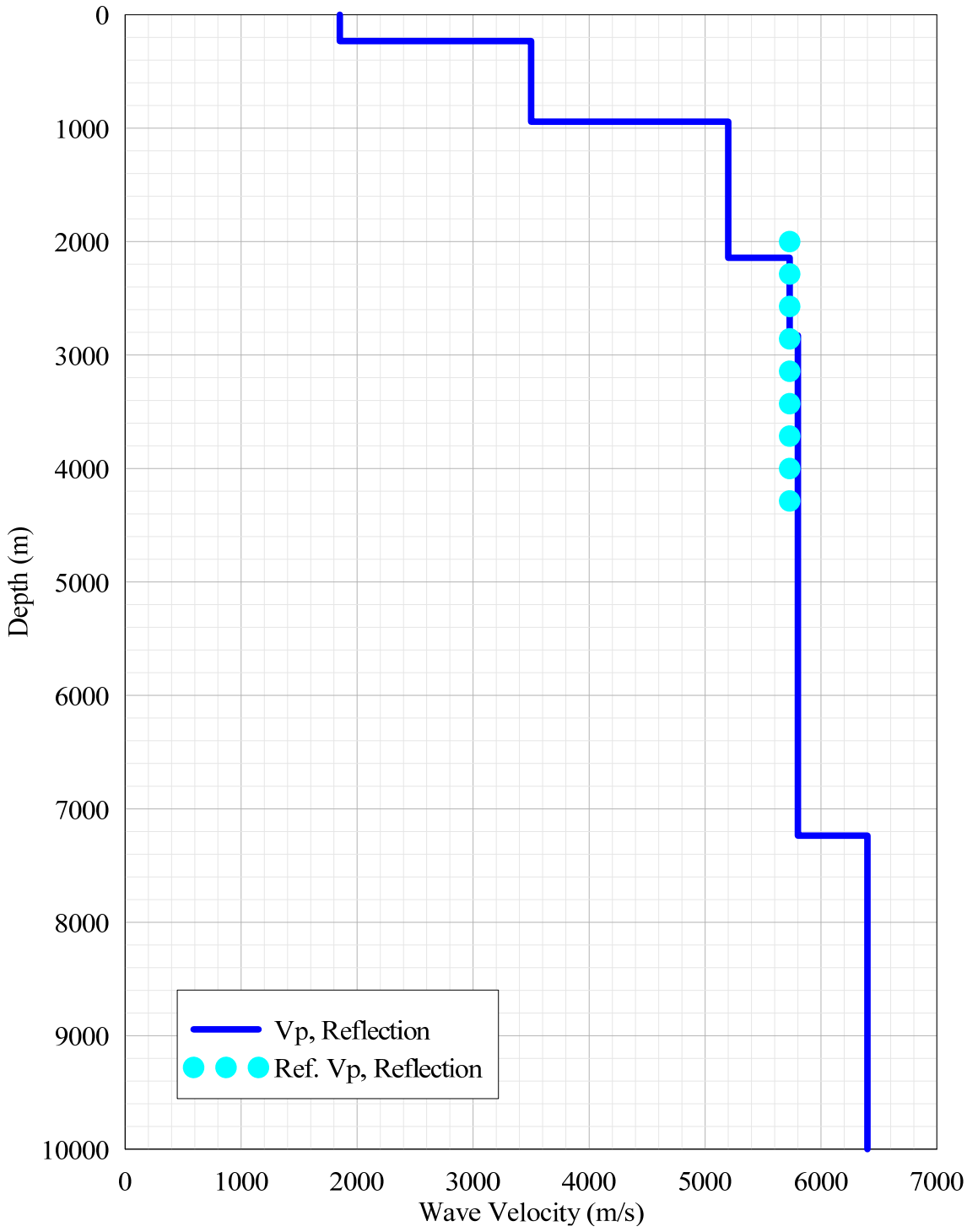

Figure A-33 Wave velocity at SP4 [Luetgert et al. 1994].

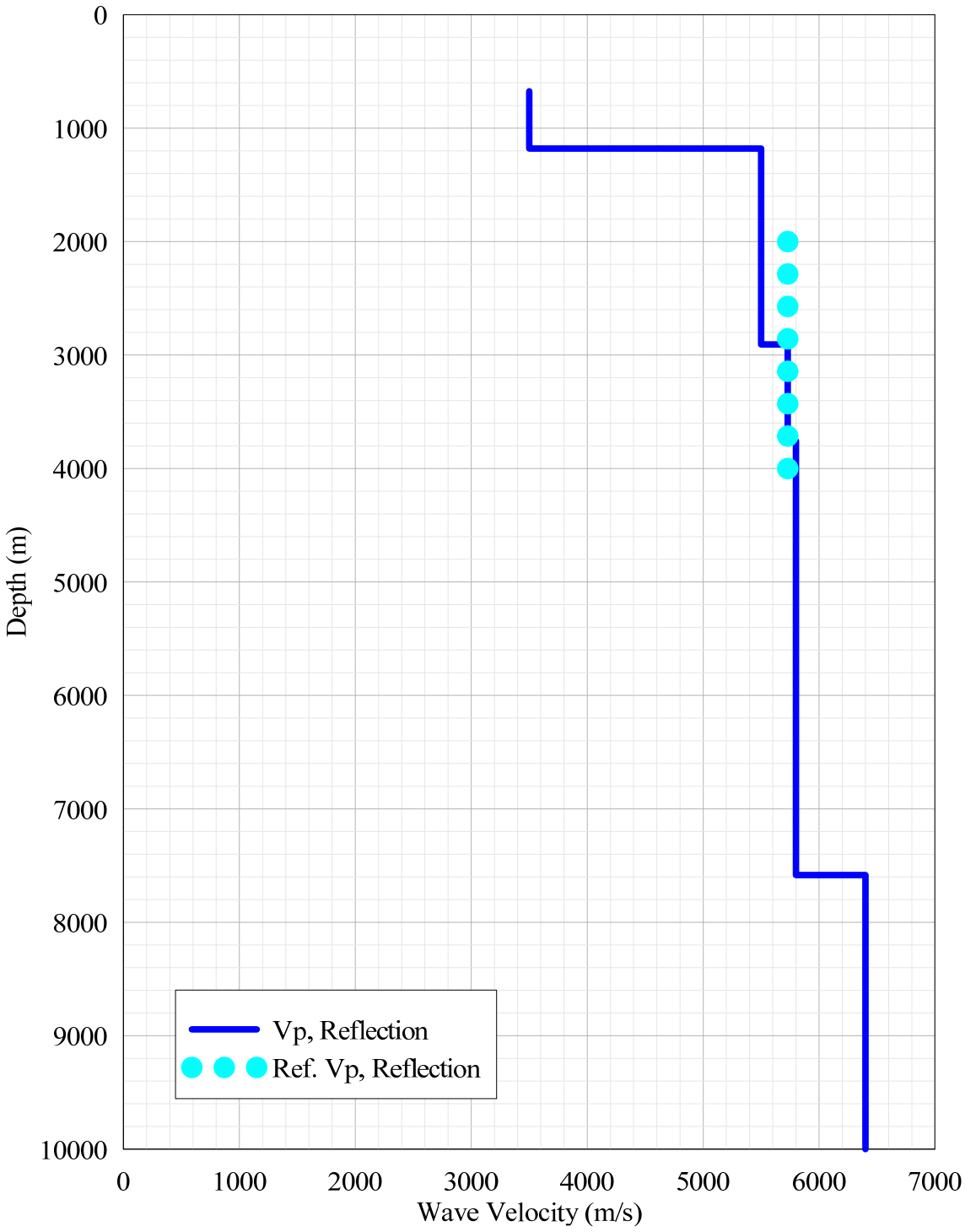

Figure A-34 Wave velocity at SP5 [Luetgert et al. 1994].

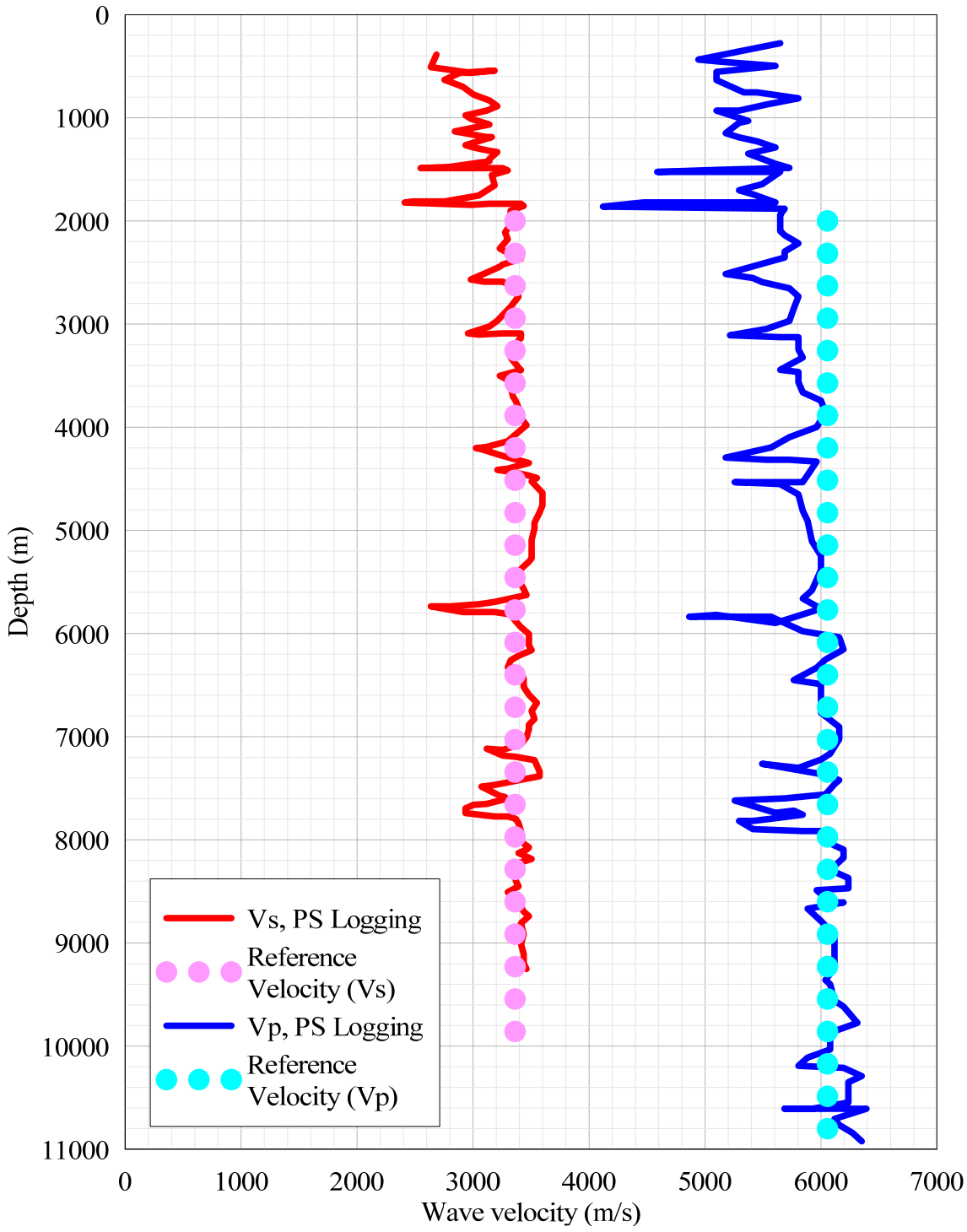

Figure A-35 Wave velocities at Monticello Reservoir [Moos and Zoback 1983, Figure 4].

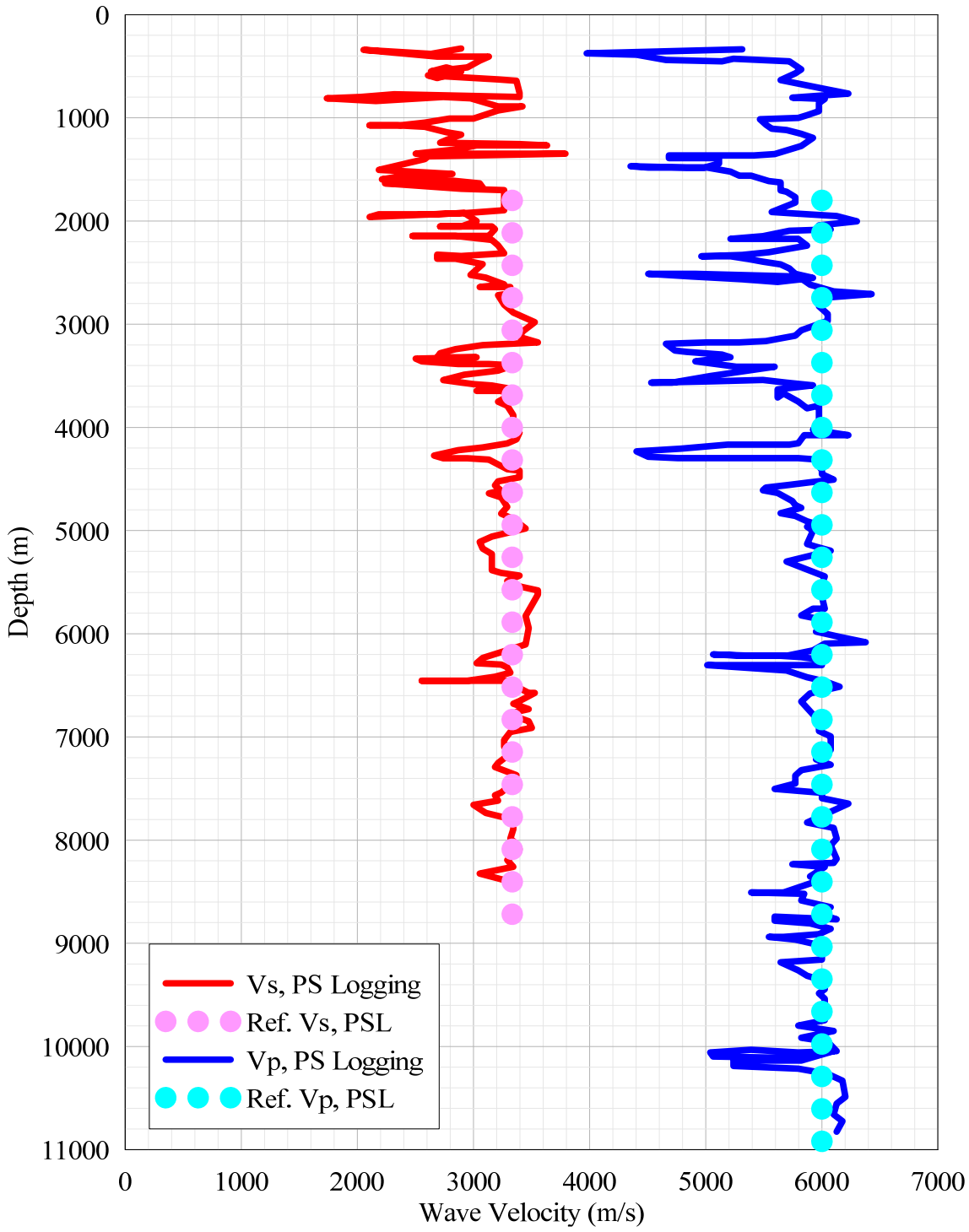

Figure A-36 Wave velocities at Monticello Reservoir [Moos and Zoback 1983, Figure 5].

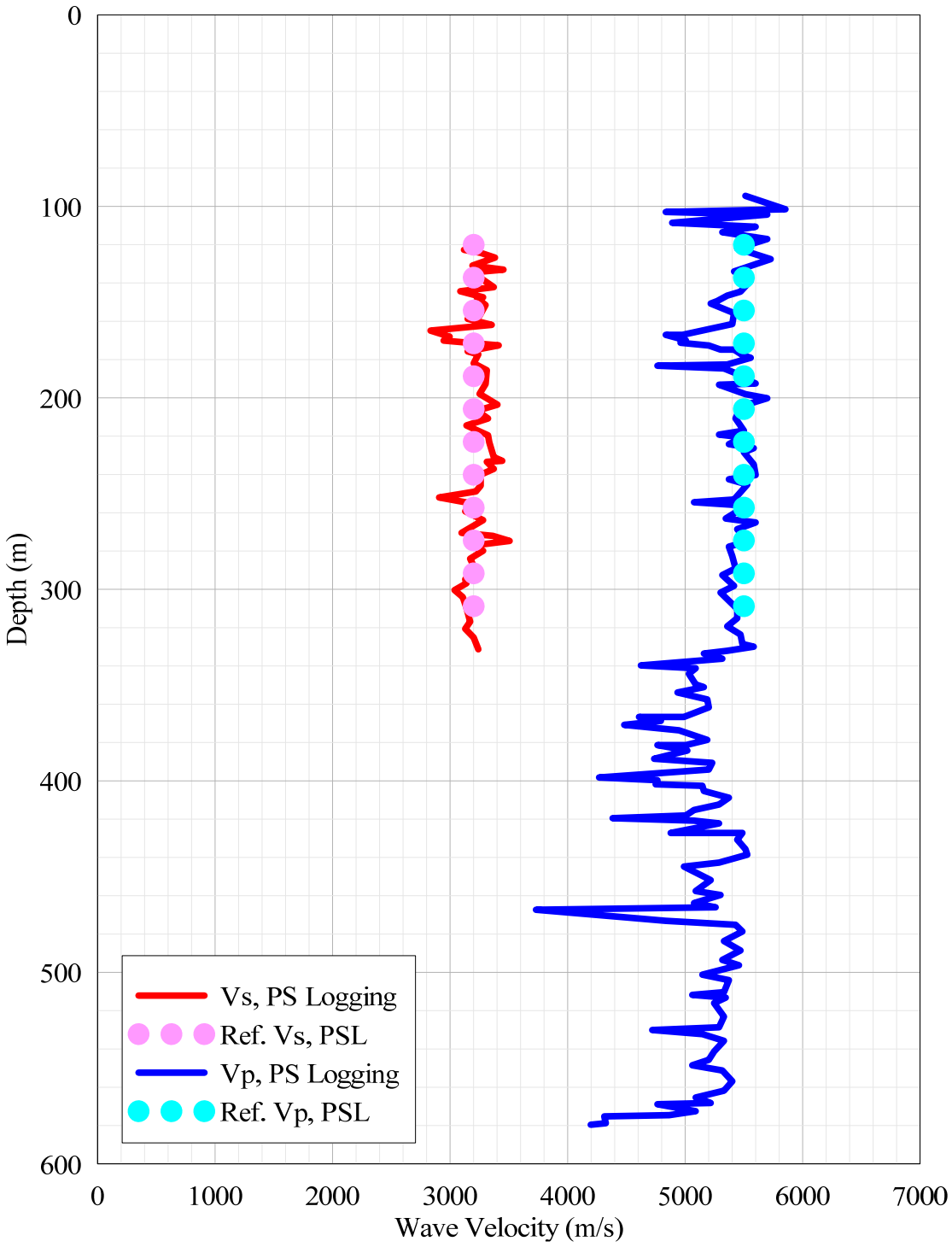

Figure A-37 Wave velocities at Monticello Reservoir [Moos and Zoback 1983, Figure 7].

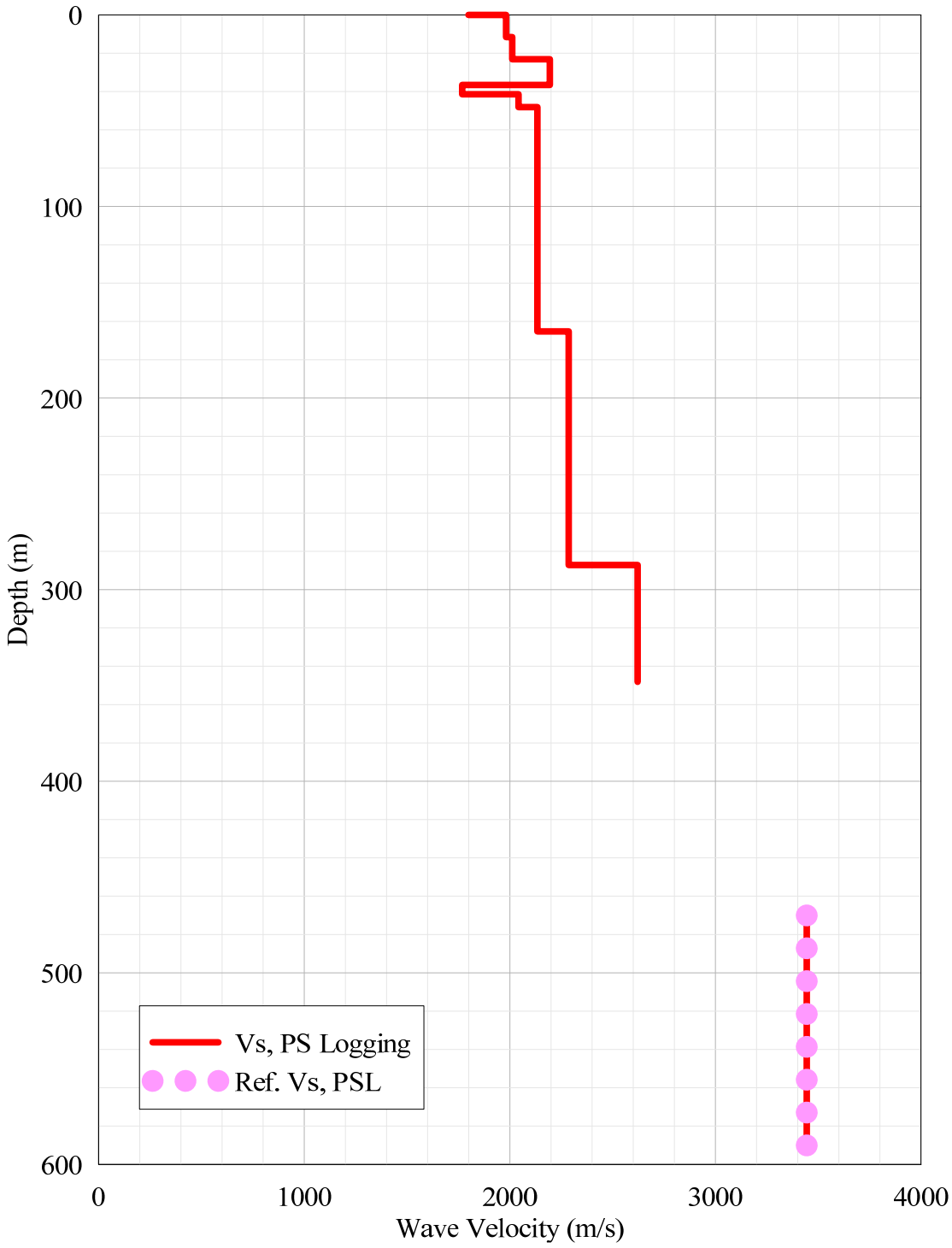

Figure A-38 Wave velocity at Nine Mile NPP (FSAR Table 2.5-58).

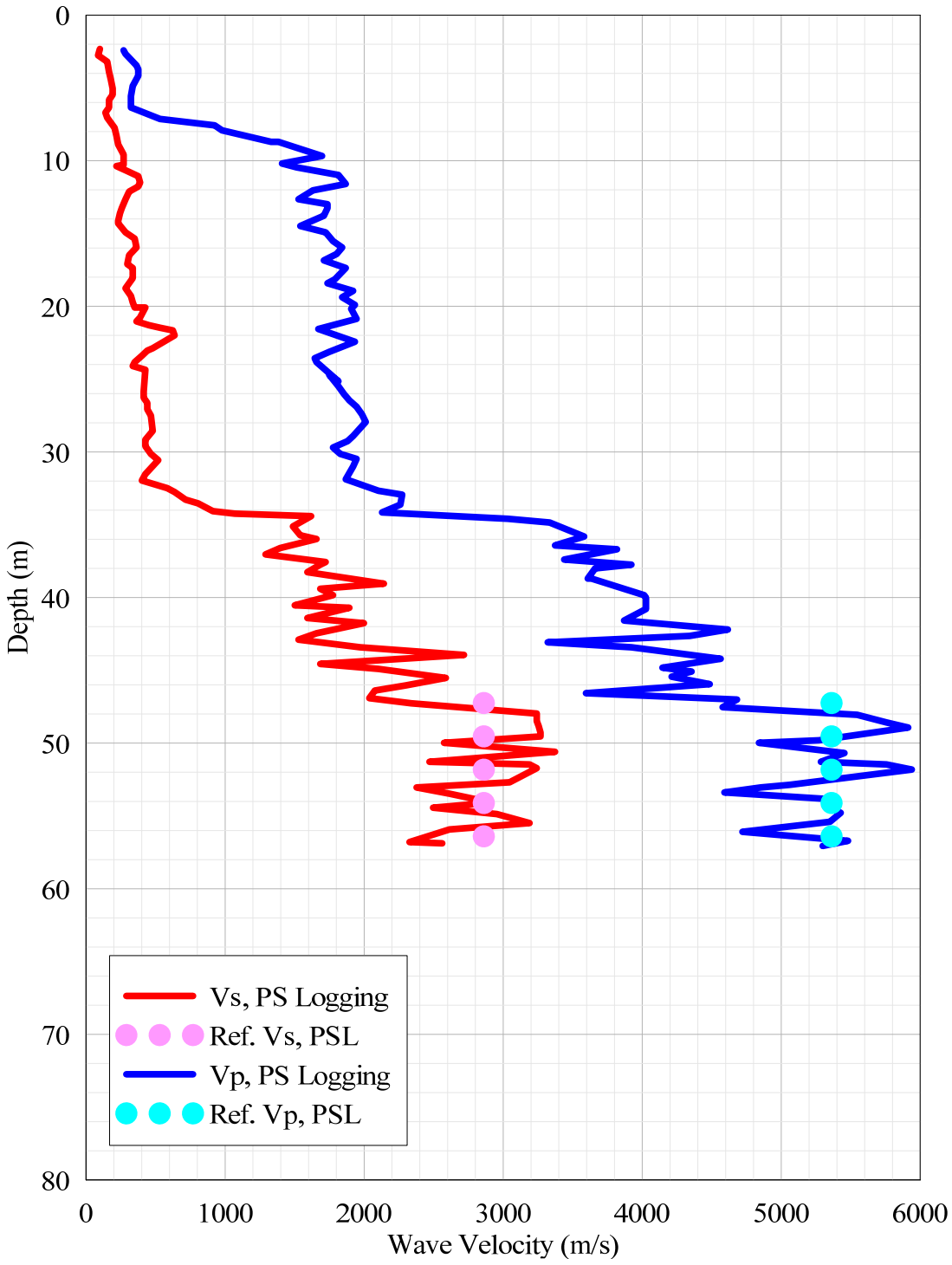

Figure A-39 Wave velocities at North Anna NPP (ESP Geophysics Figure 5).

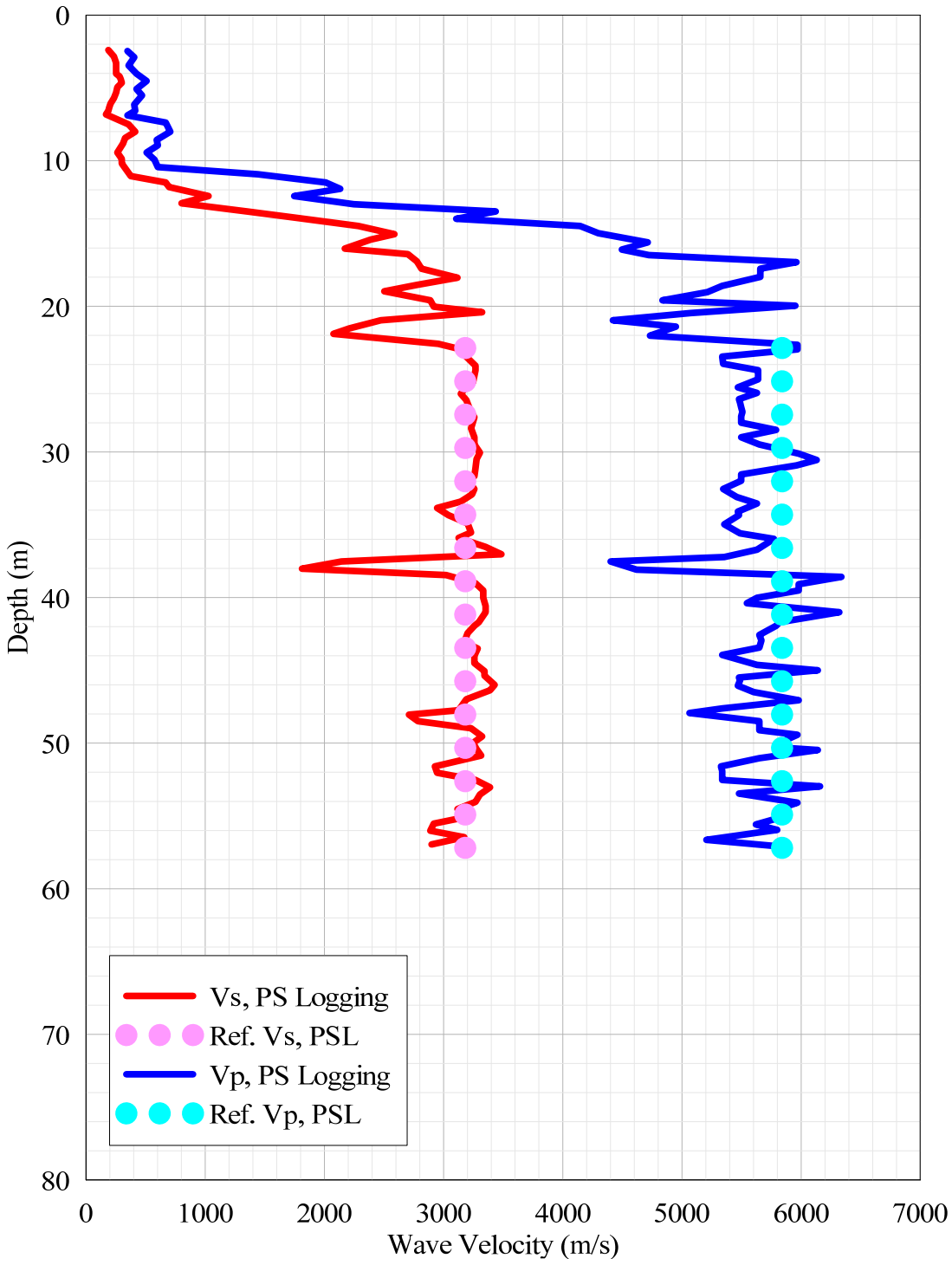

Figure A-40 Wave velocities at North Anna NPP (ESP Geophysics Figure 8).

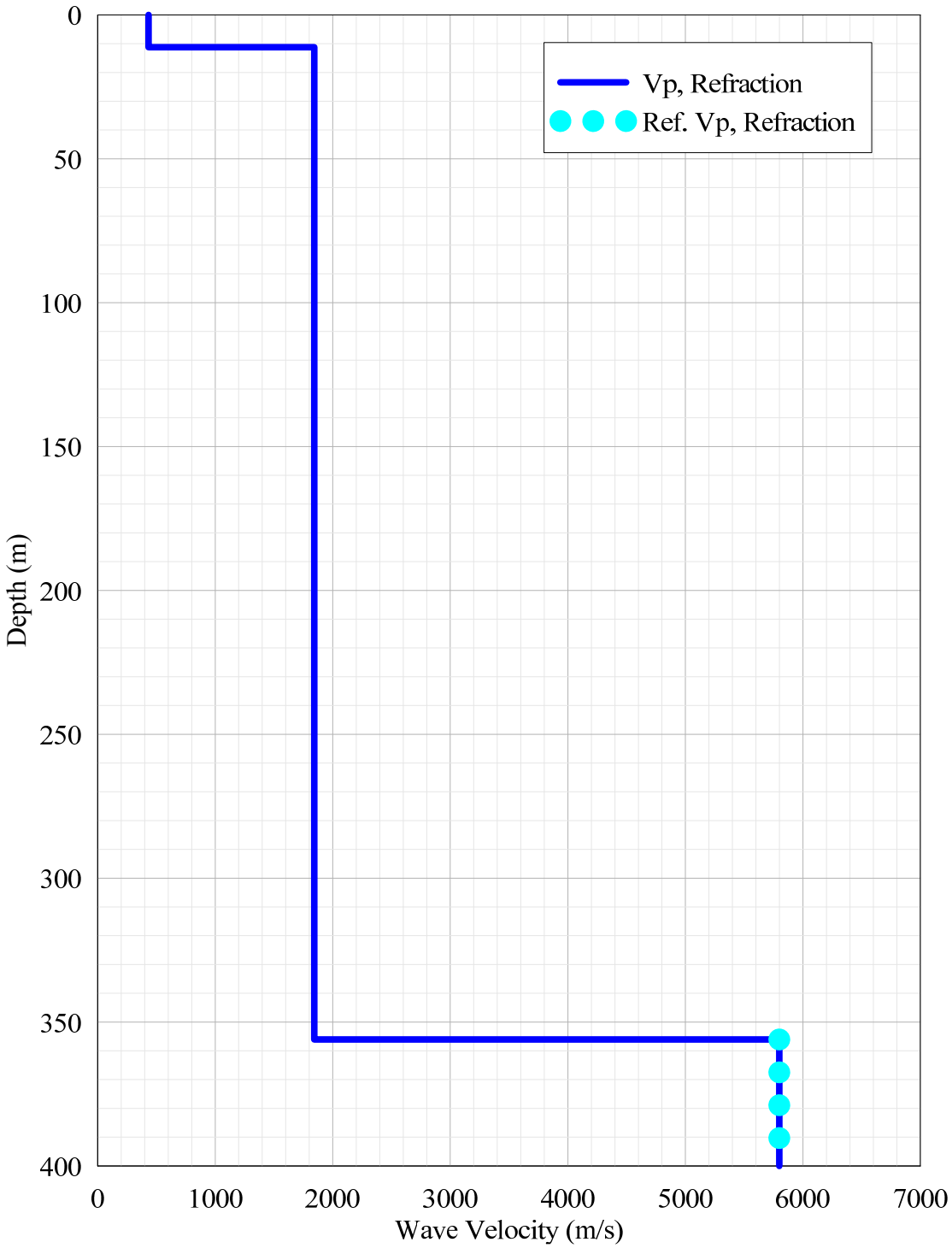

Figure A-41 Wave velocities at PSEG NPP (ESP, Figure 2.5.4.7-14, Line 1).

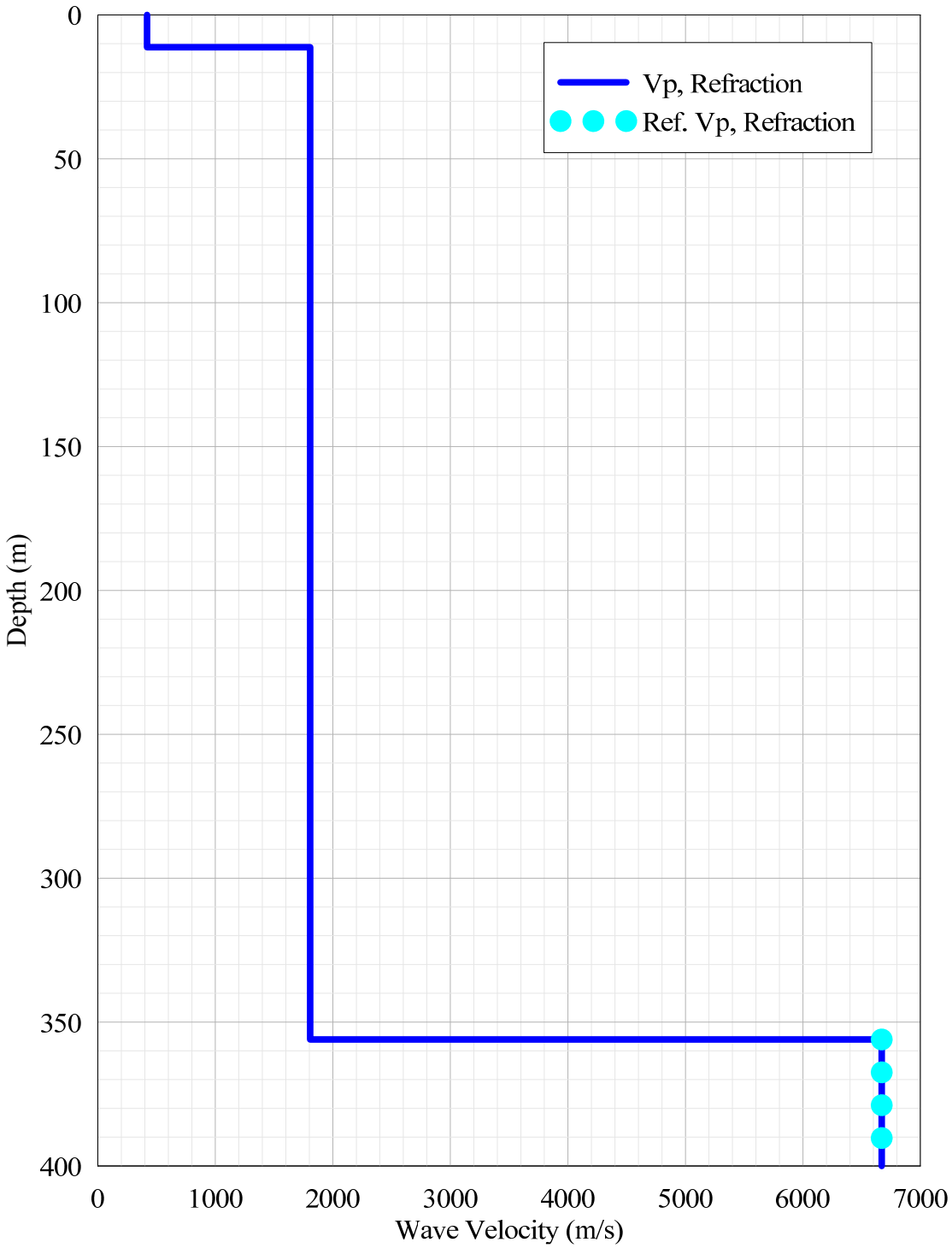

Figure A-42 Wave velocities at PSEG NPP (ESP, Figure 2.5.4.7-14, Line 2).

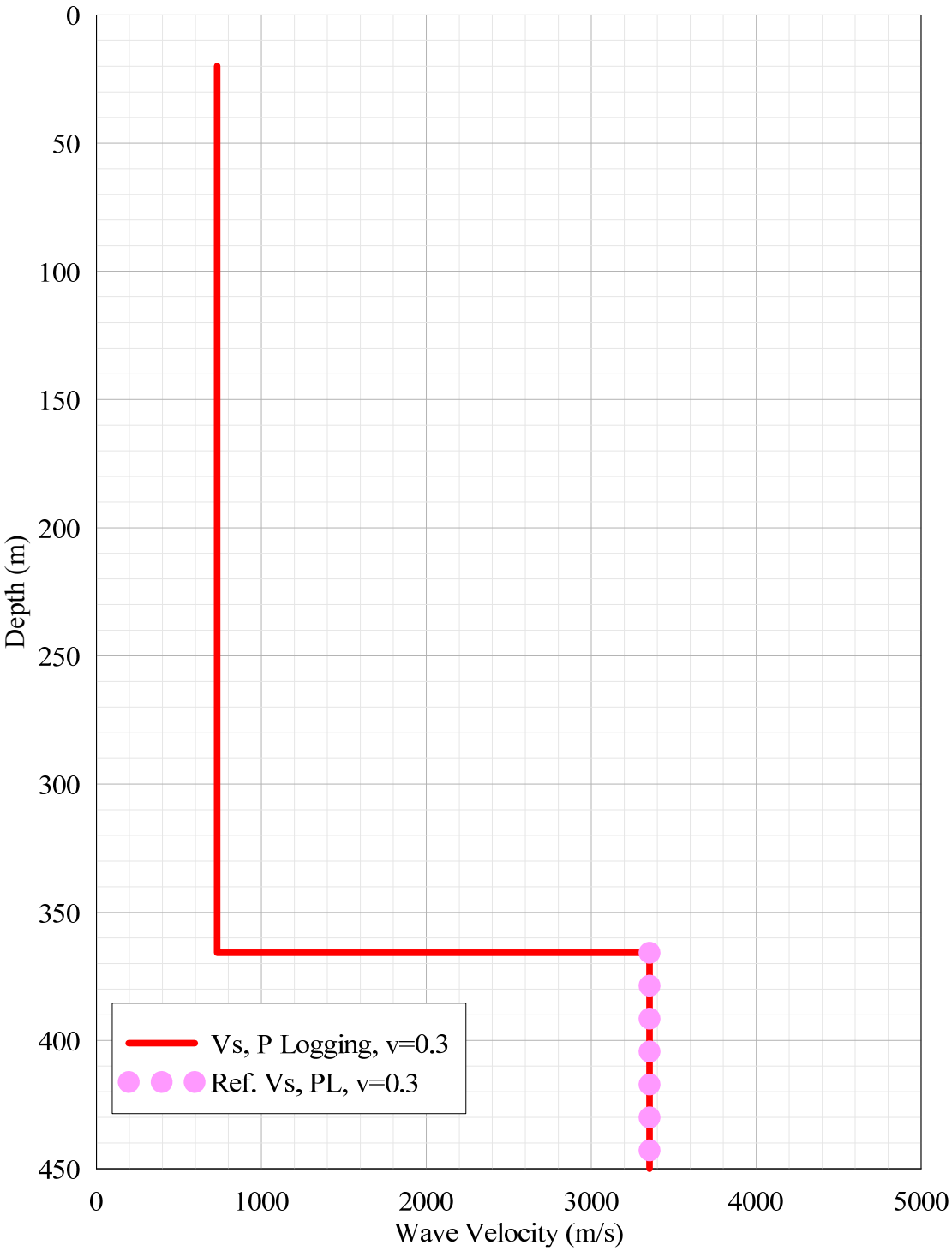

Figure A-43 Wave velocities at PSEG NPP (ESP, Figure 2.5.4.7-15).

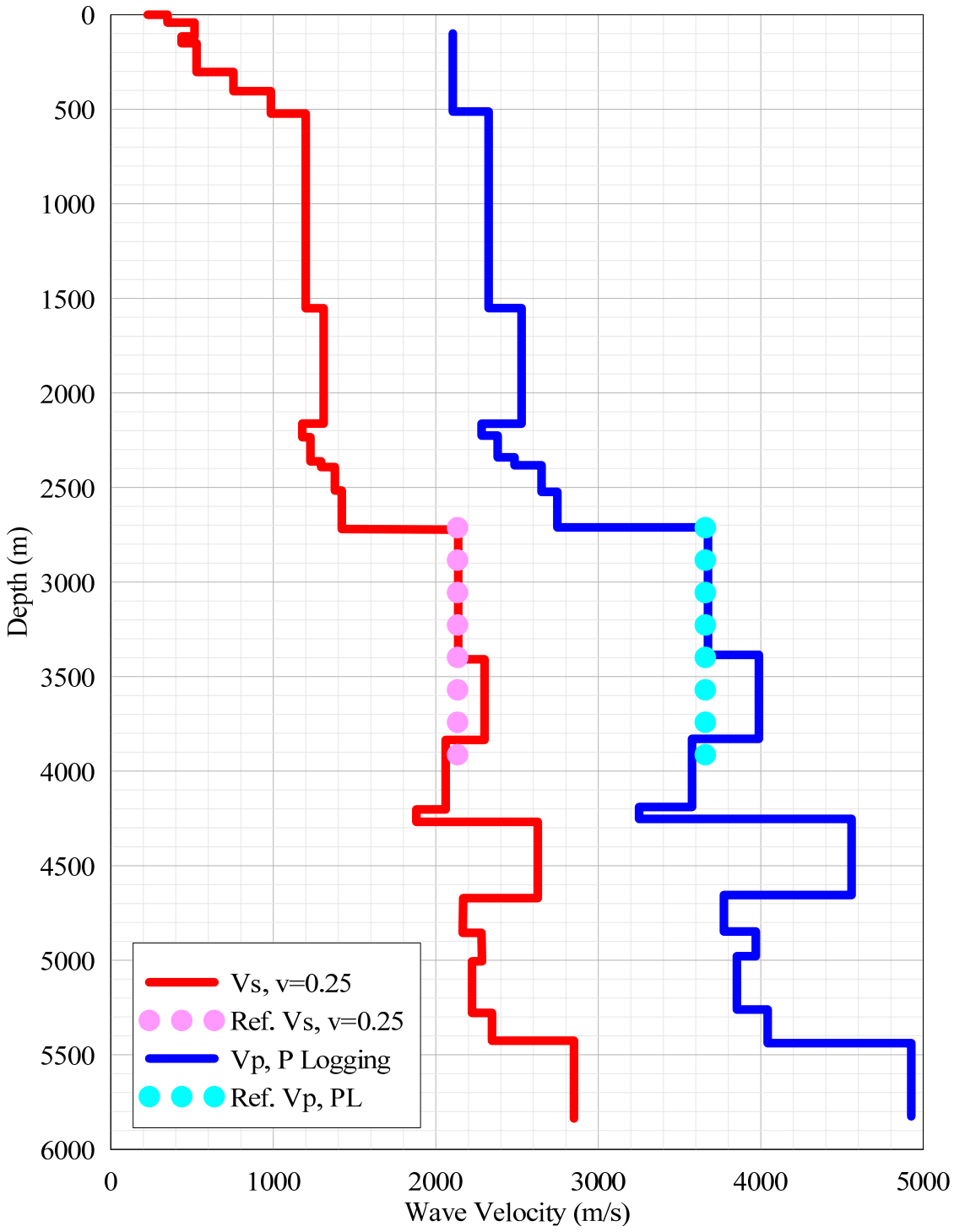

Figure A-44 Wave velocities at River Bend NPP (FSAR Figure 2.5.4-245).

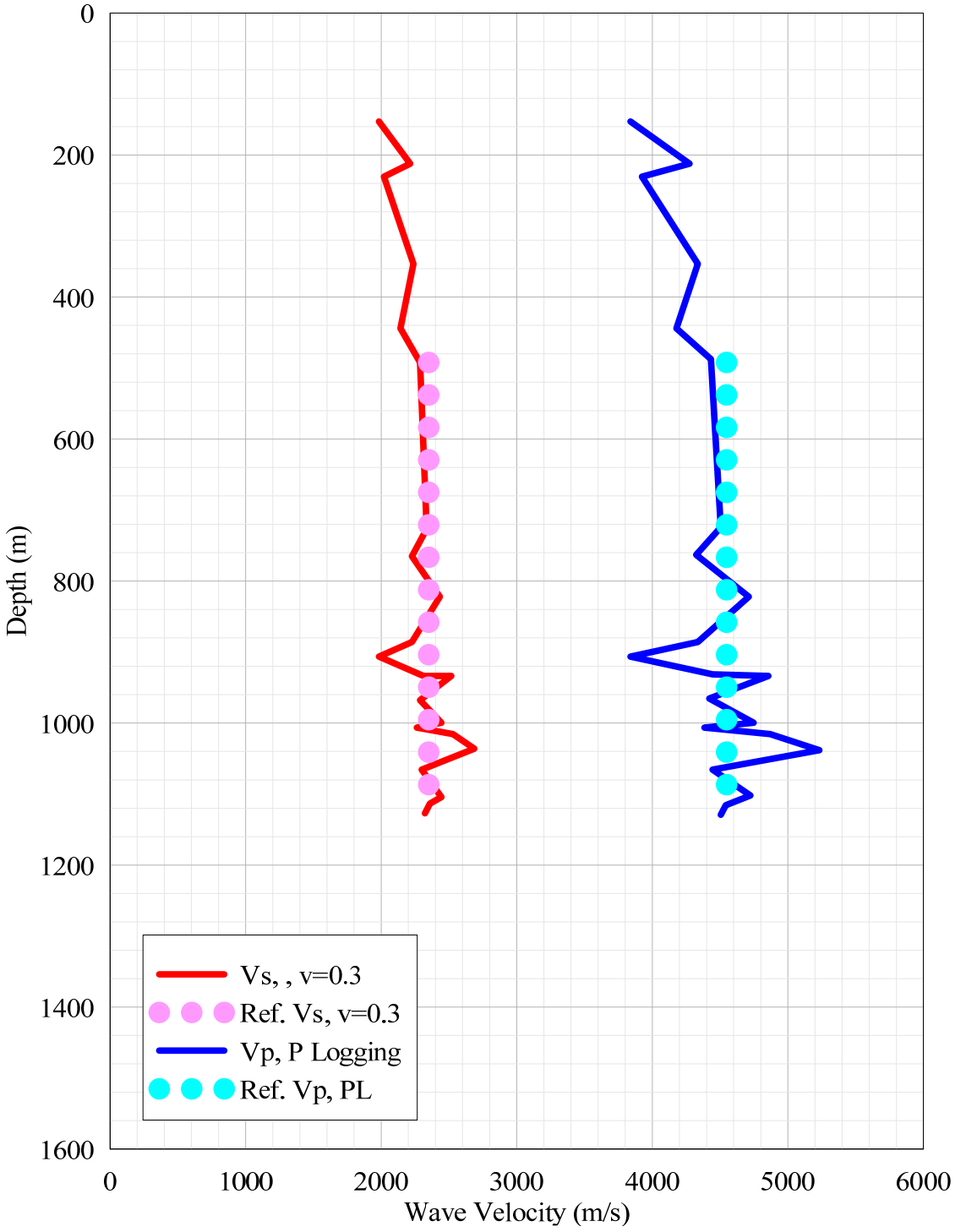

Figure A-45 Wave velocities at Shearon Harris NPP (Figure 2.5.2-262).

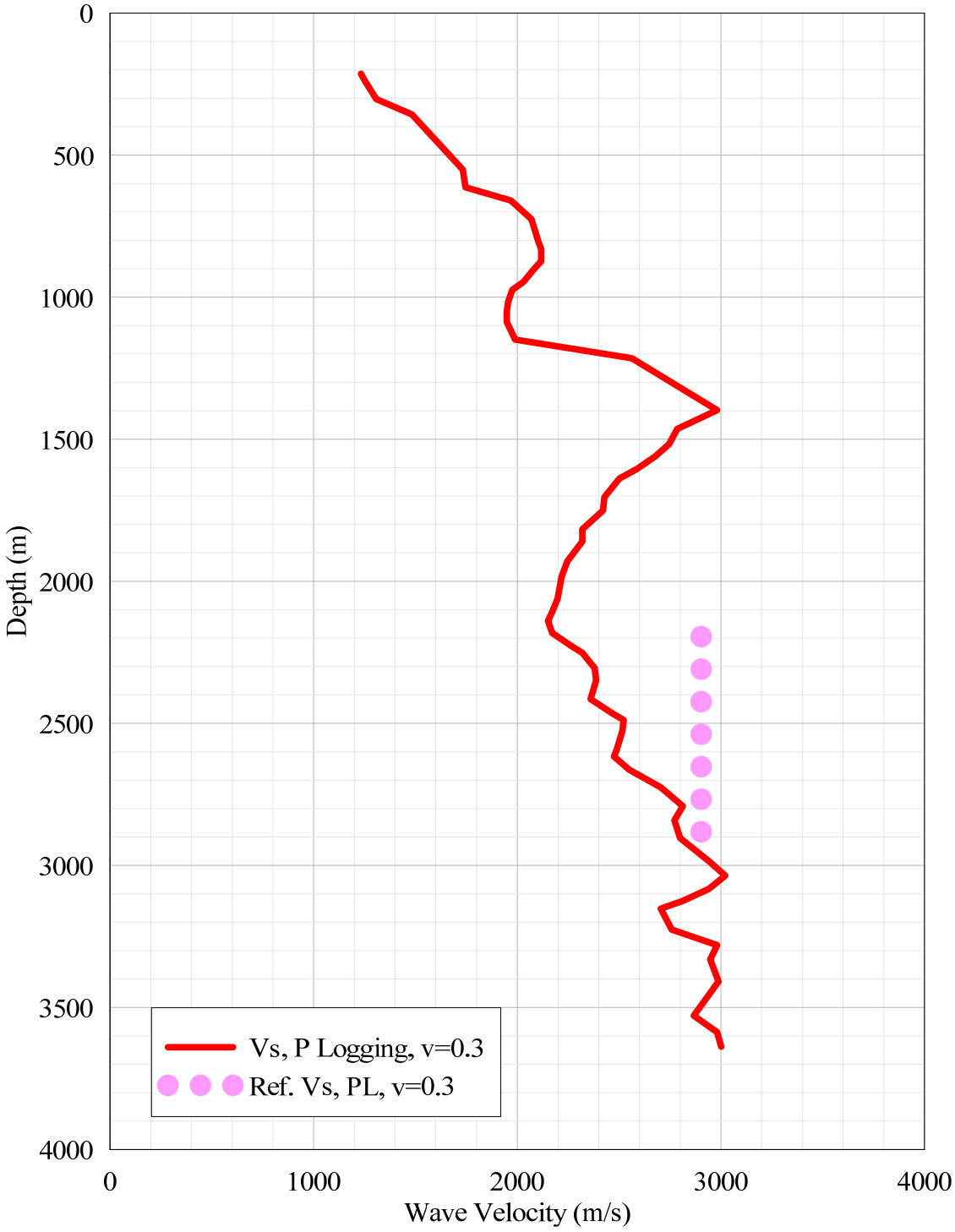

Figure A-46 Wave velocity at Turkey Point NPP (FSAR Figure 2.5.4-211).

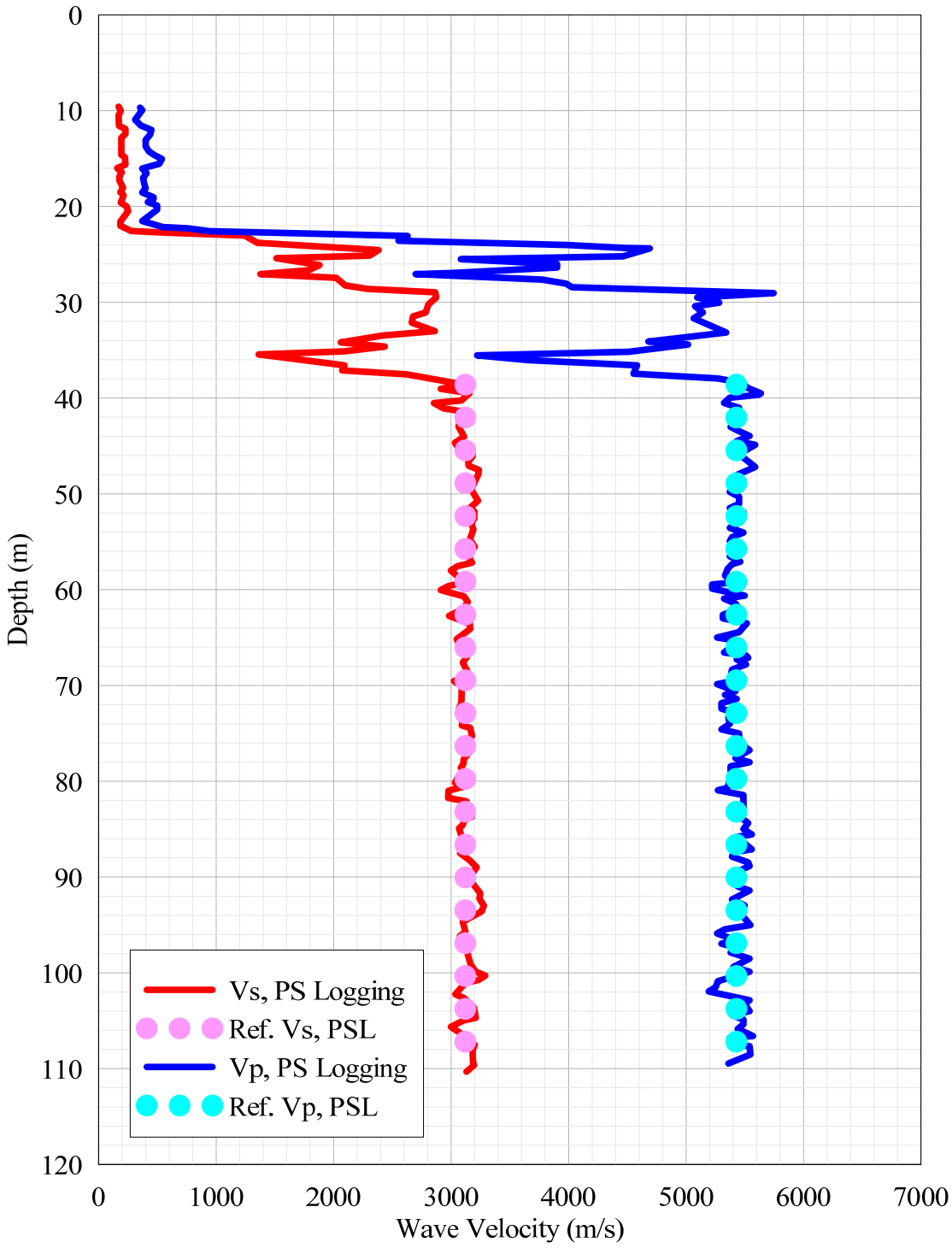

Figure A-47 Wave velocities at V.C. Summer NPP (FSAR Figure 2.5.4-224/225, BP-201).

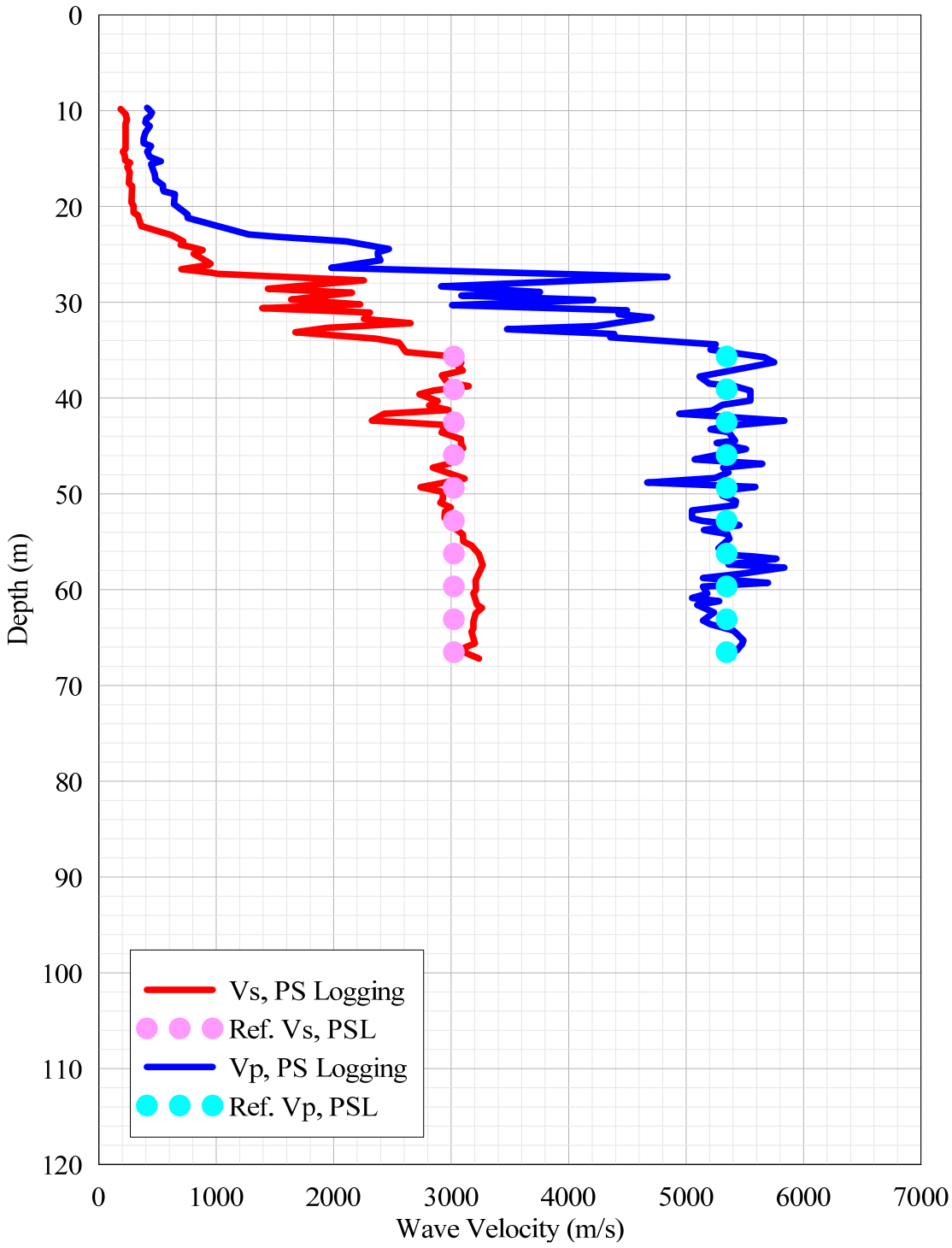

Figure A-48 Wave velocities at V.C. Summer NPP (FSAR Figure 2.5.4-224/225, BP-206).

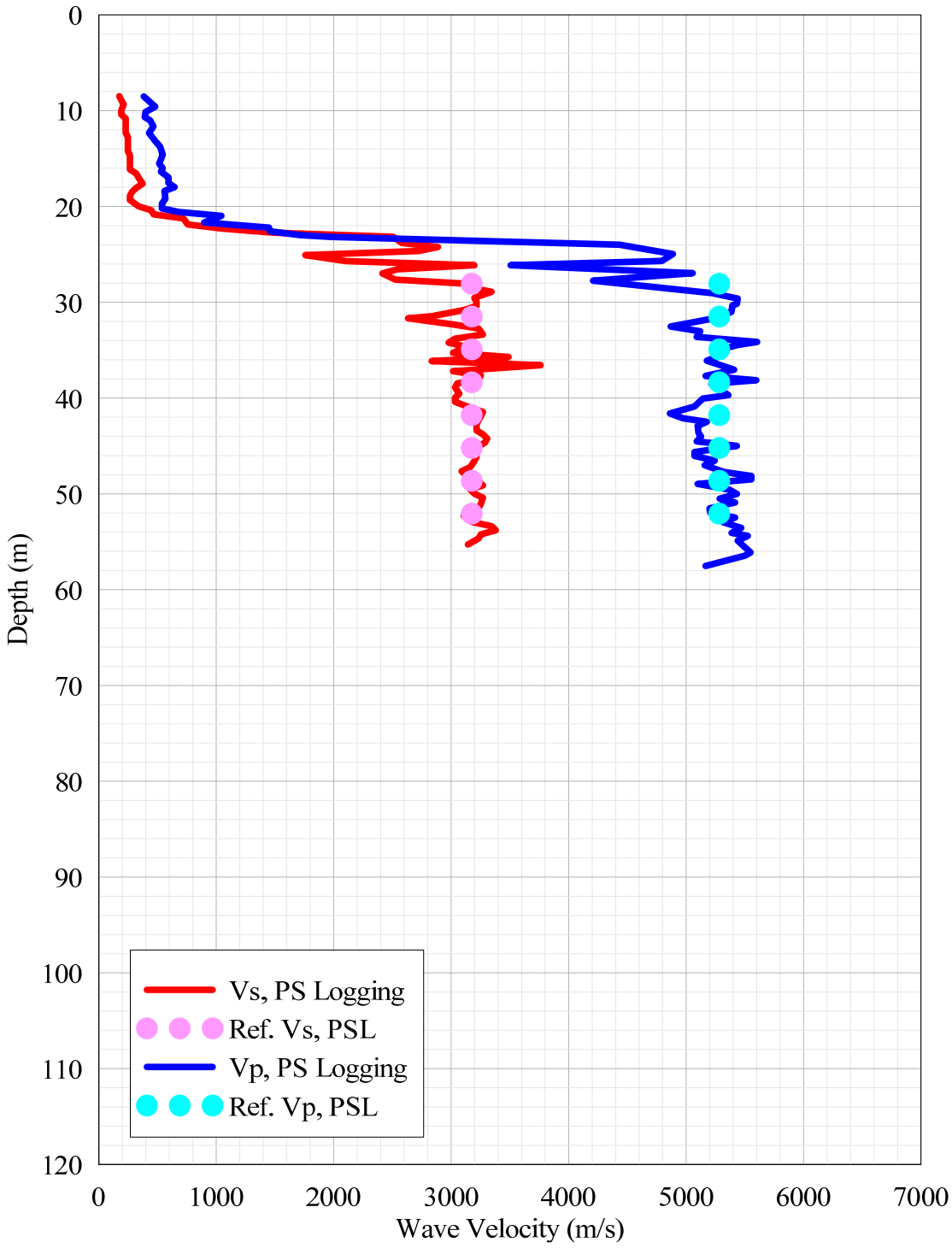

Figure A-49 Wave velocities at V.C. Summer NPP (FSAR Figure 2.5.4-224/225, BP-207).

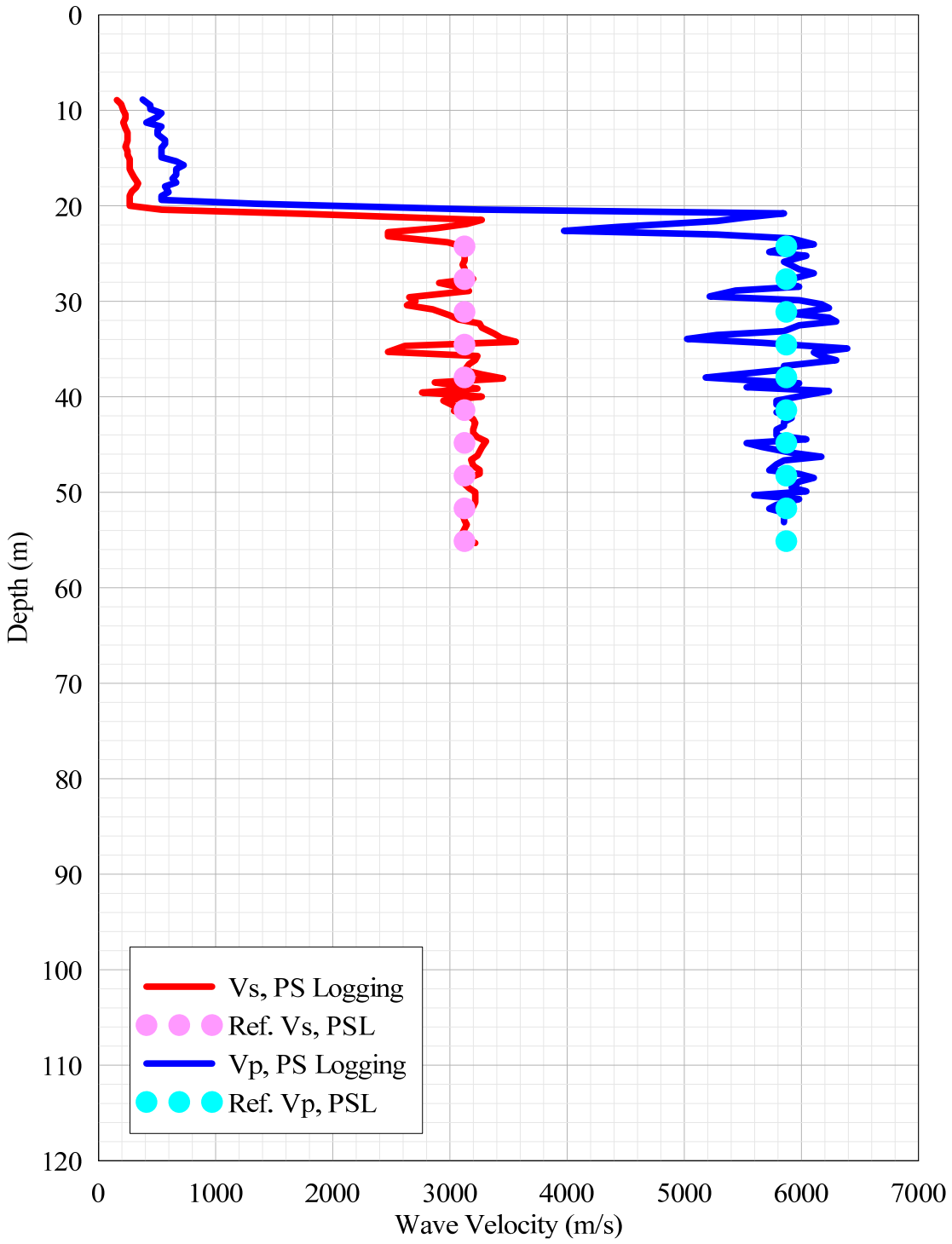

Figure A-50 Wave velocities at V.C. Summer NPP (FSAR Figure 2.5.4-224/225, BP-211).

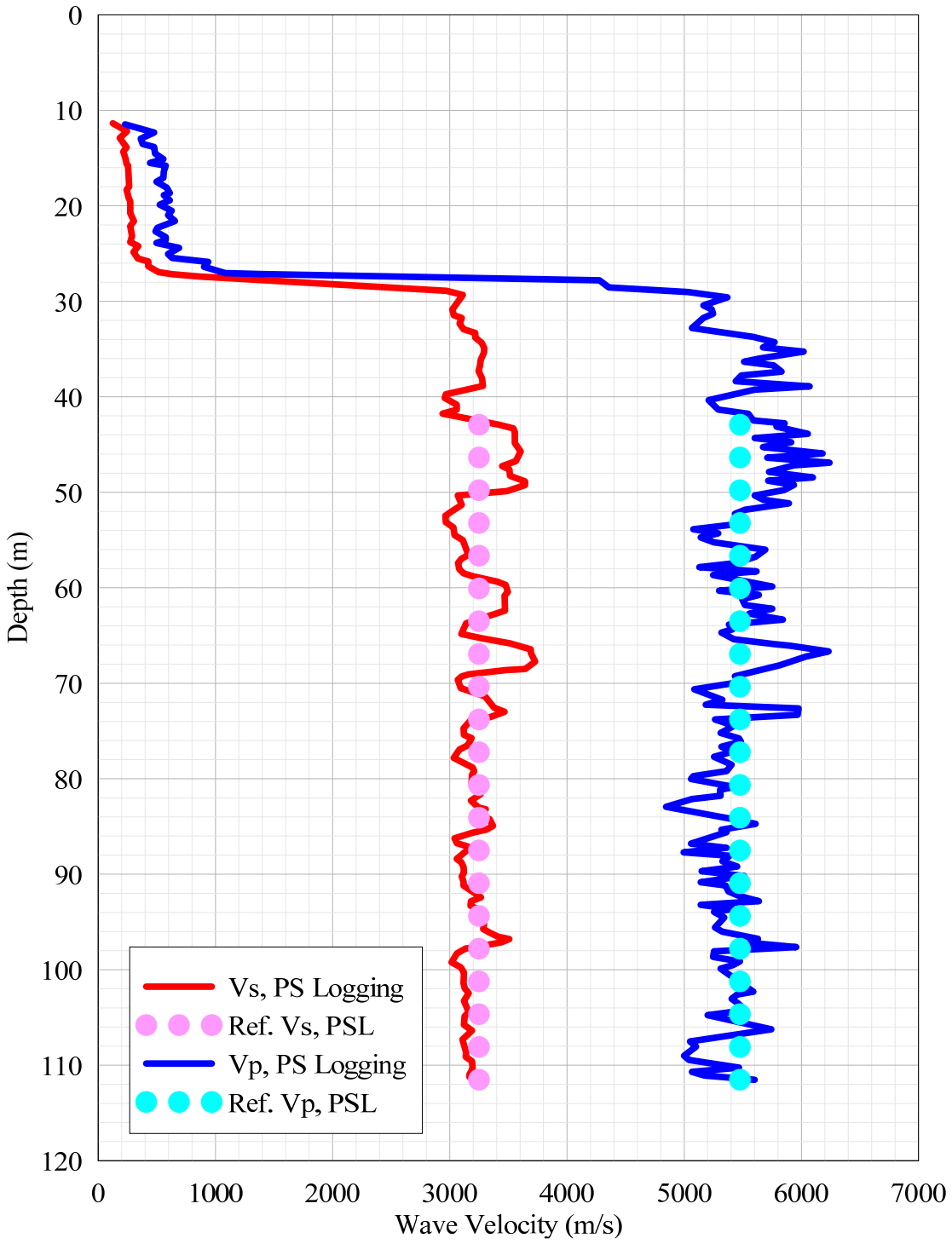

Figure A-51 Wave velocities at V.C. Summer NPP (FSAR Figure 2.5.4-224/225, BP-301).

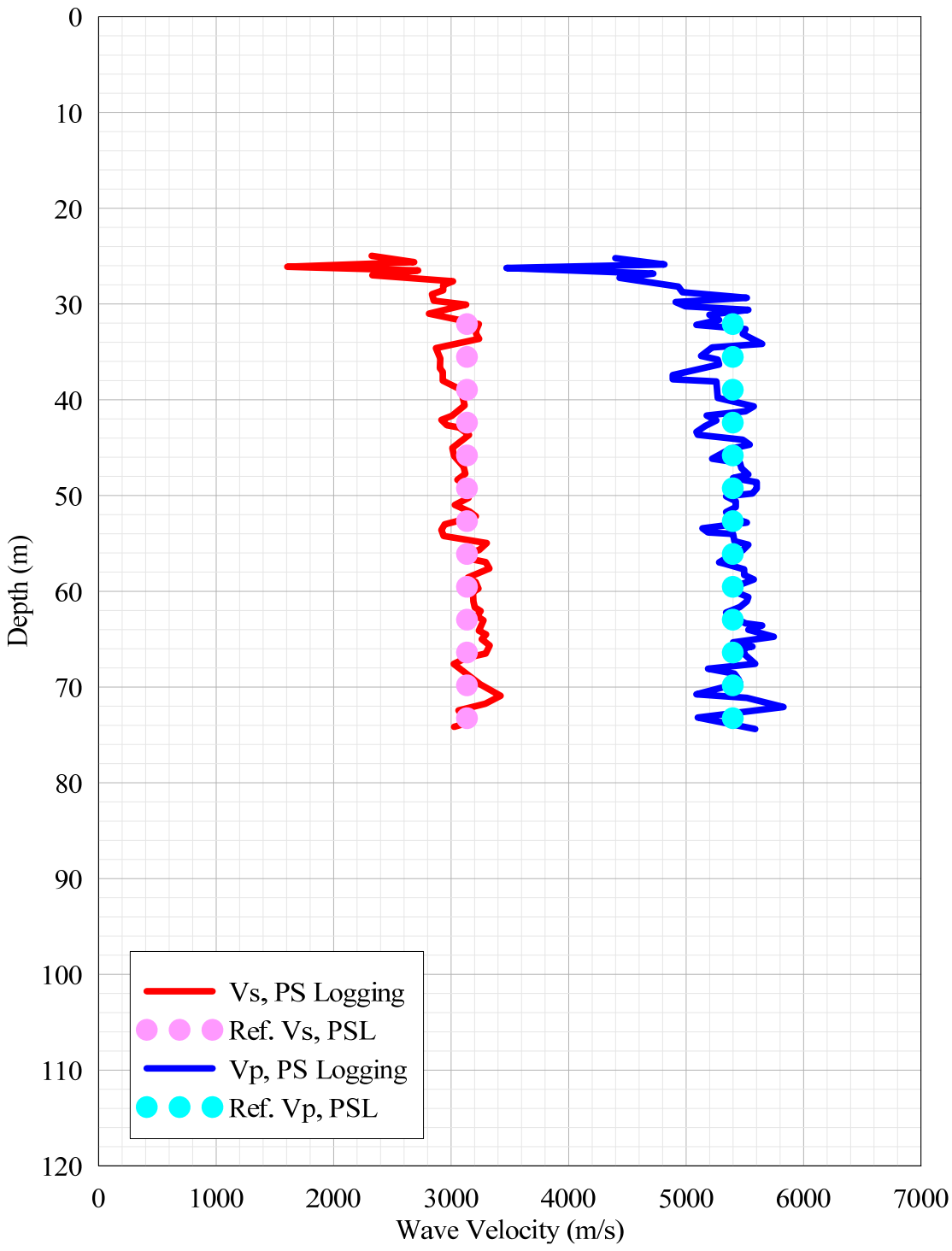

Figure A-52 Wave velocities at V.C. Summer NPP (FSAR Figure 2.5.4-224/225, BP-306).

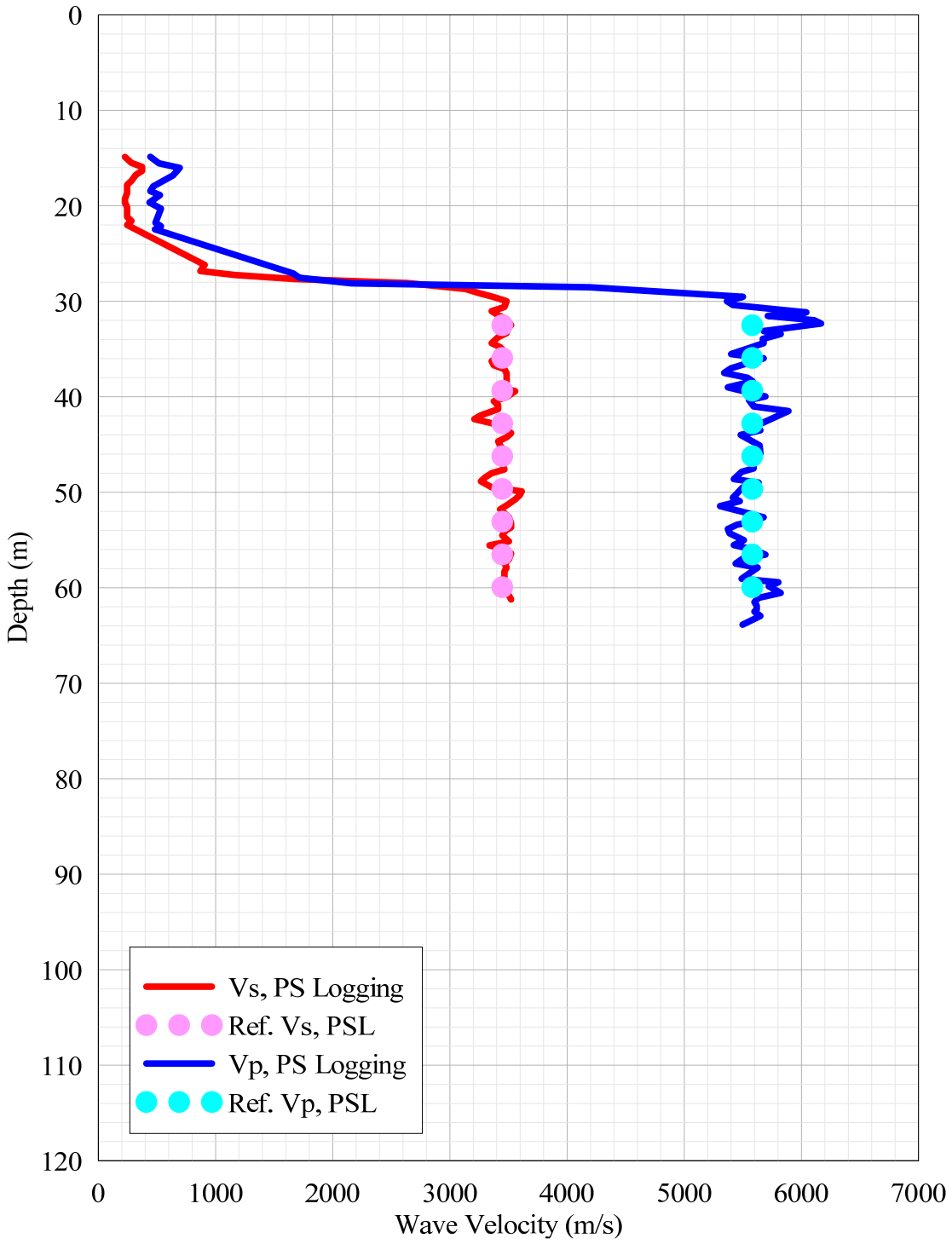

Figure A-53 Wave velocities at V.C. Summer NPP (FSAR Figure 2.5.4-224/225, BP-307).

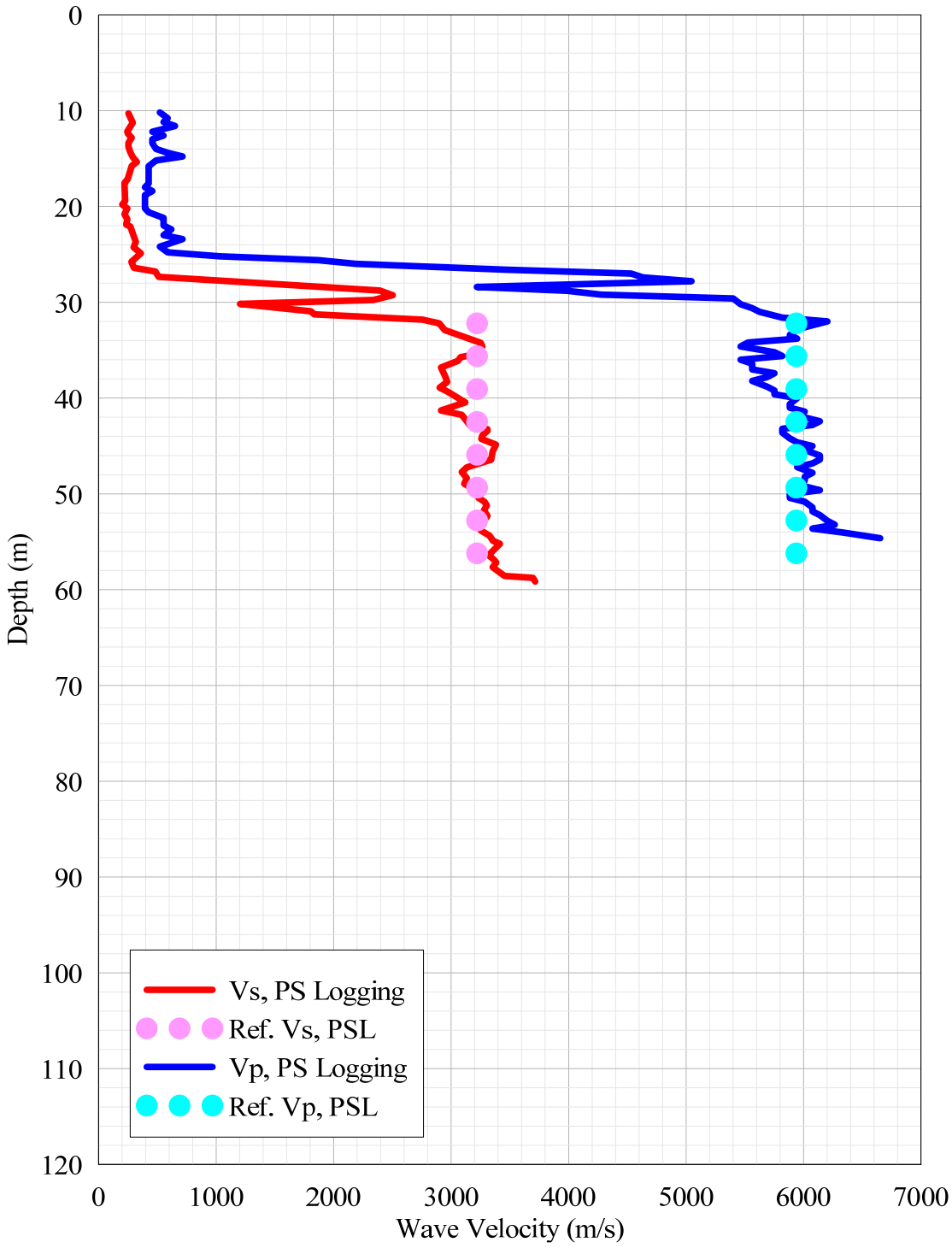

Figure A-54 Wave velocities at V.C. Summer NPP (FSAR Figure 2.5.4-224/225, BP-311).

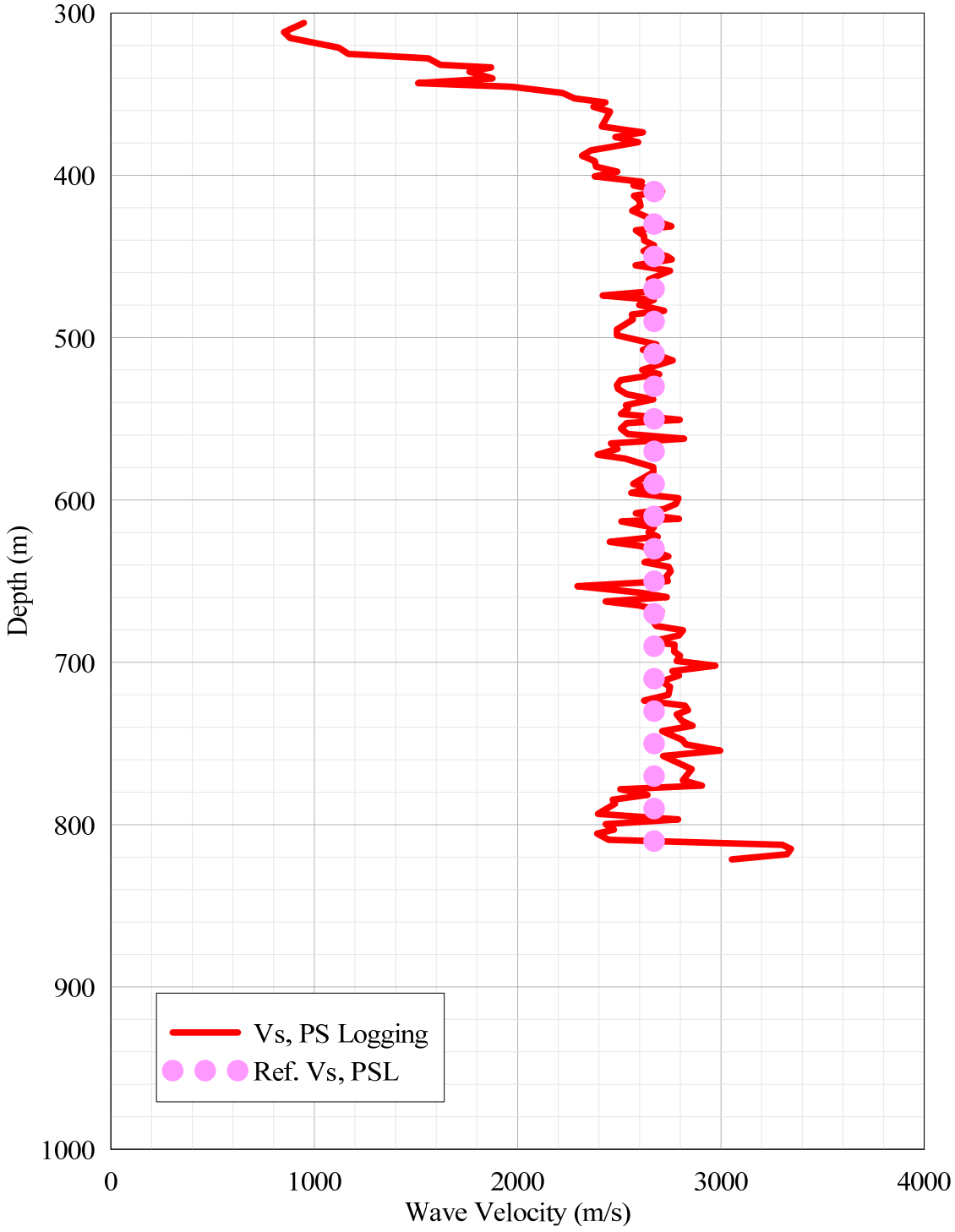

Figure A-55 Wave velocity at Vogtle NPP (DRB-9) (FSAR Figure 2.5.4-8).

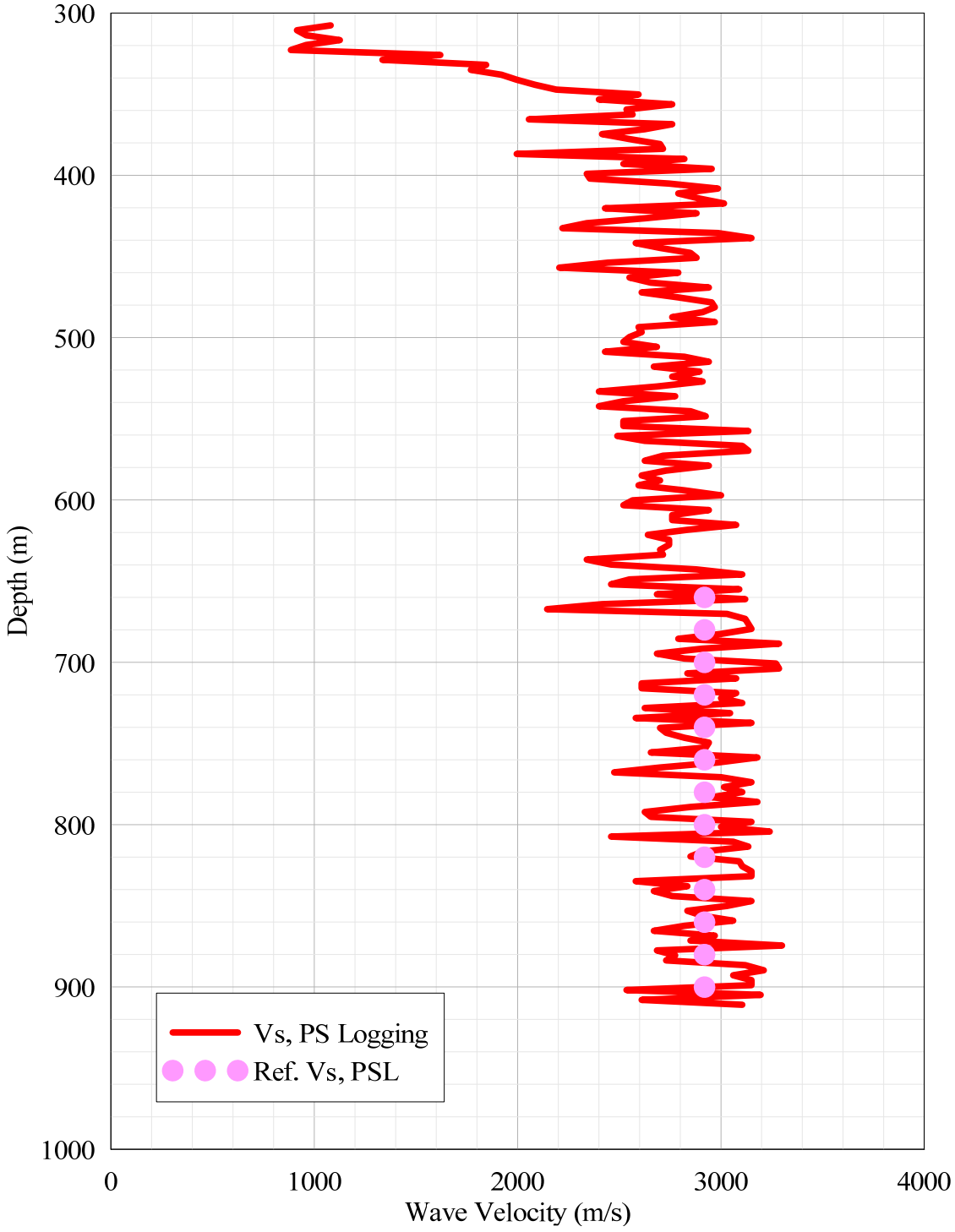

Figure A-56 Wave velocity at Vogtle NPP (DRB-10) (FSAR Figure 2.5.4-8).

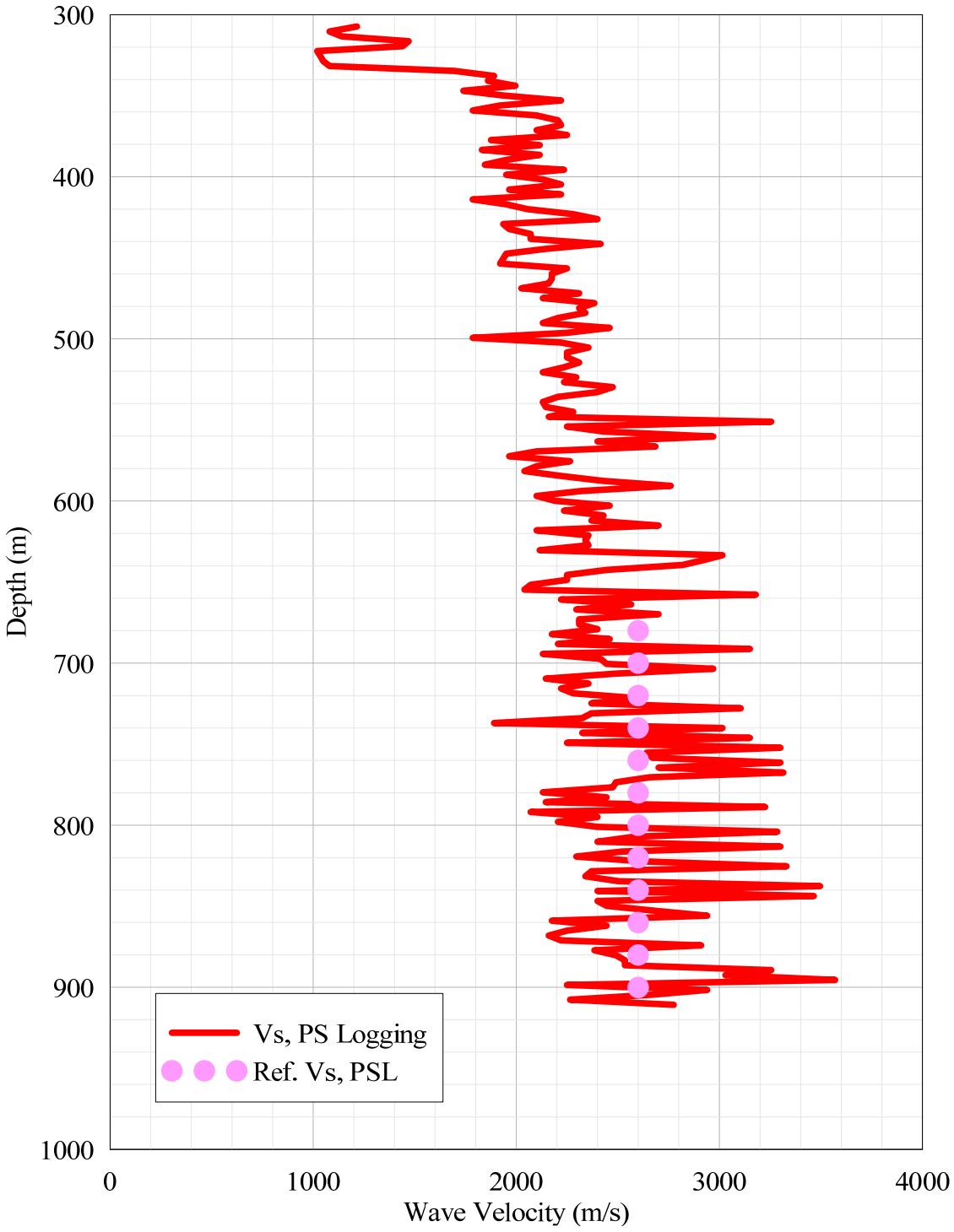

Figure A-57 Wave velocity at Vogtle NPP (DRB-11) (FSAR Figure 2.5.4-8).

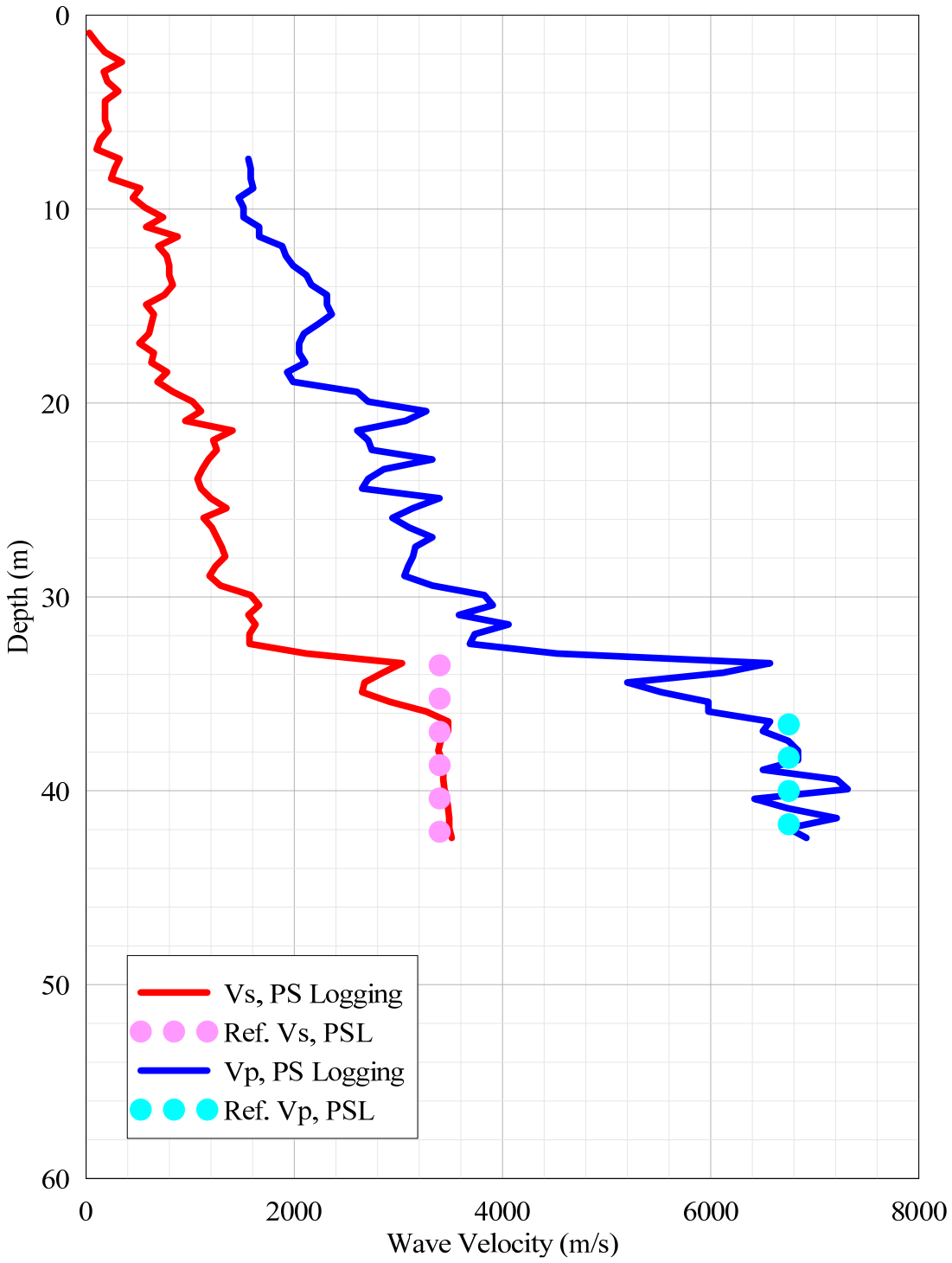

Figure A-58 Wave velocities at William States Lee III NPP (FSAR Figure 2.5.4-219).

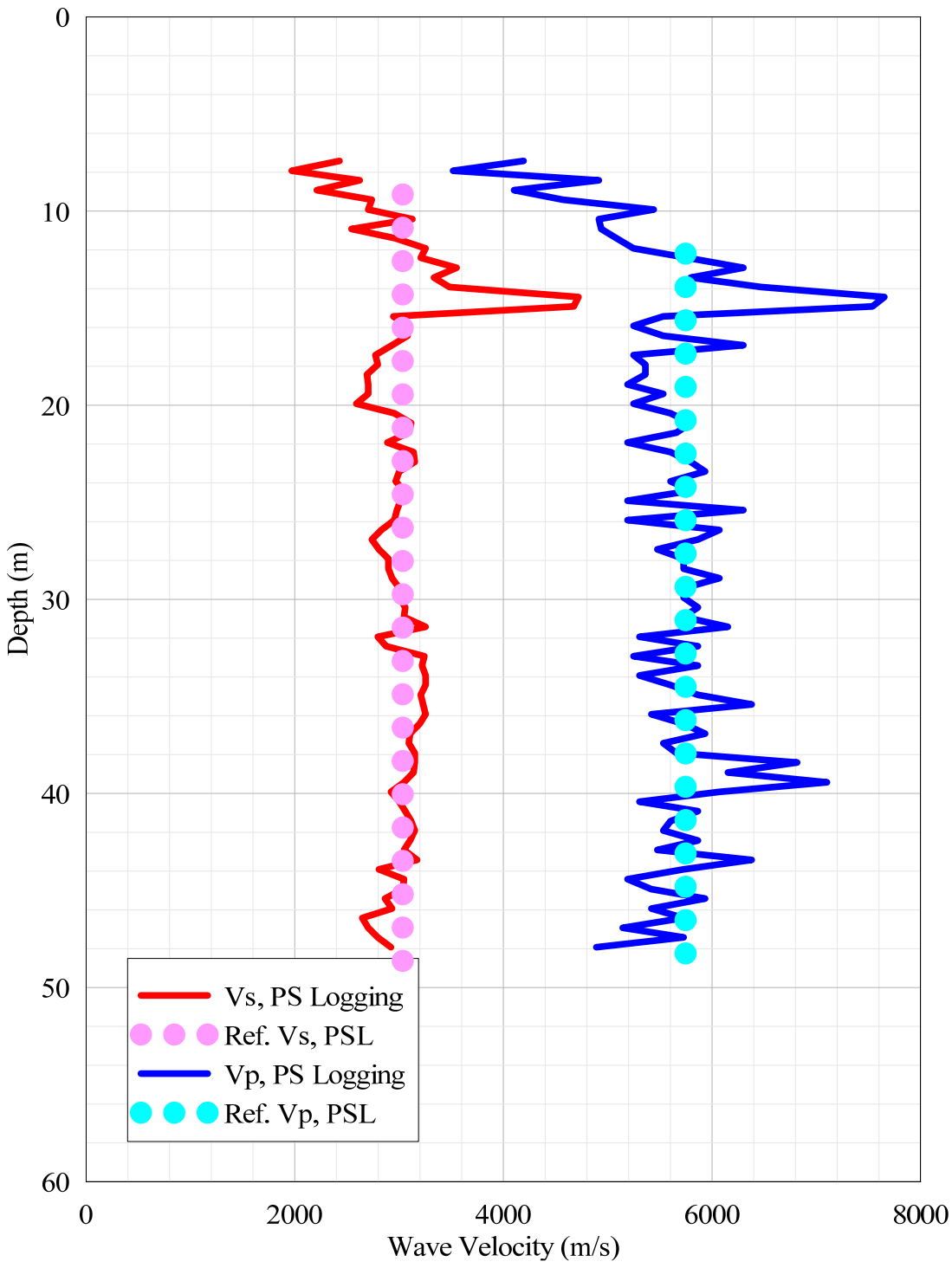

Figure A-59 Wave velocities at William States Lee III NPP (FSAR Figure 2.5.4-220).

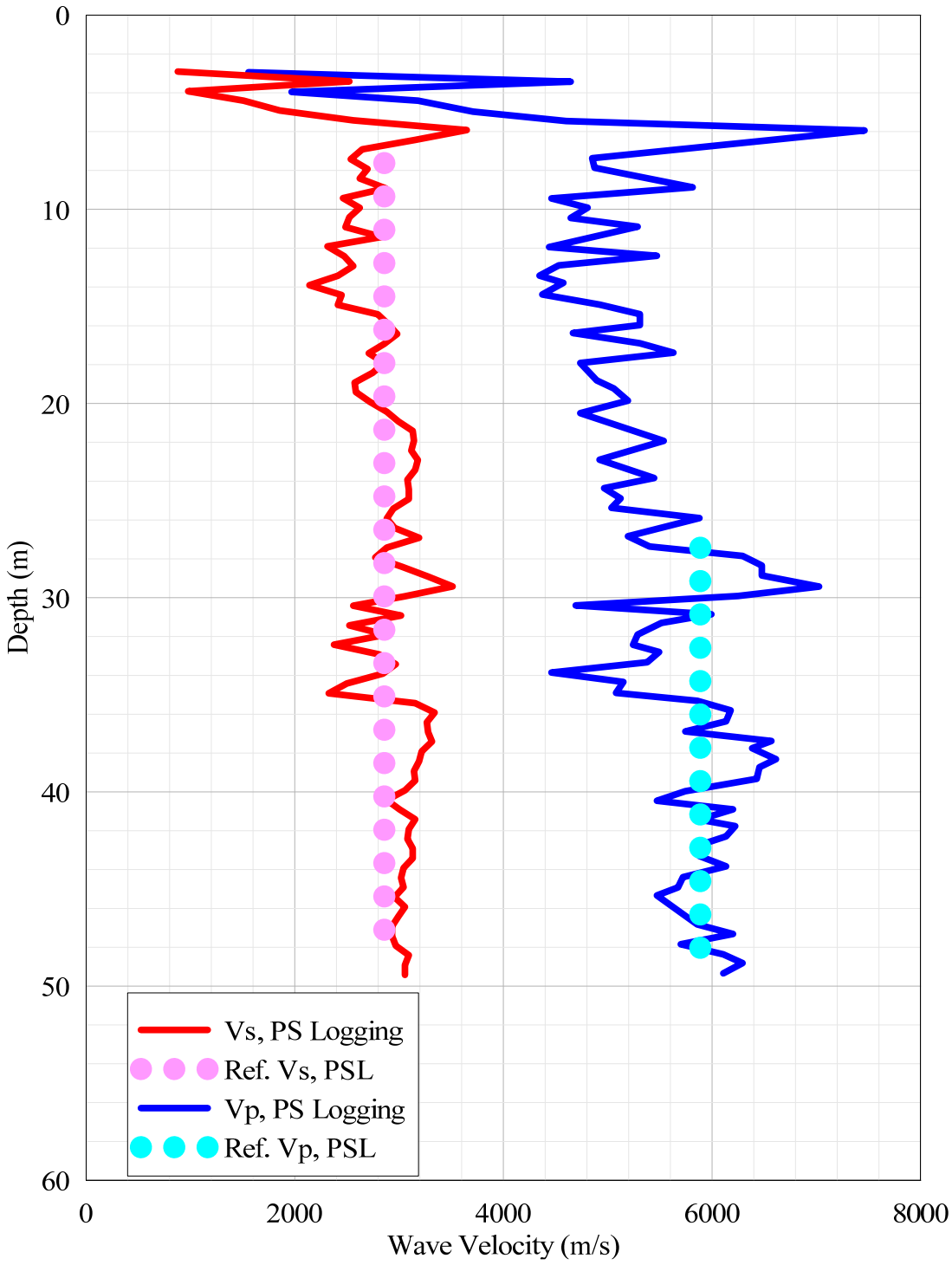

Figure A-60 Wave velocities at William States Lee III NPP (FSAR Figure 2.5.4-221).

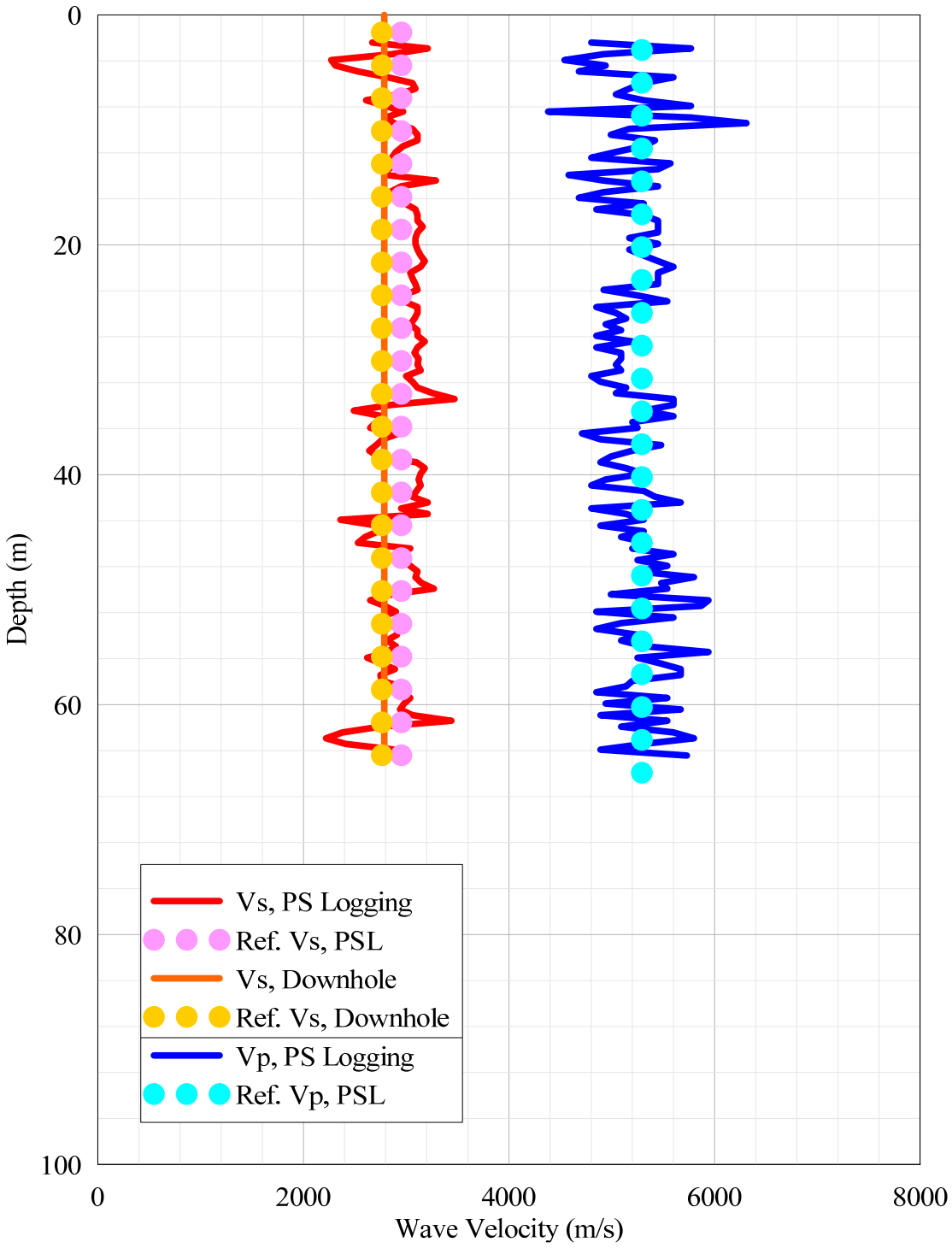

Figure A-61 Wave velocities at William States Lee III NPP (FSAR Figure 2.5.4-222).

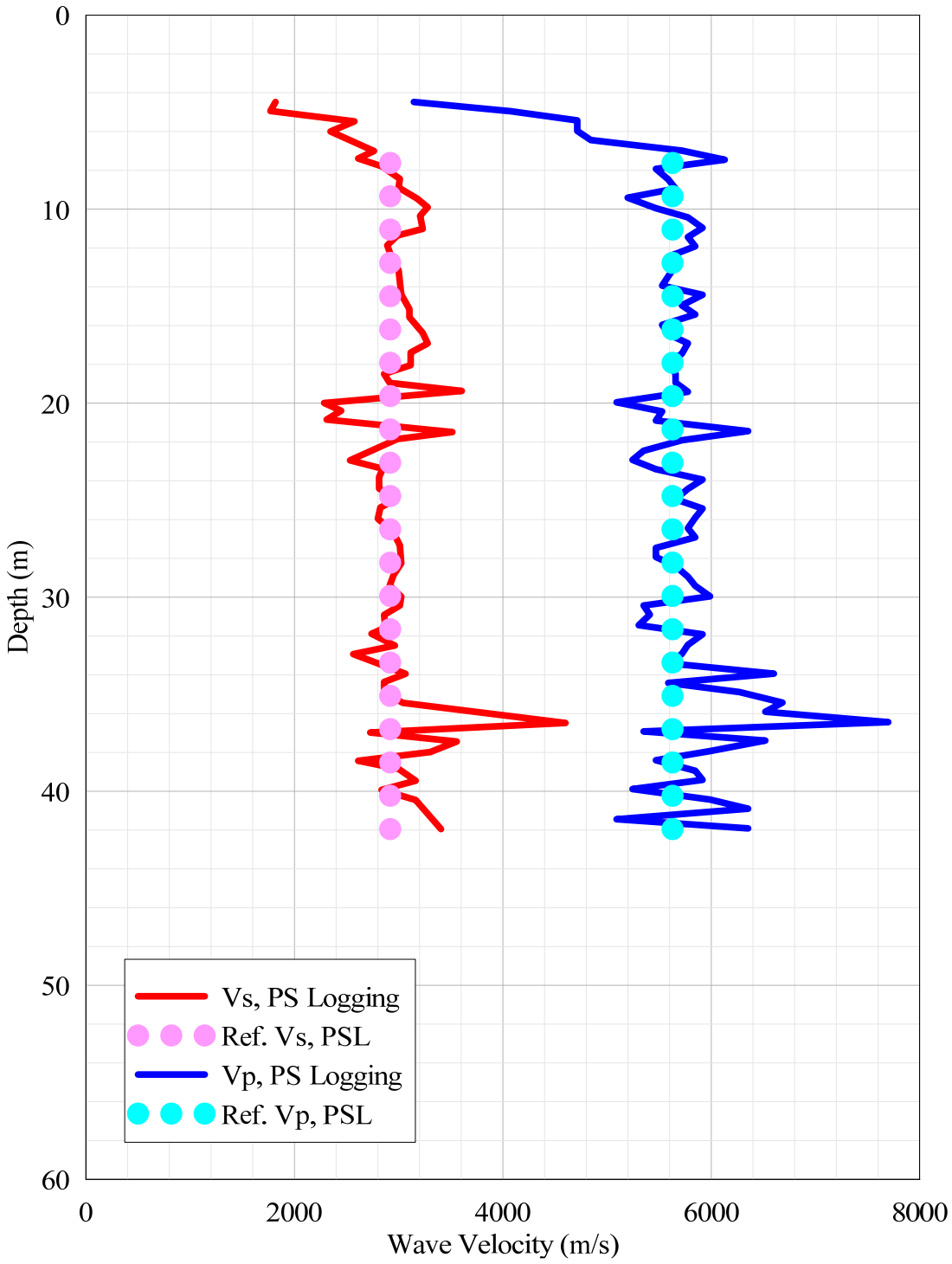

Figure A-62 Wave velocities at William States Lee III NPP (FSAR Figure 2.5.4-223).

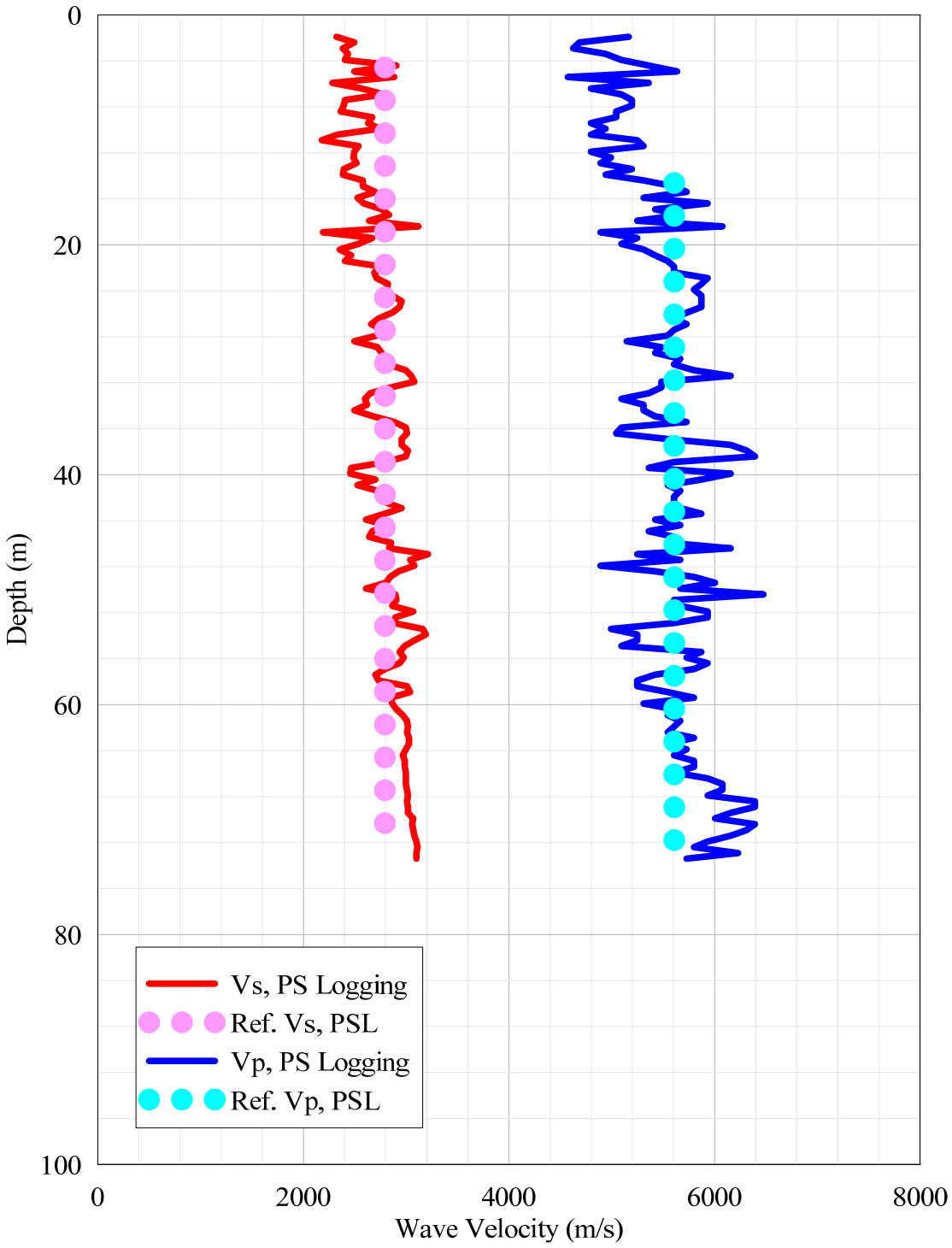

Figure A-63 Wave velocities at William States Lee III NPP (FSAR Figure 2.5.4-224).

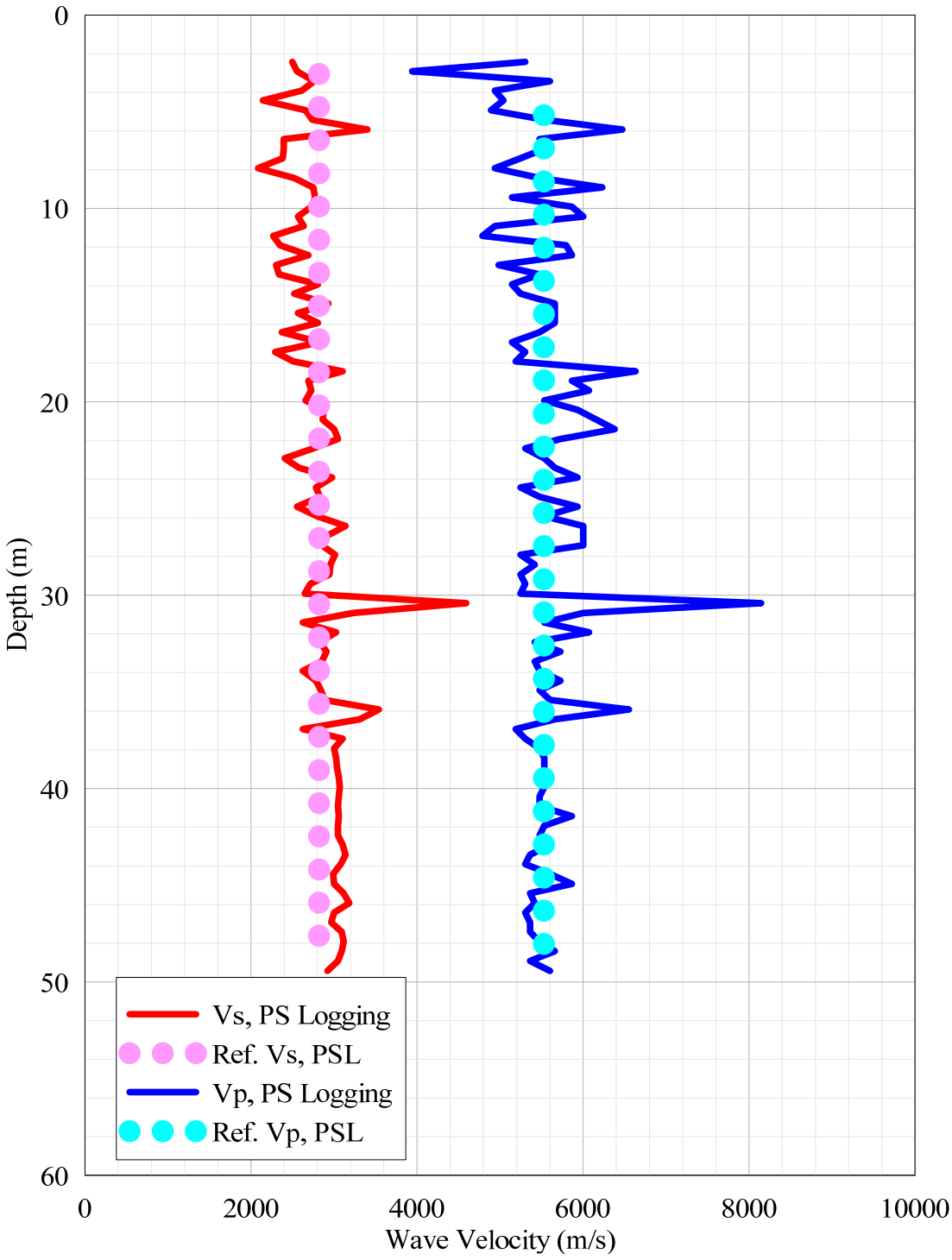

Figure A-64 Wave velocities at William States Lee III NPP (FSAR Figure 2.5.4-225).

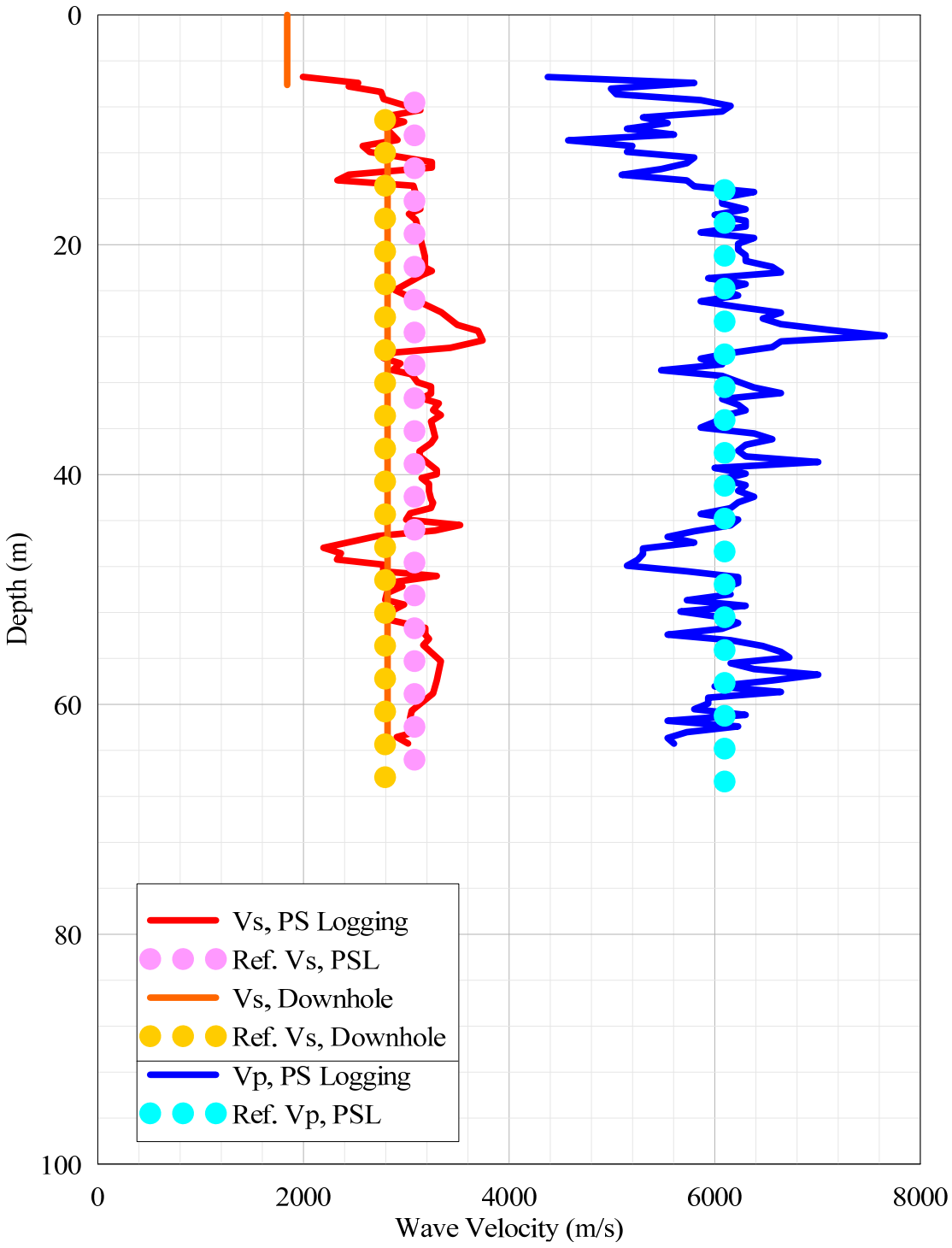

Figure A-65 Wave velocities at William States Lee III NPP (FSAR Figure 2.5.4-226).

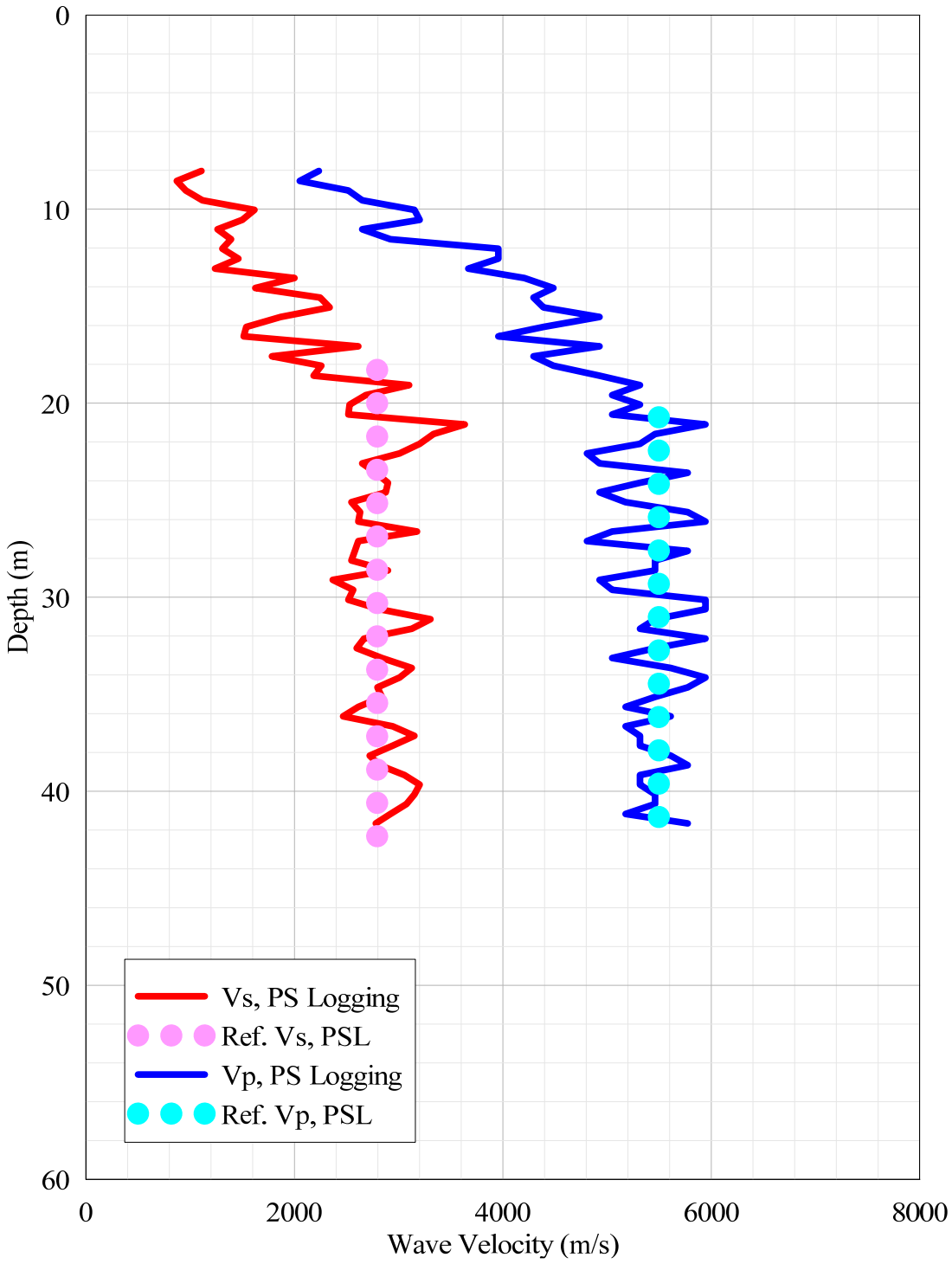

Figure A-66 Wave velocities at William States Lee III NPP (FSAR Figure 2.5.4-232).

Appendix B: Within-Profile Histograms

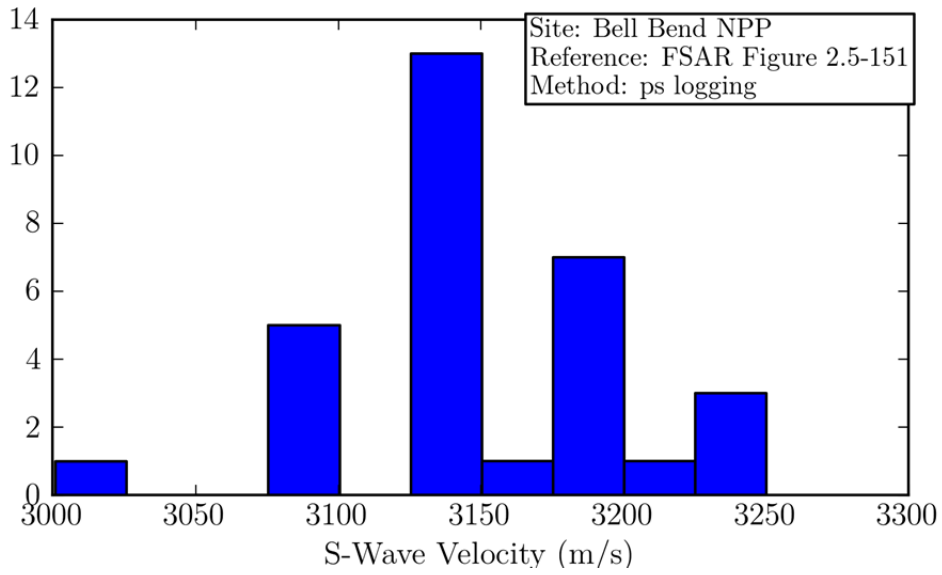

Figure B-1 **Distribution of within-profile reference velocities at Bell Bend NPP (FSAR Figure 2.5-151, PS logging).**

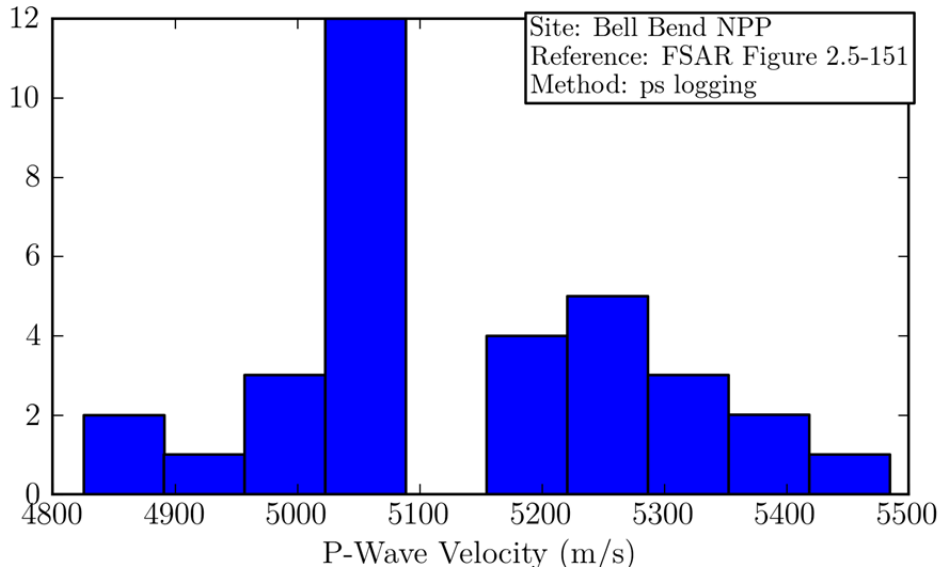

Figure B-2 **Distribution of within-profile reference velocities at Bell Bend NPP (FSAR Figure 2.5-151, PS logging).**

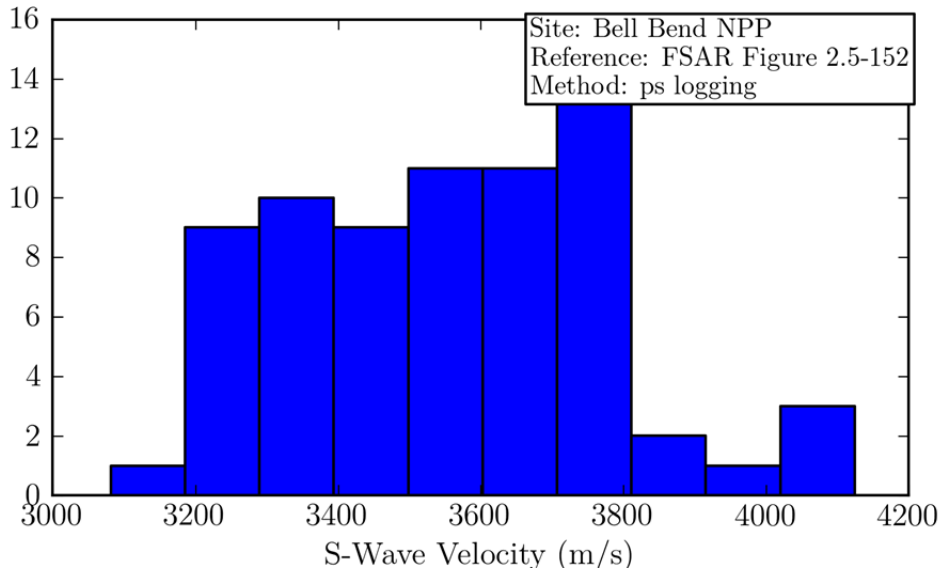

Figure B-3 **Distribution of within-profile reference velocities at Bell Bend NPP (FSAR Figure 2.5-152, PS logging).**

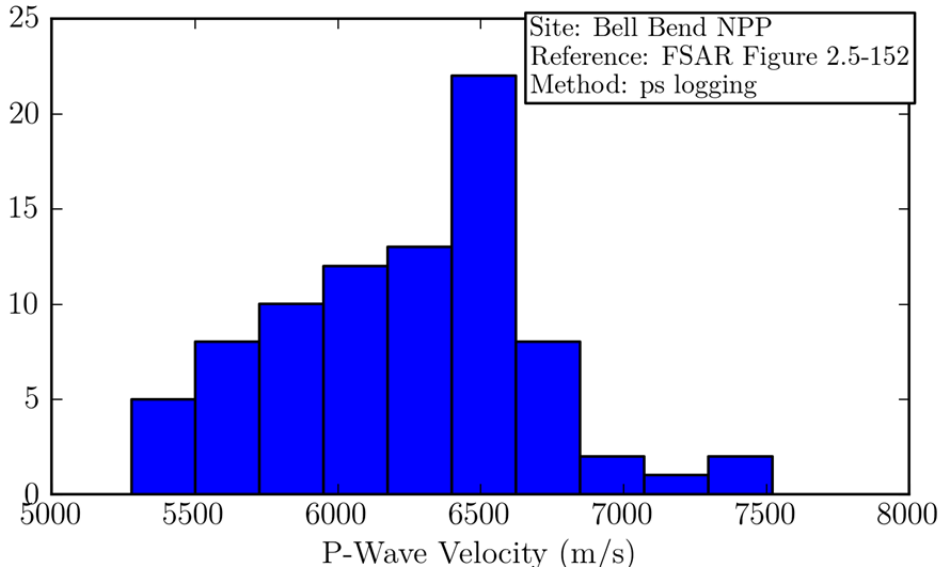

Figure B-4 **Distribution of within-profile reference velocities at Bell Bend NPP (FSAR Figure 2.5-152, PS logging).**

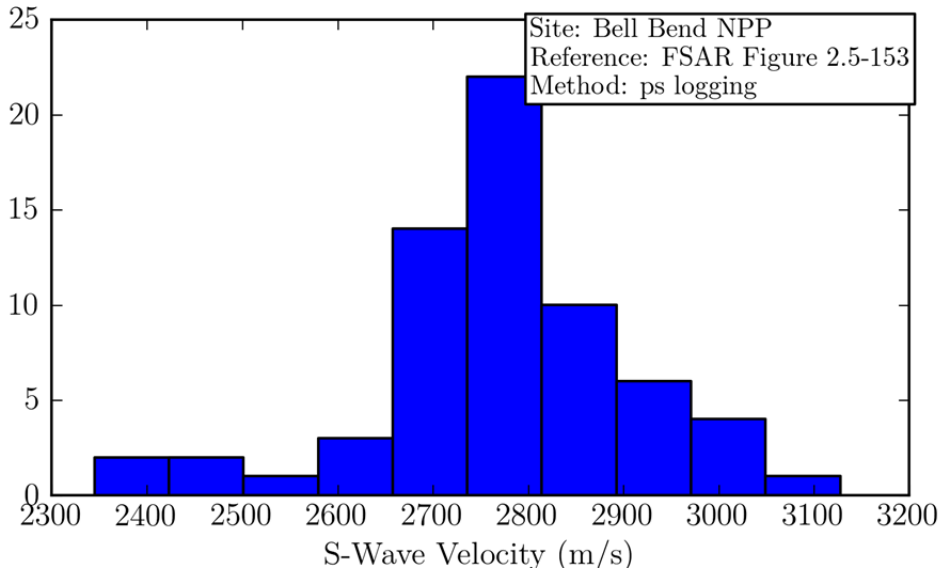

Figure B-5 **Distribution of within-profile reference velocities at Bell Bend NPP (FSAR Figure 2.5-153, PS logging).**

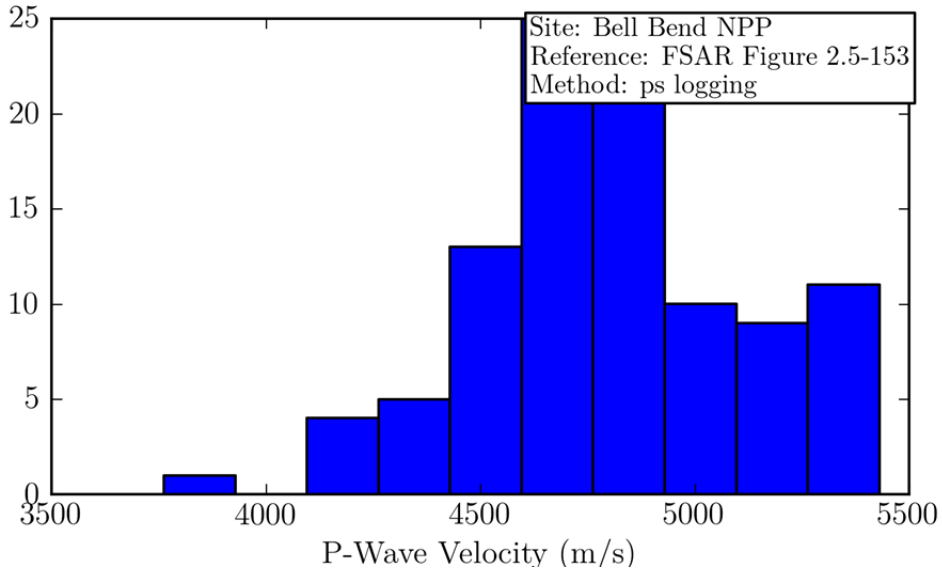

Figure B-6 **Distribution of within-profile reference velocities at Bell Bend NPP (FSAR Figure 2.5-153, PS logging).**

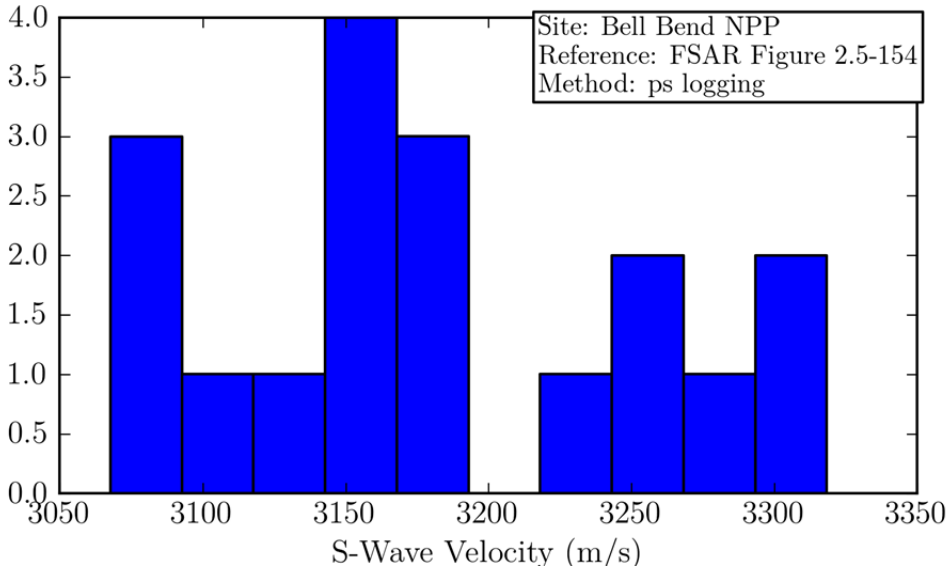

Figure B-7 **Distribution of within-profile reference velocities at Bell Bend NPP (FSAR Figure 2.5-154, PS logging).**

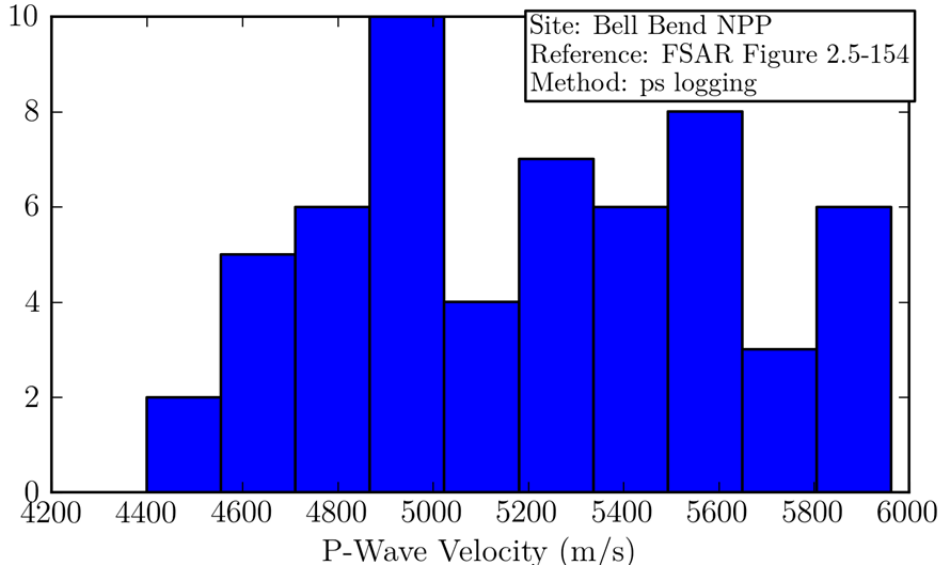

Figure B-8 **Distribution of within-profile reference velocities at Bell Bend NPP (FSAR Figure 2.5-153, PS logging).**

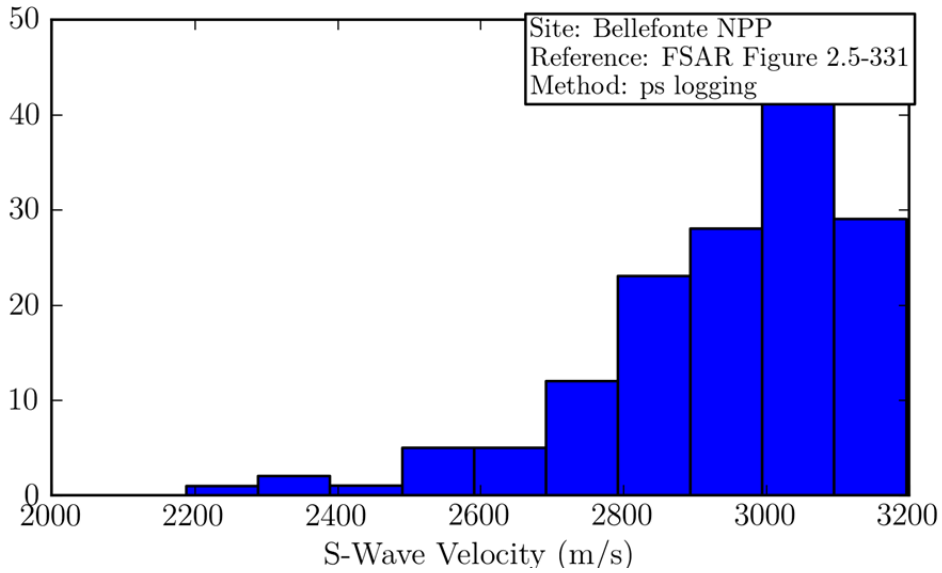

Figure B-9 **Distribution of within-profile reference velocities at Bellefonte NPP (FSAR Figure 2.5-331, PS logging).**

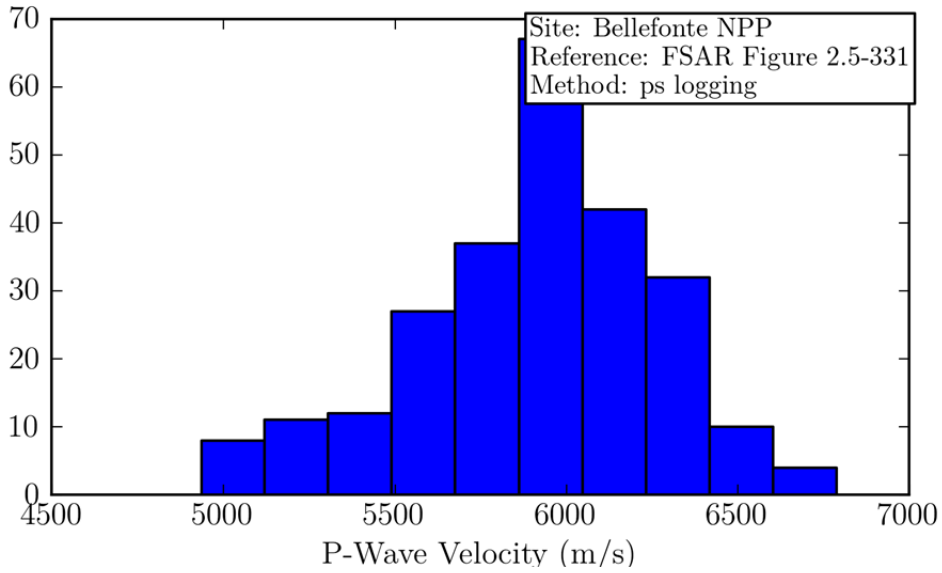

Figure B-10 **Distribution of within-profile reference velocities at Bellefonte NPP (FSAR Figure 2.5-331, PS logging).**

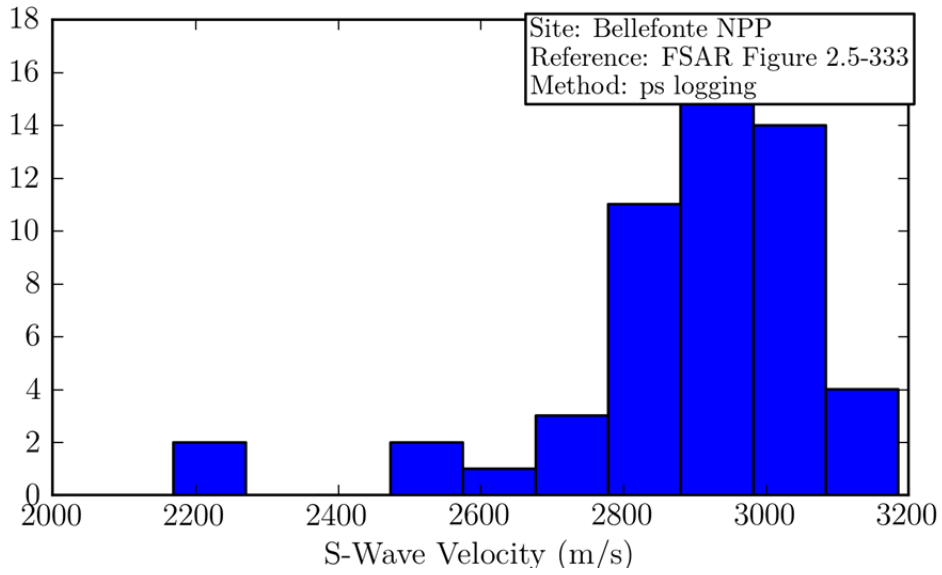

Figure B-11 Distribution of within-profile reference velocities at Bellefonte NPP (FSAR Figure 2.5-333, PS logging).

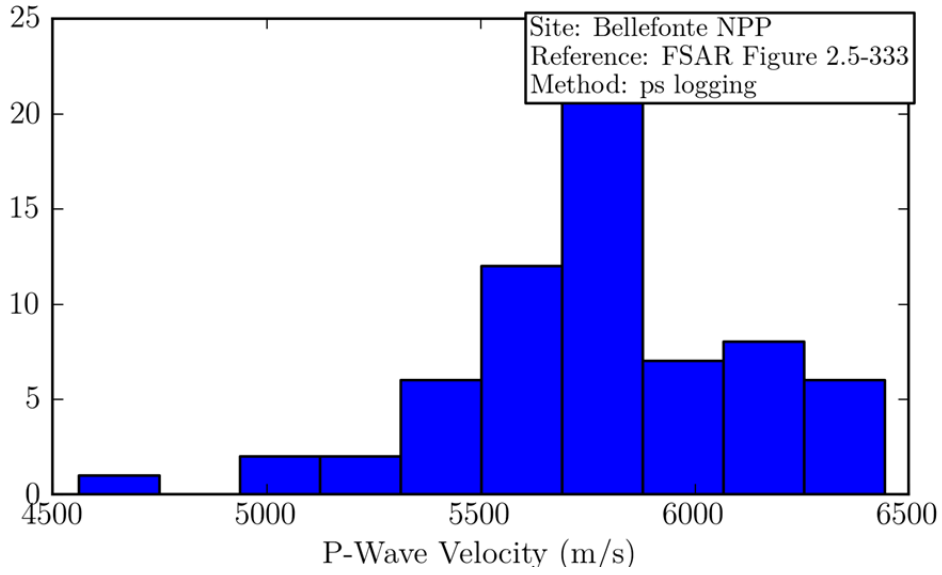

Figure B-12 Distribution of within-profile reference velocities at Bellefonte NPP (FSAR Figure 2.5-333, PS logging).

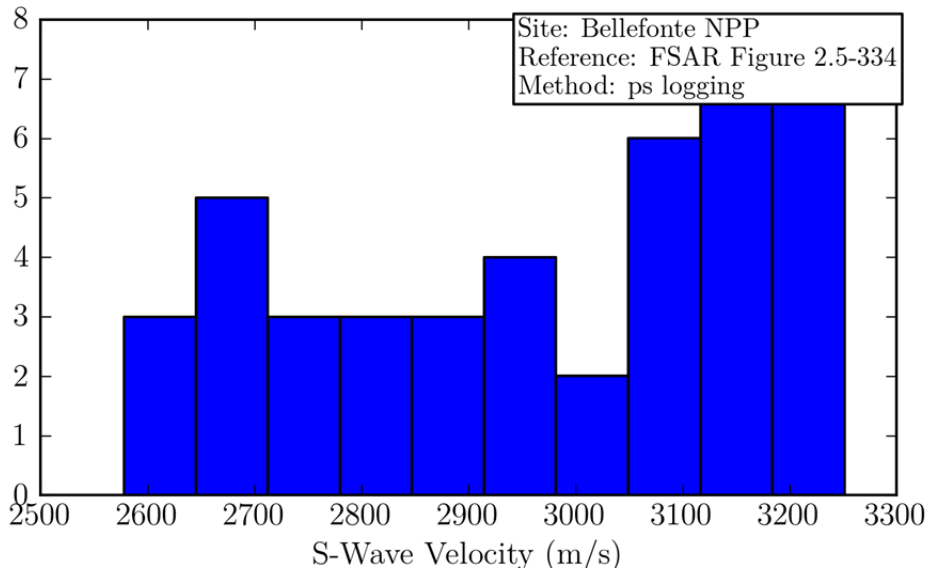

Figure B-13 Distribution of within-profile reference velocities at Bellefonte NPP (FSAR Figure 2.5-334, PS logging).

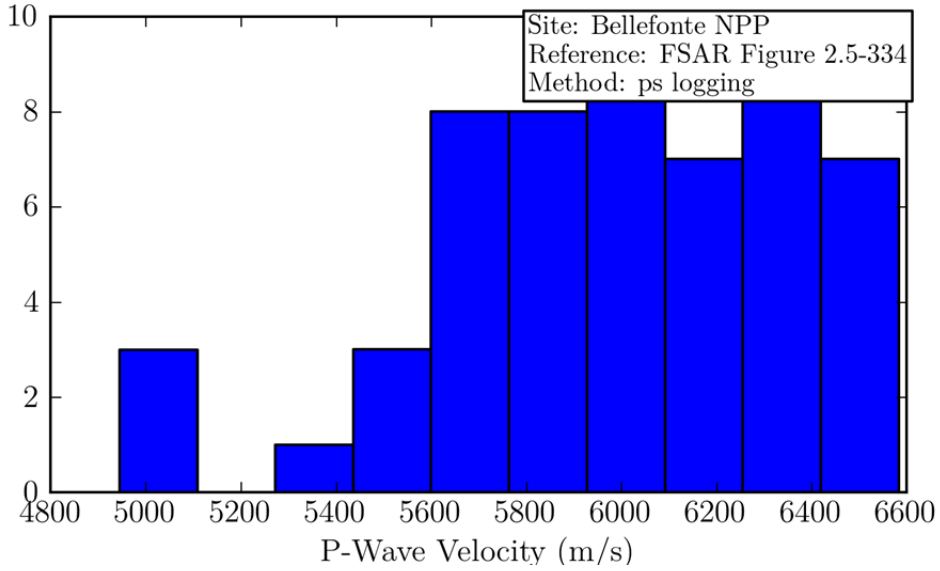

Figure B-14 Distribution of within-profile reference velocities at Bellefonte NPP (FSAR Figure 2.5-334, PS logging).

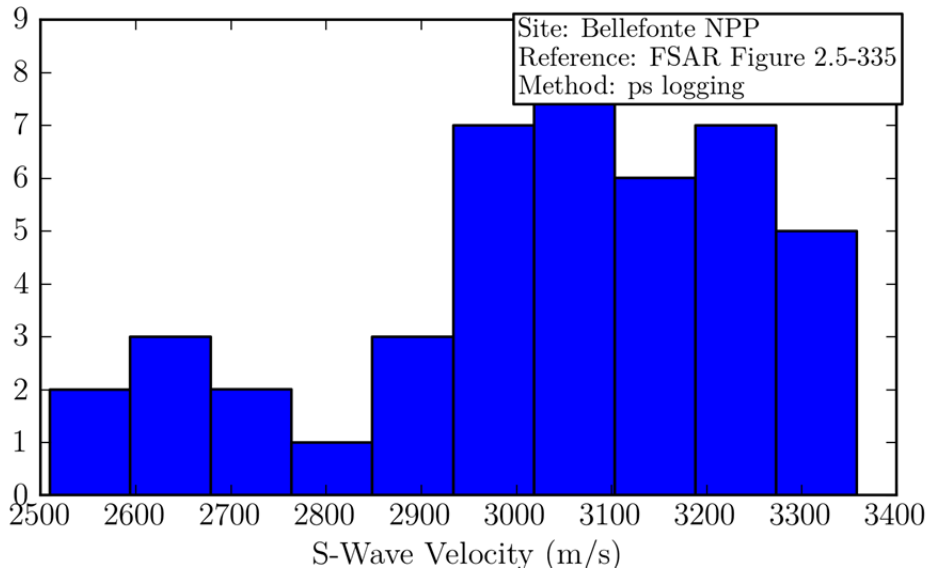

Figure B-15 Distribution of within-profile reference velocities at Bellefonte NPP (FSAR Figure 2.5-335, PS logging).

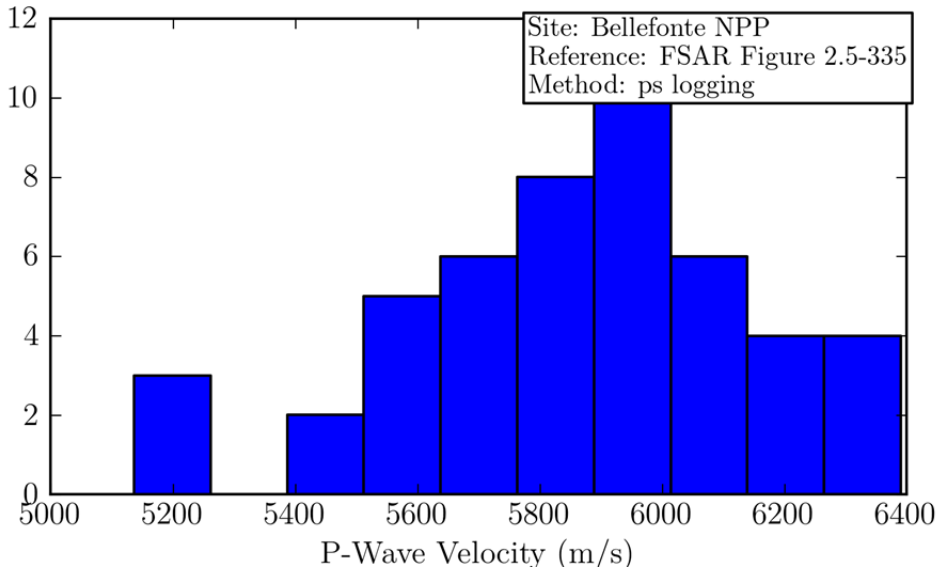

Figure B-16 Distribution of within-profile reference velocities at Bellefonte NPP (FSAR Figure 2.5-335, PS logging).

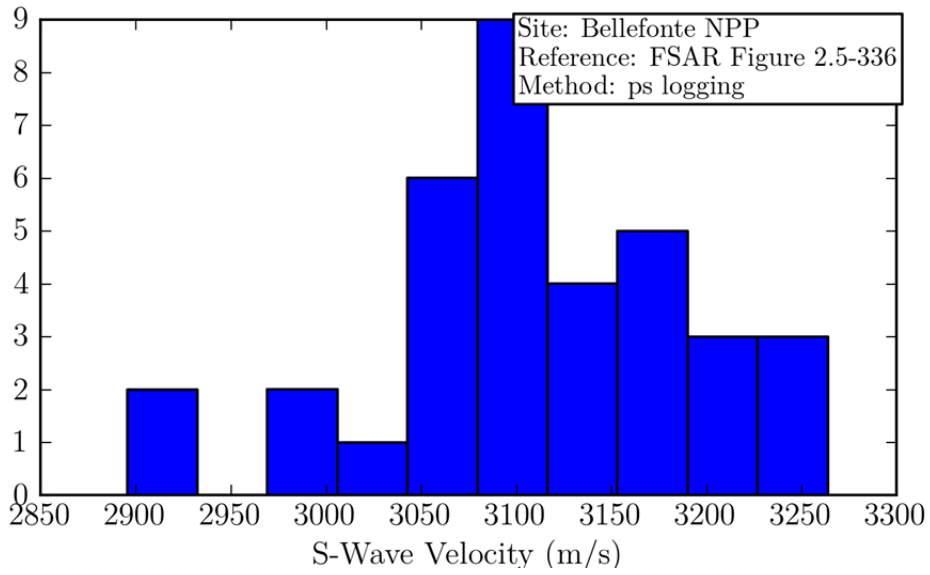

Figure B-17 Distribution of within-profile reference velocities at Bellefonte NPP (FSAR Figure 2.5-336, PS logging).

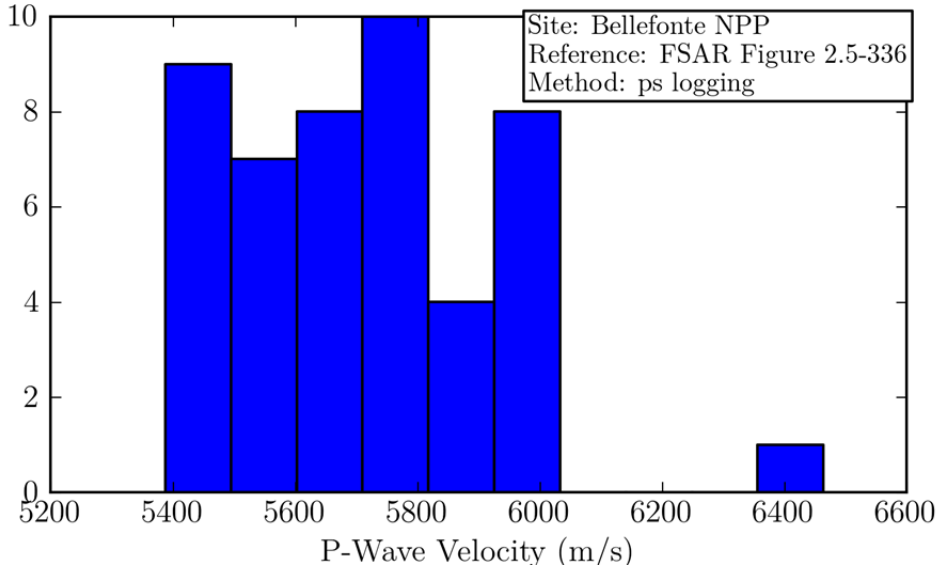

Figure B-18 Distribution of within-profile reference velocities at Bellefonte NPP (FSAR Figure 2.5-336, PS logging).

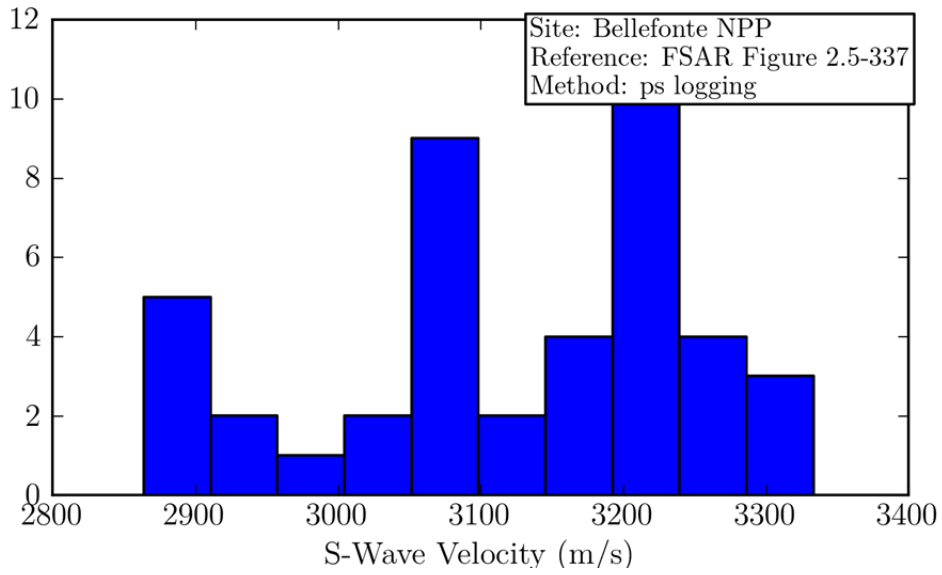

Figure B-19 Distribution of within-profile reference velocities at Bellefonte NPP (FSAR Figure 2.5-337, PS logging).

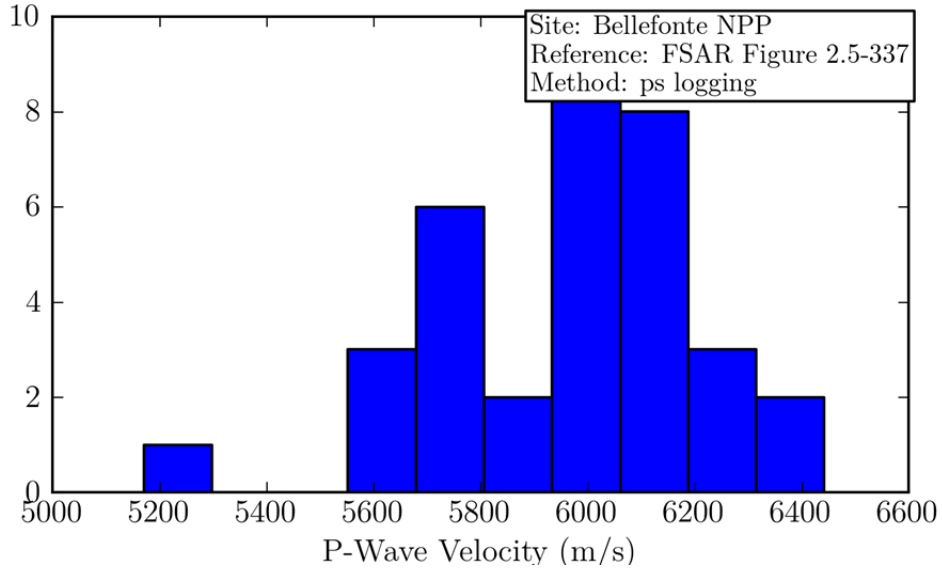

Figure B-20 Distribution of within-profile reference velocities at Bellefonte NPP (FSAR Figure 2.5-337, PS logging).

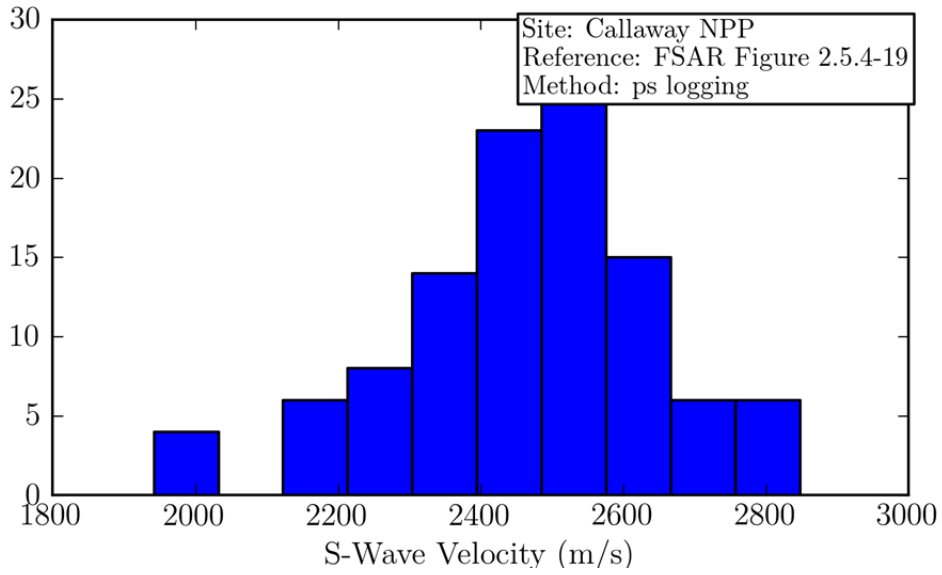

Figure B-21 Distribution of within-profile reference velocities at Callaway NPP (FSAR Figure 2.5-4.19, PS logging).

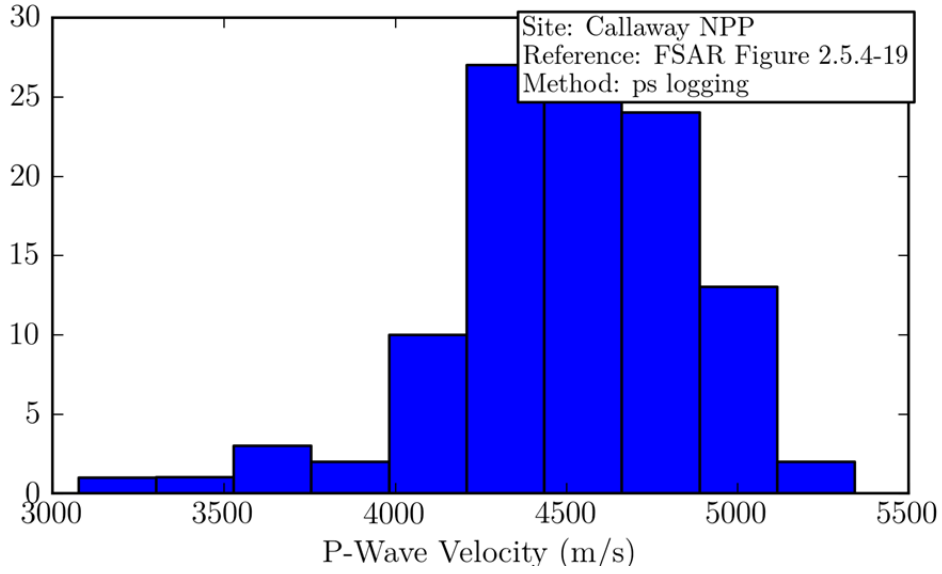

Figure B-22 Distribution of within-profile reference velocities at Callaway NPP (FSAR Figure 2.5-4.19, PS logging).

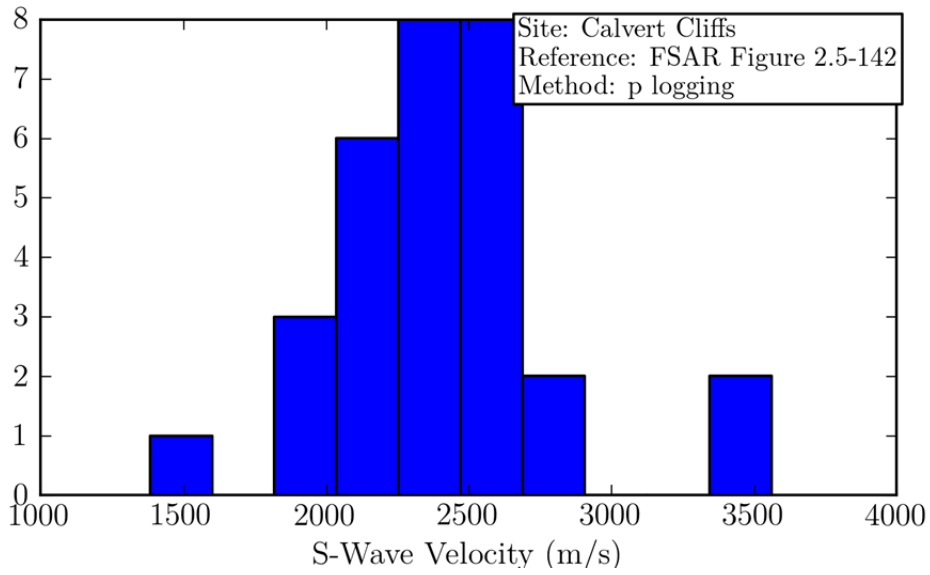

Figure B-23 Distribution of within-profile reference velocities at Calvert Cliffs NPP (FSAR Figure 2.5-142, P logging).

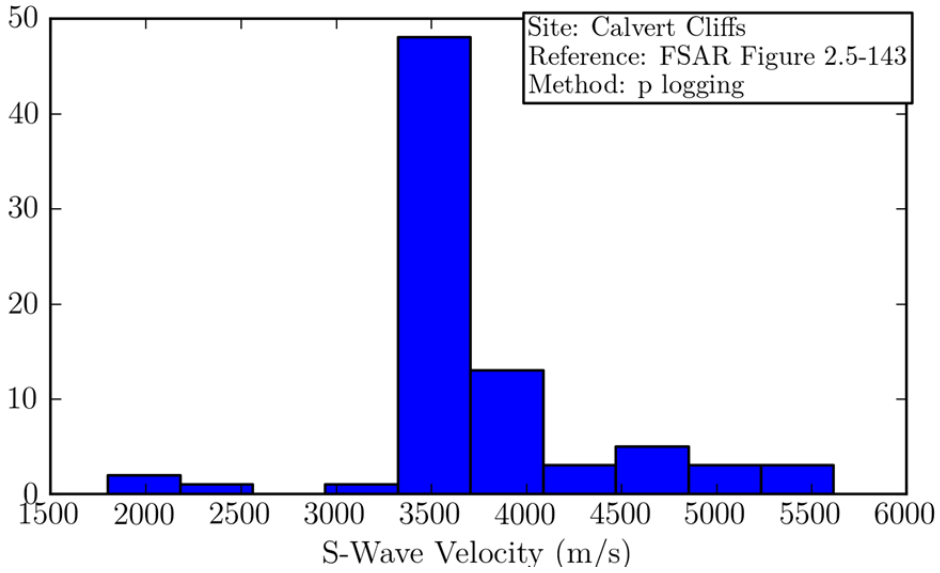

Figure B-24 Distribution of within-profile reference velocities at Calvert Cliffs NPP (FSAR Figure 2.5-143, P logging).

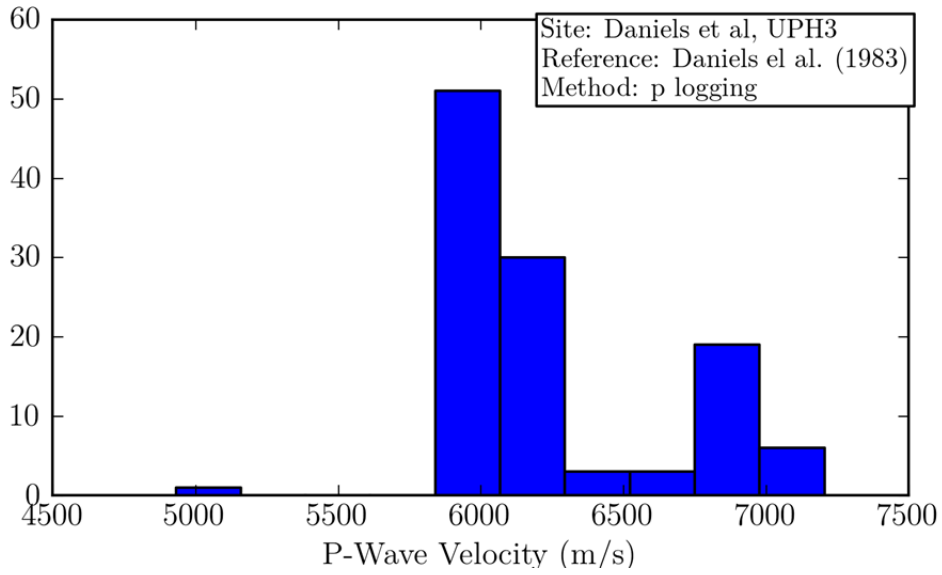

Figure B-25 Distribution of within-profile reference velocities from Daniels et al. (1983).

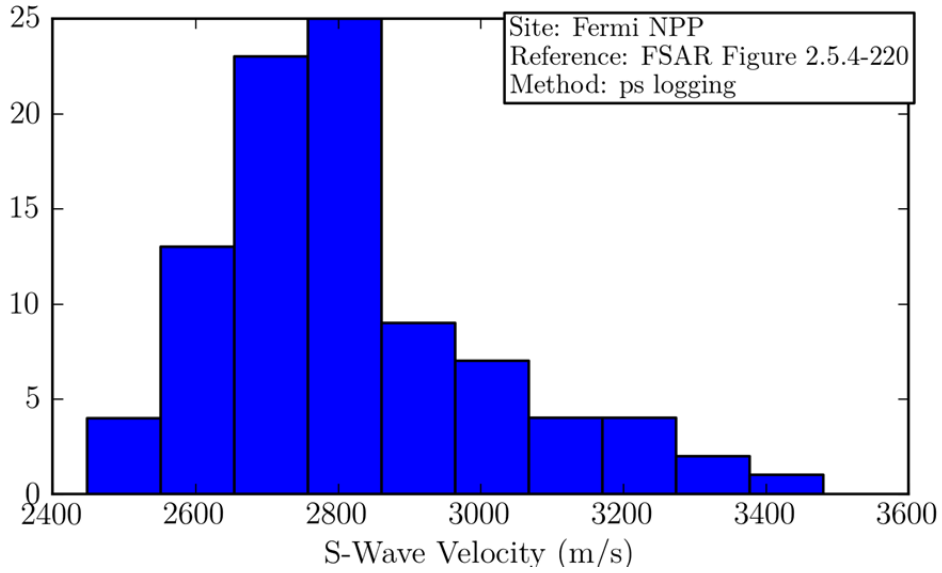

Figure B-26 Distribution of within-profile reference velocities at Fermi NPP (FSAR Figure 2.5.4-220, PS logging).

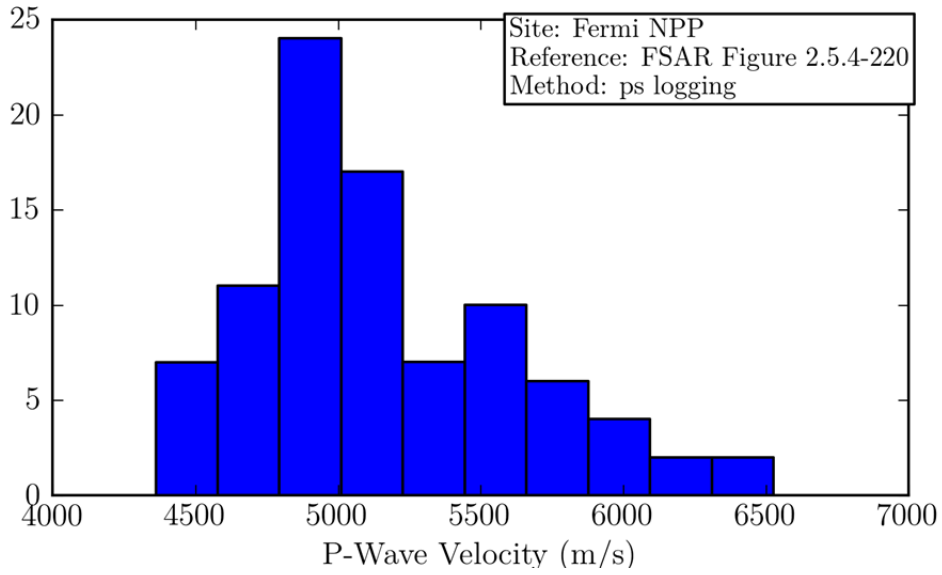

Figure B-27 Distribution of within-profile reference velocities at Fermi NPP (FSAR Figure 2.5.4-220, PS logging).

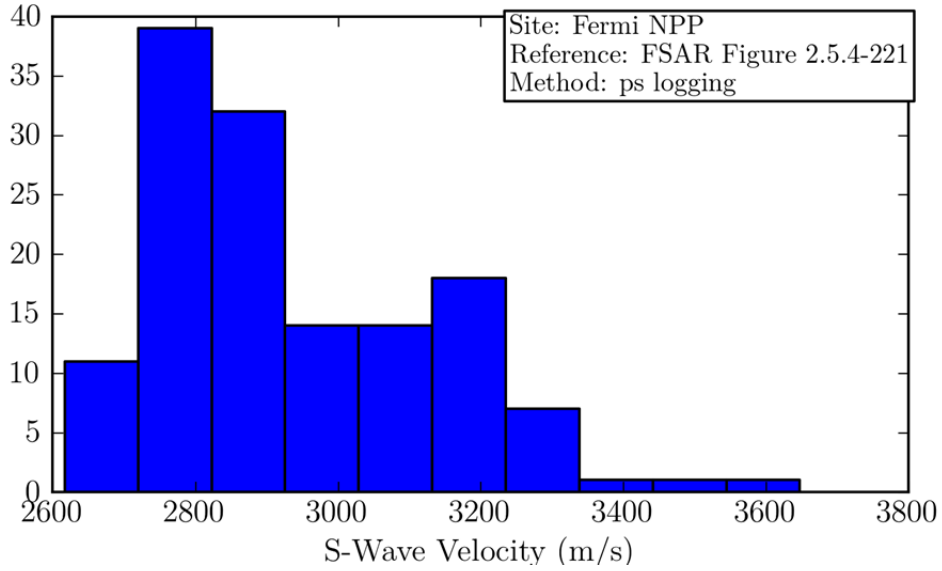

Figure B-28 Distribution of within-profile reference velocities at Fermi NPP (FSAR Figure 2.5.4-221, PS logging).

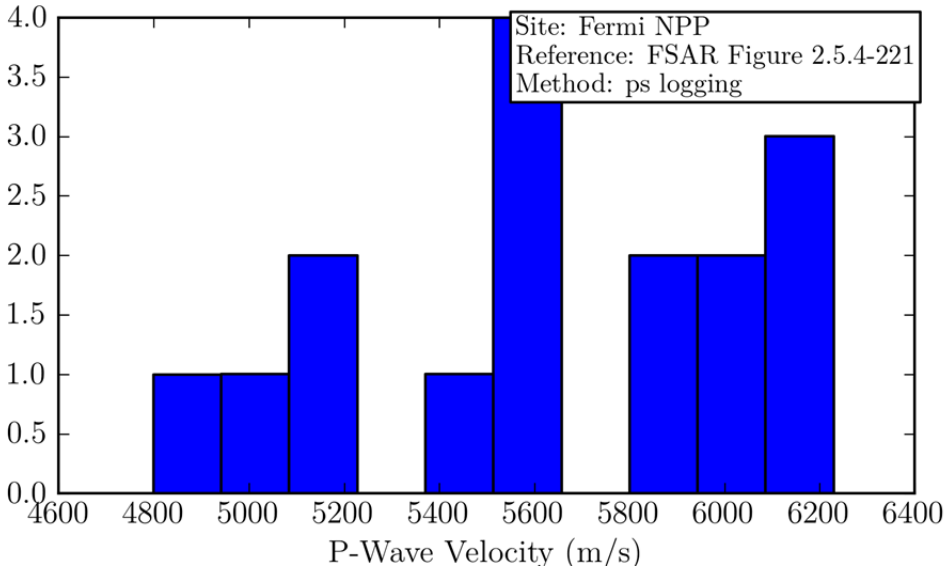

Figure B-29 Distribution of within-profile reference velocities at Fermi NPP (FSAR Figure 2.5.4-221, PS logging).

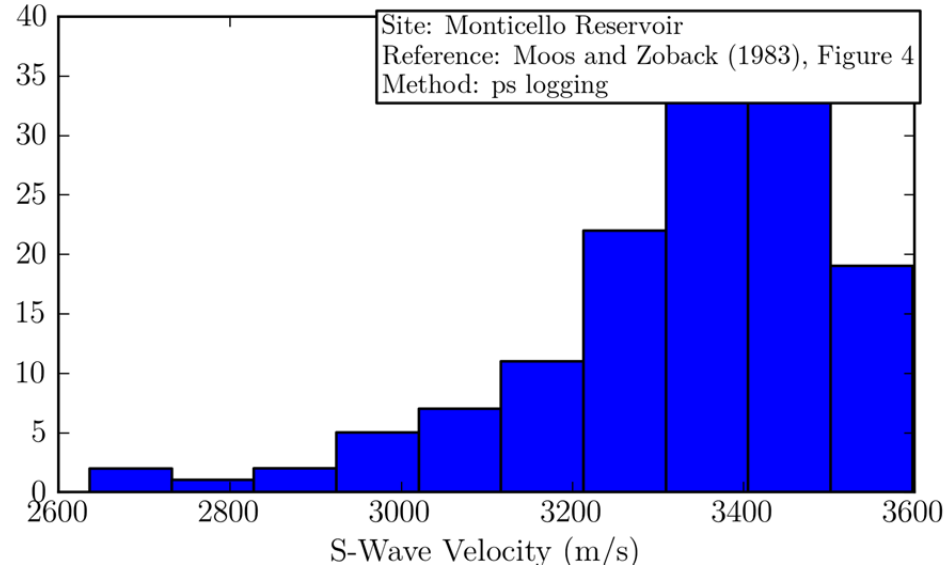

Figure B-30 Distribution of within-profile reference velocities at Monticello Reservoir [Moos and Zoback 1983, Figure 4].

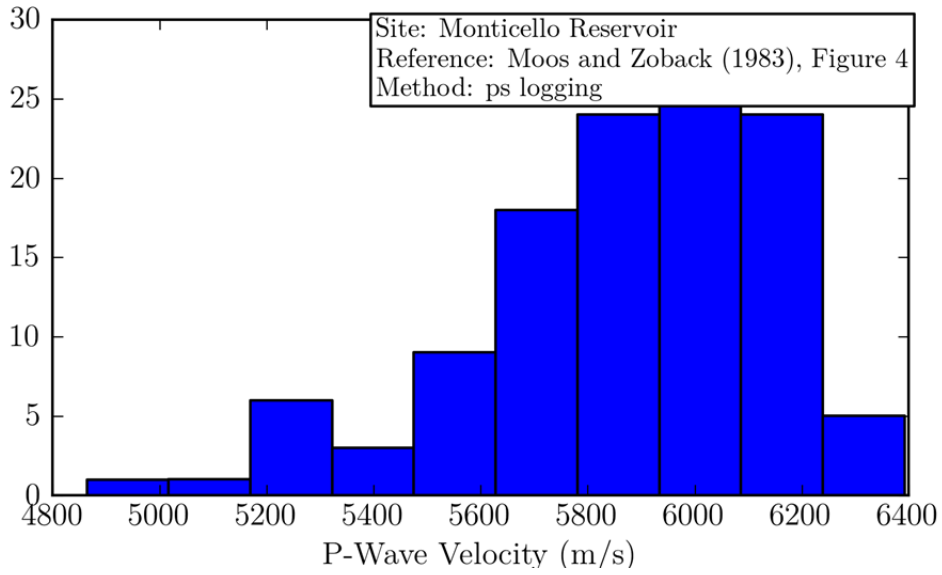

Figure B-31 **Distribution of within-profile reference velocities at Monticello Reservoir [Moos and Zoback 1983, Figure 4].**

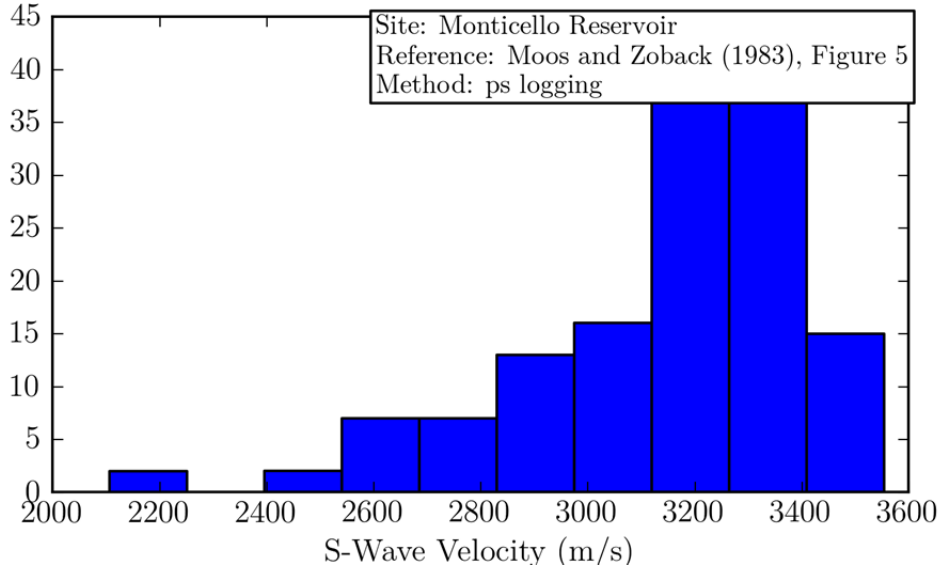

Figure B-32 **Distribution of within-profile reference velocities at Monticello Reservoir [Moos and Zoback 1983, Figure 5].**

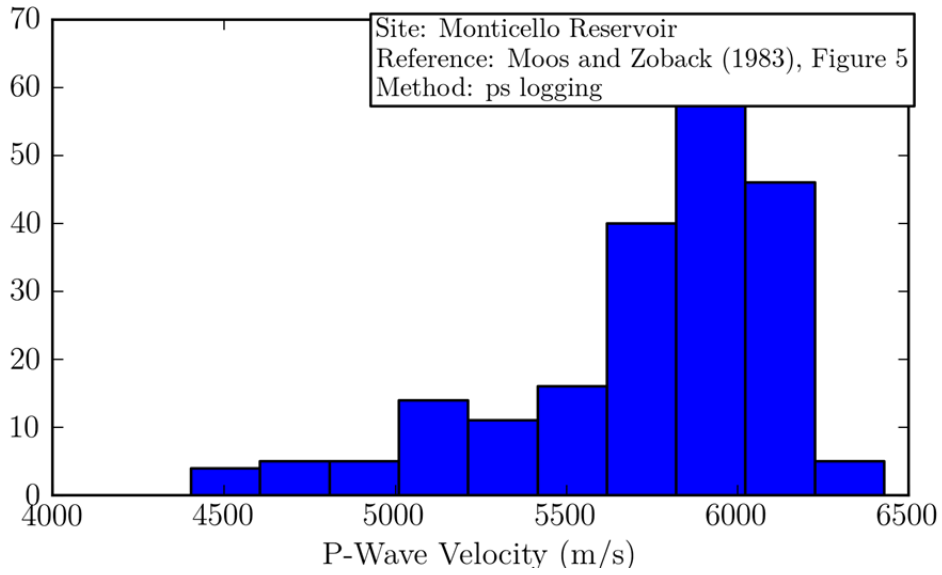

Figure B-33 +Distribution of within-profile reference velocities at Monticello Reservoir [Moos and Zoback 1983, Figure 5].

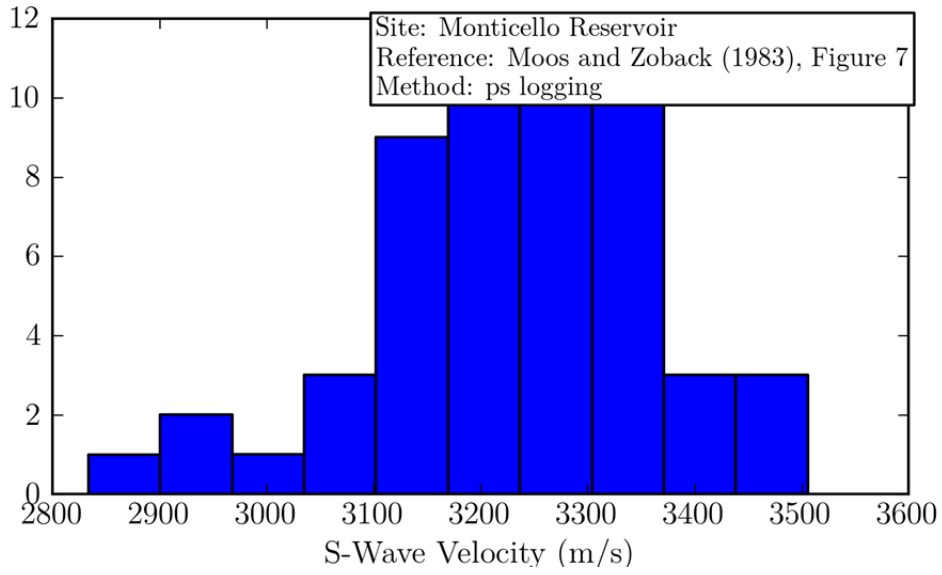

Figure B-34 Distribution of within-profile reference velocities at Monticello Reservoir [Moos and Zoback 1983, Figure 7].

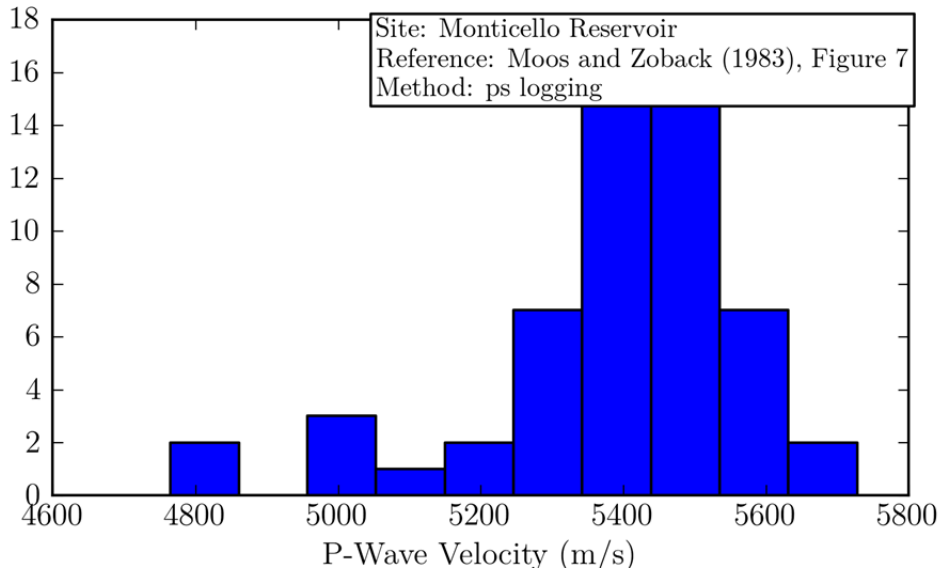

Figure B-35 Distribution of within-profile reference velocities at Monticello Reservoir [Moos and Zoback 1983, Figure 7].

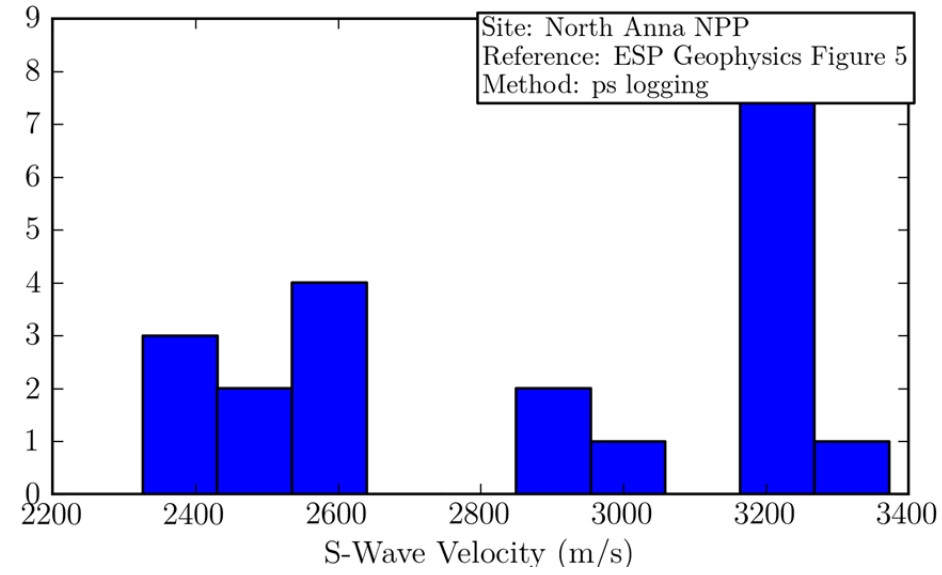

Figure B-36 Distribution of within-profile reference velocities at North Anna NPP (ESP Geophysics, Figure 5, PS logging).

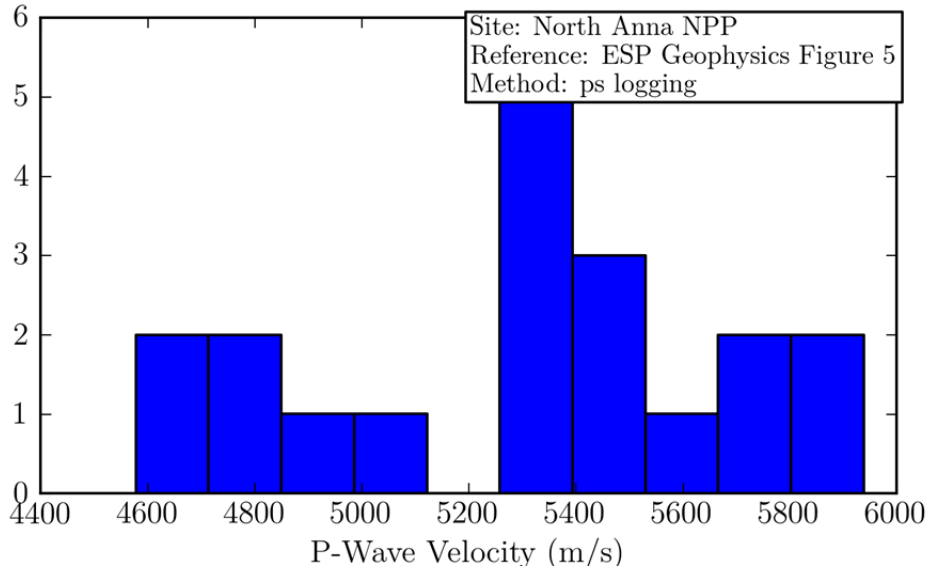

Figure B-37 Distribution of within-profile reference velocities at North Anna NPP (ESP Geophysics, Figure 5, PS logging).

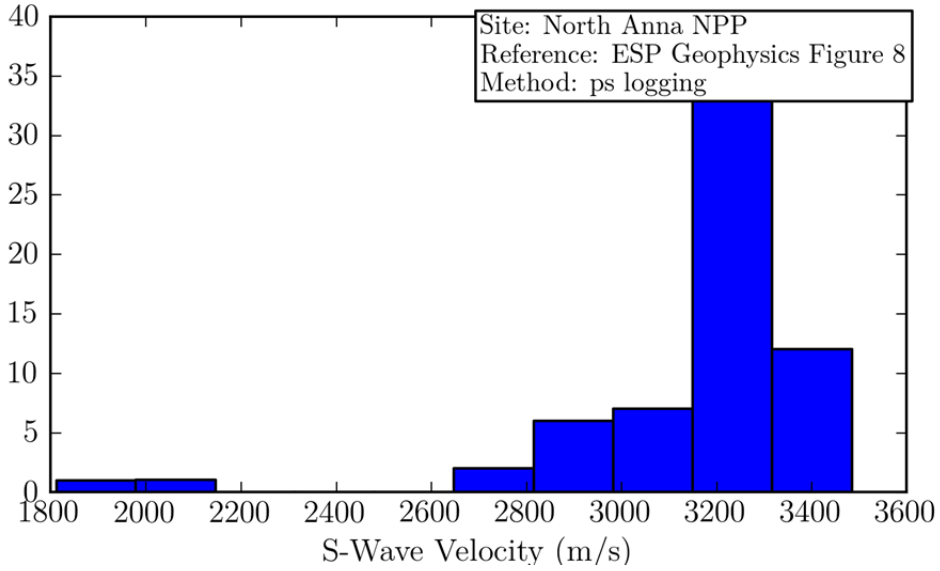

Figure B-38 Distribution of within-profile reference velocities at North Anna NPP (ESP Geophysics, Figure 8, PS logging).

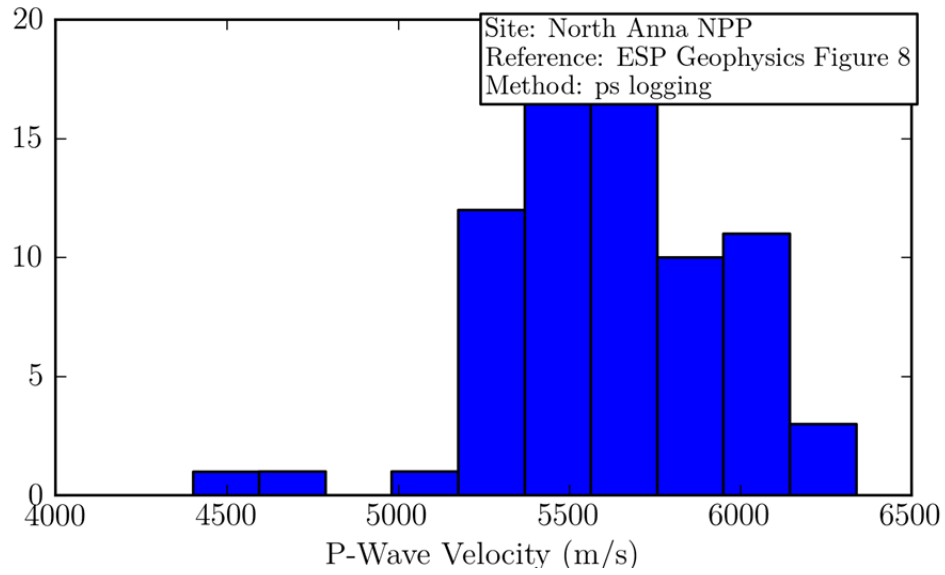

Figure B-39 Distribution of within-profile reference velocities at North Anna NPP (ESP Geophysics, Figure 8, PS logging).

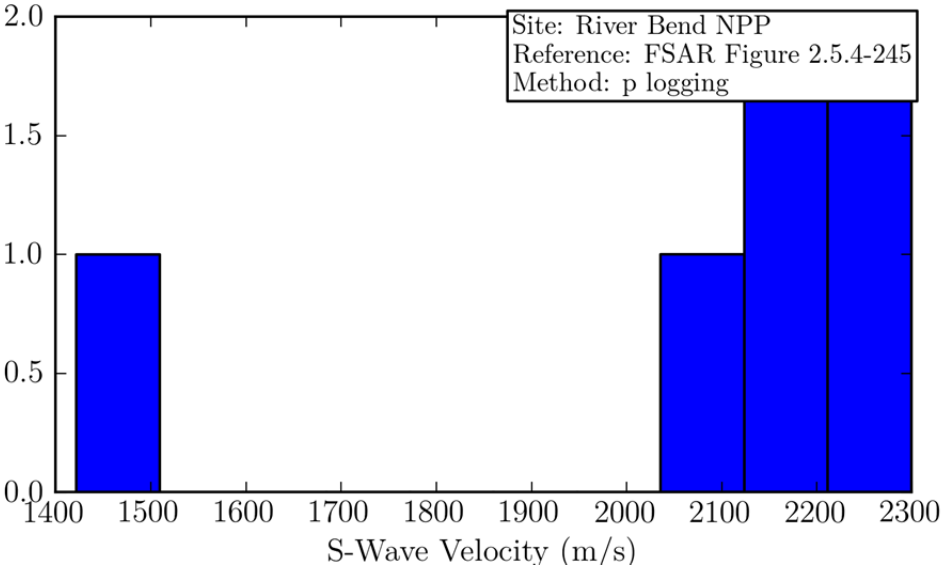

Figure B-40 Distribution of within-profile reference velocities at River Bend NPP (FSAR Figure 2.5.4-245, P logging).

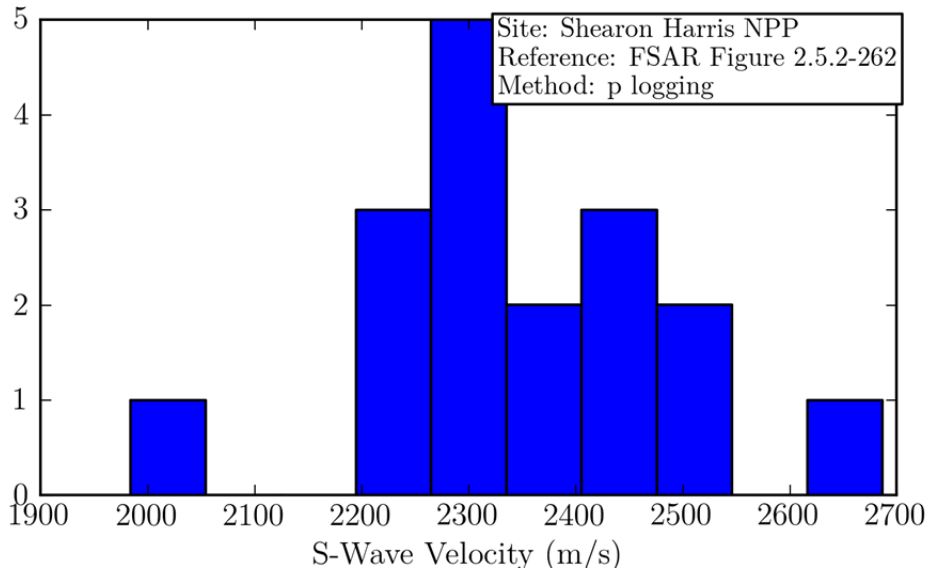

Figure B-41 Distribution of within-profile reference velocities at Shearon Harris NPP (FSAR Figure 2.5.2-262, P logging).

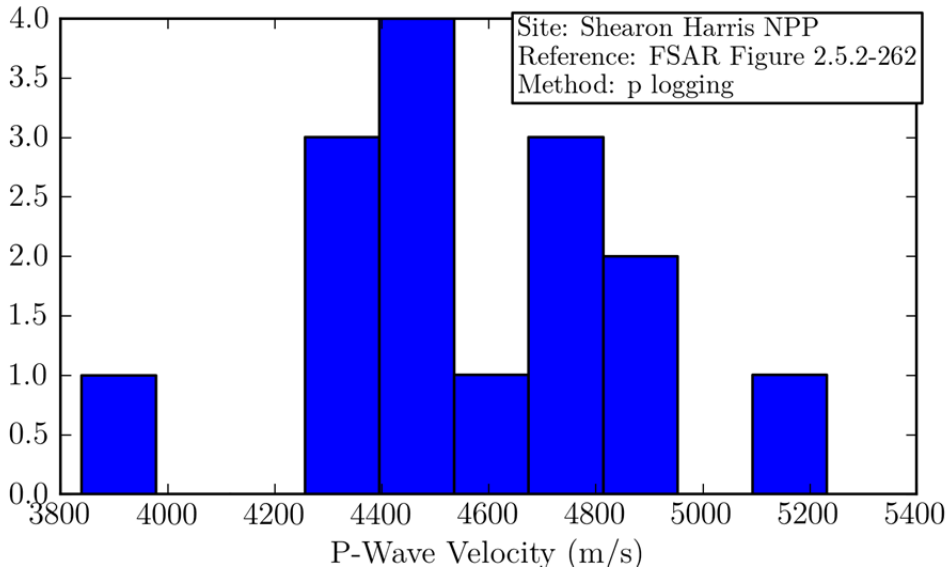

Figure B-42 Distribution of within-profile reference velocities at Shearon Harris NPP (FSAR Figure 2.5.2-262, P logging).

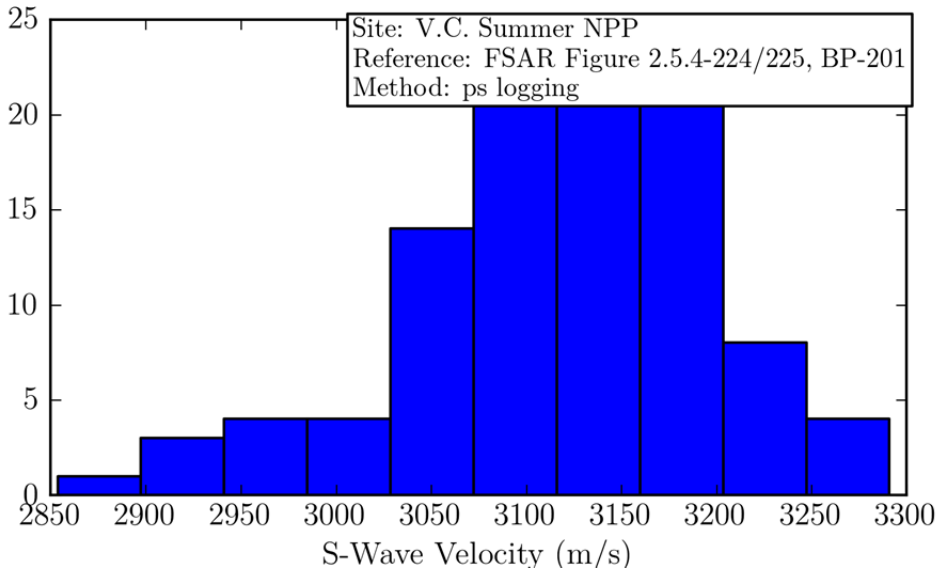

Figure B-43 Distribution of within-profile reference velocities at V.C. Summer NPP (FSAR Figure 2.5.4-224/225, BP-201, PS logging).

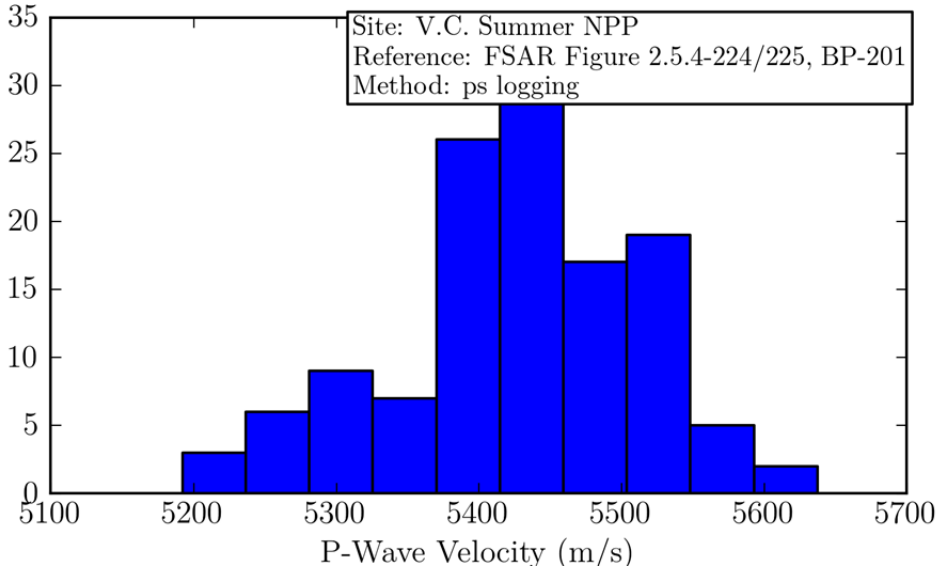

Figure B-44 Distribution of within-profile reference velocities at V.C. Summer NPP (FSAR Figure 2.5.4-224/225, BP-201, PS logging).

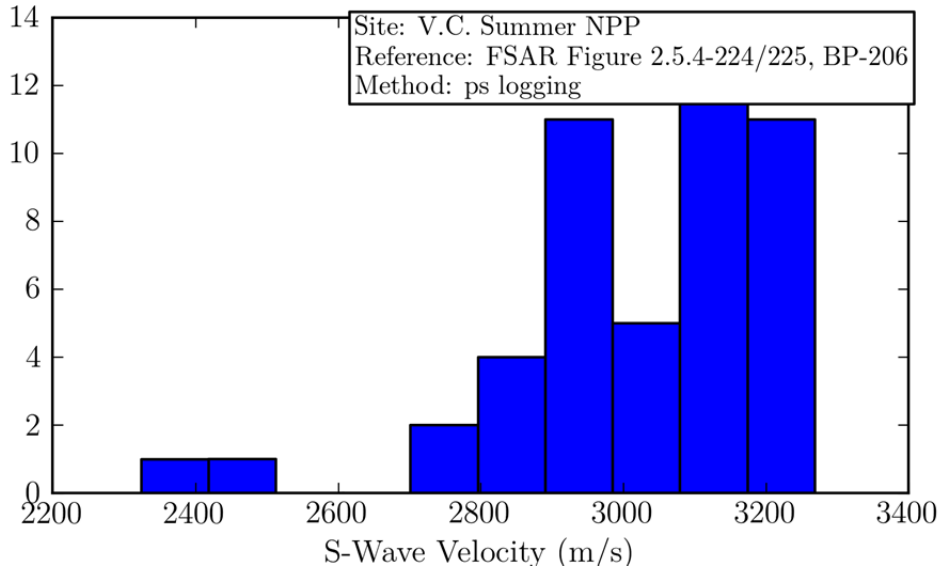

Figure B-45 Distribution of within-profile reference velocities at V.C. Summer NPP (FSAR Figure 2.5.4-224/225, BP-206, PS logging).

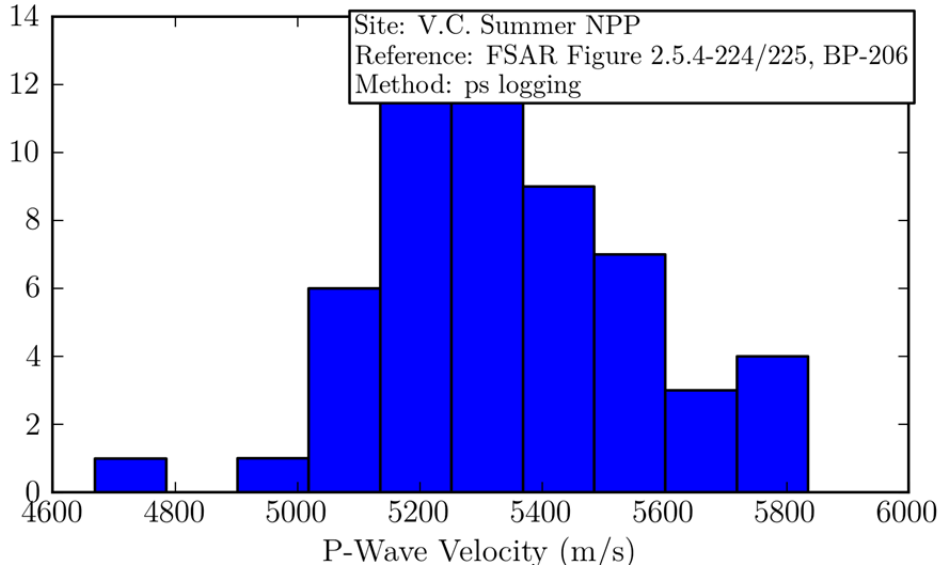

Figure B-46 Distribution of within-profile reference velocities at V.C. Summer NPP (FSAR Figure 2.5.4-224/225, BP-206, PS logging).

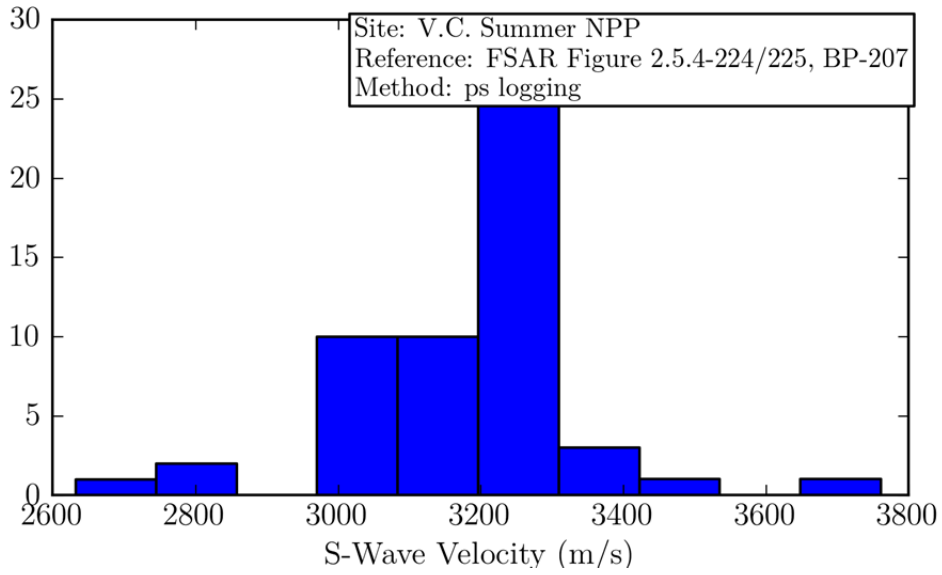

Figure B-47 Distribution of within-profile reference velocities at V.C. Summer NPP (FSAR Figure 2.5.4-224/225, BP-207, PS logging).

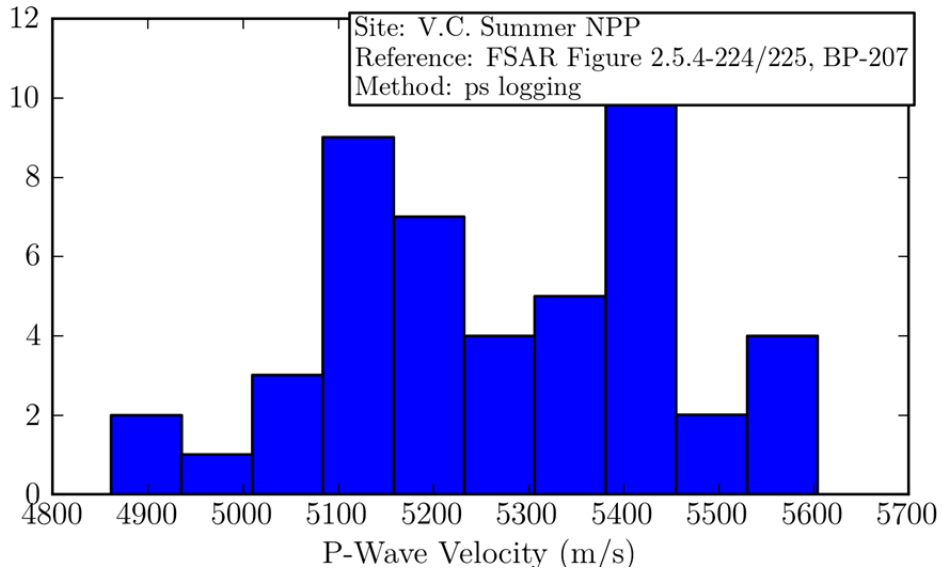

Figure B-48 Distribution of within-profile reference velocities at V.C. Summer NPP (FSAR Figure 2.5.4-224/225, BP-207, PS logging).

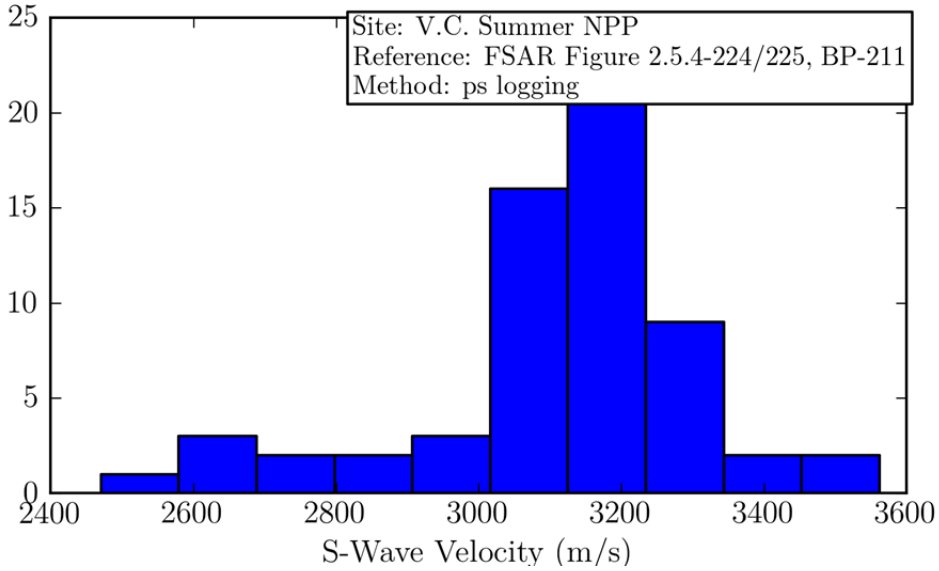

Figure B-49 Distribution of within-profile reference velocities at V.C. Summer NPP (FSAR Figure 2.5.4-224/225, BP-211, PS logging).

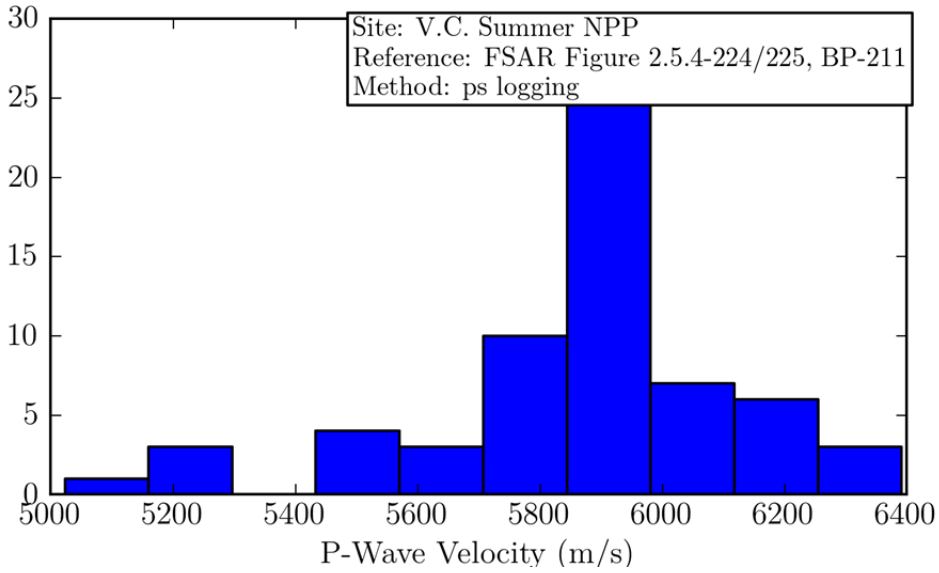

Figure B-50 Distribution of within-profile reference velocities at V.C. Summer NPP (FSAR Figure 2.5.4-224/225, BP-211, PS logging).

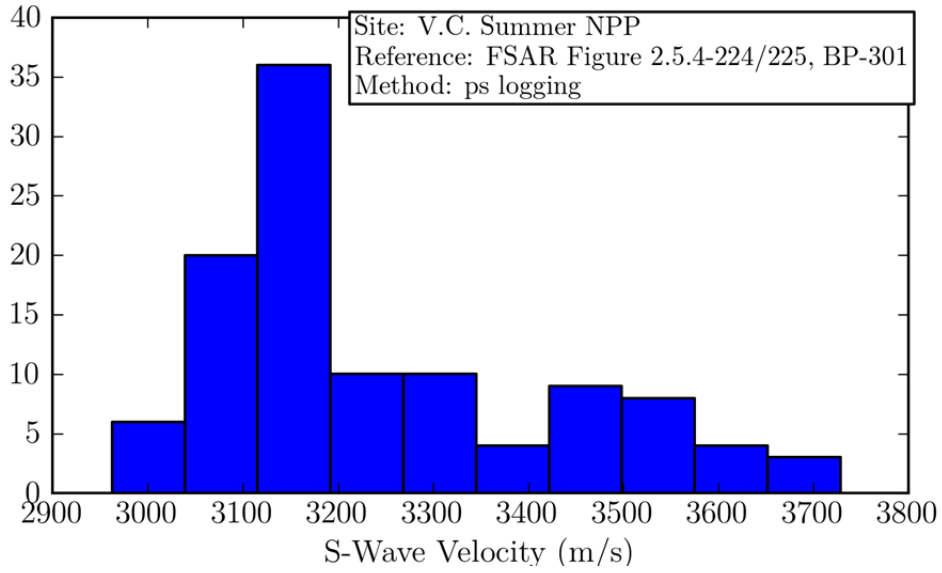

Figure B-51 Distribution of within-profile reference velocities at V.C. Summer NPP (FSAR Figure 2.5.4-224/225, BP-301, PS logging).

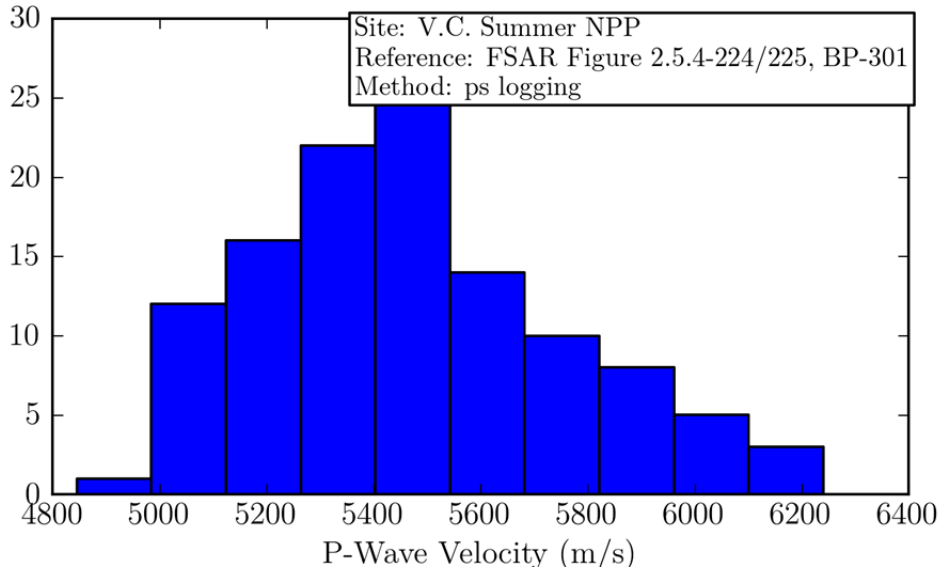

Figure B-52 Distribution of within-profile reference velocities at V.C. Summer NPP (FSAR Figure 2.5.4-224/225, BP-301, PS logging).

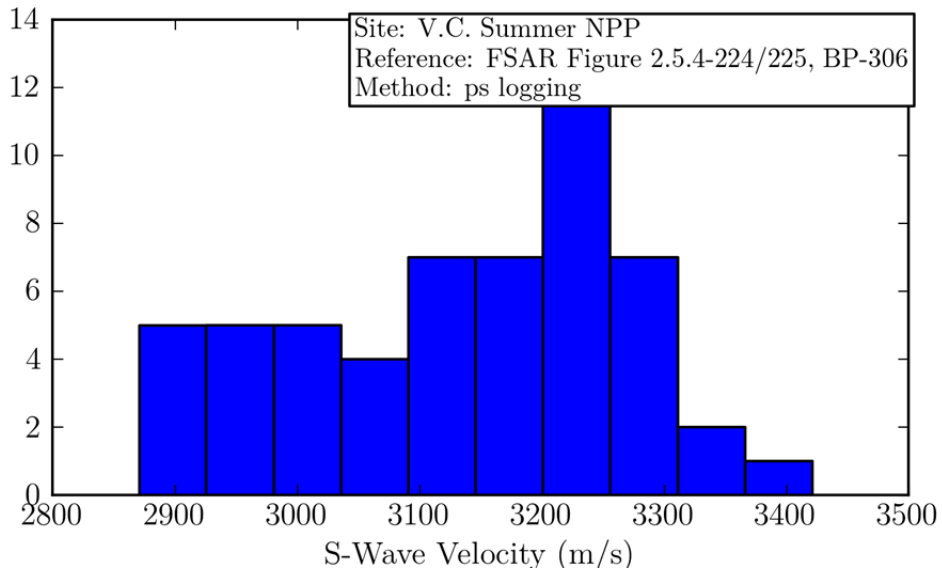

Figure B-53 Distribution of within-profile reference velocities at V.C. Summer NPP (FSAR Figure 2.5.4-224/225, BP-306, PS logging).

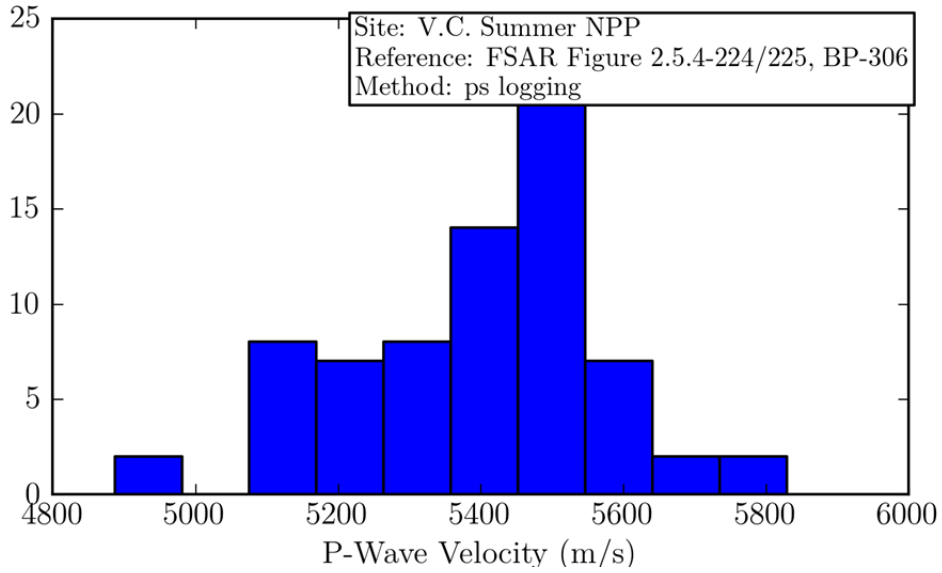

Figure B-54 Distribution of within-profile reference velocities at V.C. Summer NPP (FSAR Figure 2.5.4-224/225, BP-306, PS logging).

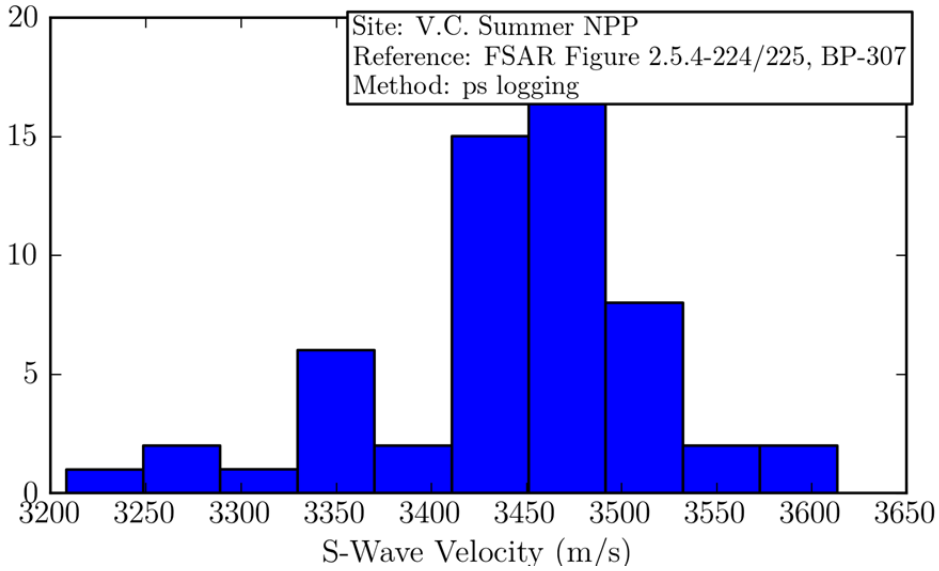

Figure B-55 Distribution of within-profile reference velocities at V.C. Summer NPP (FSAR Figure 2.5.4-224/225, BP-307, PS logging).

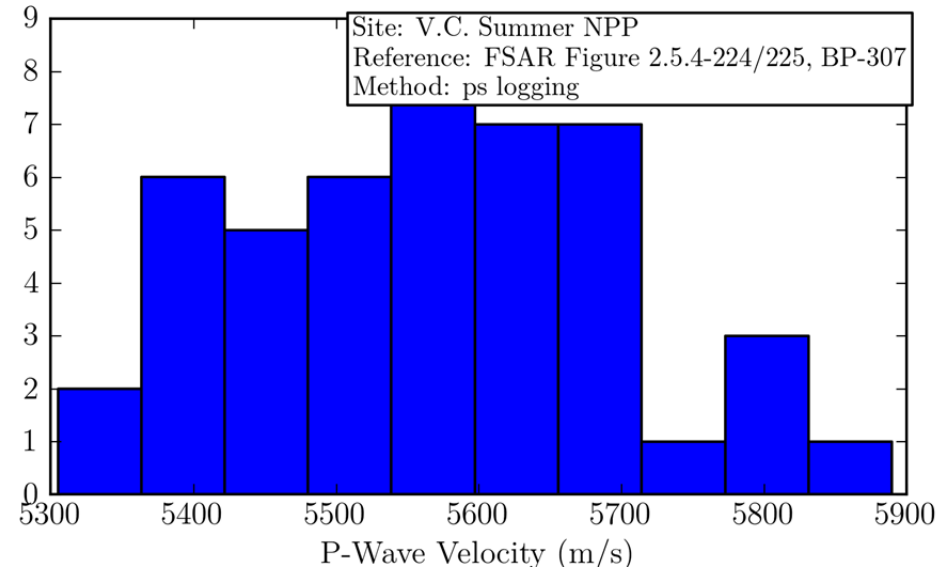

Figure B-56 Distribution of within-profile reference velocities at V.C. Summer NPP (FSAR Figure 2.5.4-224/225, BP-307, PS logging).

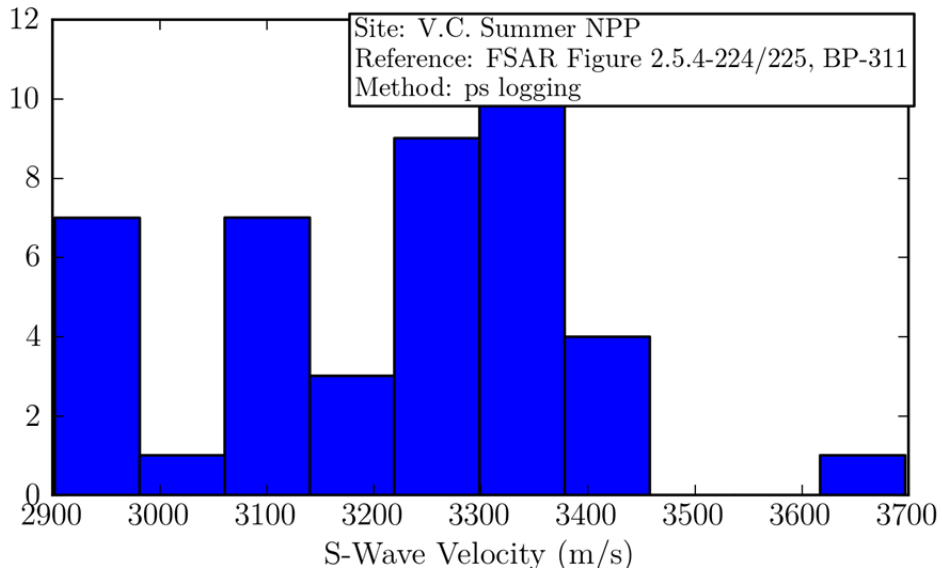

Figure B-57 Distribution of within-profile reference velocities at V.C. Summer NPP (FSAR Figure 2.5.4-224/225, BP-311, PS logging).

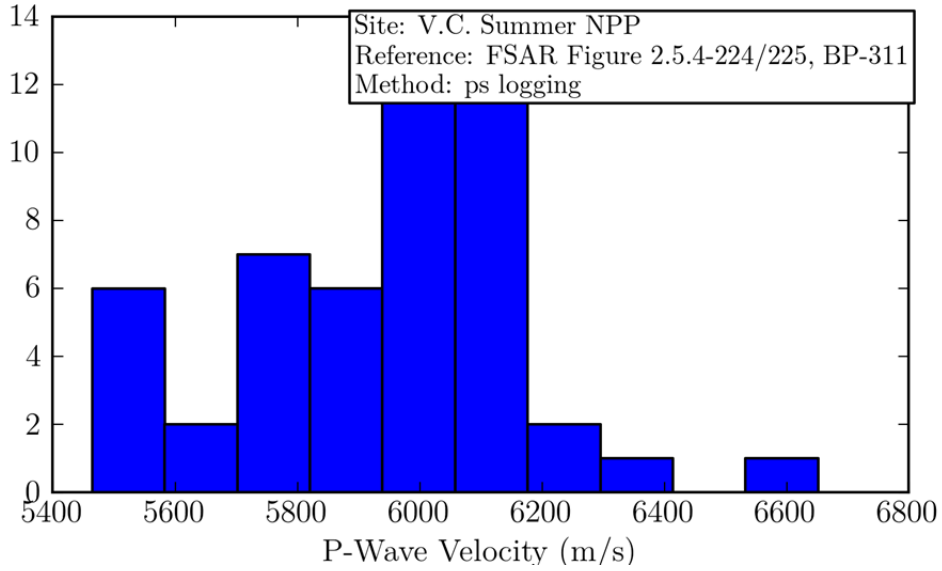

Figure B-58 Distribution of within-profile reference velocities at V.C. Summer NPP (FSAR Figure 2.5.4-224/225, BP-311, PS logging).

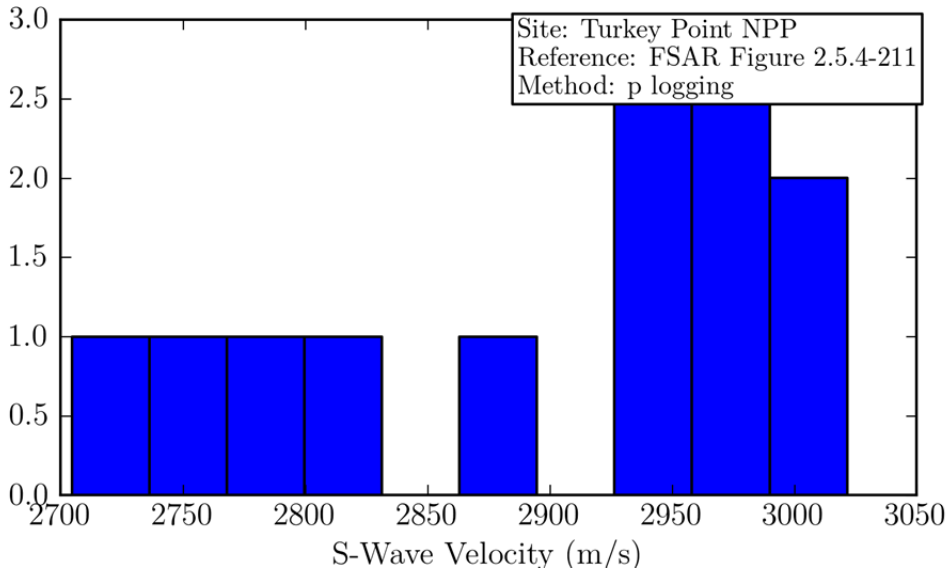

Figure B-59 Distribution of within-profile reference velocities at Turkey Point NPP (FSAR Figure 2.5.4-211, P logging).

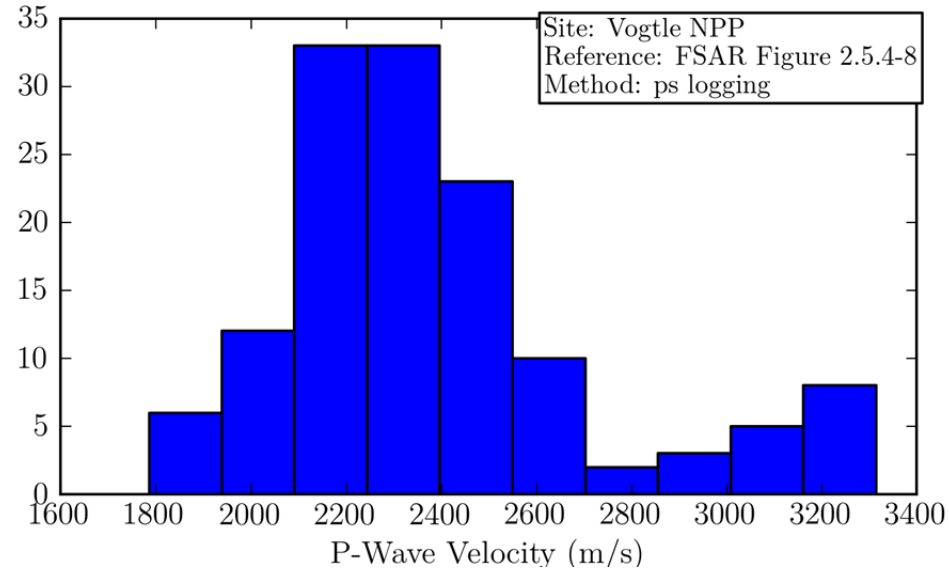

Figure B-60 Distribution of within-profile reference velocities at Vogtle NPP (FSAR Figure 2.5.4-8, PS logging).

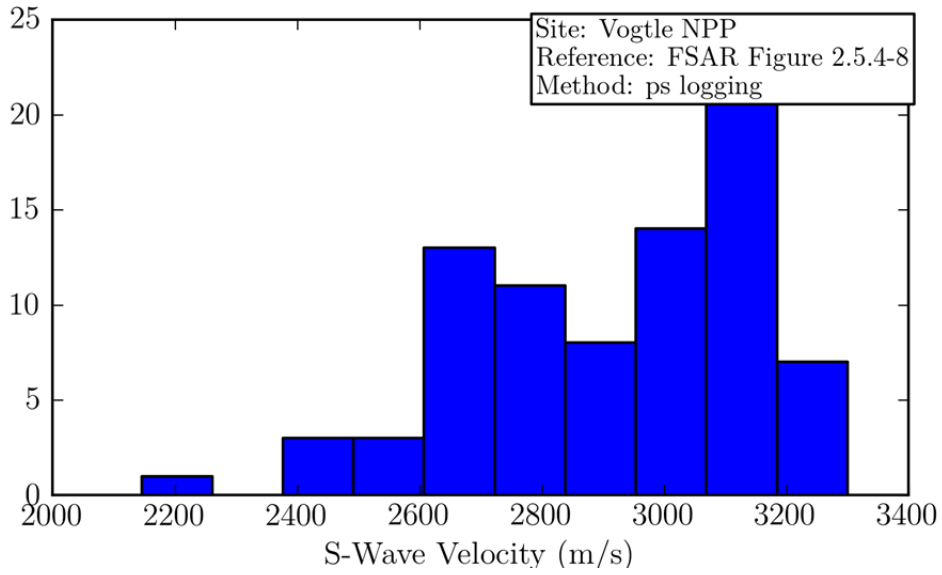

Figure B-61 Distribution of within-profile reference velocities at Vogtle NPP (FSAR Figure 2.5.4-8, PS logging).

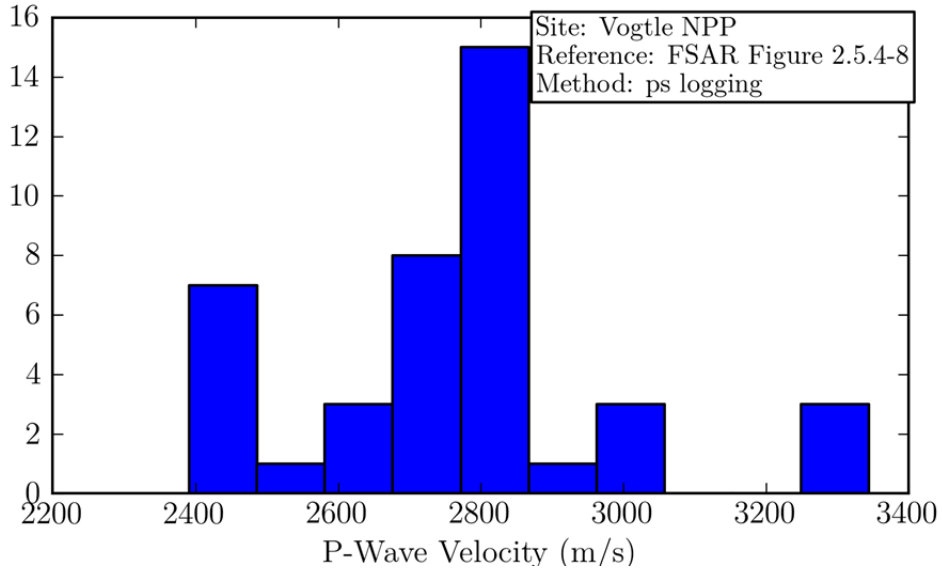

Figure B-62 Distribution of within-profile reference velocities at Vogtle NPP (FSAR Figure 2.5.4-8, PS logging).

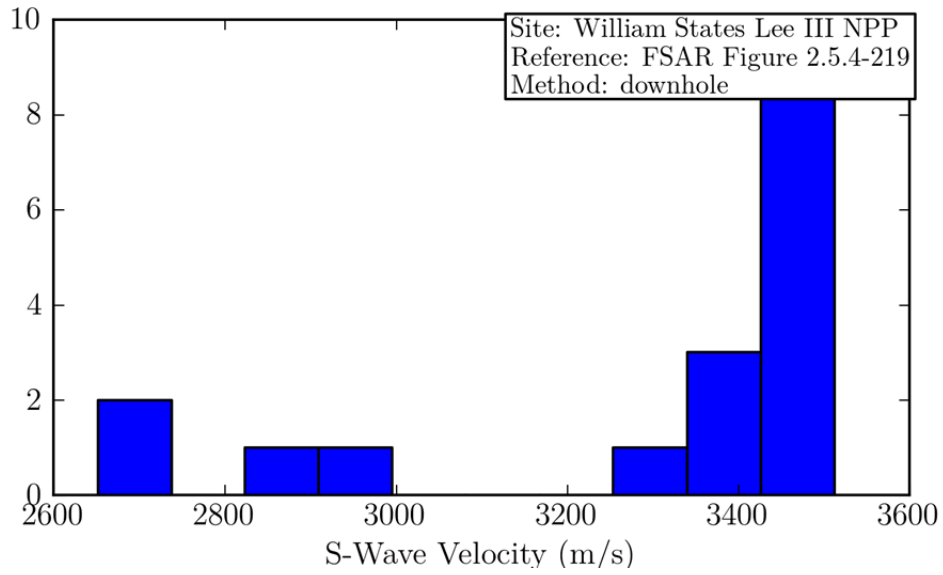

Figure B-63 Distribution of within-profile reference velocities at William States Lee III NPP (FSAR Figure 2.5.4-219, downhole).

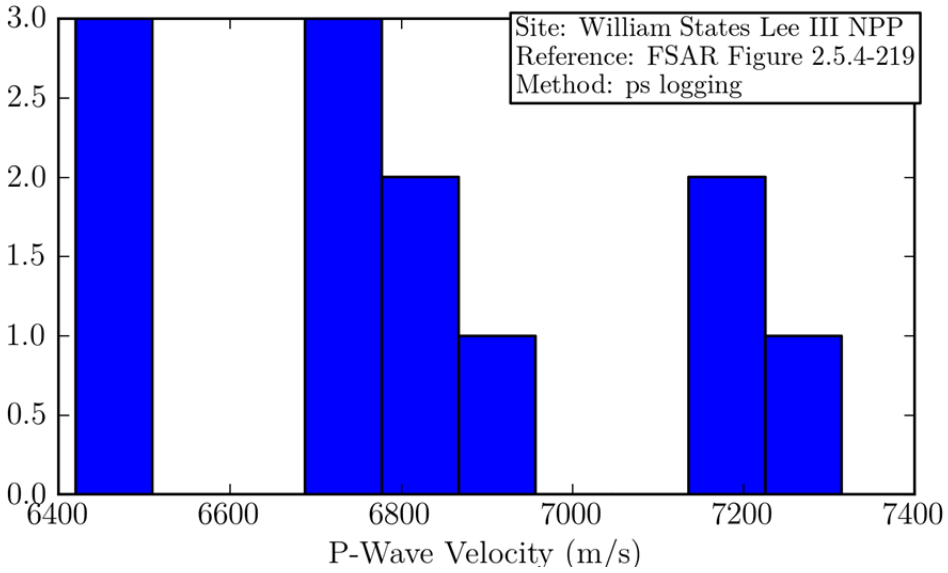

Figure B-64 Distribution of within-profile reference velocities at William States Lee III NPP (FSAR Figure 2.5.4-219, PS logging).

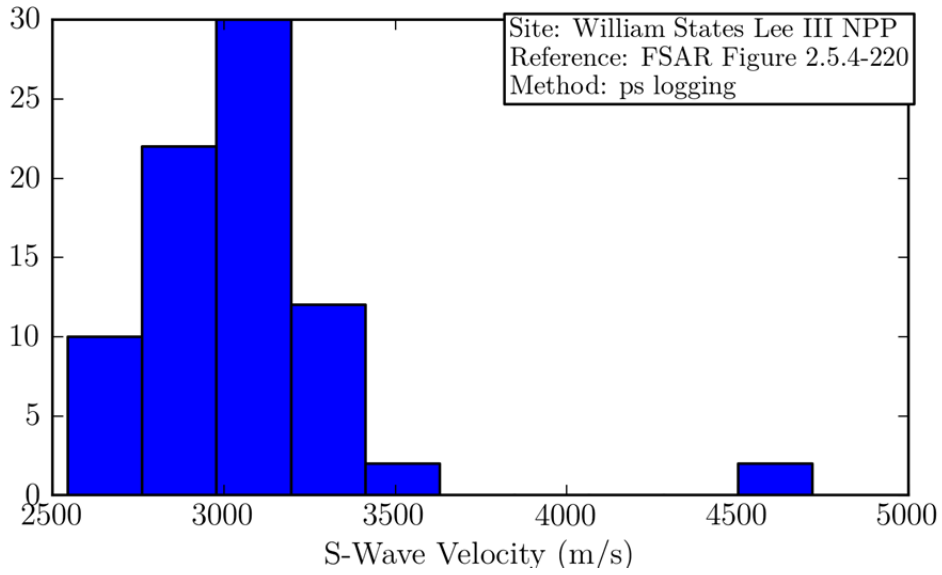

Figure B-65 Distribution of within-profile reference velocities at William States Lee III NPP (FSAR Figure 2.5.4-220, PS logging).

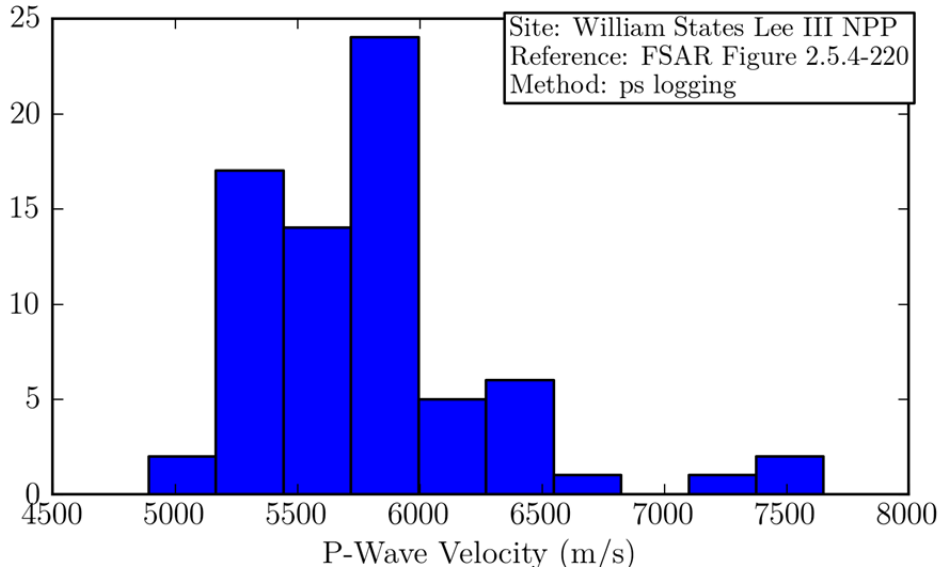

Figure B-66 Distribution of within-profile reference velocities at William States Lee III NPP (FSAR Figure 2.5.4-220, PS logging).

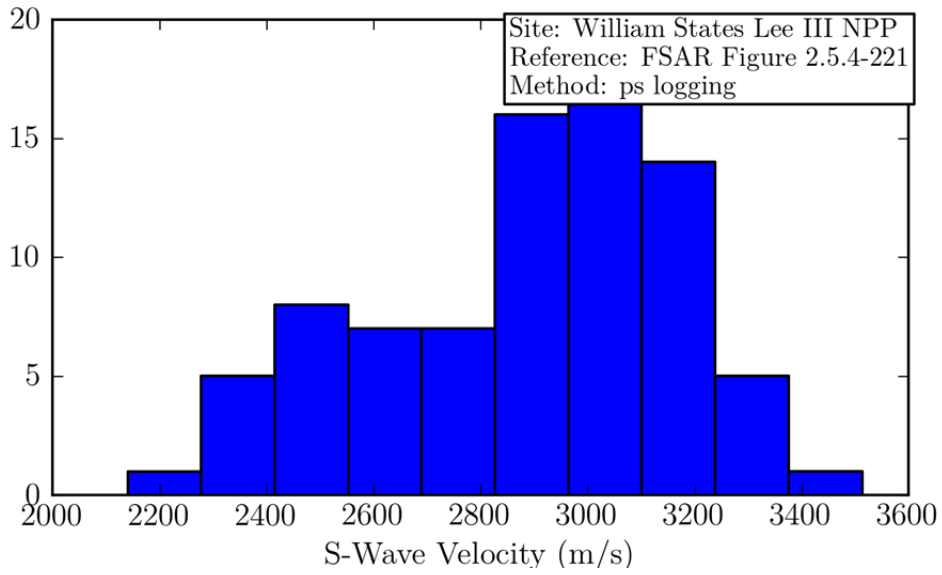

Figure B-67 Distribution of within-profile reference velocities at B William States Lee III NPP (FSAR Figure 2.5.4-221, PS logging).

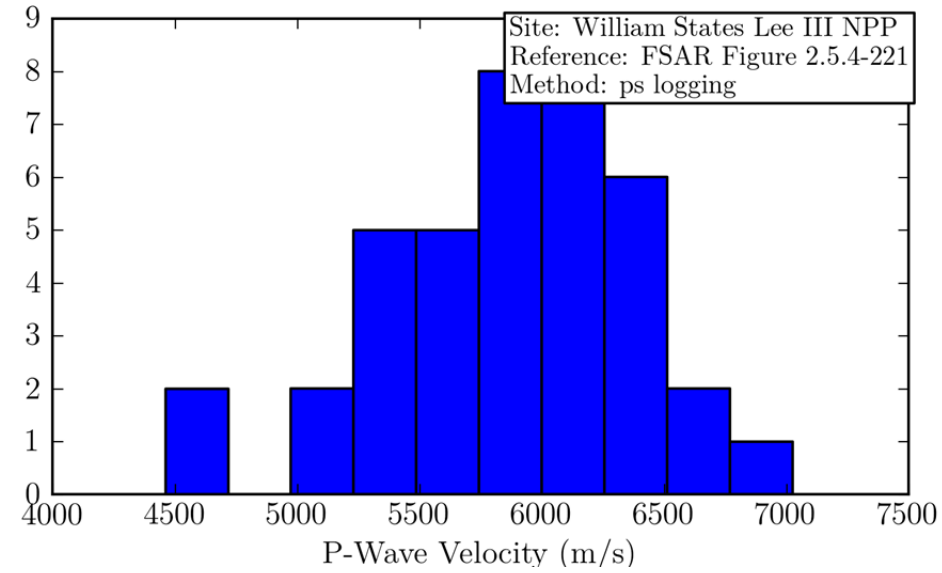

Figure B-68 Distribution of within-profile reference velocities at William States Lee III NPP (FSAR Figure 2.5.4-221, PS logging).

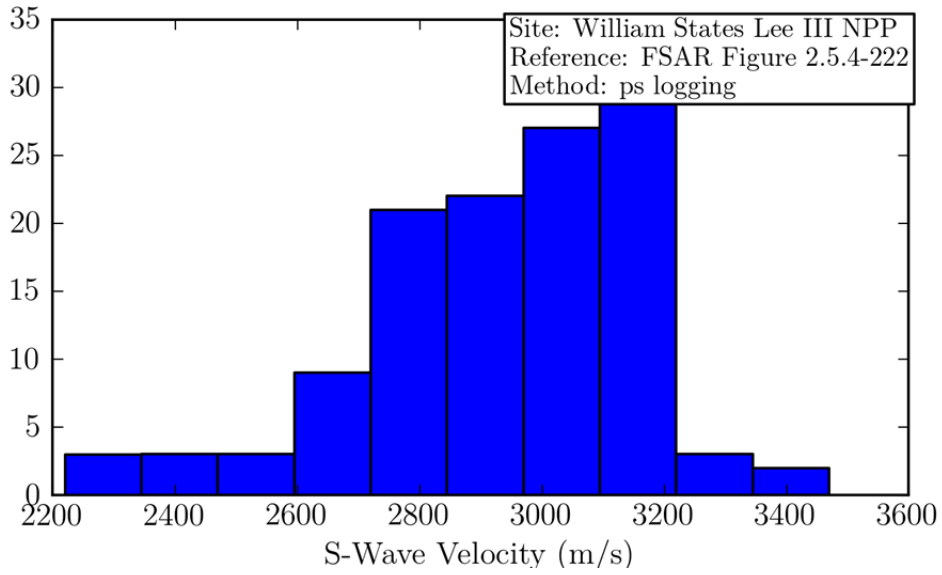

Figure B-69 Distribution of within-profile reference velocities at William States Lee III NPP (FSAR Figure 2.5.4-222, PS logging).

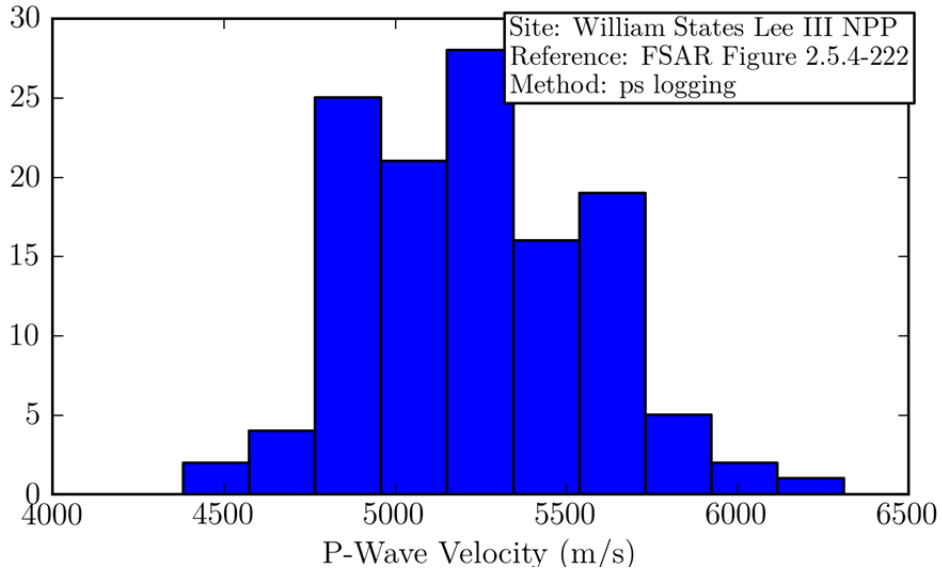

Figure B-70 Distribution of within-profile reference velocities at William States Lee III NPP (FSAR Figure 2.5.4-222, PS logging).

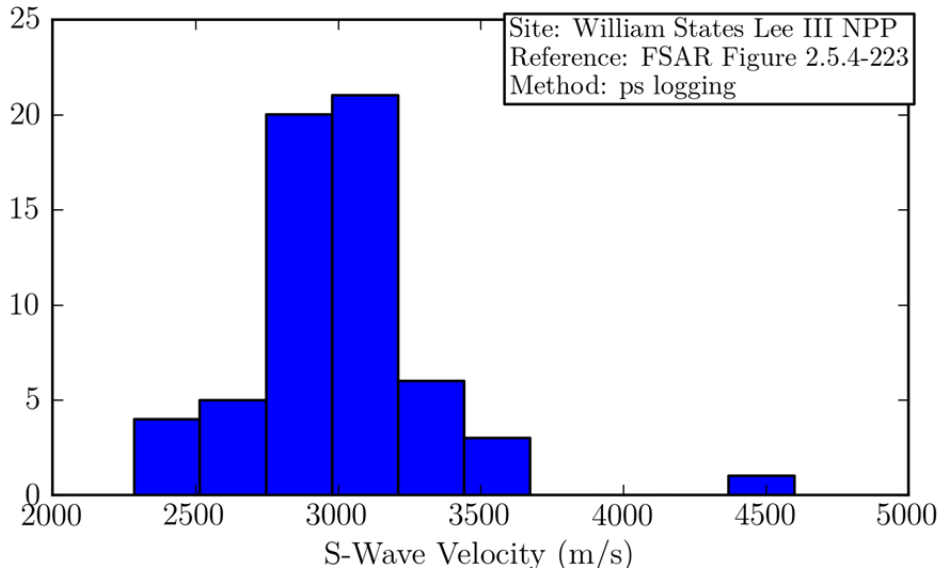

Figure B-71 Distribution of within-profile reference velocities at William States Lee III NPP (FSAR Figure 2.5.4-223, PS logging).

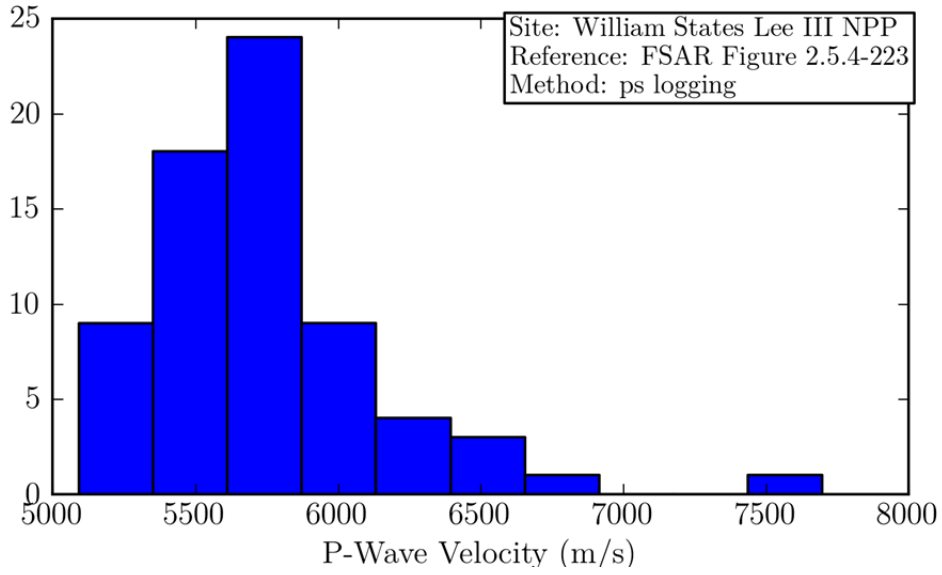

Figure B-72 Distribution of within-profile reference velocities at William States Lee III NPP (FSAR Figure 2.5.4-223, PS logging).

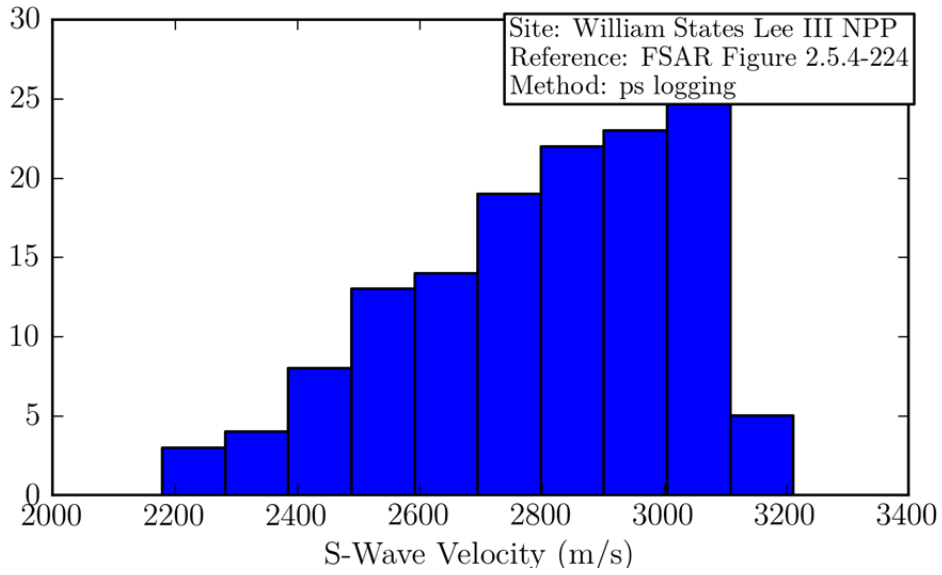

Figure B-73 Distribution of within-profile reference velocities at William States Lee III NPP (FSAR Figure 2.5.4-224, PS logging).

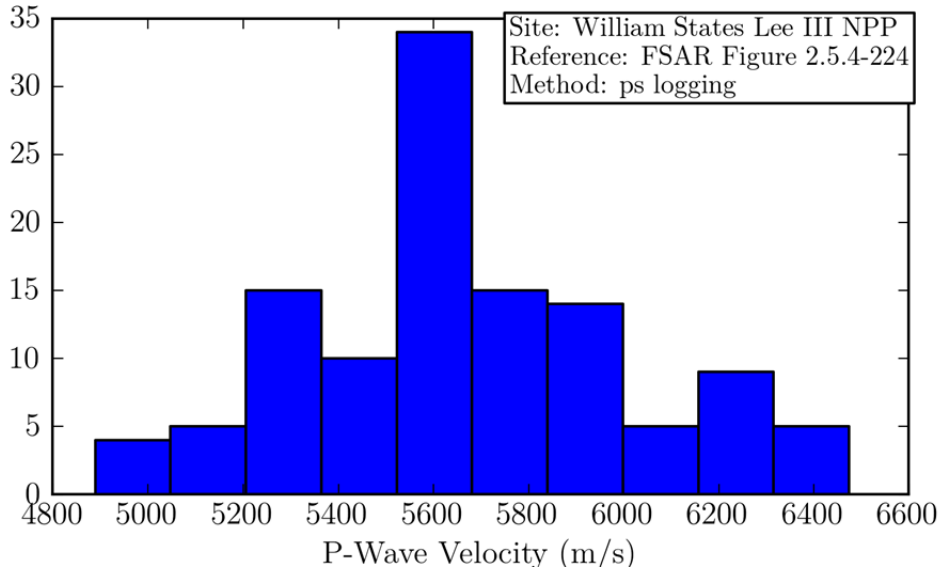

Figure B-74 Distribution of within-profile reference velocities at William States Lee III NPP (FSAR Figure 2.5.4-224, PS logging).

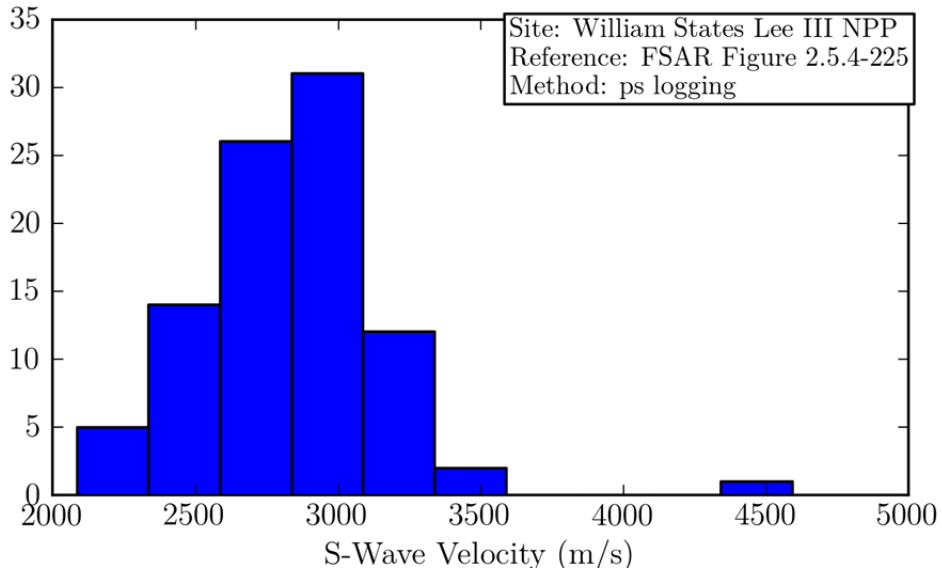

Figure B-75 Distribution of within-profile reference velocities at William States Lee III NPP (FSAR Figure 2.5.4-225, PS logging).

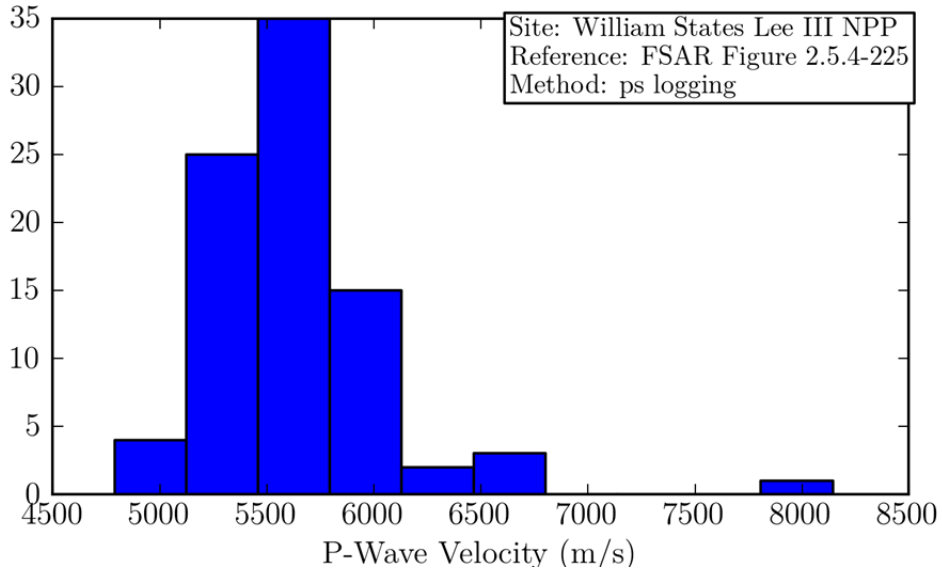

Figure B-76 Distribution of within-profile reference velocities at William States Lee III NPP (FSAR Figure 2.5.4-225, PS logging).

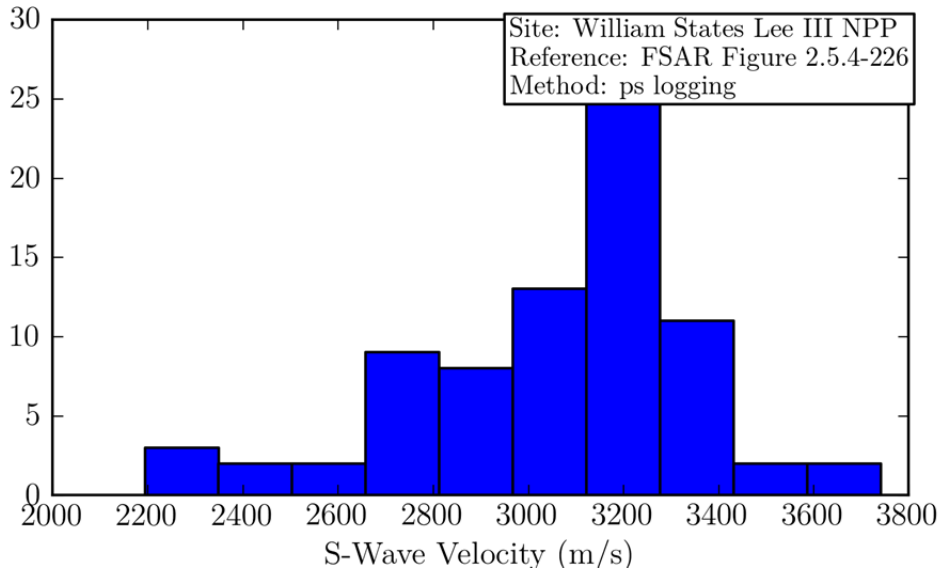

Figure B-77 Distribution of within-profile reference velocities at William States Lee III NPP (FSAR Figure 2.5.4-226, PS logging).

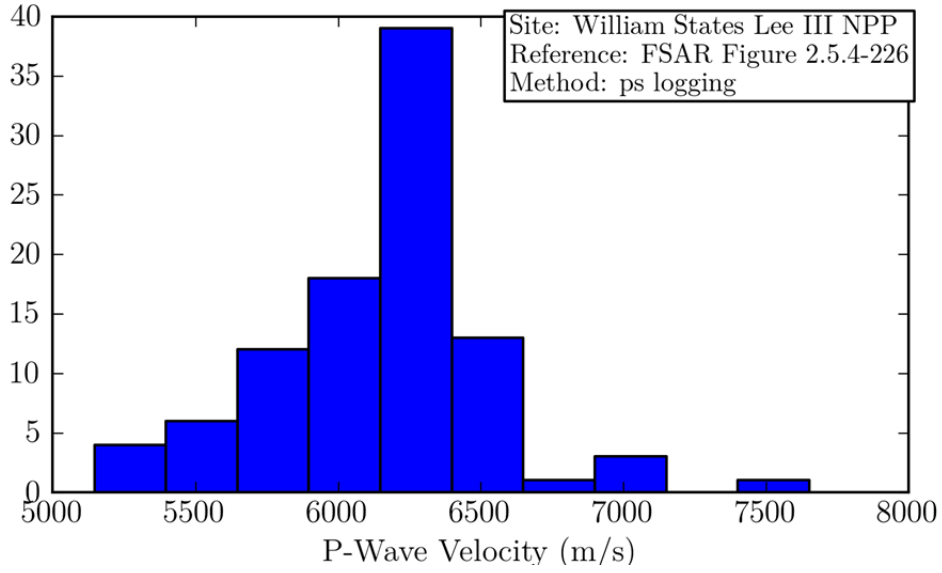

Figure B-78 Distribution of within-profile reference velocities at William States Lee III NPP (FSAR Figure 2.5.4-226, PS logging).

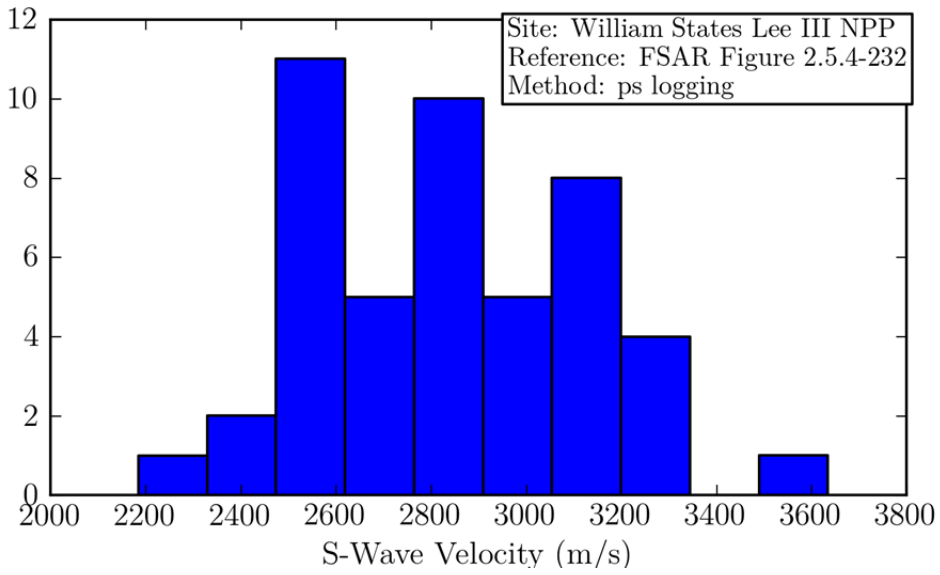

Figure B-79 **Distribution of within-profile reference velocities at William States Lee III NPP (FSAR Figure 2.5.4-232, PS logging).**

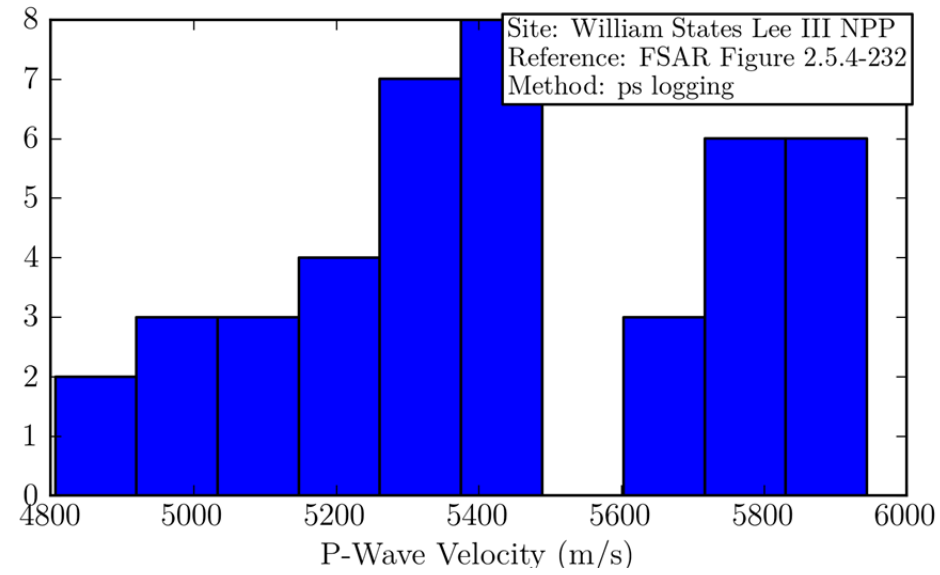

Figure B-80 **Distribution of within-profile reference velocities at William States Lee III NPP (FSAR Figure 2.5.4-232, PS logging).**

PEER REPORTS

PEER reports are available as a free PDF download from http://peer.berkeley.edu/publications/peer_reports_complete.html. Printed hard copies of PEER reports can be ordered directly from our printer by following the instructions at http://peer.berkeley.edu/publications/peer_reports.html. For other related questions about the PEER Report Series, contact the Pacific Earthquake Engineering Research Center, 325 Davis Hall mail code 1792, Berkeley, CA 94720. Tel.: (510) 642-3437; Fax: (510) 665-1655; Email: peer_editor@berkeley.edu

PEER 2014/11 *Reference-Rock Site Conditions for Central and Eastern North America: Part I - Velocity Definition*. Youssef M.A. Hashash, Albert R. Kottke, Jonathan P. Stewart, Kenneth W. Campbell, Byungmin Kim, Ellen M. Rathje, Walter J. Silva, Sissy Nikolaou, and Cheryl Moss. August 2014.

PEER 2014/10 *Evaluation of Collapse and Non-Collapse of Parallel Bridges Affected by Liquefaction and Lateral Spreading*. Benjamin Turner, Scott J. Brandenberg, and Jonathan P. Stewart. August 2014.

PEER 2014/09 *PEER Arizona Strong-Motion Database and GMPEs Evaluation*. Tadahiro Kishida, Robert E. Kayen, Olga-Joan Ktenidou, Walter J. Silva, Robert B. Darragh, and Jennie Watson-Lamprey. June 2014.

PEER 2014/08 *Unbonded Pretensioned Bridge Columns with Rocking Detail*. Jeffrey A. Schaefer, Bryan Kennedy, Marc O. Eberhard, John F. Stanton. June 2014.

PEER 2014/07 *Northridge 20 Symposium Summary Report: Impacts, Outcomes, and Next Steps*. May 2014.

PEER 2014/06 *Report of the Tenth Planning Meeting of NEES/E-Defense Collaborative Research on Earthquake Engineering*. December 2013.

PEER 2014/05 *Seismic Velocity Site Characterization of Thirty-One Chilean Seismometer Stations by Spectral Analysis of Surface Wave Dispersion.* Robert Kayen, Brad D. Carkin, Skye Corbet, Camilo Pinilla, Allan Ng, Edward Gorbis, and Christine Truong. April 2014.

PEER 2014/04 *Effect of Vertical Acceleration on Shear Strength of Reinforced Concrete Columns.* Hyerin Lee and Khalid M. Mosalam. April 2014.

PEER 2014/03 *Retest of Thirty-Year-Old Neoprene Isolation Bearings.* James M. Kelly and Niel C. Van Engelen. March 2014.

PEER 2014/02 *Theoretical Development of Hybrid Simulation Applied to Plate Structures.* Ahmed A. Bakhaty, Khalid M. Mosalam, and Sanjay Govindjee. January 2014.

PEER 2014/01 *Performance-Based Seismic Assessment of Skewed Bridges.* Peyman Kaviani, Farzin Zareian, and Ertugrul Taciroglu. January 2014.

PEER 2013/26 *Urban Earthquake Engineering. Proceedings of the U.S.-Iran Seismic Workshop.* December 2013.

PEER 2013/25 *Earthquake Engineering for Resilient Communities: 2013 PEER Internship Program Research Report Collection.* Heidi Tremayne (Editor), Stephen A. Mahin (Editor), Jorge Archbold Monterossa, Matt Brosman, Shelly Dean, Katherine deLaveaga, Curtis Fong, Donovan Holder, Rakeeb Khan, Elizabeth Jachens, David Lam, Daniela Martinez Lopez, Mara Minner, Geffen Oren, Julia Pavicic, Melissa Quinonez, Lorena Rodriguez, Sean Salazar, Kelli Slaven, Vivian Steyert, Jenny Taing, and Salvador Tena. December 2013.

PEER 2013/24 *NGA-West2 Ground Motion Prediction Equations for Vertical Ground Motions.* September 2013.

PEER 2013/23 *Coordinated Planning and Preparedness for Fire Following Major Earthquakes.* Charles Scawthorn. November 2013.

PEER 2013/22 *GEM-PEER Task 3 Project: Selection of a Global Set of Ground Motion Prediction Equations.* Jonathan P. Stewart, John Douglas, Mohammad B. Javanbarg, Carola Di Alessandro, Yousef Bozorgnia, Norman A. Abrahamson, David M. Boore, Kenneth W. Campbell, Elise Delavaud, Mustafa Erdik and Peter J. Stafford. December 2013.

PEER 2013/21 *Seismic Design and Performance of Bridges with Columns on Rocking Foundations.* Grigorios Antonellis and Marios Panagiotou. September 2013.

PEER 2013/20 *Experimental and Analytical Studies on the Seismic Behavior of Conventional and Hybrid Braced Frames.* Jiun-Wei Lai and Stephen A. Mahin. September 2013.

PEER 2013/19 *Toward Resilient Communities: A Performance-Based Engineering Framework for Design and Evaluation of the Built Environment.* Michael William Mieler, Bozidar Stojadinovic, Robert J. Budnitz, Stephen A. Mahin and Mary C. Comerio. September 2013.

PEER 2013/18 *Identification of Site Parameters that Improve Predictions of Site Amplification.* Ellen M. Rathje and Sara Navidi. July 2013.

PEER 2013/17 *Response Spectrum Analysis of Concrete Gravity Dams Including Dam-Water-Foundation Interaction.* Arnkjell Løkke and Anil K. Chopra. July 2013.

PEER 2013/16 *Effect of hoop reinforcement spacing on the cyclic response of large reinforced concrete special moment frame beams.* Marios Panagiotou, Tea Visnjic, Grigorios Antonellis, Panagiotis Galanis, and Jack P. Moehle. June 2013.

PEER 2013/15 *A Probabilistic Framework to Include the Effects of Near-Fault Directivity in Seismic Hazard Assessment.* Shrey Kumar Shahi, Jack W. Baker. October 2013.

PEER 2013/14 *Hanging-Wall Scaling using Finite-Fault Simulations.* Jennifer L. Donahue and Norman A. Abrahamson. September 2013.

PEER 2013/13 *Semi-Empirical Nonlinear Site Amplification and its Application in NEHRP Site Factors.* Jonathan P. Stewart and Emel Seyhan. November 2013.

PEER 2013/12 *Nonlinear Horizontal Site Response for the NGA-West2 Project.* Ronnie Kamai, Norman A. Abramson, Walter J. Silva. May 2013.

PEER 2013/11 *Epistemic Uncertainty for NGA-West2 Models.* Linda Al Atik and Robert R. Youngs. May 2013.

PEER 2013/10 *NGA-West 2 Models for Ground-Motion Directionality.* Shrey K. Shahi and Jack W. Baker. May 2013.

PEER 2013/09 *Final Report of the NGA-West2 Directivity Working Group.* Paul Spudich, Jeffrey R. Bayless, Jack W. Baker, Brian S.J. Chiou, Badie Rowshandel, Shrey Shahi, and Paul Somerville. May 2013.

PEER 2013/08 *NGA-West2 Model for Estimating Average Horizontal Values of Pseudo-Absolute Spectral Accelerations Generated by Crustal Earthquakes.* I. M. Idriss. May 2013.

PEER 2013/07 *Update of the Chiou and Youngs NGA Ground Motion Model for Average Horizontal Component of Peak Ground Motion and Response Spectra.* Brian Chiou and Robert Youngs. May 2013.

PEER 2013/06 *NGA-West2 Campbell-Bozorgnia Ground Motion Model for the Horizontal Components of PGA, PGV, and 5%-Damped Elastic Pseudo-Acceleration Response Spectra for Periods Ranging from 0.01 to 10 sec.* Kenneth W. Campbell and Yousef Bozorgnia. May 2013.

PEER 2013/05 *NGA-West 2 Equations for Predicting Response Spectral Accelerations for Shallow Crustal Earthquakes.* David M. Boore, Jonathan P. Stewart, Emel Seyhan, Gail M. Atkinson. May 2013.

PEER 2013/04 *Update of the AS08 Ground-Motion Prediction Equations Based on the NGA-West2 Data Set.* Norman Abrahamson, Walter Silva, and Ronnie Kamai. May 2013.

PEER 2013/03 *PEER NGA-West2 Database.* Timothy D. Ancheta, Robert B. Darragh, Jonathan P. Stewart, Emel Seyhan, Walter J. Silva, Brian S.J. Chiou, Katie E. Wooddell, Robert W. Graves, Albert R. Kottke, David M. Boore, Tadahiro Kishida, and Jennifer L. Donahue. May 2013.

PEER 2013/02 *Hybrid Simulation of the Seismic Response of Squat Reinforced Concrete Shear Walls.* Catherine A. Whyte and Bozidar Stojadinovic. May 2013.

PEER 2013/01 *Housing Recovery in Chile: A Qualitative Mid-program Review.* Mary C. Comerio. February 2013.

PEER 2012/08 *Guidelines for Estimation of Shear Wave Velocity.* Bernard R. Wair, Jason T. DeJong, and Thomas Shantz. December 2012.

PEER 2012/07 *Earthquake Engineering for Resilient Communities: 2012 PEER Internship Program Research Report Collection.* Heidi Tremayne (Editor), Stephen A. Mahin (Editor), Collin Anderson, Dustin Cook, Michael Erceg, Carlos Esparza, Jose Jimenez, Dorian Krausz, Andrew Lo, Stephanie Lopez, Nicole McCurdy, Paul Shipman, Alexander Strum, Eduardo Vega. December 2012.

PEER 2012/06 *Fragilities for Precarious Rocks at Yucca Mountain.* Matthew D. Purvance, Rasool Anooshehpoor, and James N. Brune. December 2012.

PEER 2012/05 *Development of Simplified Analysis Procedure for Piles in Laterally Spreading Layered Soils.* Christopher R. McGann, Pedro Arduino, and Peter Mackenzie–Helnwein. December 2012.

PEER 2012/04 *Unbonded Pre-Tensioned Columns for Bridges in Seismic Regions.* Phillip M. Davis, Todd M. Janes, Marc O. Eberhard, and John F. Stanton. December 2012.

PEER 2012/03 *Experimental and Analytical Studies on Reinforced Concrete Buildings with Seismically Vulnerable Beam-Column Joints.* Sangjoon Park and Khalid M. Mosalam. October 2012.

PEER 2012/02 *Seismic Performance of Reinforced Concrete Bridges Allowed to Uplift during Multi-Directional Excitation.* Andres Oscar Espinoza and Stephen A. Mahin. July 2012.

PEER 2012/01 *Spectral Damping Scaling Factors for Shallow Crustal Earthquakes in Active Tectonic Regions.* Sanaz Rezaeian, Yousef Bozorgnia, I. M. Idriss, Kenneth Campbell, Norman Abrahamson, and Walter Silva. July 2012.

PEER 2011/10 *Earthquake Engineering for Resilient Communities: 2011 PEER Internship Program Research Report Collection.* Eds. Heidi Faison and Stephen A. Mahin. December 2011.

PEER 2011/09 *Calibration of Semi-Stochastic Procedure for Simulating High-Frequency Ground Motions.* Jonathan P. Stewart, Emel Seyhan, and Robert W. Graves. December 2011.

PEER 2011/08 *Water Supply in regard to Fire Following Earthquake.* Charles Scawthorn. November 2011.

PEER 2011/07 *Seismic Risk Management in Urban Areas. Proceedings of a U.S.-Iran-Turkey Seismic Workshop.* September 2011.

PEER 2011/06 *The Use of Base Isolation Systems to Achieve Complex Seismic Performance Objectives.* Troy A. Morgan and Stephen A. Mahin. July 2011.

PEER 2011/05 *Case Studies of the Seismic Performance of Tall Buildings Designed by Alternative Means.* Task 12 Report for the Tall Buildings Initiative. Jack Moehle, Yousef Bozorgnia, Nirmal Jayaram, Pierson Jones, Mohsen Rahnama, Nilesh Shome, Zeynep Tuna, John Wallace, Tony Yang, and Farzin Zareian. July 2011.

PEER 2011/04 *Recommended Design Practice for Pile Foundations in Laterally Spreading Ground.* Scott A. Ashford, Ross W. Boulanger, and Scott J. Brandenberg. June 2011.

PEER 2011/03 *New Ground Motion Selection Procedures and Selected Motions for the PEER Transportation Research Program.* Jack W. Baker, Ting Lin, Shrey K. Shahi, and Nirmal Jayaram. March 2011.

PEER 2011/02 *A Bayesian Network Methodology for Infrastructure Seismic Risk Assessment and Decision Support.* Michelle T. Bensi, Armen Der Kiureghian, and Daniel Straub. March 2011.

PEER 2011/01 *Demand Fragility Surfaces for Bridges in Liquefied and Laterally Spreading Ground.* Scott J. Brandenberg, Jian Zhang, Pirooz Kashighandi, Yili Huo, and Minxing Zhao. March 2011.

PEER 2010/05 *Guidelines for Performance-Based Seismic Design of Tall Buildings.* Developed by the Tall Buildings Initiative. November 2010.

PEER 2010/04 *Application Guide for the Design of Flexible and Rigid Bus Connections between Substation Equipment Subjected to Earthquakes.* Jean-Bernard Dastous and Armen Der Kiureghian. September 2010.

PEER 2010/03 *Shear Wave Velocity as a Statistical Function of Standard Penetration Test Resistance and Vertical Effective Stress at Caltrans Bridge Sites.* Scott J. Brandenberg, Naresh Bellana, and Thomas Shantz. June 2010.

PEER 2010/02 *Stochastic Modeling and Simulation of Ground Motions for Performance-Based Earthquake Engineering.* Sanaz Rezaeian and Armen Der Kiureghian. June 2010.

PEER 2010/01 *Structural Response and Cost Characterization of Bridge Construction Using Seismic Performance Enhancement Strategies.* Ady Aviram, Božidar Stojadinović, Gustavo J. Parra-Montesinos, and Kevin R. Mackie. March 2010.

PEER 2009/03 *The Integration of Experimental and Simulation Data in the Study of Reinforced Concrete Bridge Systems Including Soil-Foundation-Structure Interaction.* Matthew Dryden and Gregory L. Fenves. November 2009.

PEER 2009/02 *Improving Earthquake Mitigation through Innovations and Applications in Seismic Science, Engineering, Communication, and Response. Proceedings of a U.S.-Iran Seismic Workshop.* October 2009.

PEER 2009/01 *Evaluation of Ground Motion Selection and Modification Methods: Predicting Median Interstory Drift Response of Buildings.* Curt B. Haselton, Ed. June 2009.

PEER 2008/10 *Technical Manual for Strata.* Albert R. Kottke and Ellen M. Rathje. February 2009.

PEER 2008/09 *NGA Model for Average Horizontal Component of Peak Ground Motion and Response Spectra.* Brian S.-J. Chiou and Robert R. Youngs. November 2008.

PEER 2008/08 *Toward Earthquake-Resistant Design of Concentrically Braced Steel Structures.* Patxi Uriz and Stephen A. Mahin. November 2008.

PEER 2008/07 *Using OpenSees for Performance-Based Evaluation of Bridges on Liquefiable Soils.* Stephen L. Kramer, Pedro Arduino, and HyungSuk Shin. November 2008.

PEER 2008/06 *Shaking Table Tests and Numerical Investigation of Self-Centering Reinforced Concrete Bridge Columns.* Hyung IL Jeong, Junichi Sakai, and Stephen A. Mahin. September 2008.

PEER 2008/05 *Performance-Based Earthquake Engineering Design Evaluation Procedure for Bridge Foundations Undergoing Liquefaction-Induced Lateral Ground Displacement.* Christian A. Ledezma and Jonathan D. Bray. August 2008.

PEER 2008/04 *Benchmarking of Nonlinear Geotechnical Ground Response Analysis Procedures.* Jonathan P. Stewart, Annie On-Lei Kwok, Yousseff M. A. Hashash, Neven Matasovic, Robert Pyke, Zhiliang Wang, and Zhaohui Yang. August 2008.

PEER 2008/03 *Guidelines for Nonlinear Analysis of Bridge Structures in California.* Ady Aviram, Kevin R. Mackie, and Božidar Stojadinović. August 2008.

PEER 2008/02 *Treatment of Uncertainties in Seismic-Risk Analysis of Transportation Systems.* Evangelos Stergiou and Anne S. Kiremidjian. July 2008.

PEER 2008/01 *Seismic Performance Objectives for Tall Buildings.* William T. Holmes, Charles Kircher, William Petak, and Nabih Youssef. August 2008.

PEER 2007/12 *An Assessment to Benchmark the Seismic Performance of a Code-Conforming Reinforced Concrete Moment-Frame Building.* Curt Haselton, Christine A. Goulet, Judith Mitrani-Reiser, James L. Beck, Gregory G. Deierlein, Keith A. Porter, Jonathan P. Stewart, and Ertugrul Taciroglu. August 2008.

PEER 2007/11 *Bar Buckling in Reinforced Concrete Bridge Columns.* Wayne A. Brown, Dawn E. Lehman, and John F. Stanton. February 2008.

PEER 2007/10 *Computational Modeling of Progressive Collapse in Reinforced Concrete Frame Structures.* Mohamed M. Talaat and Khalid M. Mosalam. May 2008.

PEER 2007/09 *Integrated Probabilistic Performance-Based Evaluation of Benchmark Reinforced Concrete Bridges.* Kevin R. Mackie, John-Michael Wong, and Božidar Stojadinović. January 2008.

PEER 2007/08 *Assessing Seismic Collapse Safety of Modern Reinforced Concrete Moment-Frame Buildings.* Curt B. Haselton and Gregory G. Deierlein. February 2008.

PEER 2007/07 *Performance Modeling Strategies for Modern Reinforced Concrete Bridge Columns.* Michael P. Berry and Marc O. Eberhard. April 2008.

PEER 2007/06 *Development of Improved Procedures for Seismic Design of Buried and Partially Buried Structures.* Linda Al Atik and Nicholas Sitar. June 2007.

PEER 2007/05 *Uncertainty and Correlation in Seismic Risk Assessment of Transportation Systems.* Renee G. Lee and Anne S. Kiremidjian. July 2007.

PEER 2007/04 *Numerical Models for Analysis and Performance-Based Design of Shallow Foundations Subjected to Seismic Loading.* Sivapalan Gajan, Tara C. Hutchinson, Bruce L. Kutter, Prishati Raychowdhury, José A. Ugalde, and Jonathan P. Stewart. May 2008.

PEER 2007/03 *Beam-Column Element Model Calibrated for Predicting Flexural Response Leading to Global Collapse of RC Frame Buildings.* Curt B. Haselton, Abbie B. Liel, Sarah Taylor Lange, and Gregory G. Deierlein. May 2008.

PEER 2007/02 *Campbell-Bozorgnia NGA Ground Motion Relations for the Geometric Mean Horizontal Component of Peak and Spectral Ground Motion Parameters.* Kenneth W. Campbell and Yousef Bozorgnia. May 2007.

PEER 2007/01 *Boore-Atkinson NGA Ground Motion Relations for the Geometric Mean Horizontal Component of Peak and Spectral Ground Motion Parameters.* David M. Boore and Gail M. Atkinson. May. May 2007.

PEER 2006/12 *Societal Implications of Performance-Based Earthquake Engineering.* Peter J. May. May 2007.

PEER 2006/11 *Probabilistic Seismic Demand Analysis Using Advanced Ground Motion Intensity Measures, Attenuation Relationships, and Near-Fault Effects.* Polsak Tothong and C. Allin Cornell. March 2007.

PEER 2006/10 *Application of the PEER PBEE Methodology to the I-880 Viaduct.* Sashi Kunnath. February 2007.

PEER 2006/09 *Quantifying Economic Losses from Travel Forgone Following a Large Metropolitan Earthquake.* James Moore, Sungbin Cho, Yue Yue Fan, and Stuart Werner. November 2006.

PEER 2006/08 *Vector-Valued Ground Motion Intensity Measures for Probabilistic Seismic Demand Analysis.* Jack W. Baker and C. Allin Cornell. October 2006.

PEER 2006/07 *Analytical Modeling of Reinforced Concrete Walls for Predicting Flexural and Coupled–Shear-Flexural Responses.* Kutay Orakcal, Leonardo M. Massone, and John W. Wallace. October 2006.

PEER 2006/06 *Nonlinear Analysis of a Soil-Drilled Pier System under Static and Dynamic Axial Loading.* Gang Wang and Nicholas Sitar. November 2006.

PEER 2006/05 *Advanced Seismic Assessment Guidelines.* Paolo Bazzurro, C. Allin Cornell, Charles Menun, Maziar Motahari, and Nicolas Luco. September 2006.

PEER 2006/04 *Probabilistic Seismic Evaluation of Reinforced Concrete Structural Components and Systems.* Tae Hyung Lee and Khalid M. Mosalam. August 2006.

PEER 2006/03 *Performance of Lifelines Subjected to Lateral Spreading.* Scott A. Ashford and Teerawut Juirnarongrit. July 2006.

PEER 2006/02 *Pacific Earthquake Engineering Research Center Highway Demonstration Project.* Anne Kiremidjian, James Moore, Yue Yue Fan, Nesrin Basoz, Ozgur Yazali, and Meredith Williams. April 2006.

PEER 2006/01 *Bracing Berkeley. A Guide to Seismic Safety on the UC Berkeley Campus.* Mary C. Comerio, Stephen Tobriner, and Ariane Fehrenkamp. January 2006.

PEER 2005/16 *Seismic Response and Reliability of Electrical Substation Equipment and Systems.* Junho Song, Armen Der Kiureghian, and Jerome L. Sackman. April 2006.

PEER 2005/15 *CPT-Based Probabilistic Assessment of Seismic Soil Liquefaction Initiation.* R. E. S. Moss, R. B. Seed, R. E. Kayen, J. P. Stewart, and A. Der Kiureghian. April 2006.

PEER 2005/14 *Workshop on Modeling of Nonlinear Cyclic Load-Deformation Behavior of Shallow Foundations.* Bruce L. Kutter, Geoffrey Martin, Tara Hutchinson, Chad Harden, Sivapalan Gajan, and Justin Phalen. March 2006.

PEER 2005/13 *Stochastic Characterization and Decision Bases under Time-Dependent Aftershock Risk in Performance-Based Earthquake Engineering.* Gee Liek Yeo and C. Allin Cornell. July 2005.

PEER 2005/12 *PEER Testbed Study on a Laboratory Building: Exercising Seismic Performance Assessment.* Mary C. Comerio, editor. November 2005.

PEER 2005/11 *Van Nuys Hotel Building Testbed Report: Exercising Seismic Performance Assessment.* Helmut Krawinkler, editor. October 2005.

PEER 2005/10 *First NEES/E-Defense Workshop on Collapse Simulation of Reinforced Concrete Building Structures.* September 2005.

PEER 2005/09 *Test Applications of Advanced Seismic Assessment Guidelines.* Joe Maffei, Karl Telleen, Danya Mohr, William Holmes, and Yuki Nakayama. August 2006.

PEER 2005/08 *Damage Accumulation in Lightly Confined Reinforced Concrete Bridge Columns.* R. Tyler Ranf, Jared M. Nelson, Zach Price, Marc O. Eberhard, and John F. Stanton. April 2006.

PEER 2005/07 *Experimental and Analytical Studies on the Seismic Response of Freestanding and Anchored Laboratory Equipment.* Dimitrios Konstantinidis and Nicos Makris. January 2005.

PEER 2005/06 *Global Collapse of Frame Structures under Seismic Excitations*. Luis F. Ibarra and Helmut Krawinkler. September 2005.

PEER 2005//05 *Performance Characterization of Bench- and Shelf-Mounted Equipment.* Samit Ray Chaudhuri and Tara C. Hutchinson. May 2006.

PEER 2005/04 *Numerical Modeling of the Nonlinear Cyclic Response of Shallow Foundations.* Chad Harden, Tara Hutchinson, Geoffrey R. Martin, and Bruce L. Kutter. August 2005.

PEER 2005/03 *A Taxonomy of Building Components for Performance-Based Earthquake Engineering.* Keith A. Porter. September 2005.

PEER 2005/02 *Fragility Basis for California Highway Overpass Bridge Seismic Decision Making*. Kevin R. Mackie and Božidar Stojadinović. June 2005.

PEER 2005/01 *Empirical Characterization of Site Conditions on Strong Ground Motion.* Jonathan P. Stewart, Yoojoong Choi, and Robert W. Graves. June 2005.

PEER 2004/09 *Electrical Substation Equipment Interaction: Experimental Rigid Conductor Studies.* Christopher Stearns and André Filiatrault. February 2005.

PEER 2004/08 *Seismic Qualification and Fragility Testing of Line Break 550-kV Disconnect Switches.* Shakhzod M. Takhirov, Gregory L. Fenves, and Eric Fujisaki. January 2005.

PEER 2004/07 *Ground Motions for Earthquake Simulator Qualification of Electrical Substation Equipment.* Shakhzod M. Takhirov, Gregory L. Fenves, Eric Fujisaki, and Don Clyde. January 2005.

PEER 2004/06 *Performance-Based Regulation and Regulatory Regimes.* Peter J. May and Chris Koski. September 2004.

PEER 2004/05 *Performance-Based Seismic Design Concepts and Implementation: Proceedings of an International Workshop.* Peter Fajfar and Helmut Krawinkler, editors. September 2004.

PEER 2004/04 *Seismic Performance of an Instrumented Tilt-up Wall Building.* James C. Anderson and Vitelmo V. Bertero. July 2004.

PEER 2004/03 *Evaluation and Application of Concrete Tilt-up Assessment Methodologies.* Timothy Graf and James O. Malley. October 2004.

PEER 2004/02 *Analytical Investigations of New Methods for Reducing Residual Displacements of Reinforced Concrete Bridge Columns.* Junichi Sakai and Stephen A. Mahin. August 2004.

PEER 2004/01 *Seismic Performance of Masonry Buildings and Design Implications.* Kerri Anne Taeko Tokoro, James C. Anderson, and Vitelmo V. Bertero. February 2004.

PEER 2003/18 *Performance Models for Flexural Damage in Reinforced Concrete Columns.* Michael Berry and Marc Eberhard. August 2003.

PEER 2003/17 *Predicting Earthquake Damage in Older Reinforced Concrete Beam-Column Joints.* Catherine Pagni and Laura Lowes. October 2004.

PEER 2003/16 *Seismic Demands for Performance-Based Design of Bridges.* Kevin Mackie and Božidar Stojadinović. August 2003.

PEER 2003/15 *Seismic Demands for Nondeteriorating Frame Structures and Their Dependence on Ground Motions.* Ricardo Antonio Medina and Helmut Krawinkler. May 2004.

PEER 2003/14 *Finite Element Reliability and Sensitivity Methods for Performance-Based Earthquake Engineering.* Terje Haukaas and Armen Der Kiureghian. April 2004.

PEER 2003/13 *Effects of Connection Hysteretic Degradation on the Seismic Behavior of Steel Moment-Resisting Frames.* Janise E. Rodgers and Stephen A. Mahin. March 2004.

PEER 2003/12 *Implementation Manual for the Seismic Protection of Laboratory Contents: Format and Case Studies.* William T. Holmes and Mary C. Comerio. October 2003.

PEER 2003/11 *Fifth U.S.-Japan Workshop on Performance-Based Earthquake Engineering Methodology for Reinforced Concrete Building Structures.* February 2004.

PEER 2003/10 *A Beam-Column Joint Model for Simulating the Earthquake Response of Reinforced Concrete Frames.* Laura N. Lowes, Nilanjan Mitra, and Arash Altoontash. February 2004.

PEER 2003/09 *Sequencing Repairs after an Earthquake: An Economic Approach.* Marco Casari and Simon J. Wilkie. April 2004.

PEER 2003/08 *A Technical Framework for Probability-Based Demand and Capacity Factor Design (DCFD) Seismic Formats*. Fatemeh Jalayer and C. Allin Cornell. November 2003.

PEER 2003/07 *Uncertainty Specification and Propagation for Loss Estimation Using FOSM Methods.* Jack W. Baker and C. Allin Cornell. September 2003.

PEER 2003/06 *Performance of Circular Reinforced Concrete Bridge Columns under Bidirectional Earthquake Loading*. Mahmoud M. Hachem, Stephen A. Mahin, and Jack P. Moehle. February 2003.

PEER 2003/05 *Response Assessment for Building-Specific Loss Estimation.* Eduardo Miranda and Shahram Taghavi. September 2003.

PEER 2003/04 *Experimental Assessment of Columns with Short Lap Splices Subjected to Cyclic Loads*. Murat Melek, John W. Wallace, and Joel Conte. April 2003.

PEER 2003/03 *Probabilistic Response Assessment for Building-Specific Loss Estimation.* Eduardo Miranda and Hesameddin Aslani. September 2003.

PEER 2003/02 *Software Framework for Collaborative Development of Nonlinear Dynamic Analysis Program.* Jun Peng and Kincho H. Law. September 2003.

PEER 2003/01 *Shake Table Tests and Analytical Studies on the Gravity Load Collapse of Reinforced Concrete Frames.* Kenneth John Elwood and Jack P. Moehle. November 2003.

PEER 2002/24 *Performance of Beam to Column Bridge Joints Subjected to a Large Velocity Pulse.* Natalie Gibson, André Filiatrault, and Scott A. Ashford. April 2002.

PEER 2002/23 *Effects of Large Velocity Pulses on Reinforced Concrete Bridge Columns.* Greg L. Orozco and Scott A. Ashford. April 2002.

PEER 2002/22 *Characterization of Large Velocity Pulses for Laboratory Testing.* Kenneth E. Cox and Scott A. Ashford. April 2002.

PEER 2002/21 *Fourth U.S.-Japan Workshop on Performance-Based Earthquake Engineering Methodology for Reinforced Concrete Building Structures*. December 2002.

PEER 2002/20 *Barriers to Adoption and Implementation of PBEE Innovations.* Peter J. May. August 2002.

PEER 2002/19 *Economic-Engineered Integrated Models for Earthquakes: Socioeconomic Impacts.* Peter Gordon, James E. Moore II, and Harry W. Richardson. July 2002.

PEER 2002/18 *Assessment of Reinforced Concrete Building Exterior Joints with Substandard Details.* Chris P. Pantelides, Jon Hansen, Justin Nadauld, and Lawrence D. Reaveley. May 2002.

PEER 2002/17 *Structural Characterization and Seismic Response Analysis of a Highway Overcrossing Equipped with Elastomeric Bearings and Fluid Dampers: A Case Study.* Nicos Makris and Jian Zhang. November 2002.

PEER 2002/16 *Estimation of Uncertainty in Geotechnical Properties for Performance-Based Earthquake Engineering.* Allen L. Jones, Steven L. Kramer, and Pedro Arduino. December 2002.

PEER 2002/15 *Seismic Behavior of Bridge Columns Subjected to Various Loading Patterns.* Asadollah Esmaeily-Gh. and Yan Xiao. December 2002.

PEER 2002/14 *Inelastic Seismic Response of Extended Pile Shaft Supported Bridge Structures.* T.C. Hutchinson, R.W. Boulanger, Y.H. Chai, and I.M. Idriss. December 2002.

PEER 2002/13 *Probabilistic Models and Fragility Estimates for Bridge Components and Systems.* Paolo Gardoni, Armen Der Kiureghian, and Khalid M. Mosalam. June 2002.

PEER 2002/12 *Effects of Fault Dip and Slip Rake on Near-Source Ground Motions: Why Chi-Chi Was a Relatively Mild M7.6 Earthquake.* Brad T. Aagaard, John F. Hall, and Thomas H. Heaton. December 2002.

PEER 2002/11 *Analytical and Experimental Study of Fiber-Reinforced Strip Isolators.* James M. Kelly and Shakhzod M. Takhirov. September 2002.

PEER 2002/10 *Centrifuge Modeling of Settlement and Lateral Spreading with Comparisons to Numerical Analyses***.** Sivapalan Gajan and Bruce L. Kutter. January 2003.

PEER 2002/09 *Documentation and Analysis of Field Case Histories of Seismic Compression during the 1994 Northridge, California, Earthquake.* Jonathan P. Stewart, Patrick M. Smith, Daniel H. Whang, and Jonathan D. Bray. October 2002.

PEER 2002/08 *Component Testing, Stability Analysis and Characterization of Buckling-Restrained Unbonded Braces™.* Cameron Black, Nicos Makris, and Ian Aiken. September 2002.

PEER 2002/07 *Seismic Performance of Pile-Wharf Connections.* Charles W. Roeder, Robert Graff, Jennifer Soderstrom, and Jun Han Yoo. December 2001.

PEER 2002/06 *The Use of Benefit-Cost Analysis for Evaluation of Performance-Based Earthquake Engineering Decisions.* Richard O. Zerbe and Anthony Falit-Baiamonte. September 2001.

PEER 2002/05 *Guidelines, Specifications, and Seismic Performance Characterization of Nonstructural Building Components and Equipment.* André Filiatrault, Constantin Christopoulos, and Christopher Stearns. September 2001.

PEER 2002/04 *Consortium of Organizations for Strong-Motion Observation Systems and the Pacific Earthquake Engineering Research Center Lifelines Program: Invited Workshop on Archiving and Web Dissemination of Geotechnical Data, 4–5 October 2001.* September 2002.

PEER 2002/03 *Investigation of Sensitivity of Building Loss Estimates to Major Uncertain Variables for the Van Nuys Testbed.* Keith A. Porter, James L. Beck, and Rustem V. Shaikhutdinov. August 2002.

PEER 2002/02 *The Third U.S.-Japan Workshop on Performance-Based Earthquake Engineering Methodology for Reinforced Concrete Building Structures.* July 2002.

PEER 2002/01 *Nonstructural Loss Estimation: The UC Berkeley Case Study.* Mary C. Comerio and John C. Stallmeyer. December 2001.

PEER 2001/16 *Statistics of SDF-System Estimate of Roof Displacement for Pushover Analysis of Buildings.* Anil K. Chopra, Rakesh K. Goel, and Chatpan Chintanapakdee. December 2001.

PEER 2001/15 *Damage to Bridges during the 2001 Nisqually Earthquake.* R. Tyler Ranf, Marc O. Eberhard, and Michael P. Berry. November 2001.

PEER 2001/14 *Rocking Response of Equipment Anchored to a Base Foundation.* Nicos Makris and Cameron J. Black. September 2001.

PEER 2001/13 *Modeling Soil Liquefaction Hazards for Performance-Based Earthquake Engineering.* Steven L. Kramer and Ahmed-W. Elgamal. February 2001.

PEER 2001/12 *Development of Geotechnical Capabilities in OpenSees.* Boris Jeremić. September 2001.

PEER 2001/11 *Analytical and Experimental Study of Fiber-Reinforced Elastomeric Isolators.* James M. Kelly and Shakhzod M. Takhirov. September 2001.

PEER 2001/10 *Amplification Factors for Spectral Acceleration in Active Regions.* Jonathan P. Stewart, Andrew H. Liu, Yoojoong Choi, and Mehmet B. Baturay. December 2001.

PEER 2001/09 *Ground Motion Evaluation Procedures for Performance-Based Design.* Jonathan P. Stewart, Shyh-Jeng Chiou, Jonathan D. Bray, Robert W. Graves, Paul G. Somerville, and Norman A. Abrahamson. September 2001.

PEER 2001/08 *Experimental and Computational Evaluation of Reinforced Concrete Bridge Beam-Column Connections for Seismic Performance.* Clay J. Naito, Jack P. Moehle, and Khalid M. Mosalam. November 2001.

PEER 2001/07 *The Rocking Spectrum and the Shortcomings of Design Guidelines.* Nicos Makris and Dimitrios Konstantinidis. August 2001.

PEER 2001/06 *Development of an Electrical Substation Equipment Performance Database for Evaluation of Equipment Fragilities*. Thalia Agnanos. April 1999.

PEER 2001/05 *Stiffness Analysis of Fiber-Reinforced Elastomeric Isolators.* Hsiang-Chuan Tsai and James M. Kelly. May 2001.

PEER 2001/04 *Organizational and Societal Considerations for Performance-Based Earthquake Engineering.* Peter J. May. April 2001.

PEER 2001/03 *A Modal Pushover Analysis Procedure to Estimate Seismic Demands for Buildings: Theory and Preliminary Evaluation.* Anil K. Chopra and Rakesh K. Goel. January 2001.

PEER 2001/02 *Seismic Response Analysis of Highway Overcrossings Including Soil-Structure Interaction.* Jian Zhang and Nicos Makris. March 2001.

PEER 2001/01 *Experimental Study of Large Seismic Steel Beam-to-Column Connections.* Egor P. Popov and Shakhzod M. Takhirov. November 2000.

PEER 2000/10 *The Second U.S.-Japan Workshop on Performance-Based Earthquake Engineering Methodology for Reinforced Concrete Building Structures.* March 2000.

PEER 2000/09 *Structural Engineering Reconnaissance of the August 17, 1999 Earthquake: Kocaeli (Izmit), Turkey.* Halil Sezen, Kenneth J. Elwood, Andrew S. Whittaker, Khalid Mosalam, John J. Wallace, and John F. Stanton. December 2000.

PEER 2000/08 *Behavior of Reinforced Concrete Bridge Columns Having Varying Aspect Ratios and Varying Lengths of Confinement.* Anthony J. Calderone, Dawn E. Lehman, and Jack P. Moehle. January 2001.

PEER 2000/07 *Cover-Plate and Flange-Plate Reinforced Steel Moment-Resisting Connections.* Taejin Kim, Andrew S. Whittaker, Amir S. Gilani, Vitelmo V. Bertero, and Shakhzod M. Takhirov. September 2000.

PEER 2000/06 *Seismic Evaluation and Analysis of 230-kV Disconnect Switches.* Amir S. J. Gilani, Andrew S. Whittaker, Gregory L. Fenves, Chun-Hao Chen, Henry Ho, and Eric Fujisaki. July 2000.

PEER 2000/05 *Performance-Based Evaluation of Exterior Reinforced Concrete Building Joints for Seismic Excitation.* Chandra Clyde, Chris P. Pantelides, and Lawrence D. Reaveley. July 2000.

PEER 2000/04 *An Evaluation of Seismic Energy Demand: An Attenuation Approach.* Chung-Che Chou and Chia-Ming Uang. July 1999.

PEER 2000/03 *Framing Earthquake Retrofitting Decisions: The Case of Hillside Homes in Los Angeles.* Detlof von Winterfeldt, Nels Roselund, and Alicia Kitsuse. March 2000.

PEER 2000/02 *U.S.-Japan Workshop on the Effects of Near-Field Earthquake Shaking.* Andrew Whittaker, ed. July 2000.

PEER 2000/01 *Further Studies on Seismic Interaction in Interconnected Electrical Substation Equipment.* Armen Der Kiureghian, Kee-Jeung Hong, and Jerome L. Sackman. November 1999.

PEER 1999/14 *Seismic Evaluation and Retrofit of 230-kV Porcelain Transformer Bushings*. Amir S. Gilani, Andrew S. Whittaker, Gregory L. Fenves, and Eric Fujisaki. December 1999.

PEER 1999/13 *Building Vulnerability Studies: Modeling and Evaluation of Tilt-up and Steel Reinforced Concrete Buildings.* John W. Wallace, Jonathan P. Stewart, and Andrew S. Whittaker, editors. December 1999.

PEER 1999/12 *Rehabilitation of Nonductile RC Frame Building Using Encasement Plates and Energy-Dissipating Devices.* Mehrdad Sasani, Vitelmo V. Bertero, James C. Anderson. December 1999.

PEER 1999/11 *Performance Evaluation Database for Concrete Bridge Components and Systems under Simulated Seismic Loads.* Yael D. Hose and Frieder Seible. November 1999.

PEER 1999/10 *U.S.-Japan Workshop on Performance-Based Earthquake Engineering Methodology for Reinforced Concrete Building Structures.* December 1999.

PEER 1999/09 *Performance Improvement of Long Period Building Structures Subjected to Severe Pulse-Type Ground Motions*. James C. Anderson, Vitelmo V. Bertero, and Raul Bertero. October 1999.

PEER 1999/08 *Envelopes for Seismic Response Vectors.* Charles Menun and Armen Der Kiureghian. July 1999.

PEER 1999/07 *Documentation of Strengths and Weaknesses of Current Computer Analysis Methods for Seismic Performance of Reinforced Concrete Members.* William F. Cofer. November 1999.

PEER 1999/06 *Rocking Response and Overturning of Anchored Equipment under Seismic Excitations.* Nicos Makris and Jian Zhang. November 1999.

PEER 1999/05 *Seismic Evaluation of 550 kV Porcelain Transformer Bushings.* Amir S. Gilani, Andrew S. Whittaker, Gregory L. Fenves, and Eric Fujisaki. October 1999.

PEER 1999/04 *Adoption and Enforcement of Earthquake Risk-Reduction Measures.* Peter J. May, Raymond J. Burby, T. Jens Feeley, and Robert Wood.

PEER 1999/03 *Task 3 Characterization of Site Response General Site Categories.* Adrian Rodriguez-Marek, Jonathan D. Bray, and Norman Abrahamson. February 1999.

PEER 1999/02 *Capacity-Demand-Diagram Methods for Estimating Seismic Deformation of Inelastic Structures: SDF Systems.* Anil K. Chopra and Rakesh Goel. April 1999.

PEER 1999/01 *Interaction in Interconnected Electrical Substation Equipment Subjected to Earthquake Ground Motions.* Armen Der Kiureghian, Jerome L. Sackman, and Kee-Jeung Hong. February 1999.

PEER 1998/08 *Behavior and Failure Analysis of a Multiple-Frame Highway Bridge in the 1994 Northridge Earthquake.* Gregory L. Fenves and Michael Ellery. December 1998.

PEER 1998/07 *Empirical Evaluation of Inertial Soil-Structure Interaction Effects.* Jonathan P. Stewart, Raymond B. Seed, and Gregory L. Fenves. November 1998.

PEER 1998/06 *Effect of Damping Mechanisms on the Response of Seismic Isolated Structures.* Nicos Makris and Shih-Po Chang. November 1998.

PEER 1998/05 *Rocking Response and Overturning of Equipment under Horizontal Pulse-Type Motions.* Nicos Makris and Yiannis Roussos. October 1998.

PEER 1998/04 *Pacific Earthquake Engineering Research Invitational Workshop Proceedings, May 14–15, 1998: Defining the Links between Planning, Policy Analysis, Economics and Earthquake Engineering.* Mary Comerio and Peter Gordon. September 1998.

PEER 1998/03 *Repair/Upgrade Procedures for Welded Beam to Column Connections.* James C. Anderson and Xiaojing Duan. May 1998.

PEER 1998/02 *Seismic Evaluation of 196 kV Porcelain Transformer Bushings.* Amir S. Gilani, Juan W. Chavez, Gregory L. Fenves, and Andrew S. Whittaker. May 1998.

PEER 1998/01 *Seismic Performance of Well-Confined Concrete Bridge Columns.* Dawn E. Lehman and Jack P. Moehle. December 2000.

ONLINE PEER REPORTS

The following PEER reports are available by Internet only at http://peer.berkeley.edu/publications/peer_reports_complete.html.

PEER 2012/103 *Performance-Based Seismic Demand Assessment of Concentrically Braced Steel Frame Buildings.* Chui-Hsin Chen and Stephen A. Mahin. December 2012.

PEER 2012/102 *Procedure to Restart an Interrupted Hybrid Simulation: Addendum to PEER Report 2010/103.* Vesna Terzic and Bozidar Stojadinovic. October 2012.

PEER 2012/101 *Mechanics of Fiber Reinforced Bearings.* James M. Kelly and Andrea Calabrese. February 2012.

PEER 2011/107 *Nonlinear Site Response and Seismic Compression at Vertical Array Strongly Shaken by 2007 Niigata-ken Chuetsu-oki Earthquake.* Eric Yee, Jonathan P. Stewart, and Kohji Tokimatsu. December 2011.

PEER 2011/106 *Self Compacting Hybrid Fiber Reinforced Concrete Composites for Bridge Columns.* Pardeep Kumar, Gabriel Jen, William Trono, Marios Panagiotou, and Claudia Ostertag. September 2011.

PEER 2011/105 *Stochastic Dynamic Analysis of Bridges Subjected to Spacially Varying Ground Motions.* Katerina Konakli and Armen Der Kiureghian. August 2011.

PEER 2011/104 *Design and Instrumentation of the 2010 E-Defense Four-Story Reinforced Concrete and Post-Tensioned Concrete Buildings.* Takuya Nagae, Kenichi Tahara, Taizo Matsumori, Hitoshi Shiohara, Toshimi Kabeyasawa, Susumu Kono, Minehiro Nishiyama (Japanese Research Team) and John Wallace, Wassim Ghannoum, Jack Moehle, Richard Sause, Wesley Keller, Zeynep Tuna (U.S. Research Team). June 2011.

PEER 2011/103 *In-Situ Monitoring of the Force Output of Fluid Dampers: Experimental Investigation.* Dimitrios Konstantinidis, James M. Kelly, and Nicos Makris. April 2011.

PEER 2011/102 *Ground-motion prediction equations 1964 - 2010.* John Douglas. April 2011.

PEER 2011/101 *Report of the Eighth Planning Meeting of NEES/E-Defense Collaborative Research on Earthquake Engineering.* Convened by the Hyogo Earthquake Engineering Research Center (NIED), NEES Consortium, Inc. February 2011.

PEER 2010/111 *Modeling and Acceptance Criteria for Seismic Design and Analysis of Tall Buildings.* Task 7 Report for the Tall Buildings Initiative - Published jointly by the Applied Technology Council. October 2010.

PEER 2010/110 *Seismic Performance Assessment and Probabilistic Repair Cost Analysis of Precast Concrete Cladding Systems for Multistory Buildlings.* Jeffrey P. Hunt and Božidar Stojadinovic. November 2010.

PEER 2010/109 *Report of the Seventh Joint Planning Meeting of NEES/E-Defense Collaboration on Earthquake Engineering. Held at the E-Defense, Miki, and Shin-Kobe, Japan, September 18–19, 2009.* August 2010.

PEER 2010/108 *Probabilistic Tsunami Hazard in California.* Hong Kie Thio, Paul Somerville, and Jascha Polet, preparers. October 2010.

PEER 2010/107 *Performance and Reliability of Exposed Column Base Plate Connections for Steel Moment-Resisting Frames.* Ady Aviram, Božidar Stojadinovic, and Armen Der Kiureghian. August 2010.

PEER 2010/106 *Verification of Probabilistic Seismic Hazard Analysis Computer Programs.* Patricia Thomas, Ivan Wong, and Norman Abrahamson. May 2010.

PEER 2010/105 *Structural Engineering Reconnaissance of the April 6, 2009, Abruzzo, Italy, Earthquake, and Lessons Learned.* M. Selim Günay and Khalid M. Mosalam. April 2010.

PEER 2010/104 *Simulating the Inelastic Seismic Behavior of Steel Braced Frames, Including the Effects of Low-Cycle Fatigue.* Yuli Huang and Stephen A. Mahin. April 2010.

PEER 2010/103 *Post-Earthquake Traffic Capacity of Modern Bridges in California.* Vesna Terzic and Božidar Stojadinović. March 2010.

PEER 2010/102 *Analysis of Cumulative Absolute Velocity (CAV) and JMA Instrumental Seismic Intensity (I_{JMA}) Using the PEER–NGA Strong Motion Database.* Kenneth W. Campbell and Yousef Bozorgnia. February 2010.

PEER 2010/101 *Rocking Response of Bridges on Shallow Foundations.* Jose A. Ugalde, Bruce L. Kutter, and Boris Jeremic. April 2010.

PEER 2009/109 *Simulation and Performance-Based Earthquake Engineering Assessment of Self-Centering Post-Tensioned Concrete Bridge Systems.* Won K. Lee and Sarah L. Billington. December 2009.

PEER 2009/108 *PEER Lifelines Geotechnical Virtual Data Center.* J. Carl Stepp, Daniel J. Ponti, Loren L. Turner, Jennifer N. Swift, Sean Devlin, Yang Zhu, Jean Benoit, and John Bobbitt. September 2009.

PEER 2009/107 *Experimental and Computational Evaluation of Current and Innovative In-Span Hinge Details in Reinforced Concrete Box-Girder Bridges: Part 2: Post-Test Analysis and Design Recommendations.* Matias A. Hube and Khalid M. Mosalam. December 2009.

PEER 2009/106 *Shear Strength Models of Exterior Beam-Column Joints without Transverse Reinforcement.* Sangjoon Park and Khalid M. Mosalam. November 2009.

PEER 2009/105 *Reduced Uncertainty of Ground Motion Prediction Equations through Bayesian Variance Analysis.* Robb Eric S. Moss. November 2009.

PEER 2009/104 *Advanced Implementation of Hybrid Simulation.* Andreas H. Schellenberg, Stephen A. Mahin, Gregory L. Fenves. November 2009.

PEER 2009/103 *Performance Evaluation of Innovative Steel Braced Frames.* T. Y. Yang, Jack P. Moehle, and Božidar Stojadinovic. August 2009.

PEER 2009/102 *Reinvestigation of Liquefaction and Nonliquefaction Case Histories from the 1976 Tangshan Earthquake.* Robb Eric Moss, Robert E. Kayen, Liyuan Tong, Songyu Liu, Guojun Cai, and Jiaer Wu. August 2009.

PEER 2009/101 *Report of the First Joint Planning Meeting for the Second Phase of NEES/E-Defense Collaborative Research on Earthquake Engineering.* Stephen A. Mahin et al. July 2009.

PEER 2008/104 *Experimental and Analytical Study of the Seismic Performance of Retaining Structures.* Linda Al Atik and Nicholas Sitar. January 2009.

PEER 2008/103 *Experimental and Computational Evaluation of Current and Innovative In-Span Hinge Details in Reinforced Concrete Box-Girder Bridges. Part 1: Experimental Findings and Pre-Test Analysis.* Matias A. Hube and Khalid M. Mosalam. January 2009.

PEER 2008/102 *Modeling of Unreinforced Masonry Infill Walls Considering In-Plane and Out-of-Plane Interaction.* Stephen Kadysiewski and Khalid M. Mosalam. January 2009.

PEER 2008/101 *Seismic Performance Objectives for Tall Buildings.* William T. Holmes, Charles Kircher, William Petak, and Nabih Youssef. August 2008.

PEER 2007/101 *Generalized Hybrid Simulation Framework for Structural Systems Subjected to Seismic Loading.* Tarek Elkhoraibi and Khalid M. Mosalam. July 2007.

PEER 2007/100 *Seismic Evaluation of Reinforced Concrete Buildings Including Effects of Masonry Infill Walls.* Alidad Hashemi and Khalid M. Mosalam. July 2007.

The Pacific Earthquake Engineering Research Center (PEER) is a multi-institutional research and education center with headquarters at the University of California, Berkeley. Investigators from over 20 universities, several consulting companies, and researchers at various state and federal government agencies contribute to research programs focused on performance-based earthquake engineering.

These research programs aim to identify and reduce the risks from major earthquakes to life safety and to the economy by including research in a wide variety of disciplines including structural and geotechnical engineering, geology/seismology, lifelines, transportation, architecture, economics, risk management, and public policy.

PEER is supported by federal, state, local, and regional agencies, together with industry partners.

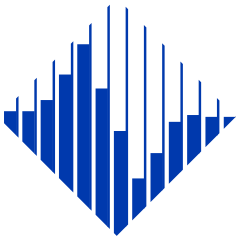

PEER Core Institutions:
University of California, Berkeley (Lead Institution)
California Institute of Technology
Oregon State University
Stanford University
University of California, Davis
University of California, Irvine
University of California, Los Angeles
University of California, San Diego
University of Southern California
University of Washington

PEER reports can be ordered at http://peer.berkeley.edu/publications/peer_reports.html or by contacting

Pacific Earthquake Engineering Research Center
University of California, Berkeley
325 Davis Hall, mail code 1792
Berkeley, CA 94720-1792
Tel: 510-642-3437
Fax: 510-642-1655
Email: peer_editor@berkeley.edu

ISSN 1547-0587X